NASA CONTRACT
NASW 1932

SPACE GEODESY ALTIMETRY

AIRCRAFT EXPERIMENT

May 1970

RAYTHEON COMPANY | EQUIPMENT DIVISION

SPACE GEODESY ALTIMETRY AIRCRAFT EXPERIMENT, DATED MAY 1970, PREPARED UNDER NASW-1932

FINAL REPORT ERRATA SHEET

7/24/70

PAGE	CHANGE
iv	Add new sentence after 2nd paragraph "E. Weiss was technically responsible for the Flight Test Plan".
v	Fourth line, change from "meansurators" to "mensurators".
xii	For Figure 5-43 change caption from "(Camera Looking in $Y^{(3)}$ Direction of Figure 14) to "(Camera Looking in $Y^{(3)}$ Direction of Figure 14 in Appendix B)".
1-7	Figure 1-5 printed upside down.
2-6	Figure 2-3 printed upside down.
3-3	Fifth line from bottom, change from "morevoer" to "moreover'
3-4	For Flight 3, under Stilwell Parameters, change altitude from "80, 000" to "20, 000".
3-5	For Flight 4, change location from "7°07' x 33°38''" to "37°07' x 73°38' ".
3-7	For Flight 16, under Stilwell Parameters, add new data in column to the right of 8, 1500 ft, 1/200 a f 22, new data should read:

No. of Runs	4
Altitude	10, 000 ft.
Camera Parameters	1/200 at f 22

4-11	Sixth line, change from "P_r" to "P_R".
4-13	Thirteenth line, change from "P_r" to "P_R".
5-6	Tenth line from bottom, after Molo Christianson change "and" to "are".
5-9	Tenth line, change from "P_r" to "P_R".

PAGE	CHANGE
5-12	Change equation (5-14),

From: $$\theta_e = \frac{\theta_{H1}\,\theta_{H2}}{\theta_{H\theta}+\theta_{H2}} + \frac{\theta_{E1}\,\theta_{E2}}{\theta_{E1}\,\theta_{E2}}$$

To: $$\theta_e = \frac{\theta_{H1}\,\theta_{H2}}{\theta_{H1}+\theta_{H2}} + \frac{\theta_{E1}\,\theta_{E2}}{\theta_{E\theta}\,\theta_{E2}}$$

PAGE	CHANGE
5-23	Fifth line, change from "5-21" to "5-17".
5-23	Ninth line, change from "5-30" to "5-23".
5-23	Seventeenth line, change from "10,000 ft." to "5,000 ft".
5-34	First line, change from "5-57" to "5-37".
5-41	In caption, change from "(Camera Looking in $Y^{(3)}$ Direction of Figure 14) to "(Camera Looking in $Y^{(3)}$ Direction of Figure 14 in Appendix B)".
A-1	Second line, change from "4.1.4" to "4.4".
B-37	Third line, change from "(which is not gaussian!" to "(which is not gaussian)".

SPACE GEODESY AIRCRAFT EXPERIMENT

FINAL REPORT

MAY 1970

Prepared Under

NASA Contract NASW 1932

for

A. Selser
Technical Monitor
NASA
Code RED-IDP-RSS
Wallops Station
Wallops Island, Va. 2337

by

RAYTHEON COMPANY
Equipment Division
Wayland Laboratories
Advanced Technology Programs
Sudbury, Massachusetts

Prepared by: E Genest
E. Genest
Project Engineer

Approved by: M Kolker
M. Kolker
Program Manager

C Mundo
C. Mundo
Program Scientist

FOREWORD

This report contains the results of the Space Geodesy Aircraft Experiment awarded Raytheon Company under Contract No. NASW-1932 by the Geodetic Satellite Program Office, Office of Space Science and Applications, National Aeronautics and Space Administration.

The experiment was conducted by the Equipment Division of Raytheon Company under the direction of Mr. Myer Kolker as Program Manager with Mr. Emile Genest as Project Engineer and Dr. Charles J. Mundo, Jr., as Program Scientist.

Successful implementation of this effort was due largely to Mr. Jerome D. Rosenberg, Manager, Geodetic Satellite Programs, NASA OSSA, who initiated the effort, and provided the necessary initial direction and guidance, and to Mr. Allen Selser, Technical Monitor, NASA Wallops Station, who continued the direction and guidance through the conclusion of the experiment.

The primary objective of this experiment was to obtain measurements at normal incidence of radar backscatter and waveforms for varied ocean conditions.

ABSTRACT

Measurements of the radar pulse shape and cross section per unit area, σ^o, at vertical incidence from various ocean conditions were made during the 1969-1970 Winter approximately 120 miles east of Norfolk, Va. The radar equipment consisted of an X-band transmitter, receiver and antenna system generating pulses of ten through one hundred nanoseconds. The reflections were received on a high speed oscilloscope inside an aircraft flying at 10,000 feet. Ocean truth was provided: (1) by two cameras located in the aircraft, one of which obtained pictures which were subsequently processed to provide two-dimensional Fourier transforms of the ocean surface; (2) by a NASA ship on location which provided measurements of ocean and atmospheric conditions, and; (3) by a second aircraft with a laser profilometer which provided precise measurements of the ocean waves. The results indicate a σ^o ranging from 8 to 21 dB and a noticeable trend for σ^o versus wind speed. The waveform of the return compared favorably with the expected waveform.

ACKNOWLEDGEMENT

The Space Geodesy Altimetry Aircraft Experiment Program was initiated by Jerome D. Rosenberg and Dr. Martin J. Swetnick, NASA Office of Space Science and Applications. The Technical Monitor for the program was Alan R. Selser of NASA Wallops Station.

Myer Kolker of Raytheon was Manager of the program, assisted by Dr. Charles Mundo as Program Scientist. Project Engineer of the program at Raytheon was Emile Genest, assisted by Neil Lacey, John Bartlett and John Westphal. The latter three engineers, in addition to participating in the design and fabrication of the radar system at the Raytheon Sudbury Engineering Center, also flew with the equipment and operated it during the runs over the test areas.

Robert Nock and Robert Long of NASA Wallops Station directed aircraft and ship operations and supplied weather information. Lawrence Chase of the National Oceanographic Instrumentation Center provided guidance in measuring ocean parameters from the U.S. Naval Ship Range Recoverer which participated throughout the experiment. Special mention should be made of the officers and crew who spent many days and nights on location so that "ocean truth" would be available when the NASA Wallops Station C-54 aircraft made flights to gather the experimental data.

J. Beck, J. Buck, and T. Brown of Lockheed piloted the C-54 and also provided assistance in planning the flight patterns. C. Linton, RCA, operated the side-looking camera on board the aircraft to take pictures of the ocean for later use in correlating ocean conditions with the radar data. R. Johnson and R. Smith, NASA Wallops Station, developed the films from the side-looking camera.

Denzil Stilwell and W. Keller of NRL provided guidance on applying the Stilwell technique for making Fourier transforms of the side-looking camera photographs. S. Henriksen and H. Hockeborn of Raytheon analyzed the films on meansurators and densitometers at the Raytheon Autometric Operation.

On several test flights, additional ocean truth was provided by W. Kielhorn of ONR who flew a Cessna-310 aircraft with a laser profilometer on board for measuring and recording wave heights at the same time and place where radar and camera data were obtained by the C-54 aircraft. Duncan Ross and Richard Shields of the Naval Oceanographic Office reduced the laser profilometer data.

Professor Blair Kinsman of the Chesapeake Bay Institute, Johns Hopkins University, provided overall guidance on ocean wave theory and measurement techniques, both in the early planning stages of the experiment and in the evaluation phase.

As can be seen from the foregoing, the experiment depended upon the combined efforts of a large number of people in many different organizations. Much of the credit for coordinating these many activities goes to Alan R. Selser, NASA Wallops Station, who provided overall direction for the program.

This report was edited by L. F. Coppenrath of Raytheon's Advanced Development Laboratory.

CONTENTS

CONTENTS (Continued)

CONTENTS (Continued)

CONTENTS (Continued)

ILLUSTRATIONS

ILLUSTRATIONS (Continued)

TABLES

SPACE GEODESY AIRCRAFT EXPERIMENT

EXECUTIVE SUMMARY

During December, 1969 and January, 1970 sixteen test flights were flown out of NASA's Wallops Station, Virginia with the purpose of measuring radar pulse shapes and radar cross sections per unit area, σ^o, at vertical incidence from various ocean conditions.

The radar equipment consisted of an X-band (9 GHz) transmitter, receiver, and antennas (standard gain horns) capable of generating pulses as narrow as ten nanoseconds. The transmitter was a low level local oscillator with a TWT amplifier (12 watts) after the pulse modulation. There were two receiving antennas (standard gain horns of 22 dB with a 12° beamwidth) that were cross polarized with respect to each other permitting measurements of both direct and cross polarized return energy. The transmitting antenna (8° beamwidth) was mechanically boresighted to the same axis as the receiving antennas. The receiver was a fixed gain superheterodyne type. A wide band oscilloscope was used to indicate the sea echos which were photographically recorded. The number of pulses that were integrated, displayed and photographed varied from one to 278. Most of the flights were flown at 10,000 feet using a 20 nanosecond pulse width which resulted in pulse limited returns (rather than beam limited).

Ocean truth data was provided by (1) a down-looking camera which photographed the ocean corresponding to the radar scope photographs, (2) a second camera which obtained photos which were subsequently processed to provide two-dimensional Fourier transforms of the ocean surface, (Stilwell process), (3) a NASA ship on location at the test area which supplied measurements of ocean and atmospheric condition, and (4) an ONR aircraft with a laser profilometer which yielded precise measurements of the ocean waves.

Approximately 600 frames from ten of the flights were selected for further examination. A point coordinate mensurator was used to precisely measure the return pulse peak and noise level, and digitally record these points on to punched cards. All the pertinent radar and environmental data were recorded onto cards. These cards were used as the input data for a processing program which calculated, by using a form of the radar equation, the radar cross section, σ^o, for each frame. For each flight and for a selected number of runs, the mean, the standard deviation, and frequency distribution were then calculated.

The spread of values of σ^o ranged from approximately 8 dB to 21 dB for wave heights up to 12 ft and wind speeds up to 26 knots. In comparing σ^o for each flight with the sea condition, there appears to be correlation between σ^o and wind speed. Since the capillary waves are directly related to wind speed, the data indicates that at X-band σ^o is probably more dependent on capillary wave formations than any other ocean parameter. The data also showed no significant change in σ^o when the aircraft was flying at various headings with the sea direction. Expected pulse shapes, calculated for various pulsewidths, altitudes and σ^o, compared favorably with the actual pulse shapes. The rise times were linear and equal to the pulsewidth and the decay times were related to altitude and beamwidth.

It is recommended that the analysis be further extended to measurements of rise and decay times along with amplitude distributions as a function of time. The Stilwell process should be further developed by analyzing all the available photographs. The relation between σ^o and capillary waves should be further investigated by implementing a method of measuring the capillaries and performing further aircraft experiments. These aircraft experiments should also include measurements of correlation between pulses, altitude bias from wave heights, waveform sampling techniques, and candidate data processors.

SECTION 1. INTRODUCTION & SUMMARY

The Space Geodesy Altimetry Aircraft Experiment Program supports the goal of developing a satellite radar altimeter which will be capable of measuring the distance between the orbit and the ocean surface to accuracies of ± 1 meter or better. At the present time, there is a lack of empirical data on the way in which radar pulses are backscattered by the ocean at vertical incidence.

During this Aircraft Experiment empirical data was taken which will aid in developing a valid electromagnetic model of the ocean at X-Band as a function of pulse-length, sea-state, and altitude. Radar returns from a variety of ocean conditions were observed, recorded, and analyzed. This data will be useful for designing a satellite radar altimeter capable of measuring heights above the ocean to accuracies of ± 1 meter or better at altitudes of 1000 to 1500 kilometers and at orbital velocities of 7 to 8 kilometers per second. In addition, the data will also be useful in interpreting the data from the GEOS C Radar Altimeter Experiment in which accuracies of ± 5 meters are expected and in which consideration is being given to recovering the shape of the return waveform.

The objectives of the flight tests were to measure the pulse shape as reflected from different ocean conditions and to attempt to find a correlation between the return pulse shape and the ocean parameters. Specifically, the intent was to obtain a measure of σ^o (radar scattering coefficient) and $H(\omega)$ (impulse response) for various states of the sea or ocean.

This final report describes the equipment used for making the measurements (see Figure 1-1). It describes both the radar equipment and the auxiliary equipment for making the necessary measurements of ocean and aircraft characteristics. Briefly stated, the basic radar system consisted of three antennas, a receiver rack and a transmitter rack. The antennas were mechically installed, and boresighted in the NASA C54 aircraft. The receiver and transmitter units were mounted in standard nineteen inch racks in the aircraft. Three operators were required to operate the radar equipment, auxiliary data recording equipment, and the three cameras (oscilloscope, ground viewing, and ocean spectra).

The data gathered in this experiment consisted of approximately 10, 000 frames of oscilloscope photographs, 10, 000 frames of ocean photographs at vertical incidence, and 150 frames of ocean photographs at 45° incidence. 600 frames of oscilloscope photographs were reduced in order to obtain σ^o and pulse shape measurements. The process used in reducing the 600 frames of data is described in Section 4. 0.

This report also attempts to relate σ^o to wave height, wave period, wind speed and roll angle. The σ^o measurements are made with narrow pulse returns as would be encountered in a satellite radar altimeter. The relations between pulse shape, altitude, pulse width and wind speed are derived and compared to actual measurements. Various methods of obtaining ocean parameters are described and compared. These include "eyeball" estimates, laser profilometer measurements, and two dimensional Fourier transforms using photographs. The "eyeball" estimates of wave height, and wave period and anemometer readings of wind speed were obtained from the NASA Range Recoverer ship (Figure 1-2) on location in the measurement area. The laser profilometer measurements were obtained by ONR personnel who used a Cessna 310 aircraft with the laser equipment aboard (see Figure 1-3) in the same area. The ocean spectra photographs were obtained from photos taken by a side looking camera on the NASA C54 aircraft used in the experiment (see Figure 1-4, 1-5).

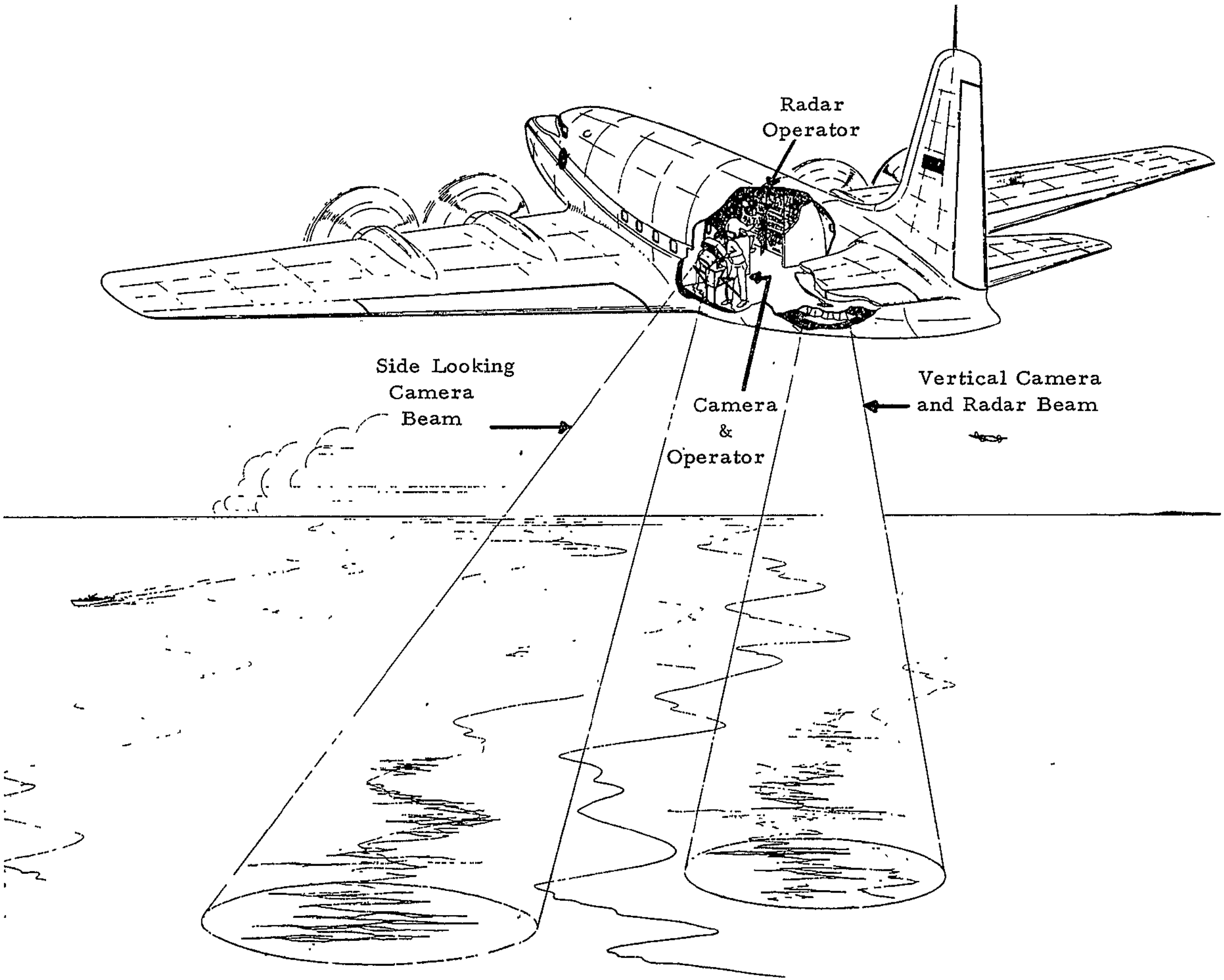

Figure 1-1. Artist Concept of Aircraft Experiment

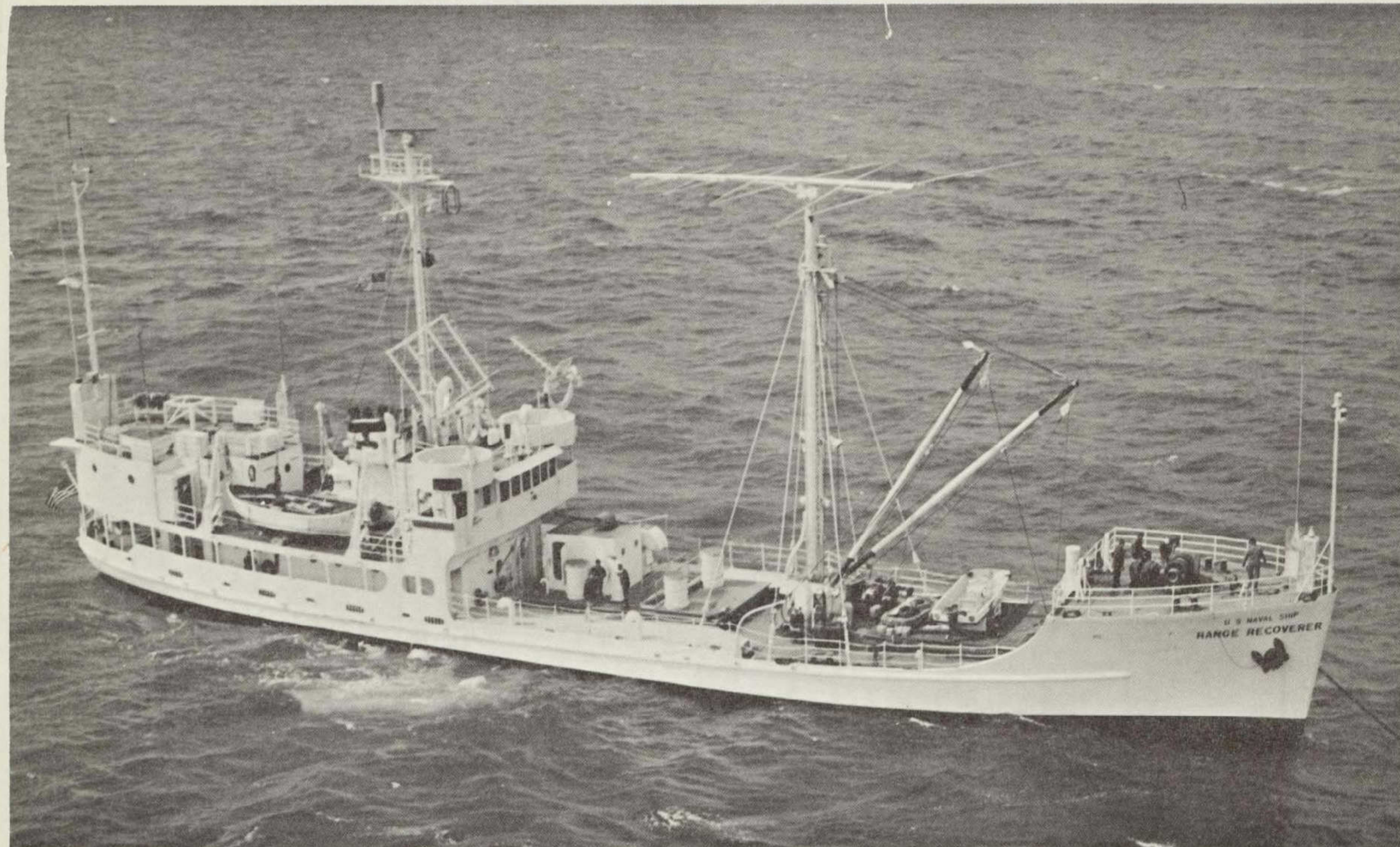

Figure 1-2. NASA Recovery Ship

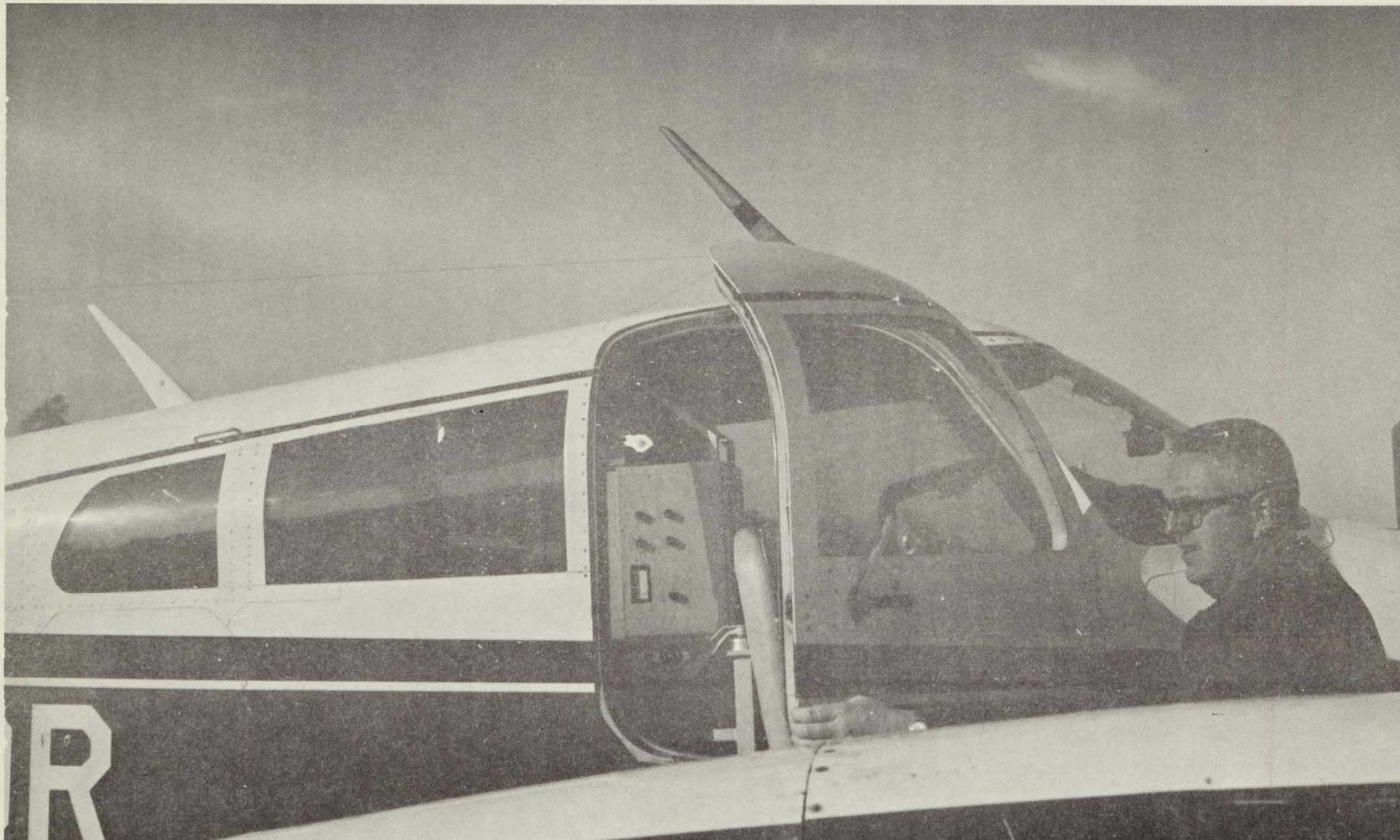

Figure 1-3. CESSNA 310 Aircraft With Laser Equipment Aboard

Figure 1-4. Ocean Spectra Camera (Internal)

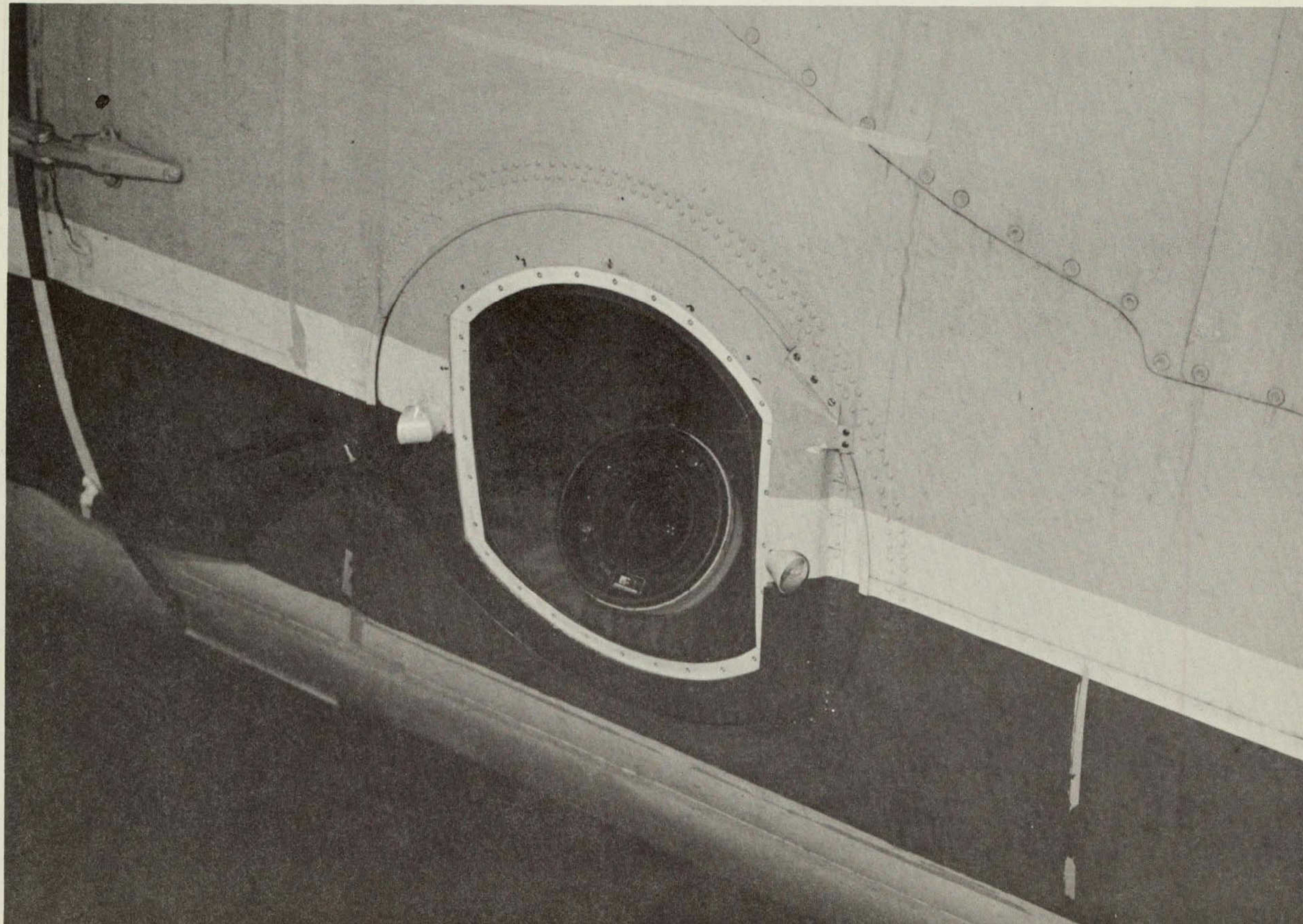

Figure 1-5. Ocean Spectra Camera (External)

Summarizing the conclusions and recommendations:

Conclusions

1. σ^o appears to have a functional relation to wind speed but none to wave height, period, or direction.

2. Variations in σ^o over the looking angles of 0 to 4 degrees are small.

3. The distribution of the amplitude of the return signal and hence σ^o, appears to be Rayleigh.

4. Cross polarized returns at normal incidence were 30 dB down from direct polarized returns.

5. The return waveform and σ^o are unrelated to sea direction.

6. The leading edge of the return waveform was a consistent ramp with little fluctuations.

7. The trailing edge of the return waveform contained large fluctuations for the individual pulse but the average value had a predictable decay functionally related to altitude, pulsewidth and beamwidth.

8. The average characteristics of the measured return waveforms agreed with the computed waveforms.

9. Ocean parameters were consistently obtained by visual observations.

10. Implemented techniques for measurement of ocean parameters included Stilwell photography and laser profilometry. The former is simpler but it requires further development. The latter is more complex and provides one dimension spectrum.

Recommendations

1. The same analyses conducted on the chosen 600 frames of data be extended to the remaining frames to fully exploit the data from this experiment.

2. Measure rise times and decay times and correlate with theoretical values.

3. Analyze the distribution of pulse amplitude as a function of time using a densitometer.

4. The Stilwell process should be further developed by processing all the available photographs and extending the analysis of the results. This includes, at least, analyzing frames from the same flight for self consistency, correlation of Stilwell and laser profilometry data from flight 5, and correlation with surface "eye ball" reports.

5. The relationship of σ^o to surface wind should be further investigated including flying over areas where the surface has no capillary waves (no wind) present and includes conditions of no waves present and swell waves present.

6. Altitude biases as a function of sea state should be investigated. This includes ground range calibration and an independent accurate source of aircraft altitude.

7. Correlation measurements between pulses as a function of time and frequency shift should be performed to compare with satellite measurements.

8. A waveform sampler should be implemented in addition to the oscilloscope and camera.

9. Candidate data processors should be flown and compared.

10. Methods for ground truth measuring of capillary waves should be investigated.

11. In planning future aircraft experiments, major emphasis should be given to methods, availability, and confidence level for the ground truth measurement of the ocean surface conditions.

SECTION 2. TEST SYSTEM

2.1 System Parameters

Table 2-1 gives the system parameters used in making the measurements. Much of the data was taken at 10,000 ft with 20 nsec pulses because: (1) sufficient S/N was available at this altitude; (2) pulse limiting conditions prevailed; and (3) the higher altitudes created operational problems because of oxygen requirements.

The parameter values used were dictated by various practical and operational considerations. The altitude of 20,000 feet is the maximum limit that aircraft available for this operation can fly. The pulsewidth values are those which future radar altimeter designs will be considering and also those which can be generated with present available equipment and a minimum of in-house design effort. The transmitted power of 12 watts is obtained by using a TWT amplifier unit packaged complete with its power supply. Higher power units proved to be proportionately more expensive and impractical for this application. The antennas are standard gain horns which are readily available and have well controlled characteristics. The transmitted wavelength is approximately 3 cm or X-band. The entire X-band from 8 to 12 GHz was capable of being used although the experiment concentrated at one arbitrarily chosen frequency (9 GHz). X-band was used because previous studies have indicated that future GEOS radar altimeters will probably operate in that band.

The oscilloscope camera has a shutter speed of 1/50 of a second and the prf was determined so that one pulse or up to 278 integrated pulses can be displayed on an oscilloscope and photographed. This permits an evaluation of individual pulse returns as well as the integrated effect of many pulses.

Table 2-1. System Parameters

Altitude (ft)	1500, 5000, 10000, 15000, 20000
Pulsewidth (nsec)	10, 20, 100
Transmitted Power (w)	3, 12
Antenna Gain (dB) (two way)	47.3
Frequency (GHz)	9.0
Roll and Pitch (deg.)	0, 3, 5
Radar Output	Scope Photographs
Auxiliary Data	Vertical Photos Side Looking Photos Roll & Pitch Recordings Ship Reports on Sea & Weather Laser Profilometer
Pulse Repetition Rate	0 to 5 KHz
Bandwidth (IF)	200 MHz
Antenna Beamwidth - Transmit	8 degrees
Antenna Beamwidth - Receive	12 degrees
Detector	Square Law
Signal-to-Noise	18 dB or greater
Prime Power	1200 watts
Size-Receiver	19-inch rack 4 ft high
Size Transmitter	19-inch rack 4 ft high
Weight per Rack Unit	300 lbs.

A wide IF bandwidth (200 MHz) was deemed desirable in order to obtain clear pictures of the expected fast rise times. Bandwidths wider than 200 MHz would have made the system much more complex and expensive.

The antenna beamwidths were selected so that the system remained pulse limited at the operating altitudes and yet provided sufficient gain.

The detector operated as a square law device and permitted convenient calibration between power and voltage.

Signal-to-noise was kept high in order to see the effect of ocean parameters on the pulses independently of the thermal noise.

The prime power, size and weight for all the necessary equipment were not critical parameters.

2.2 Radar System Components

The equipment (see Figure 2-1, 2-2) can be broken down into three functional and physical subsystems. They are the transmitter, receiver, and antenna. The transmitter and receiver subsystems consist of rack-mounted units of general purpose equipments with a minimum of in-house designed and fabricated units.

The antenna assembly (Figure 2-3) consists of two receiving standard gain horns cross polarized with respect to each other and fed by a waveguide switch selecting either receiving horn. A standard gain transmitting horn completes the antenna assembly. The E-plane vector of the transmitting horn is perpendicular to the line of flight.

2.3 Transmitter

The type of transmitter selected for this application is a low level local oscillator with a TWT amplifier after the pulse modulation (see Figure 2-4). This is preferred over the magnetron type because it permits wide

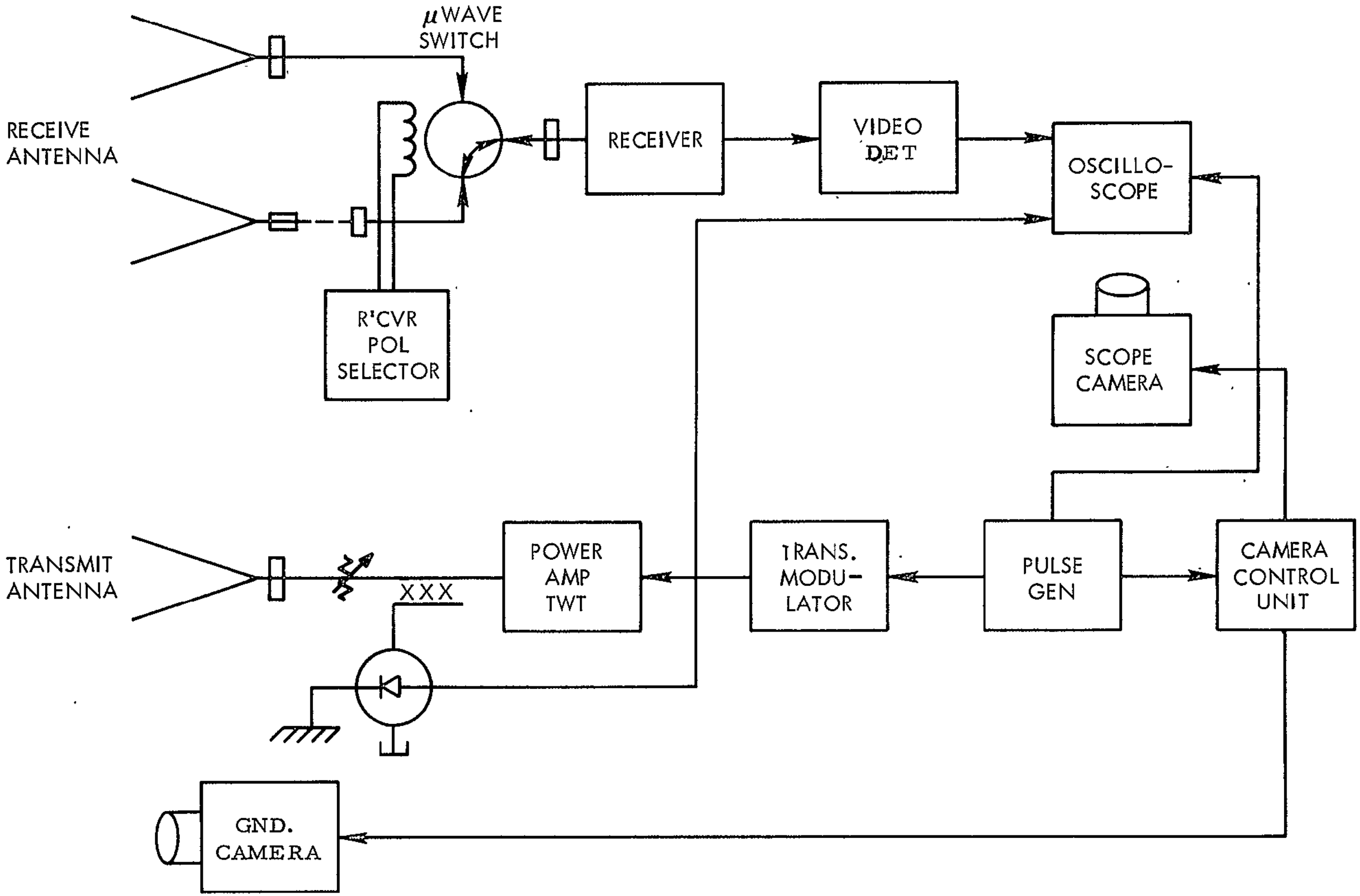

Figure 2-1. Altimeter System Block Diagram

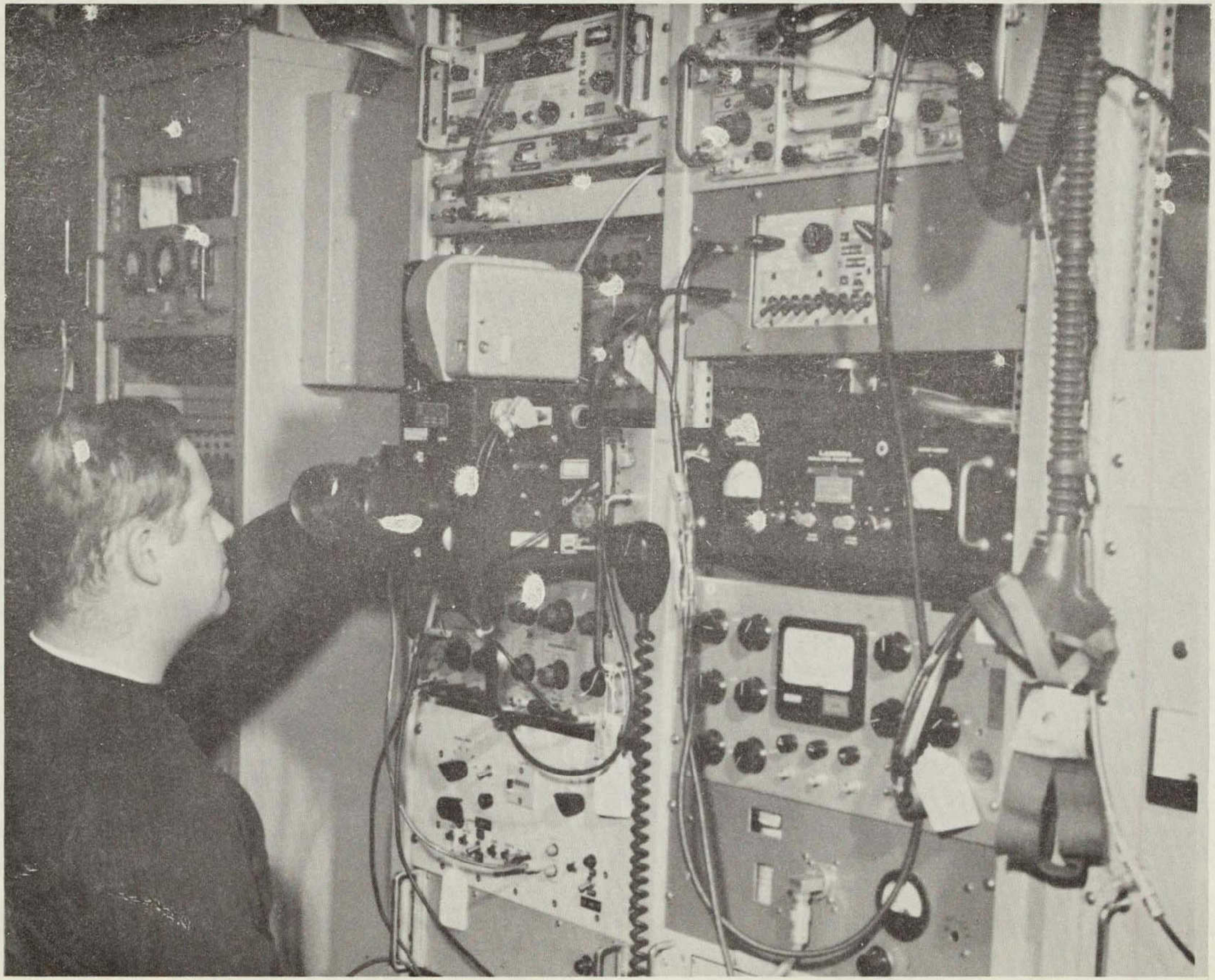

Figure 2-2. Aircraft Installation

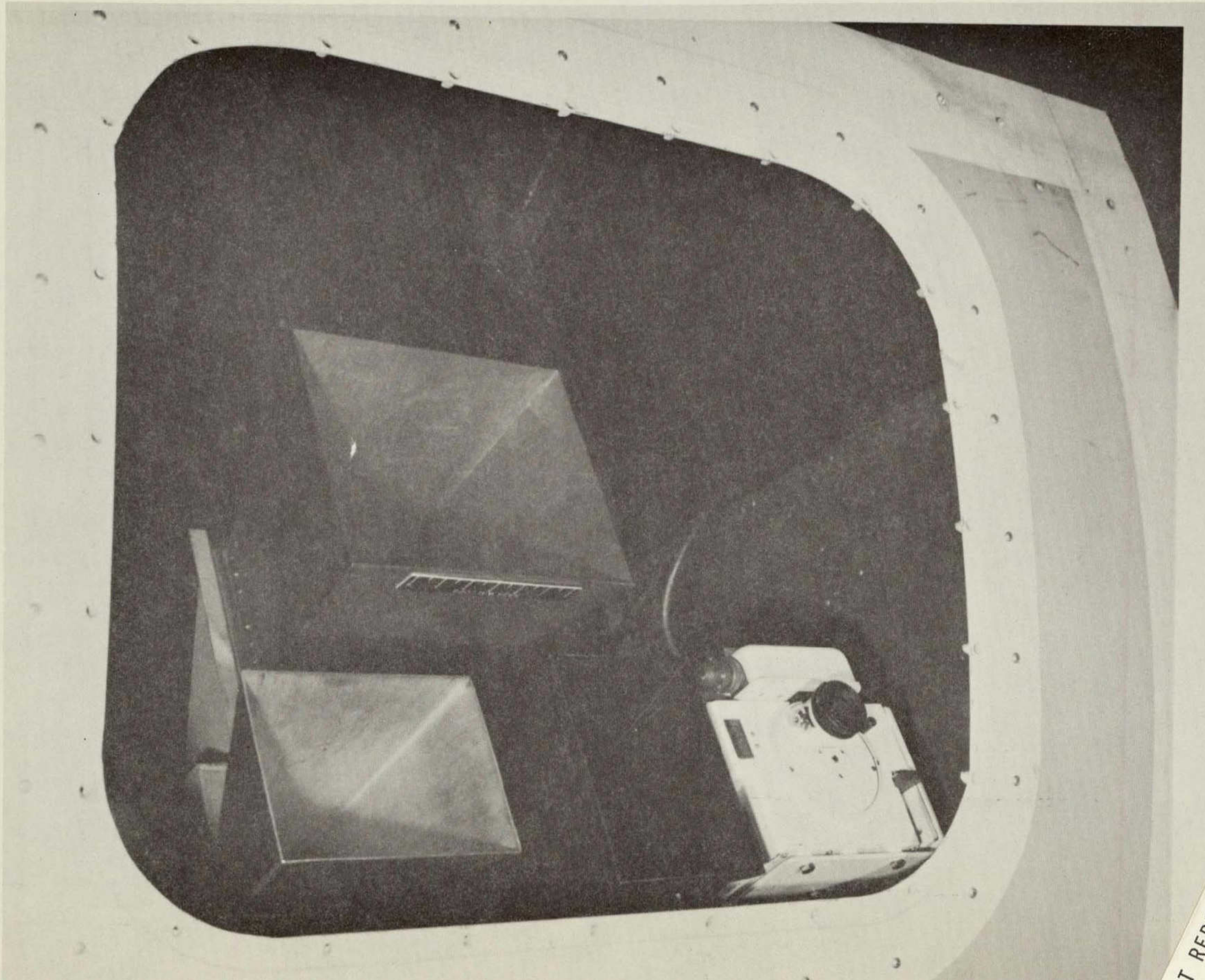

Figure 2-3. Antenna Assembly

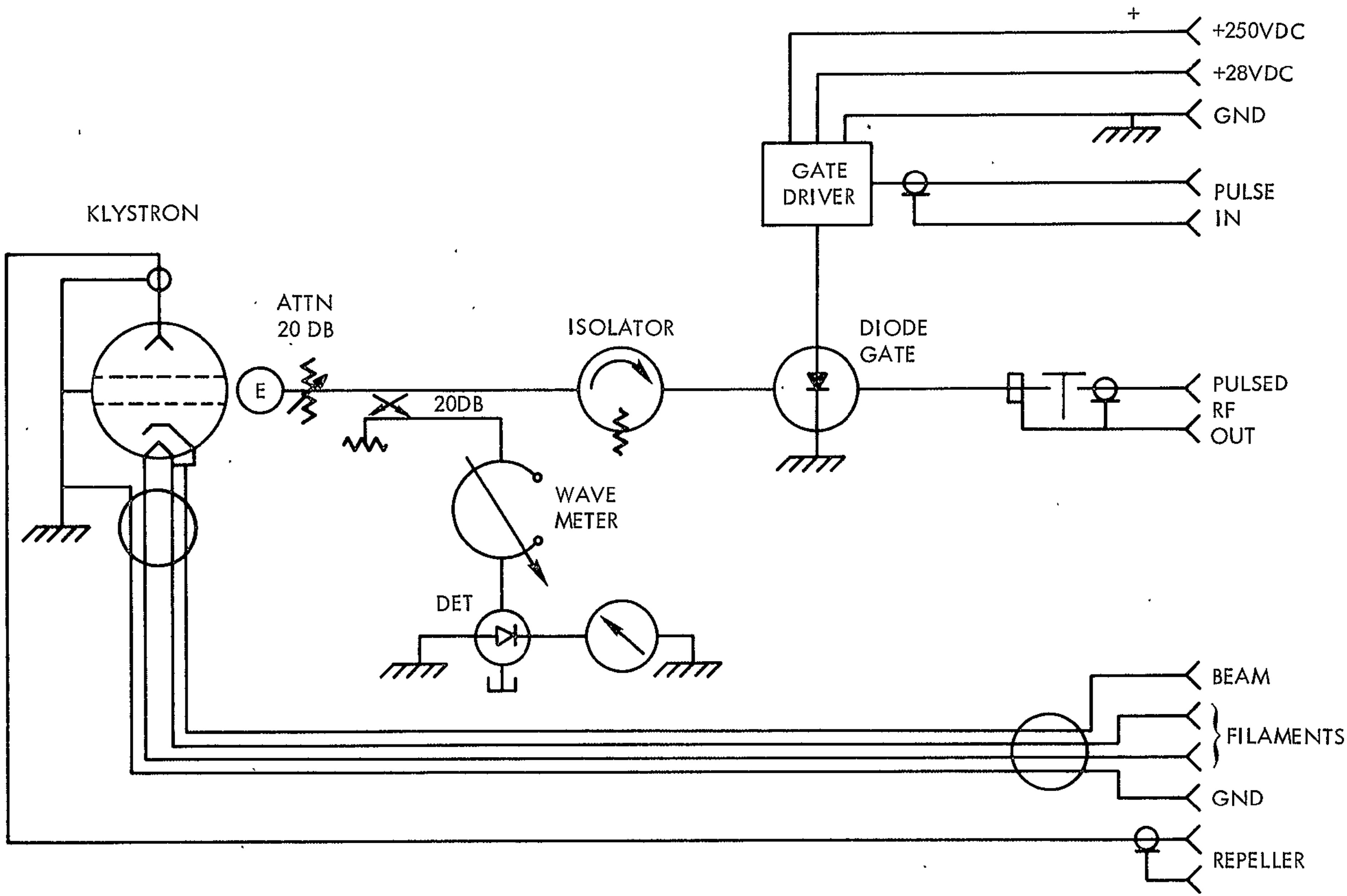

Figure 2-4. Transmitter Chassis RF Source and Modulator

bandwidth or fast rise time pulses. It also permits variable pulsewidths and pulse repetition rates to be used, thereby giving flexibility to the experiment.

The equipment shown in Figure 2-2 consists of various pieces of general purpose lab instruments such as the klystron power supply, pulse generator, TWT amplifier, and variable attenuator. The other units were designed and built by Raytheon. This approach of using as much off-the-shelf equipment was used in order to minimize the design effort and have equipment available on a short schedule. It also has proved to be the most economical approach and provides flexibility in parameter variations.

The local oscillator is a low level klystron (2k25 or equivalent) which is readily powered with standard laboratory voltage power supplies. The same power supply is also used for the receiver local oscillator. The klystron is a very stable oscillator which also can be mechanically adjusted over the entire X-band.

The requirement for fast rise times (5 nsec) and narrow pulses (20 nsec) necessitates the use of a varactor switch which in turn requires an avalanche transistor switch driver. These are shown in Figure 2-5. The rise time is controlled by the switching speed of the avalanche transistor and the varactor diode. These have been tested and shown to produce better than 5 nsec rise times . The pulsewidth is controlled by the length of the delay line used in the circuit of Figure 2-5. The delay lines are various lengths of coaxial cables (1.5 nsec delay/ft).

The switch driver is triggered by a standard pulse generator such as those manufactured by Hewlett Packard or Data Pulse. This will permit selection of pulse repetition rates up to 5 KHz and as low as one pulse (by manual trigger). The pulse generator is also used to provide the synch signals for the oscilloscope and to provide the triggers for the camera controls

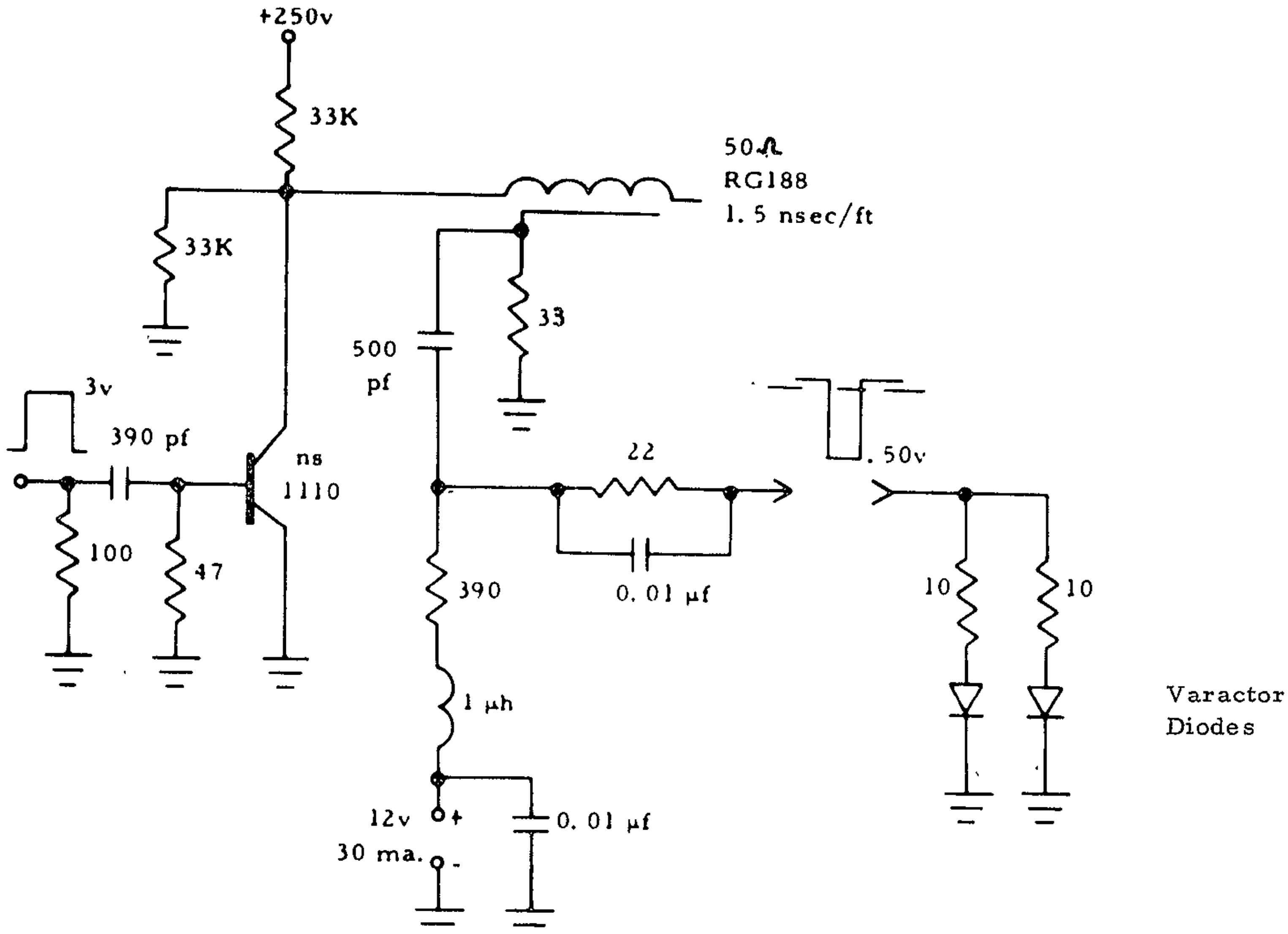

Figure 2-5. Switch Driver

The pulses are amplified in a TWT amplifier which has the necessary bandwidth to preserve the pulse shape. The amplifier can provide a minimum of 10 w peak CW power.

A variable attenuator (0 to 30 dB) on the output of the transmitter permits the use of the system at low altitudes without imposing a requirement for large dynamic range on the receiver.

2.4 Antenna and Microwave Assembly

The transmitted and received signals are fed to the antennas through waveguide runs in the aircraft. Waveguide is required in order to keep the losses to a minimum.

A mechanical antenna switch connects either of two receiving antennas to the receiver. The two receiving antennas are cross polarized with respect to each other permitting measurements of the direct and cross polarized return energy during flights. The receiving antennas are standard gain horns of 22 dB gain with a 12 degree nominal beamwidth. They have low sidelobe levels (less than 20 dB). Switching between antennas is remotely controlled from the operator's console.

The transmitting antenna has an 8 degree nominal beamwidth. It is mechanically boresighted to the same axis as the receiving antennas. The H-plane of the transmitting antenna is parallel to the line of flight.

The isolation between the transmitting and receiving antennas is required to be in excess of 60 dB in order to avoid transmitter leakage. Tests were run on the antenna prior to aircraft installation (see Figure 2-6) with a simulation of the aircraft skin area in order to assure proper alignment, isolation, and beam characteristics.

2.5 Receiver

The receiver used in this experiment (see Figure 2-7) is a fixed gain superheterodyne type. The RF (9.00 GHz) received by the receiving antenna

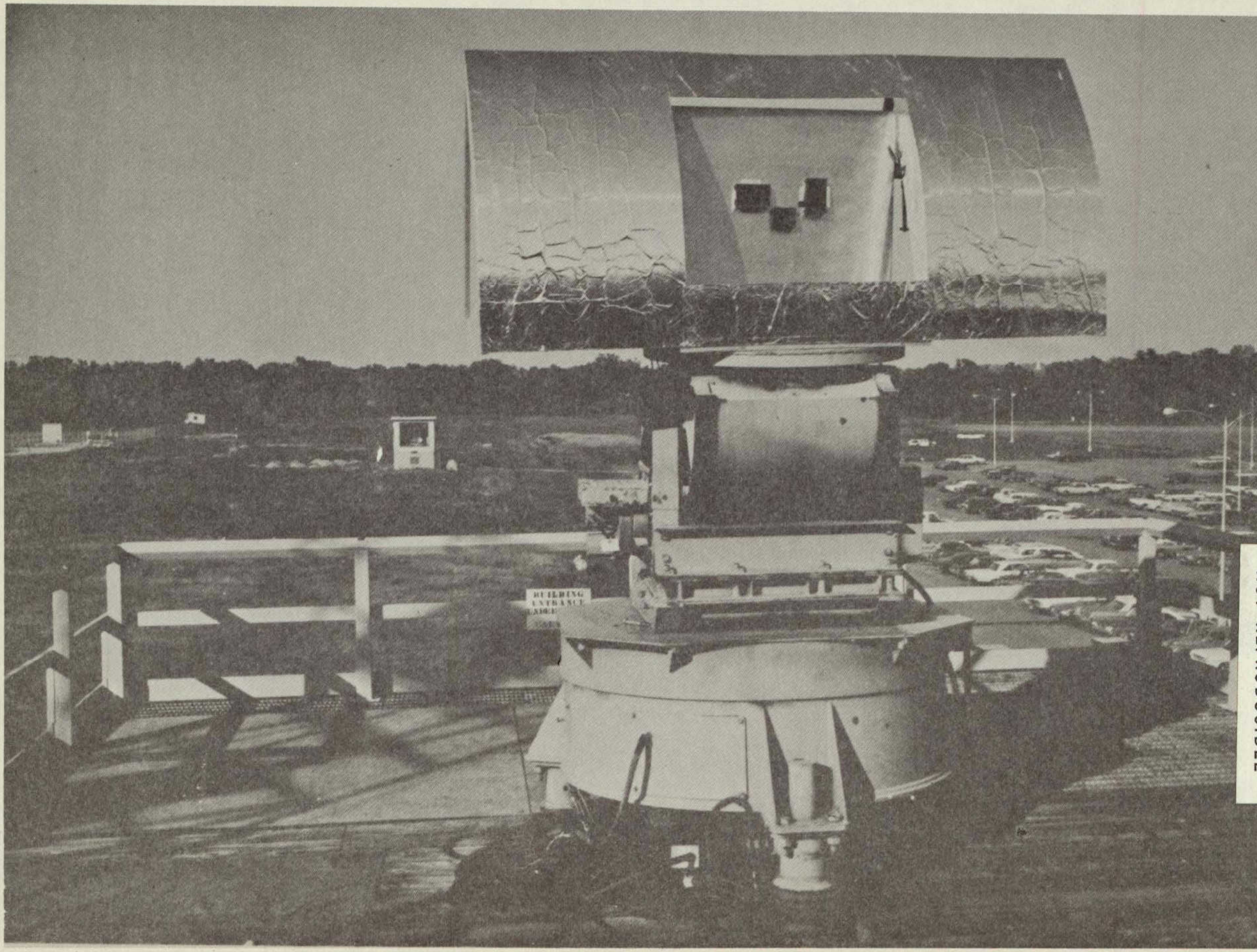

Figure 2-6. Antenna Mockup (Front View)

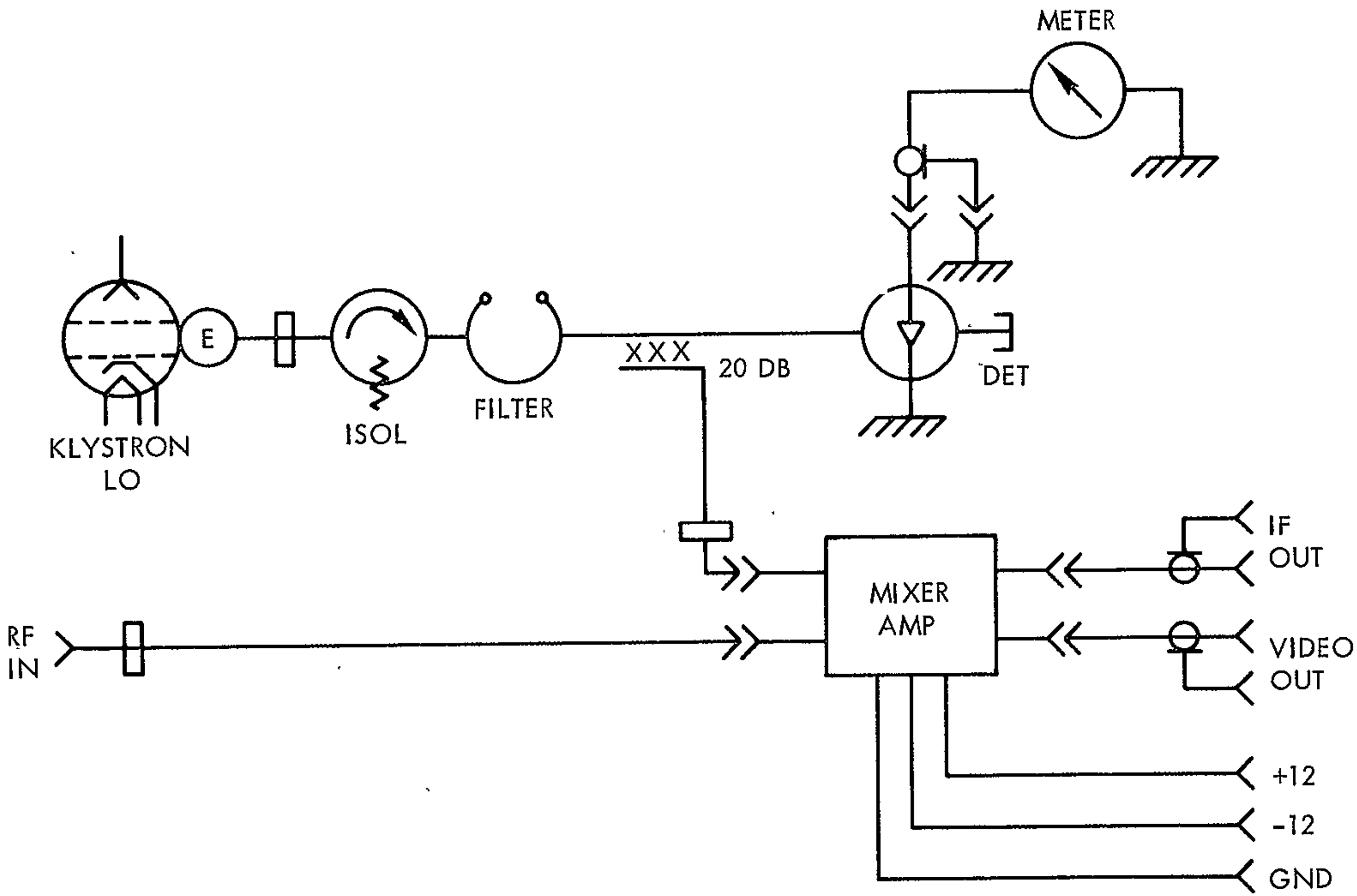

Figure 2-7. 9.00 GHz Receiver

is converted to an intermediate frequency of about 120 MHz in a crystal mixer with no RF preselection. The local oscillator signal needed to perform this mixing action is obtained from a low power klystron oscillator (Varian VA-203B/6975). Both this local oscillator klystron and the klystron used to produce the transmitted signal are powered from the same power supply.

The intermediate signal produced by the mixer is amplified in a wide band IF amplifier (see Figure 2-8).

The IF amplifier provides sufficient gain to produce an output noise signal after video detection of approximately 10 mV. This means that with a noise figure of 10 dB and a video rectification efficiency of 50 percent, the rms noise signal from the IF amplifier will be 20 mV (IF noise power of 8 μW).

The gain (RF input power to IF output power) needed to produce this size signal is therefore

$$A = \frac{N_{IF}}{KTBF} = 10^6 \quad (2\text{-}1)$$

$$\text{Gain A in dB} = 60 \text{ dB.} \quad (2\text{-}2)$$

These gains are necessary in order to produce useful signal levels at the input to the oscilloscope to be used for recording the signals returned from the sea surface. With a S/N of 20 dB, the voltages at the scope input will be 100 mV and, with 20 mV/cm deflection, produce 5 cm of deflection on the scope face. The IF amplifier has a useful dynamic range of greater than 40 dB. The unit requires power supplies of ± 12 volts dc. Both the IF and a video output are available on this unit so that other kinds of detectors could be used if needed (square law, coherent, etc.). The physical size of this mixer IF amplifier is shown in Figure 2-8.

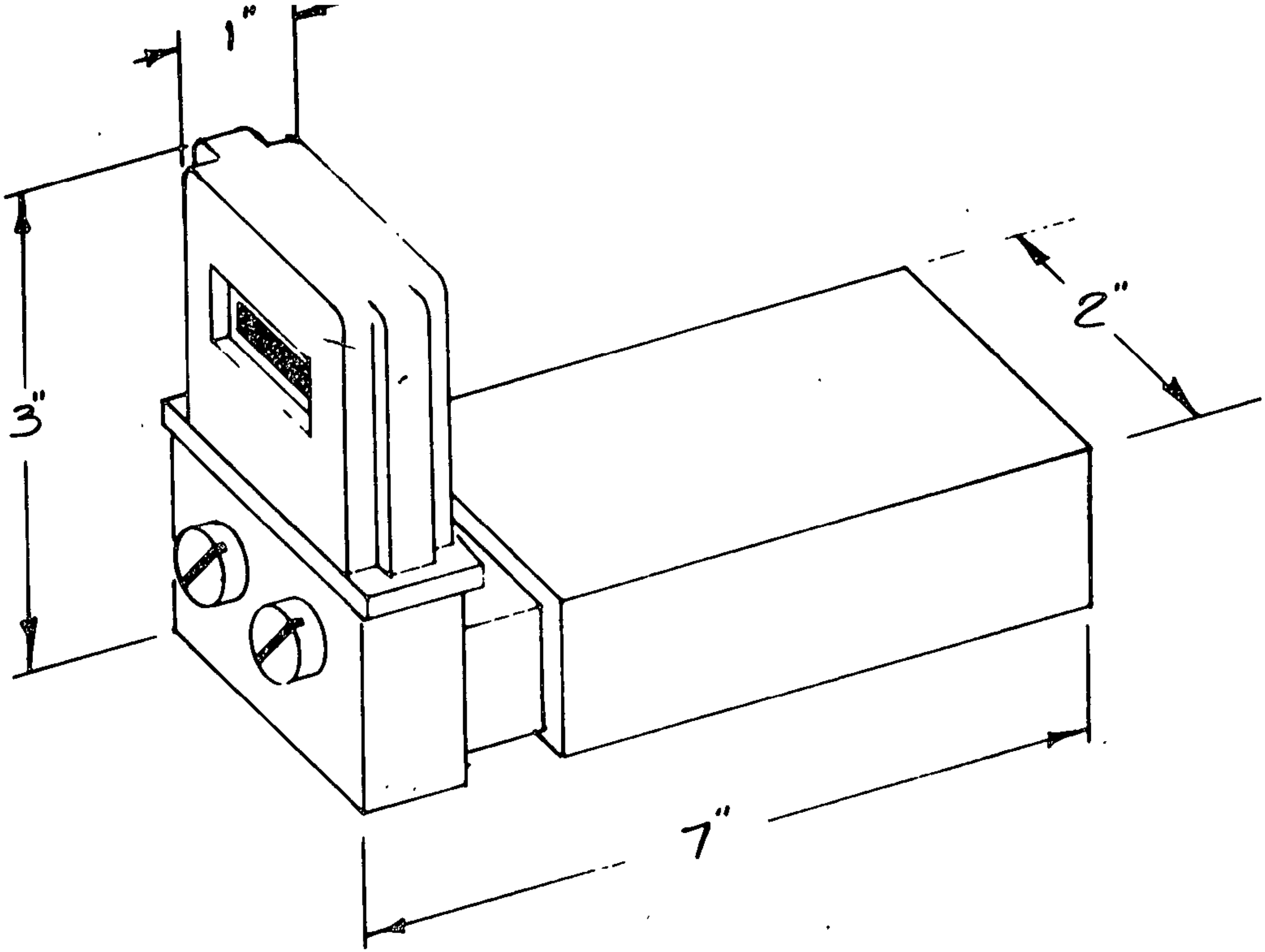

Figure 2-8. Mixer IF Amplifier

A wide-band oscilloscope (Tektronix model 585) is used to indicate the return from the sea. This unit has a frequency response sufficiently wide to obtain pulse rise times of 3 to 4 nsec. A Beattie Coleman camera was utilized to obtain photographic records of the resulting waveforms. Special films (Kodak 2485) were used to permit recording single pulse returns as well as multiple returns.

2.6 Ground Support Equipment

The purpose of the Ground Support Equipment (GSE) (see Figure 2-9) is to permit field maintenance, calibration, and sparing of the radar system. The sparing is accomplished by providing units in the GSE which are identical to the onboard equipment. The receiver and transmitter units in the GSE have already been described in the previous sections.

For purposes of maintenance, a power meter, a VSWR meter, and a Polaroid camera have been included as part of the GSE.

Preflight calibration of the onboard equipment is accomplished by disconnecting the aircraft antennas and attaching the GSE at the coax terminations.

A special purpose for which the GSE was used was that of runway calibration checks. The equipment was used as a transponder by attaching receiving and transmitting antennas.

The equipment is conveniently packaged in a mobile rack unit (see Figure 2-10) for use and for transporting.

2.7 Component Specifications

Specifications for transmitter and receiver are shown in Tables 2-2 and 2-3.

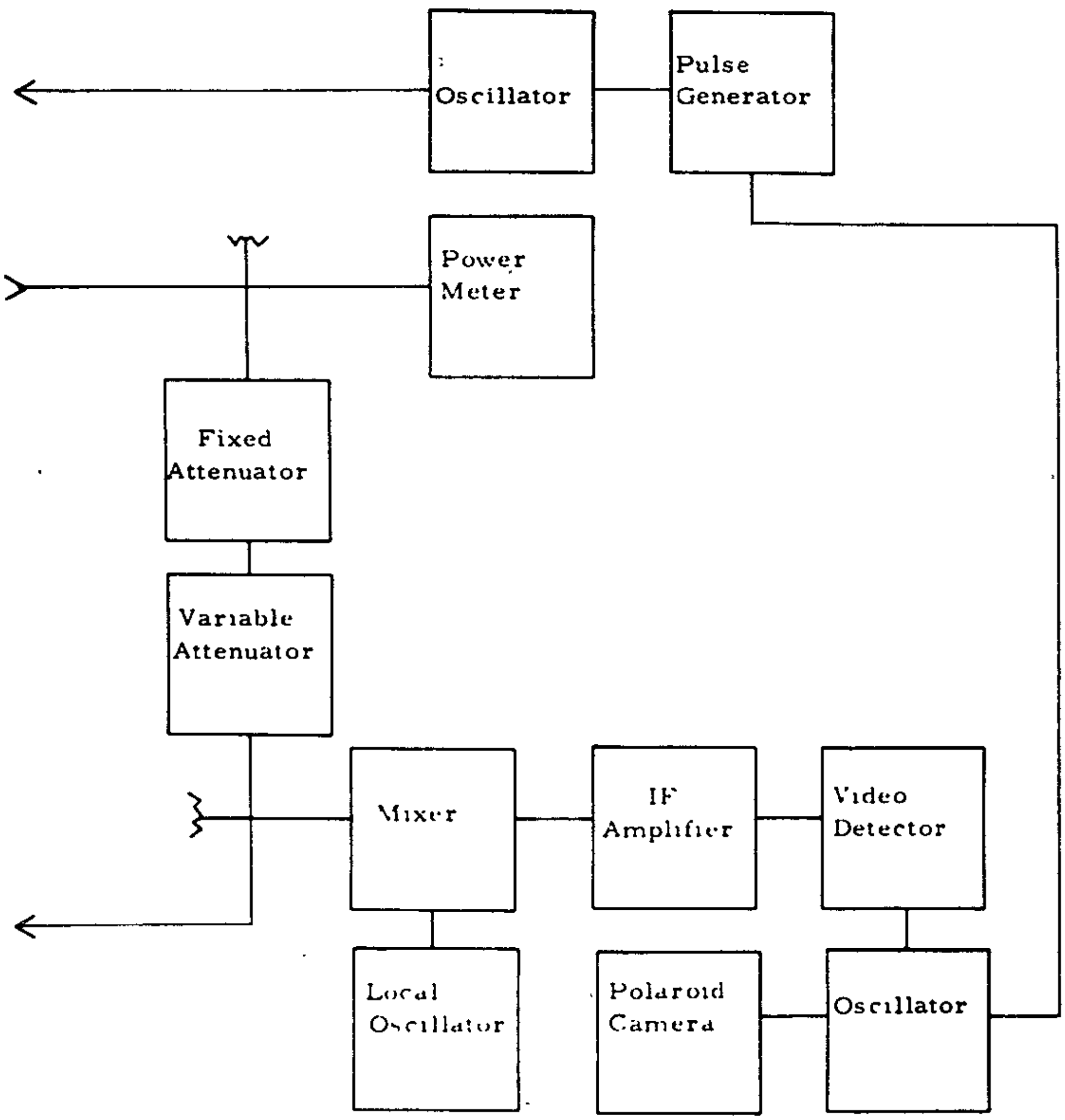

Figure 2-9. Ground Support Equipment Block Diagram

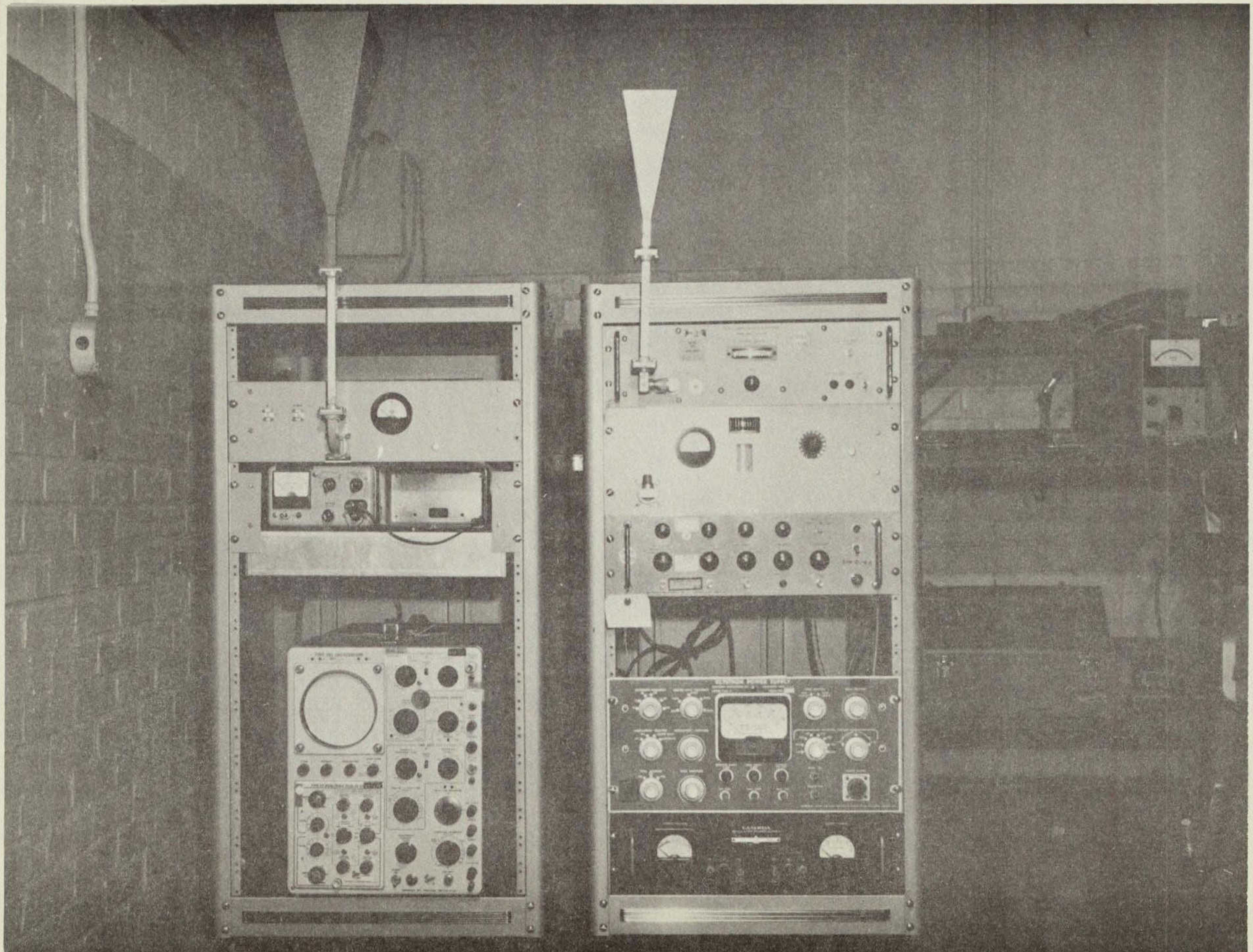

Figure 2-10. Ground Support Equipment In Mobile Rack

Table 2-2. Transmitter Specification

Transmitter LO:	
Low power klystron oscillator	
Power	20 mW
Tunable frequency	8.5 to 9.6 GHz
Output connections -	UG39/U
Convection cooled.	
Diode Switch:	
Bandwidth	8.5 to 9.6 GHz
Connections	Waveguide - UG39/U
Switching Time	5 nanosec
Incident power	50 mW cw
Max I_{ms} Loss	1.0 dB
Isolation	> 25 dB
TWT Amplifier:	
Gain	$\geq$ 30 dB
Bandwidth	8.5 to 9.6 GHz
NF	30 dB
Max power out at gain of 30 dB $\geq$ 10 watts	
Integral Power Supplies rack mounted.	

Table 2-3. Receiver Specification

Mixer IF Amplifier:

RF input	9.0 GHz
RF input conn.	Waveguide (UG39/U flange)
IF frequency	120 MHz
Bandwidth	200 MHz
Noise Figure	~10 dB
IF output	Z_o = 50 ohm
RF to IF gain	~56 to 60 dB
Video Output Required	
video det. efficiency ≥ 50%	
video bandwidth	~ 100 MHz
	into reasonable resistive load 50 ohm → 1 kohm
1 dB IF compression pt	0 dBm

Oscilloscope Requirement:

1. Delayed sweep greater than 5 μsec delay time delay jitter < 0.5 nanoseconds
2. Rise time < 5 nanoseconds
3. Vertical sensitivity adjust. min. of 10 mV/cm
4. Sweep speeds up to 5 nanoseconds/cm.

Camera (Oscilloscope):

1. Solenoid activated shutter
2. f/16 lens or better, shutter speed 1/50
3. Capable of using at least 100 ft of 35 mm film
4. Data storage on film
5. Simple to load.

2.8 Output Data

The outputs of the system are pulses photographed from the face of an oscilloscope. A single pulse display or an integrated pulse display can be provided and photographed. The transmitted and received pulses can be both displayed on an expanded time scale and photographed.

The oscilloscope photographs also contain a counter reading and clock which aid in the data reduction.

2.9 Ground Camera

Photographs of the ocean were taken at the same time that radar pictures were taken via the oscilloscope. These photos permitted a check on the sea conditions and more importantly helped to explain any anomalies in the data, such as returns from ships and clouds.

The ground camera (Flight Research Model IV) is a 35 mm roll-film camera. The camera shutter is controlled by the circuits that control the oscilloscope camera at the operator's console. Data synchronization is obtained through use of a counter and clock which are photographed on the film.

2.10 Ocean Wave Measurements

The main requirement of auxiliary data was to obtain some quantitative measure of the ocean characteristics to be compared with the radar data. Ocean wave heights, directions, and wavelengths were the quantities of interest.

Wind direction and wind speed indicators were furnished by the NASA ship stationed in the test areas. Experienced personnel aboard the ship also provided some "eyeball" estimates of wave height and period.

Photographic techniques were used to provide an optical Fourier transform of the photographed ocean and thereby provide the directional energy spectra of the ocean. This technique was developed by D. Stilwell of NRL and is referred in this report as the "Stilwell" or "Ocean Spectra" process. A side looking camera (see Figure 1-4 and 1-5) provided high resolution photographs for use in this technique. The camera uses nine inch film of low graininess. It is mounted to look out the side of the aircraft at an angle of approximately 45 degrees from the vertical. Photographs were taken while climbing to the operating altitude and at the end of the run when descending. Sets of photographs were taken at angles of 0, 90, 180, and 270 degrees with respect to sea direction.

2.11 Aircraft Data

Roll and pitch data was continuously recorded on a strip chart-recorder. Aircraft altitude, cabin temperature, outside temperature and weather were monitored and recorded by the operators.

SECTION 3. FLIGHT OPERATIONS

3.1 Source of Data

The data collected on these flights came from many sources. This section lists the sources and the data supplied by each.

3.1.1 Raytheon

A) Radar Data

1. Transmitted power
2. Antenna beamwidth, gain, and polarization
3. Transmitted frequency
4. Pulse width
5. System losses
6. Number of pulses per frame

B) Oscilloscope Data

1. Oscilloscope settings

3.1.2 NASA Aircraft Data

1. A/C Altitude
2. A/C Heading
3. A/C Speed
4. A/C Location

3.1.3 Strip Chart Data

1. A/C Roll Angle
2. A/C Pitch Angle
3. Oscilloscope Camera Synchronization
4. Time of Day

3.1.4 NASA Range Recoverer Ship

A) Ocean Truth Data

1. Wave direction
2. Wave height
3. Wave period
4. Wind velocity (speed and direction)
5. Air and Sea temperature
6. Air Pressure

3.1.5 Oscilloscope Film

1. Received power
2. Pulse shape

3.1.6 Ocean Film (Flight Research Camera)

1. Ocean photograph for each oscilloscope photograph

3.1.7 Dr. Stilwell - Ocean Specta Film (K-17 Camera)

1. Ocean spectra data

3.1.8 ONR - Laser Profilometer

1. Ocean spectra data

3.2 Summary of Flights

The value of the flights is determined primarily from the availability of useful data. Table 3-1 is a summary of the radar and environmental parameters that were recorded for each flight. In the following paragraphs each flight is briefly summarized. Included also are various observations that were made during the flights.

3.2.1 Flight 1 - Nov-24-1969

This flight, the first of three shakedown flights, was flown over coastal waters near Wallops. From a height of 6000 feet, 8 Stilwell photographs were taken and 4 radar runs were made using Flight Pattern 3, (Figure 3-3) the rectangular pattern. However, it was observed that sea direction is difficult to obtain accurately at this altitude, and that morevoer any estimate is likely to be off by 180°. The strip-chart was not recording for the entire flight and the ground camera worked only for a short while. Also, according to the NASA FPS-16 radar, the C-54 altimeter (SCR-718) could be off by 400-600 feet at 6000 ft. This flight lasted two hours.

Table 3-1. Summary of the Radar and Environmental Parameters

RADAR PARAMETERS	FLIGHT 1 11/29/69	FLIGHT 2 12/11/69		FLIGHT 3 12/12/69	
Pulse Width	.100 μs			.100 μs	
Polarization	cross			direct	
Pulse/Frame	50			50	
Frame Rate	1/sec			1/sec	
Pulse Repetition Freq.	2500	NO DATA		2500	
Peak Power	12 watts			12 watts	
Attenuation				16 dB	
Sweep Speed				.1 μs/cm	
Amplitude Set.				.01 v/cm	
Time Delay				2.0 μs	41.5 μs
ENVIRONMENTAL PARAMETERS					
Sky Condition	Clear	Clear		Partly Cloudy	
Cabin Temp.	75°F	75°F		75°F	
Water Temp.					
Wind Direction					
Wind Speed					
Sea Direction	146° or 326°	150° or 330°			
Altitude	6000 Ft.			1000 Ft	20,000 Ft
A/C Velocity				150 Knots	145
No. of Runs	4			2	6
Location	Off Shore	Off Shore		37°50' x 75° 20'	
Air Surface Temp.					
Wave Heights					
Wave Period					
STILWELL PARAMETERS					
No. of Runs	4	8	4	8	4
Altitude	6000 Ft	1000	18,000	1000	80,000
Camera Parameters		f11	f11	$\frac{1}{200}$ @f16	$\frac{1}{200}$ @f22

Table 3-1. Summary of the Radar and Environmental Parameters (Cont.)

RADAR PARAMETERS	FLIGHT 4 12/15/69			FLIGHT 5 12/17/69		FLIGHT 6 12/18/69					FLIGHT 7 1/6/70	FLIGHT 8 1/8/70				FLIGHT 9 1/9/70
Pulse Width	.100 µs	.100 µs	.020 µs	.020 µs →		.100 µs →					.020 µs	.020 µs →				NO DATA TWT FAILURE
Polarization	direct →			direct →		cross	direct	cross	direct	direct	direct	direct				
Pulse/Frame	1	50	50	50 →		1	50	50	50	1	50, 47 278, 500	1	2	50	278	
Frame Rate	NA	1/sec	1/sec	1/sec →		NA	1/sec	1/sec	1/sec	NA	NA	NA →				
P. R. F.	NA	2500	2500	2500		NA	2500	2500	2500	NA	VAR.	NA	NA	2500	13900	
Peak Power	12 watts →			12 watts →		12 watts →					12 watts	12 watts →				
Attenuation	10 dB →			0 dB →							0 dB	0 dB →				
Sweep Speed	.050 µs/cm			.05 µs/cm →		.05 µs/cm →				.500	.050 µs/cm	.05 µs/cm →				
Amplitude Set.	.050 v/cm 1-4 .200 v/cm 21-25	.050 v/cm	.020 v/cm	.5 v/cm	.1 v/cm	.200 v/cm	.100	.010	.050?	2.9 µs	.100 v/cm	.1 v/cm	.1	.05	.05	
Time Delay	3.1 µs	10 µs	10 µs	2.8 µs	20 µs	3.2 µs	36.0 µs	36.0 µs	54.0 µs?			20 µs →				
ENVIRONMENTAL PARAMETERS																
Sky Condition	Partly Cloudy →			Partly Cloudy →		Partly Cloudy →					Cloudy	Cloudy →				Cloudy
Cabin Temp.	75°F →			75°F →		75°F →					75°F	70°F →				70°F
Water Temp.	NA →			NA		NA					58°F	53°F →				61°F
Wind Direction	293° →			320° →		330° →					310°	350° →				290°
Wind Speed	26 knots →			16 knots →		8-16 knots →					3 knots	19 knots →				30 knots
Sea Direction	290° →			320° →		330° →					320°	340° →				290°
Altitude	1500 ft	5000 ft	5000 ft	1500 ft	10,000 ft	1500 ft	15,000 ft	15,000 ft	20,000 ft	1500	15,000 ft	10,000 ft →				
A/C Velocity	165 →			155	165	160	160	160	150	165	198	208 →			186	
No. of Runs	8	12	6	4	6	4	6	6	6	4	6	6	6	6	6	
Location	7°07'x33°38'			37°07'x73°38'		37°07'x73°28'					37°07'x73°38'	37°07' x 73°28'				37°07' x 73°38'
Air Surface Temp.	46.4°F →			4.5°C →		6.2°C →					9.6°C					-2.3°C
Wave Heights	8 ft →			4-6 ft →		3-5 ft →					3 ft	12 ft →				7 ft
Wave Period	8 sec →			7 sec →		NA					5 sec	8 sec →				NA
STILWELL PARAMETERS																
No. of Runs	8			8		8					NONE	4				4
Altitude	1500			1500		1500						1000				1000 @ f16
Camera Parameters	$\frac{1}{200}$ @ f11 Focal Length			$\frac{1}{200}$ at f11		$\frac{1}{200}$ @ f11 Laser Data Available						$\frac{1}{200}$ @ f16				$\frac{1}{200}$ and f11

Laser Data Available   Laser Data Available

Table 3-1. Summary of the Radar and Environmental Parameters (Cont.)

RADAR PARAMETERS	FLIGHT 10 1/20/70					FLIGHT 11 1/21/70	FLIGHT 12 1/22/70					
Pulse Width	.010 µs	→	→	→	→	NO DATA (ICE COVER)	.020 µs	→	→	→	→	→
Polarization	direct	→	→	→	→		direct	→	→	→	→	→
Pulse/Frame	1	2	10	50	148		1	2	10	50	148	278
Frame Rate	NA	NA	NA	1	1/2		NA	NA	NA	1	1/2	1/2
PRF	NA	NA	500	2500	5400		NA	NA	500	2500	5400	13900
Peak Power	3 watts	→	→	→	→		3 watts	→	→	→	→	→
Attenuation	20 dB	→	→	→	→		0 dB	→	→	→	→	→
Sweep Speed	.100 µs/cm	→	.05	→	→		.050 µs/cm	→	→	→	→	→
Amplitude Set.	.010/cm	→	→	→	→		.05 v/cm	→	→	.02	→	→
Time Delay	10 µs	→	→	→	→		21 µs					
ENVIRONMENTAL PARAMETERS												
Sky Condition	Cloudy	→	→	→	→		Clear	→	→	→	→	→
Cabin Temp.	70°F	→	→	→	→		70°F	→	→	→	→	→
Water Temp.	32°F	→	→	→	→		NA	→	→	→	→	→
Wind Direction	080°	→	→	→	→		330°	→	→	→	→	→
Wind Speed	3 knots	→	→	→	→		15 knot	→	→	→	→	→
Sea Direction	None	→	→	→	→		265°	→	→	→	→	→
Altitude	5000 ft	→	→	→	→		10,000 ft	→	→	→	→	→
A/C Velocity	160 knots	→	→	→	→		164 knots	→	→	→	→	→
# of Runs	4	4	4	4	4		4	4	4	4	4	4
Location	Tangier Sound					Tangier	Long Island Sound					
Air Surface Temp.	27°F	→	→	→	→		NA					
Wave Heights	Calm	→	→	→	→		2 ft					
Wave Period	Calm	→	→	→	→		NA					
STILWELL PARAMETERS												
# of Runs	4	4					NA	NA		NONE		
Altitude	1500 ft	5000 ft					NA	NA				
Camera Parameters	$\frac{1}{200}$ @ f8	$\frac{1}{200}$ @ f8					NA	NA				

Table 3-1. Summary of the Radar and Environmental Parameters (Cont.)

RADAR PARAMETERS	FLIGHT 13 1/26/70					
Pulse Width	.020µs	→				
Polarization	direct	→				cross
Pulse/Frame	1	10	50	148	278	50
Frame Rate	NA	NA	1	1/2	1/2	1
PRF	NA	500	4500	5400	13900	2500
Peak Power	3 watts	→				
Attenuation	odB	→				
Sweep Speed	.05µs/cm	→				
Amplitude Set	.02v/cm	→				.01v/cm
Time Delay	21µs	→				
Environmental Parameters						
Sky Condition	Cloudy	→				
Cabin Temp	75°F	→				
Water Temp	58°F	→				
Wind Direction	220°	→				
Wind Speed	26 kts	→				
Sea Direction	220°	→				
Altitude	10,000 ft	→				
A/C Velocity	159 kts	→				
No. of Runs	4	4	4	4	4	4
Location	37°07' N x 73°38'1w					
Air Surface Temp.	55°F	→				
Wave Height	9 ft	→				
Wave Period	8 sec	→				
Stilwell Parameters						
No. of Runs	8	4				
Altitude	1500 ft	1500 ft				
Camera Parameters	1/200 @ f 11	1/200 @ f 16				

RADAR PARAMETERS	FLIGHT 14 1/27/70						
Pulse Width	.02µs	→					.01µs
Polarization	direct	→		cross		dir	dir.
Pulse/Frame	1	10	50	148	50	50	50
Frame Rate	NA	NA	1	1/2	1	1	1
PRF	NA	500	2500	5400	4500	2500	2500
Peak Power	12 watts	→					
Attenuation	odB –	→					
Sweep Speed	.05µs/cm	→					.20
Amplitude Set	.05v/cm	.02	.02	.05	.01	.05	.05
Time Delay	.	.02	.02	.05	.01	.05	.05
Environmental Parameters		Roll Angle 3°					
Sky Condition	Partly Cloudy	→					Clear
Cabin Temp	70°F	→					70°
Water Temp	55°F	→					
Wind Direction	360°	→					
Wind Speed	12 kts	→					
Sea Direction	350°	→					
Altitude	10,000 ft	→					2460 ft
A/C Velocity	177 kts	→					300
No. of Runs	4	4	4	4	4	4	Frames
Location	37°07N x 73°38' w						Ice Land
Air Surface Temp.	43°F	→					
Wave Height	5 ft	→					
Wave Period	5 sec	→					
Stilwell Parameters							
No. of Runs	4	4	4				
Altitude	1500 ft	10,000 ft	1500 ft				
Camera Parameters	1/200 @ f 16	1/200 @ f 22	1/200 @ f 22				

RADAR PARAMETERS	FLIGHT 15 1/28/70					
Pulse Width	.020µs	→				
Polarization	direct	→				
Pulse/Frame	1	10	50	148	278	50
Frame Rate	NA	NA	1	1/2	1/2	1
PRF	NA	500	2500	5400	13700	2500
Peak Power	12 watts	→				
Attenuation	odB	→				
Sweep Speed	.05µs/cm	→				
Amplitude Set	.10v/cm				.05	.05
Time Delay						
Environmental Parameters						5°
Sky Condition	Clear	→				
Cabin Temp	75°F	→				
Water Temp	55°F	→				
Wind Direction	10°	→				
Wind Speed	6 kts	→				
Sea Direction	10°	→				
Altitude	10,000 ft	→				
A/C Velocity	185 kts	→				
No. of Runs	4	4	4	4	4	4
Location	37°07' N x 73°38' w					
Air Surface Temp.	51°F	→				
Wave Height	3 ft	→				
Wave Period	4 sec	→				
Stilwell Parameters						
No. of Runs	4	4	4			
Altitude	1500 ft	10,000ft	1500 ft			
Camera Parameters	1/200 @f22	1/200 @ f22	1/200 @ f16			

RADAR PARAMETERS	FLIGHT 16 1/29/70					
Pulse Width	.020µs	→				
Polarization	direct	→				
Pulse/Frame	1	10	50	148	50	148
Frame Rate	NA	NA	1	1/2	1	1/2
PRF	NA	500	2500	5400	2600	5400
Peak Power	12 watts	→				
Attenuation	odB	→				
Sweep Speed	.05µs/cm	→				
Amplitude Set	.02v/cm	→			.05	.05
Time Delay	21.5µs	→				
Environmental Parameters					Color Film	
Sky Condition	Clear	→				
Cabin Temp	75°F	→				
Water Temp	55°F	→				
Wind Direction	210°	→				
Wind Speed	22 kts	→				
Sea Direction	210°	→				
Altitude	10,000 ft	→				
A/C Velocity	177 kts	→				
No. of Runs	4	4	4	4	4	4
Location	37°07' N x 73°38' w					
Air Surface Temp.	60°F	→				
Wave Height	7 ft	→				
Wave Period	7 sec	→				
Stilwell Parameters						
No. of Runs	8					
Altitude	1500 ft					
Camera Parameters	1/200 @ f22					

3.2.2 Flight 2 - Dec-11-1969

This flight, the second shakedown flight, was flown over approximately the same area as the first flight. Upon arriving at the test area a Stilwell pattern was flown at 1000 feet without regard to sea direction. The C-54 then climbed to 18,000 feet for the radar runs. The climb took about 45 minutes, which was considerly shorter than had been predicted. Since the C-54 was above 10,000 feet, oxygen was required by the crew for the first time. The radar return signal was strong, but at approximately 17,000 feet the oscilloscope developed synchronization problems and a trace could not be obtained. All radar runs, therefore, had to be aborted. A Stilwell pattern was flow at 18,000 feet and then again at 1000 feet. The purpose of the second Stilwell pattern at 1000 feet was to observe what effect condensation on the lens had on lens resolution.

3.2.3 Flight 3 - Dec-13-1969

This was the last shakedown flight. Since there was no usable data from flight 2, a similar flight plan was used except that only the 100 nanosecond pulse width was attempted (It was extremely difficult to change pulse widths while using oxygen). The radome was removed for this and subsequent flights in order to improve the return signal level. Stilwell patterns were flown in the following order: 1000 ft., 20,000 ft., 1000 ft. Some radar data was taken at 1000 feet and a full Radar Pattern 2 was flown at 20,000 feet. It was difficult to see any return signal using cross polarization, so direct was used during the entire flight. The sea direction could not be determined, so that arbitiary headings were flown during the data runs.

3.2.4 Flight 4 - Dec-15-69

This was the first data flight. It was flown over the Atlantic Ocean about 120 miles east of Norfolk at 37° 07' N, 73° 38' W (hereafter known as GEOS test area) with ocean truth data being furnished for the first time by the

NASA Range Recoverer ship. ONR personnel were to fly with us in their Cessna with the laser profilometer but they had to cancel due to aircraft problems. However, it had been decided previously to fly at a low altitude, 5000 feet, so as to make coordination between the two aircraft easier. A low cloud ceiling forced the cancellation of the 5000 foot Stilwell pattern. Two Stilwell patterns were flown at 1500 feet, one before the radar runs and the other after. At 5000 feet Radar Pattern 1 (Figure 3-1) (12 runs) and Pattern 2 (Figure 3-2) (6 runs) were flown. Some single pulse per frame data was taken during the Stilwell patterns. The results confirmed that individual pulses are visible on the film. 10 dB of attenuation was deliberately put in the receiver so that the return signal would not be saturated. The roll and pitch gyros were operating and the strip-chart was calibrated and operating. The counter of the ground (Flight Research Camera) camera jammed although the camera itself operated.

3.2.5 Flight 5 - Dec-17-1970

This flight was flown at 10,000 feet in the GEOS test area. Due to low cloud cover Stilwell Patterns were only flown at 1500 feet. ONR personnel flew their Cessna and took laser profilometer data. The Range Recoverer was on station and relayed ocean truth data to the C-54. An attempt was made to change the pulse width but during the change a connector pin was bent, making further data runs impossible. Therefore, only one Radar Flight Pattern 2 (Figure 3-2) was flown at 10,000 feet.

3.2.6 Flight 6 - Dec-18-1970

ONR personnel accompanied the C-54 again with their laser profilometer. The low cloud cover over the GEOS test area again forced cancellation of the high altitude Stilwell pattern. Radar Flight Pattern 2 was flown twice at 15,000 feet and once at 20,000 feet. There did not seem to be any noticeable return

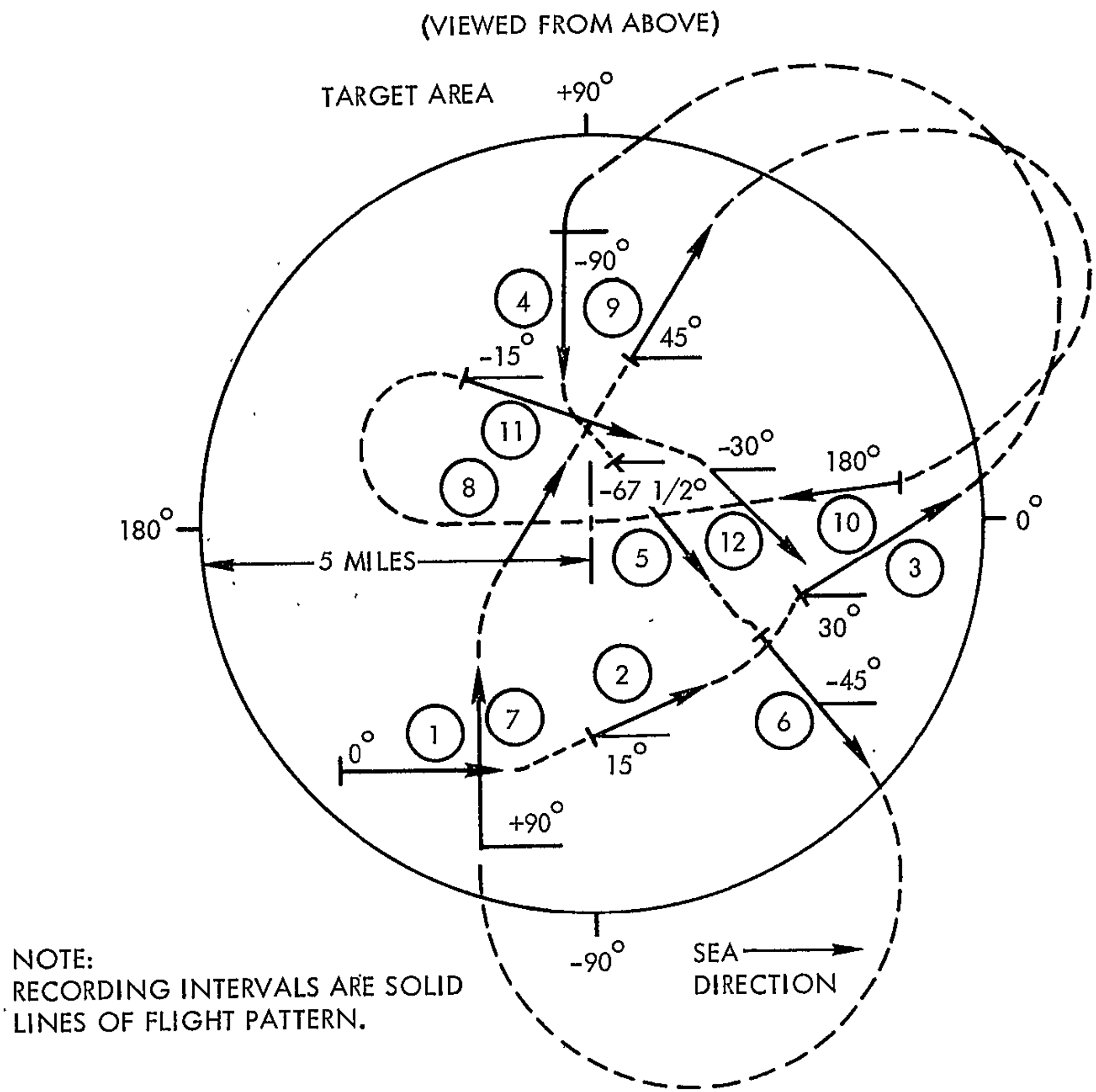

Figure 3-1. Flight Pattern 1

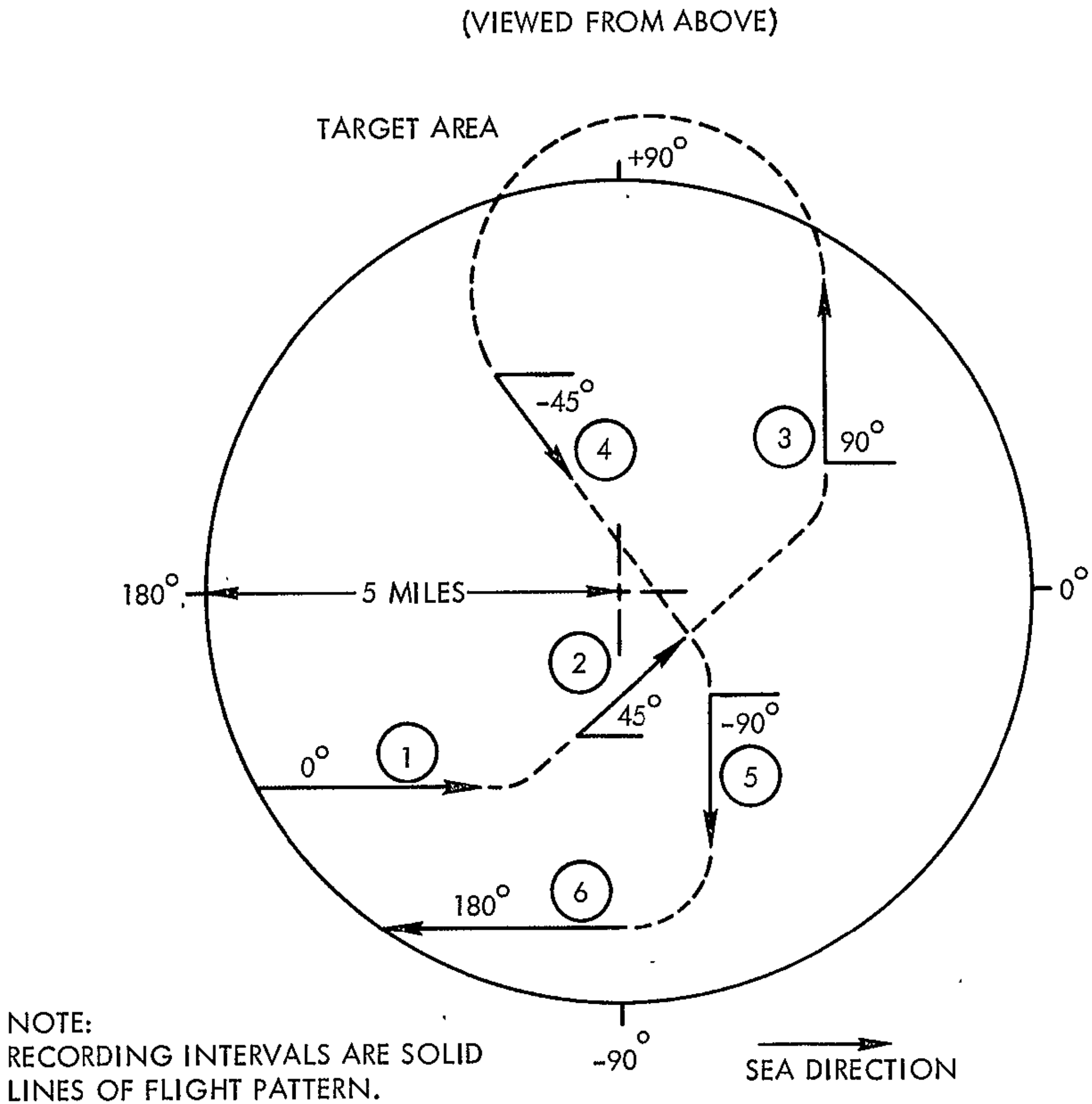

Figure 3-2. Flight Pattern 2

during any of the cross polarization runs, but there was a strong return signal when direct polarization was used. The transmitted frequency was measured to be 9.00 GHz.

3.2.7 Flight 7 - Jan-6-1970

The Range Recoverer was on station in the GEOS test area, providing the only source of ocean truth data for this flight. There was a Navy block to all aircraft in the area from 0 to 5000 feet with a cloud cover somewhat below 5000 feet. All Stilwell patterns were therefore cancelled. Also, because of the cloud condition, the ground camera was not used. Pattern 2 was flown once at 15,000 feet with the pulses per frame varied during each run. Although usable data was obtained, the procedure of varying pulses per frame during each run was time consuming causing each run to cover a large area of ocean. Therefore, on following flights pulses per frame were kept constant during each run and only changed between runs.

Upon returning to Wallops a system calibration check was attempted by flying over the GSE on the runway. The GSE picked up the aircraft signal for a very short time while the GSE signal was not received in the aircraft.

3.2.8 Flight 8 - Jan-8-1970

Before flying to the test area, another attempt was made at a system calibration check using the GSE. Four passes over the runway at 5000 feet gave very marginal returns but did permit a verification of the system calibration. Because of the low ceiling and the trouble receiving the signal from the GSE, the 10,000 foot passes were cancelled. The calibration runs scheduled upon return from the test area were cancelled due to stormy weather. After arriving at the GEOS test area (37° 07' N, 73° 38'W), it was learned that the Range Recoverer went in toward the shore during the night because of stormy seas. The ship was at that time 80 miles west of the test area, at 37°N, 75°W. Since the ship was in coastal waters, it was decided to make the radar runs at the test area rather than over the ship.

The ship's ocean truth and weather reports were used as estimates of the conditions in the test area. Because of the very low overcast and surface fog, only one Stilwell pattern was flown at 1000 feet. Flight Pattern 2 was flown 4 times at 10,000 feet with the pulses per frame varied with each pattern.

3.2.9 Flight 9 - Jan-9-1970

Two Stilwell patterns were flown at 1000 ft upon arriving at the test area. The C-54 then climbed to 10,000 feet for the radar runs where it was discovered that the TWT had failed. The transmitted and received signals were lost, and thus the radar runs were cancelled and the C-54 returned to Wallops.

3.2.10 Flight 10 - Jan 10-1970

The 12 watt TWT that failed was replaced with a 3 watt TWT. In order to get calm water conditions, this flight was flown over Tangier Sound in Chesapeake Bay. The Range Recoverer was in the sound and reported a calm surface although the surface appeared from the aircraft to have a small wave pattern. There was a considerable amount of ice along the shore of the Sound, although the center of sound was ice free except for a few small patches. Two Stilwell patterns were flown, one at 1500 feet and one at 5000 feet. Radar Pattern 3 (Figure 3-3) was flown 5 times at 5000 feet.

3.2.11 Flight 11 - Jan-21-1970

This flight was scheduled over Tangier Sound, but during the previous night the Sound became completely frozen over. The Range Recoverer, still in the Sound, was unable to get to any other possible test areas that day. Therefore, the flight was cancelled and the C-54 returned to Wallops.

STILWELL PATTERN AND RADAR PATTERN 3

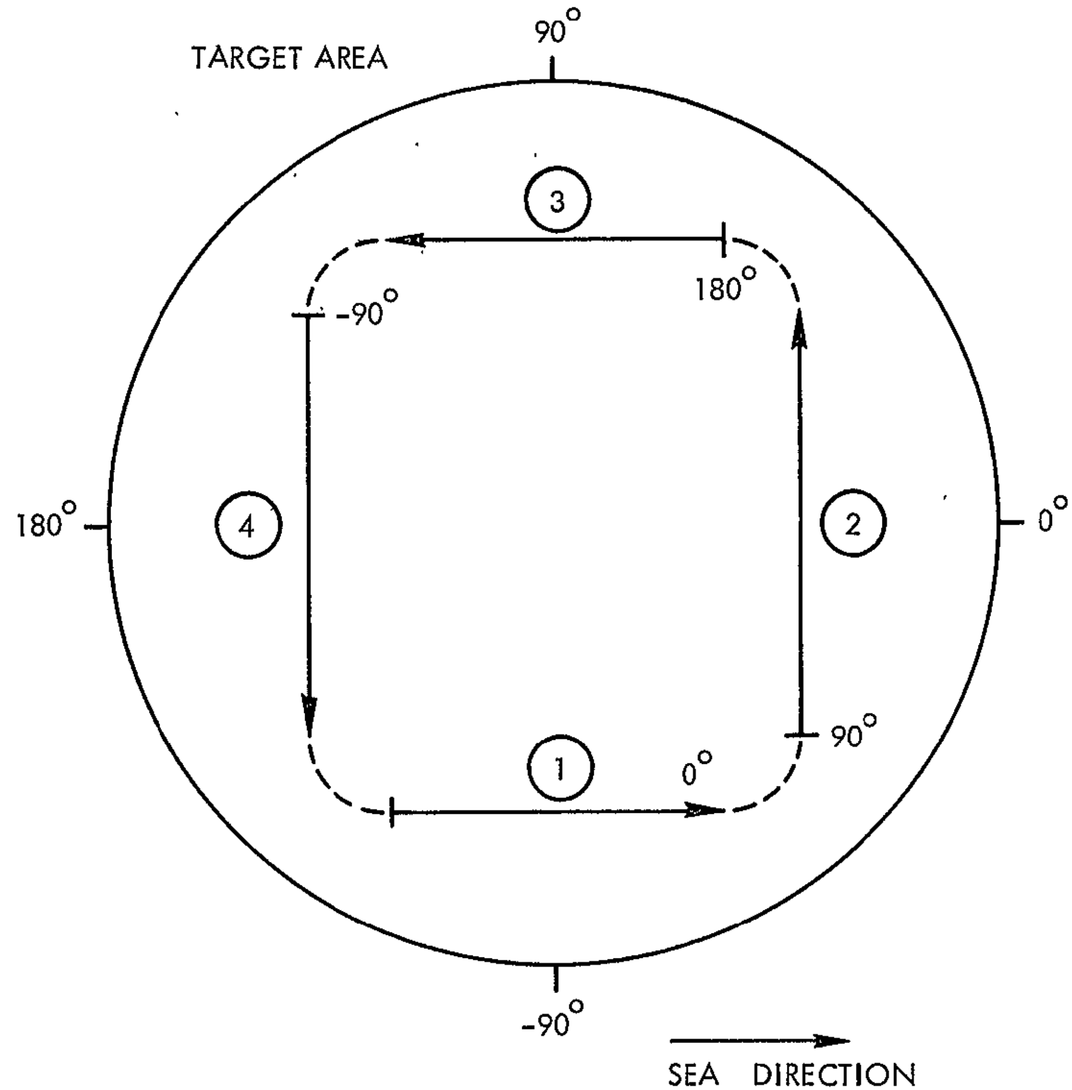

Figure 3-3. Ocean Spectra Flight Pattern

3.2.12 Flight 12 - Jan-22-1970

This flight was scheduled over Long Island Sound in an attempt to get calm water conditions. Sea direction, wave heights, and wind velocity estimates were based on observations from the aircraft and on radio conversations with the Bridgeport, Conn. Air Control Area. There were no Stilwell photos taken on this flight and all the ground film was later accidently double-exposed during flight 13. Radar Pattern 3 was flown six times with a different number of pulses per frame for each pattern. The 3 watt TWT was again used.

3.2.13 Flight 13 - Jan-27-1970

With the Range Recover again on station, the test flights resumed in the GEOS test area, 37° 07" N, 73° 38'W. Three Stilwell Patterns were flown at 1500 feet, and low cloud cover forced the cancellation of the 10,000 foot Stilwell Pattern. As mentioned above, the ground film was accidently double-exposed on the film of flight 12. Radar Pattern 3 was flow six times, five times with direct polarization and once with cross polarization. There was no signal return when the horns were cross polarized.

3.2.14 Flight 14 - Jan-27-1970

The 12 watt TWT was repaired and reinstalled for this and the remainder of the flights. This flight was over the GEOS test area with the Range Recoverer supplying ocean truth data. Three Stilwell Patterns were flown six times each. For one pattern the aircraft was kept at a constant 3° roll angle which caused a slightly reduced return signal. The cross polarized mode was tried again with no success. Before returning to Wallops, the C-54 flew over Tangier Sound and found it to be ice-bound, which precluded any further testing in that area. The ground camera was jammed for the entire flight.

3.2.15 Flight 15 - Jan-28-1970

Radar Pattern 3 was flown six times on this flight over the GEOS test area. One pattern was flown with a constant 5° roll angle, which again caused a slightly reduced return signal. Three Stilwell patterns were flown, two at 1500 feet and one at 10,000 feet.

3.2.16 Flight 16 - Jan-29-1970

This last test flight was flown over the GEOS test area. Three Stilwell patterns were flown, two at 1500 feet, and one at 10,000 feet. Radar Pattern 3 was flown six times. On the last two patterns extended range color film (E. G. G. Type XR), rather than black and white film, was used.

3.3 Typical Data Sheets

The data sheets presented in this section are the actual data sheets for flight 14. The original data sheets for the other flights are similar to the ones presented here. The data was recorded during the flight by the Raytheon controller. He received this data from the Raytheon radar operator, the aircraft pilot and/or co-pilot, the NASA Range Recoverer, and the ocean spectra (K-17) camera operator.

3.3.1 Flight Data Sheet

FLIGHT DATA SHEET (1) OF (1)

FLIGHT # 14	DATE 1/27/70 Take-off 9:45 A.M. Land 1:30 P.M.
LOCATION Wallops 9-D	NAME OF RECORDER J. Bartlett

STATUS OF OTHER ELECTRONIC EQUIPMENT

EQUIPMENT STATUS:

PULSE WIDTH:	(a) (20)	(b) 50	(c) 200	(nanosecs)
POLARIZATION:	(a) direct	(b) cross	(see below)	
PULSES/FRAME:	(see below)			
FRAME RATE:	(a) 1/2	(b) 1	(c) 2	(per sec) varied
BEAM WIDTH:	(a) 8°	(b) 16°		
PEAK POWER:	(a) 10	(b) 20	C. (12)	watts
FILM ROLL #:	(a) C ____	(b) BW ✓		

ENVIRONMENT:

SKY CONDITION:
(a) Uniformly Overcast
(b) Cloudy
(c) Partly Cloudy ✓
(d) Puff Ball Clouds
(e) Clear
(f) Rain
(g) Fog

VISIBILITY RANGE: 8m

HUMIDITY:

CABIN TEMPERATURE: 70° F

OUTSIDE AIR TEMPERATURE:

WIND VELOCITY AND DIRECTION FROM A/C:

THIS SHEET PERTAINS TO RUNS All

TOTAL NUMBER OF RUNS FOR FLIGHT 24

Run #	Pulse/Frame	Polarization	Roll Angle
1, 2, 3, 4	1	dir	0°
5, 6, 7, 8	10	dir	0°
9, 10, 11, 12	50	dir	0°
13, 14, 15, 16	148	dir	0°
17, 18, 19, 20	50	cross	0°
21, 22, 23, 24	50	dir	3°

3.3.2 Run Data Sheet

3900-3906 → Transmitted Pulse

FLIGHT #	DATE	NAME	
14	1/27/70	J. Bartlett	Sheet 1

FRAME #			AIRCRAFT	TAS		SEA	LOCATION			Amp
RUN	START	END	HEADING	VELOCITY	ALTITUDE	DIRECTION HEADING	LATITUDE	LONGITUDE	TIME DELAY	Set v/cm
1	3919	3948	350°	177 kts	10,000 ft	350°	37° 07'N	73° 38'W		.050
2	3951	3980	260°	177 kts	10,000 ft	350°	37° 07'N	73° 38'W		.050
3	3983	4012	170°	177 kts	10,000 ft	350°	37° 07'N	73° 38'W		.050
4	4016	4045	080°	177 kts	10,000 ft	350°	37° 07'N	73° 38'W		.050
5	4048	4077	350°	177 kts	10,000 ft	350°	37° 07'N	73° 38'W		.020
6	4080	4109	260°	177 kts	10,000 ft	350°	37° 07'N	73° 38'W		.020
7	4112	4141	170°	177 kts	10,000 ft	350°	37° 07''N	73° 38'W		.020
8	4144	4173	080°	177 kts	10,000 ft	350°	37° 07'N	73° 38'W		.020
9	4176	4215	350°	177 kts	10,000 ft	350°	37° 07'N	73° 38'W		.020
10	4218	4257	260°	177 kts	10,000 ft	350°	37° 07'N	73° 38'W		.020
11	4260	4299	170°	177 kts	10,000 ft	350°	37° 07'N	73° 38'W		.020
12	4302	4341	080°	177 kts	10,000 ft	350°	37° 07'N	73° 38'W		.020
13	4344	4383	350°	177 kts	10,000 ft	350°	37° 07'N	73° 38'W		.050

3.3.2 Run Data Sheet (Continued)

3900-3906 Transmitted Pulse

FLIGHT #	DATE	NAME	Sheet 2
14	1/27/70	J. Bartlett	

FRAME #			AIRCRAFT			SEA	LOCATION			
RUN	START	END	HEADING	VELOCITY	ALTITUDE	DIRECTION HEADING	LATITUDE	LONGITUDE	TIME DELAY	Amp Set
14	4386	4425	260°	177 kts	10,000 ft.	350°	37° 07'N	73° 38'W		.050
15	4428	4467	170°							
16	4470	4509	080°							
17	4512	4532	350°							.010
18	4535	4554	260°							
19	4557	4576	170°							
20	4579	4598	080°							
21	4600	4640	350°							.050
22	4643	4683	260°							
23	4686	4725	170°							
24	4728	4767	080°							
	4773	4782		TRANSMITTED PULSE						

3.3.3 Ocean Truth Data Sheet

FLIGHT #	RUN(S) #(S)	DATE	LOCATION
14	All	1/27/70	Wallops 9-D

J. Bartlett   Time: 10:10 AM

PARAMETER	VALUE	SOURCE
SURFACE WIND DIRECTION	360^0	Range Recoverer
SPEED	12 kts	"
WATER SURFACE TEMPERATURE	54.6^oF	"
AIR SURFACE TEMPERATURE	43^oF	"
WAVE HEIGHTS AVERAGE	5 ft	"
(DOMINANT) WAVE DIRECTION	350^o	"
AIR PRESSURE	1020.3 mb	"
VISIBILITY	8 miles	"
WAVE PERIOD	5 seconds	"
DEW POINT	36^o	"

3.3.4 Ocean Spectra Data Sheet

OCEAN SPECTRA CAMERA (STILWELL)

FLIGHT #	FRAME #	ALTITUDE	A/C HEADING	SEA DIRECTION	TIME	COMMENTS
14	1 + 2	1,500 Ft.	350°	350°	10:30	Before Climb
	3 + 4		260°		10:32	f16 @ $\frac{1}{200}$
	5 + 6		170°		10:33	
	7 + 8		080°		10:34	
	9 + 10	10,000 Ft.	350°		11:46	f22 @ $\frac{1}{200}$
	11 + 12		260°		11:47	
	13 + 14		170°		11:48	Broken Clouds
	15 + 16		080°		11:49	
	17 + 18	1,500 Ft.	350°		12:02	After Climb
	19 + 20		260°		12:03	f22 @ $\frac{1}{200}$
	21 + 22		170°		12:04	
	23 + 24		080°		12:05	Heavy Haze

TAS = 142 Kts

TAS = True Air Speed

SECTION 4. DATA PROCESSING

4.1 Radar Analysis

The data from the flight tests in the form of scope film, ocean film (ground camera), ocean spectra film (K-17 camera), laser profilometer output, weather and ocean condition reports from the Range Recoverer, and strip-chart recordings were gathered, correlated, and analyzed with the objective of finding the average $\sigma°$, (radar cross-section per unit area) for various ocean conditions. The $\sigma°$ was calculated for each of the selected frames and average $\sigma°$'s were calculated for each flight.

4.1.1 Procedures

Approximately 600 frames from ten of the flights (flights 4, 5, 6, 7, 8, 10, 12, 14, 15, 16) were selected for processing. All the pertinent environmental and radar information was recorded onto cards for computer processing. Using a form of the radar equation, the radar cross section, $\sigma°$, was then calculated for each frame, for each flight and for a selected number of runs. The mean, the standard deviation, the frequency distribution, and the cumulative probability distribution of $\sigma°$ were then calculated. The results are presented in Section 5 and Appendix A.

4.1.2 Analysis

The radar cross section, $\sigma°$, was calculated from the radar equation, using the relations derived below.

Derivation of Equations for $\sigma°$

The radar equation can be written in the form:

$$P_R = \frac{P_T G^2 \lambda^2 \sigma}{(4\pi)^3 h^4 L} \qquad (4\text{-}1)$$

where

P_R = received power

P_T = transmitted power

G = peak antenna gain

λ = transmitted wavelength

σ = target cross section

h = altitude

L = combined system lossed

1. waveguide loss
2. attenuation (receiver calibration correction)
3. antenna pattern loss

If the return is from an area such as terrain, then

$$\sigma = \sigma^\circ A \qquad (4\text{-}2)$$

where

σ° = radar cross section per unit area

A = area of terrain illuminated

The area illuminated is calculated from the geometry of the radar system (see Figure 4-1).

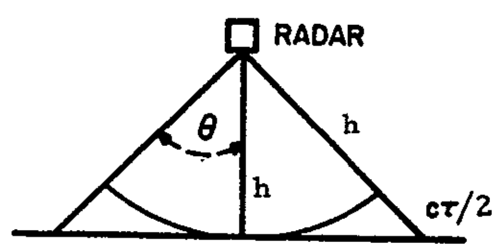

Figure 4-1. Geometry of the Radar System

The area, A, will depend on whether the radar system is pulse limited or beam limited.

From the geometry, if

$$\tau \geq \frac{h\theta^2}{c}$$

then the system is beam limited, and if

$$\tau < \frac{h\theta^2}{c}$$

then the system is pulse limited, where

τ = transmitted pulse width

h = aircraft altitude

c = speed of light

θ = incidence angle

A. Pulse Limited Case

The area illuminated for a pulse limited system is:

$$A = \pi c \tau h$$

The relationship of the range to altitude is,

$$r = h \sec P \sec R$$

where

P = pitch angle of aircraft

R = roll angle of aircraft.

For these flights, the roll and pitch angles of the aircraft during the radar operation were four degrees or less, and it can be assumed that

$$\sec P = \sec R \approx 1.0$$

therefore, $\sigma°$ can be expressed as

$$\sigma° = \frac{P_R (4\pi)^3 h^3 L}{P_T G^2 \lambda^2 \pi c \tau} \qquad (4-3)$$

B. <u>Beam Limited Case</u>

In this case, the geometry of the system leads to an illuminated area of

$$A = \pi \theta^2 h^2 \text{ (for small angle } \theta).$$

Now equation (4-1) can be expressed as

$$P_R = \frac{P_T G^2 \lambda^2 \pi\theta^2 \sigma°}{(4\pi)^3 h^2 L}$$

solving for $\sigma°$,

$$\sigma° = \frac{P_R (4\pi)^3 h^2 L}{P_T G^2 \lambda^2 \pi \theta^2} \qquad (4-4)$$

Estimation of Average $\sigma°$

The value of the received power, P_R, as expressed in equations (4-3) and (4-4) is an average of the peak power return. For these test flights, where the majority of the oscilloscope frames recorded at least 50 return pulses, the value of P_R desired for each frame is the average of the power of the pulse peaks recorded. Since a procedure of calculating the return power for each pulse and then averaging these values was not feasible, an estimate of the average peak power was made for each frame. This was possible since each frame represented integration of 50 or more pulses. Figure 4-2, the oscilloscope presentation, illustrates the maximum and average pulse peaks. Point 4 is the average pulse peak and point 3 is the maximum return pulse peak. As can be seen by this figure, point 3 can be measured rather easily, while point 4 can only be estimated.

Figure 4-3 shows a single pulse representation. Point 2 is the peak power return. The value of P_R derived from point 2 is equivalent to the P_R derived above using the average return power for multiple pulses.

Statistical Groupings of $\sigma°$ Data

Average $\sigma°$'s were found in various groupings of $\sigma°$. This data is presented in Section 5. Standard statistical equations were used to find the mean and standard deviation of $\sigma°$ (as a ratio).

$$\bar{\sigma}° = \frac{1}{n} \sum_{i=1}^{n} \sigma_i° \; ; \; n = \text{no. of frames}$$

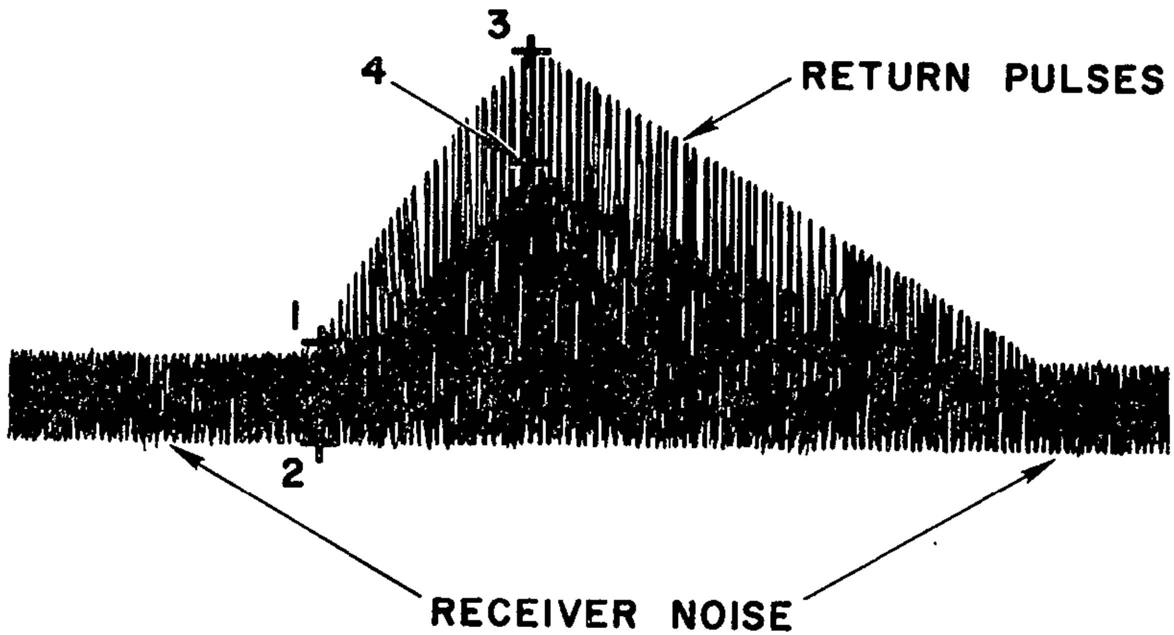

Figure 4-2. Scope Presentation: Multiple Pulses

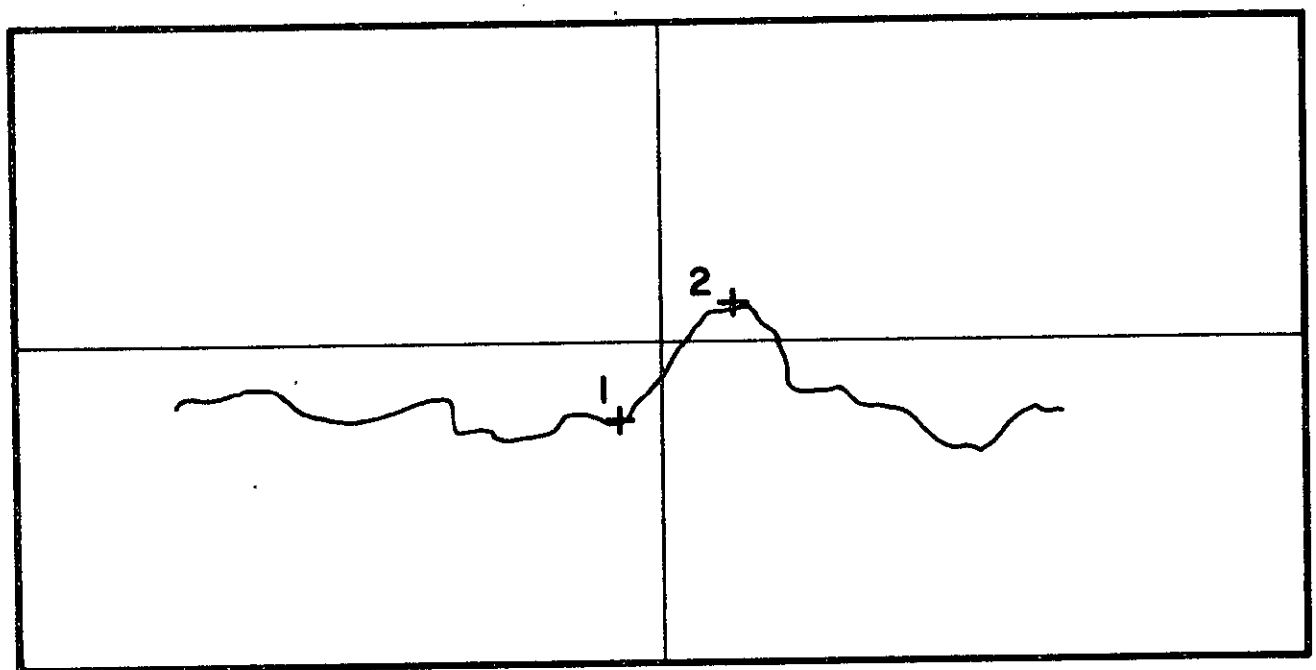

Figure 4-3. Scope Representation: Single Pulse

$$S_{\sigma^\circ} = \frac{\sum_{i=1}^{n} (\sigma_i^\circ - \overline{\sigma}^\circ)^2}{n - 1}.$$

The mean and standard deviation of σ° were later converted to dB for presentation purposes.

The histograms of σ° are based on the mean and standard deviation with each bar of the histogram being one-half of a standard deviation wide. The number of σ° values were totaled in each of the ten ranges of the histogram for each grouping. The ten ranges are as follows: (let $S = S_{\sigma^\circ}$)

$\sigma_i^\circ < \overline{\sigma}^\circ - 2.0S$

$\overline{\sigma}^\circ - 2.0S \leq \sigma_i^\circ < \overline{\sigma}^\circ - 1.5S$

$\overline{\sigma}^\circ - 1.5S \leq \sigma_i^\circ < \overline{\sigma}^\circ - 1.0S$

$\overline{\sigma}^\circ - 1.0S \leq \sigma_i^\circ < \overline{\sigma}^\circ - 0.5S$

$\overline{\sigma}^\circ - 0.5S \leq \sigma_i^\circ < \overline{\sigma}^\circ$

$\overline{\sigma}^\circ \leq \sigma_i^\circ < \overline{\sigma} + 0.5S$

$\overline{\sigma}^\circ + 0.5S \leq \sigma_i^\circ < \overline{\sigma} + 1.0S$

$\overline{\sigma}^\circ + 1.0S \leq \sigma_i^\circ < \overline{\sigma} + 1.5S$

$\overline{\sigma}^\circ + 1.5S \leq \sigma_i^\circ < \overline{\sigma} + 2.0S$

$\overline{\sigma}^\circ + 2.0 \leq \sigma_i^\circ$

The cumulative probability distributions were found by integrating the frequency distributions, i.e., the histograms. If $f(\sigma^\circ)$ is the frequency distribution of σ°, then the cumulative probability distribution is:

$$F(\sigma^\circ) = \sum_{x=-\infty}^{\sigma^\circ} f(x)$$

4.2 Selection of Flights and Frames

4.2.1 Flights Selection Criteria

Of the sixteen test flights, ten were selected for analysis. Those not selected included the three shakedown flights (flights 1, 2 and 3) which had very little ocean truth data, flights 9 and 11 which were aborted before any radar data was taken, and flight 13 which had poor multiple pulse oscilloscope film quality. Frames were selected from all of the other flights in order to get radar data for a variety of sea conditions.

4.2.2 Frame Selection Criteria

Approximately six hundred frames were selected for processing from the ten selected flights. From each flight, the frames were selected in such a manner that the effect on the return power of varying aircraft altitude, pulse width, number of pulses integrated, aircraft heading, antenna polarization, etc., could be studied. The frames that were eliminated from consideration fell into one of three categories:

1. if the return signals were saturated or were masked by the noise,
2. if the roll and pitch angles of the aircraft were excessive (greater than 5°) at the time of the recording of the return pulse, and
3. if there were any possibilities the film could be misinterpreted.

4.2.3 Point Measurement of the Scope Film

In order to calculate the radar backscatter per unit area, σ°, an accurate value of the return power, P_R, was needed. The return power was measured from the scope film using a point coordinate mensurator, a measuring instrument with a 24" x 24" viewing screen and a magnification capability of 20 X to 30 X. The procedure was to precisely locate each point of interest under the reference crosshair of the instrument, and automatically record the coordinates of the point on a punched card. The measured coordinate values are in microns.

Using Figure 4-2, the oscilloscope representation of multiple pulses as a reference, the following points were measured for each frame with multiple pulses.

Point 1 - The top of the noise level at the start of the return pulse.

Point 2 - The bottom of the noise level at the start of the return pulse.

Point 3 - The absolute return pulse peak.

Point 4 - The average return pulse peak.

A. Multiple Pulse Procedure

The value of the average return signal power, P_R, was obtained in the following manner. First, the y-coordinate of point 2 was subtracted from the y-coordinate of point 4. By knowing the amplitude setting of the oscilloscope, this value could easily be converted to volts. However, this represents both signal and noise returns and to obtain just the signal return, a minimum receiver noise level in volts had to be subtracted from the original result. This minimum noise level was found by subtracting the y-coordinate of point 2 from the y-coordinate of point 1 and then dividing this result by 2. The final value of P_R was then converted to dBm by means of a receiver calibration curve (see Figure 5-8).

B. Single Pulse Procedure

For those frames with only single pulses, the following two points were measured (see Figure 4-3):

Point 1 - The start of the return pulse

Point 2 - The peak of the return pulse

P_r was found for single pulse by subtracting the y-coordinate of point 1 from the y-coordinate of point 2 and then converting this value to volts and finally to dBm by using the receiver calibration curve.

4.2.4 Card Format

All the pertinent information concerning each frame has been stored on punched cards. There are three sets of cards. The first set, the flight cards, includes information that was constant throughtout each flight; the second set, the run cards, includes information that varied during the flight but was constant during each run; and the last set, the oscilloscope cards, includes the measured points from the oscilloscope film.

A. Flight Cards

The following information is included on each of the flight cards:

1. Flight number
2. Location code
   - 37° 07'N x 73° 38'W (120 miles east of Norfolk, Va.)
   - Tangier Sound (in Chesapeake Bay)
   - Off shore near Wallops Island, Va.
   - Long Island Sound (Middle Ground)
3. Sea Direction (°)
4. Wave Height (ft)
5. Wave Period (sec)
6. Wind Speed (knots)

7. Wind Direction (°)

8. Water Temperature (° F)

9. Air Pressure at sea level (mb)

10. Peak Power Transmitted (watts)

11. Receiver Attenuation (dB)

12. Beamwidth (°)

13. Ocean Spectra Data Available (Stilwell)

   - yes
   - no

14. Laser Profilometer Data Available

   - yes
   - no

15. Sky Condition

   - Clear
   - Cloudy
   - Partly Cloudy

16. Date of Flight

B. <u>Run Cards</u>

The run Data Cards included the following information:

1. Flight number

2. Run number

3. Aircraft Altitude (ft)

4. Oscilloscope Sweep Speed (nsec/cm)

5. Oscilloscope Amplitude Setting (millivolts/cm)

6. Number of Pulses per Frame

7. Transmitted Pulse Width (nsec)

8. Antenna Polarization Code

   - Direct
   - Cross

9. Aircraft Heading (°)

C. Oscilloscope Cards

The Oscilloscope Data Cards have the following data.

1. Flight number
2. Run number
3. Frame number
4. The x- and y-coordinates of the points of interest as described in Section 4.1. This is the output of the Point Coordinate Mensurator.

4.3 Computer Processing Program

A data processing program was developed which used the flight, run, and oscilloscope cards as input to calculate the radar cross section per unit area, $\sigma°$, and the return signal power, P_r, for each frame. It further calculated for each flight the average $\sigma°$ and its standard deviation, a histogram of the individual $\sigma°$'s, and a cumulative probability distribution of $\sigma°$. This was done for the $\sigma°$ based on the average peak return signal and for the $\sigma°$ based on the absolute peak return signal (see Section 4.1). This program (Figure 4-4) was written in FORTRAN IV for use on a CDC 6600.

4.4 Results of Processing Program

All of the output from the processing of the flight test data is presented in Appendix A in computer printout form. Further analysis and groupings of this data are found in Section 5.

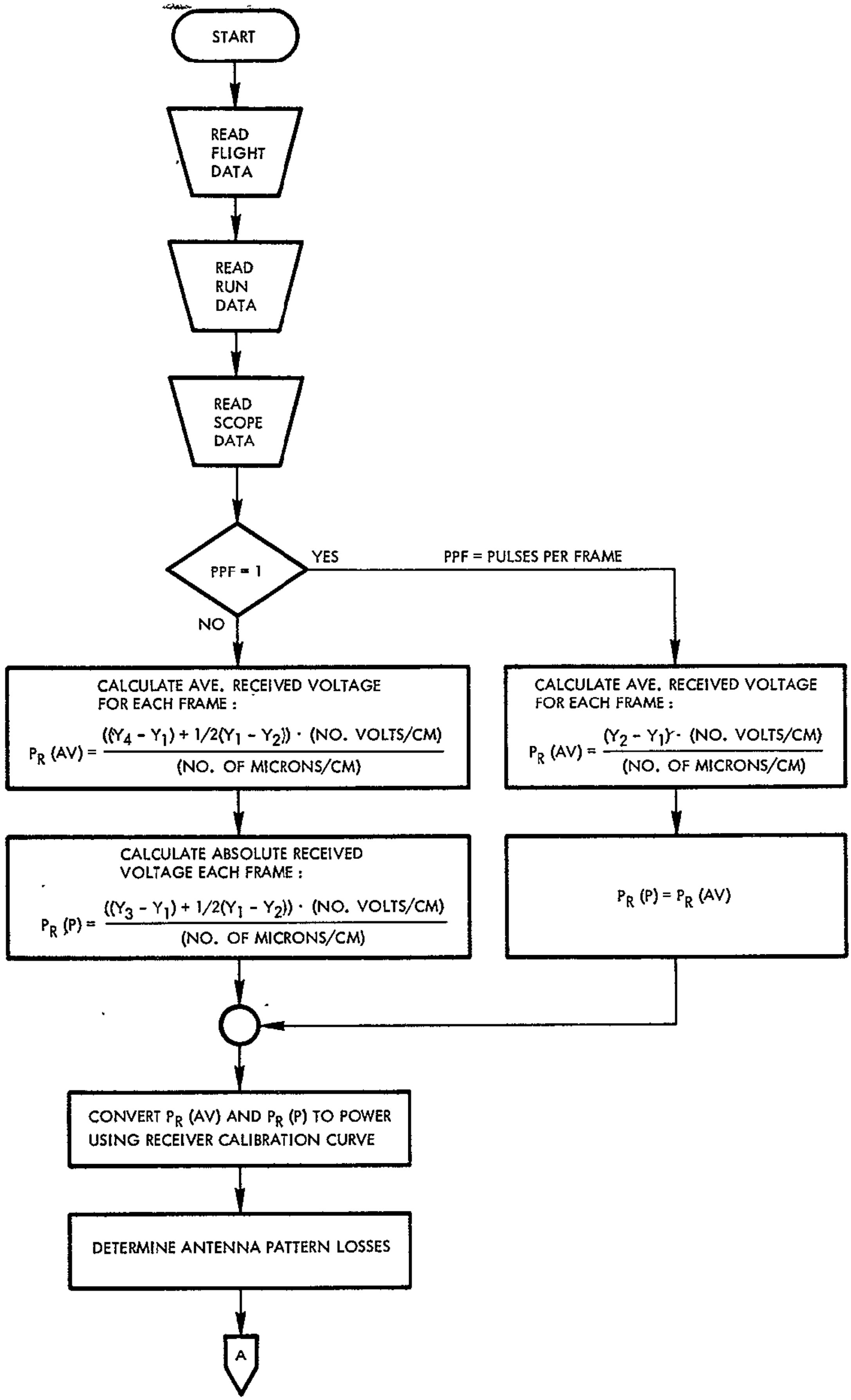

Figure 4-4. Computer Processing Program

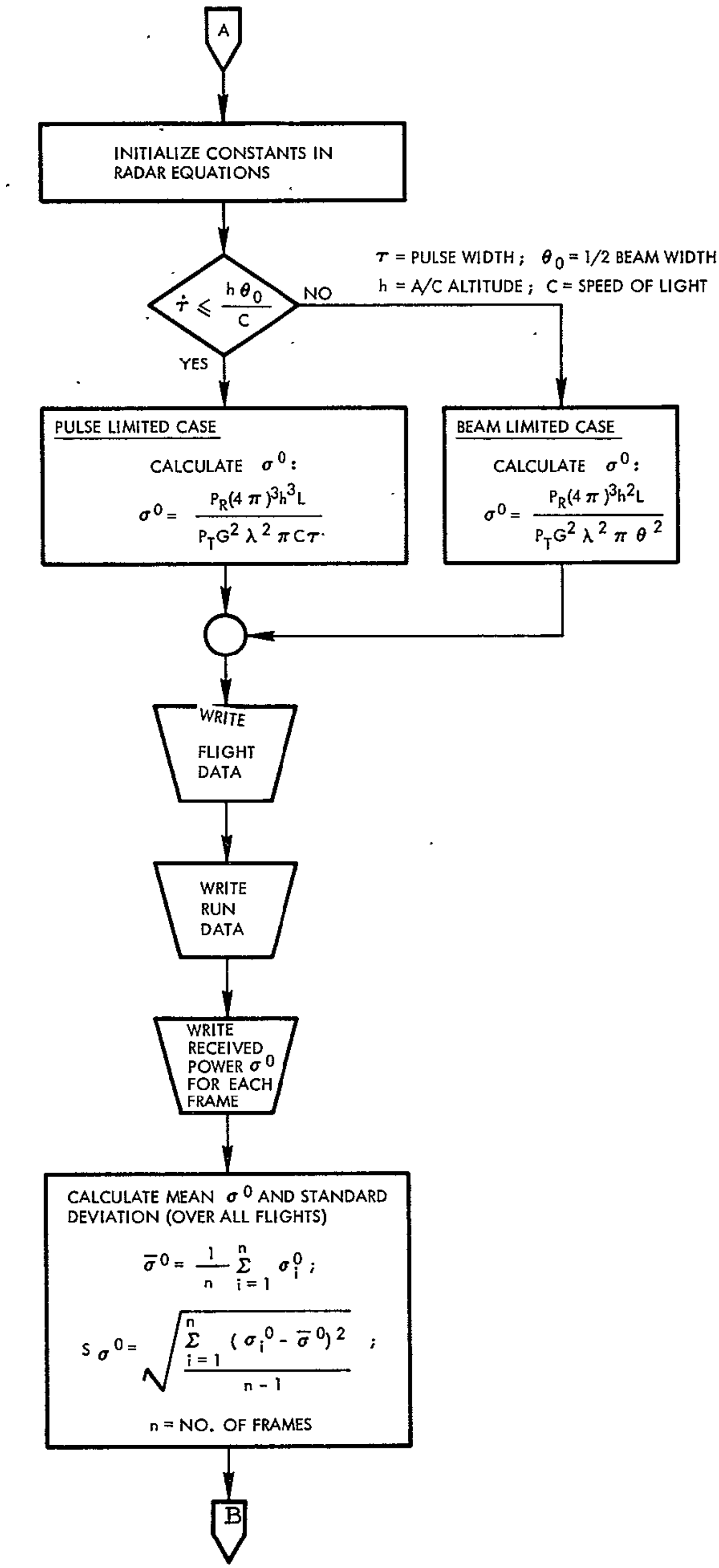

Figure 4-4. Computer Processing Program (Cont.)

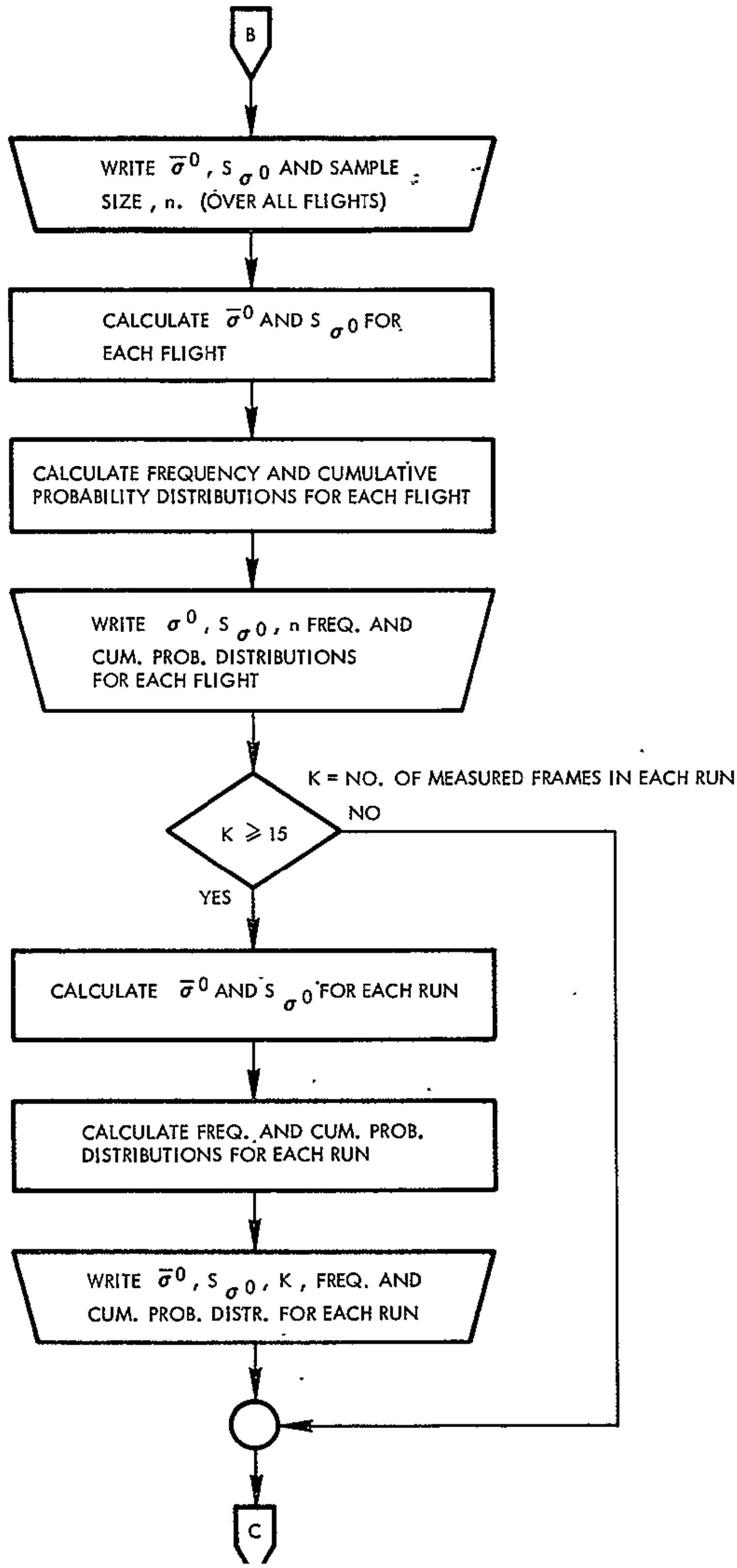

Figure 4-4. Computer Processing Program (Cont.)

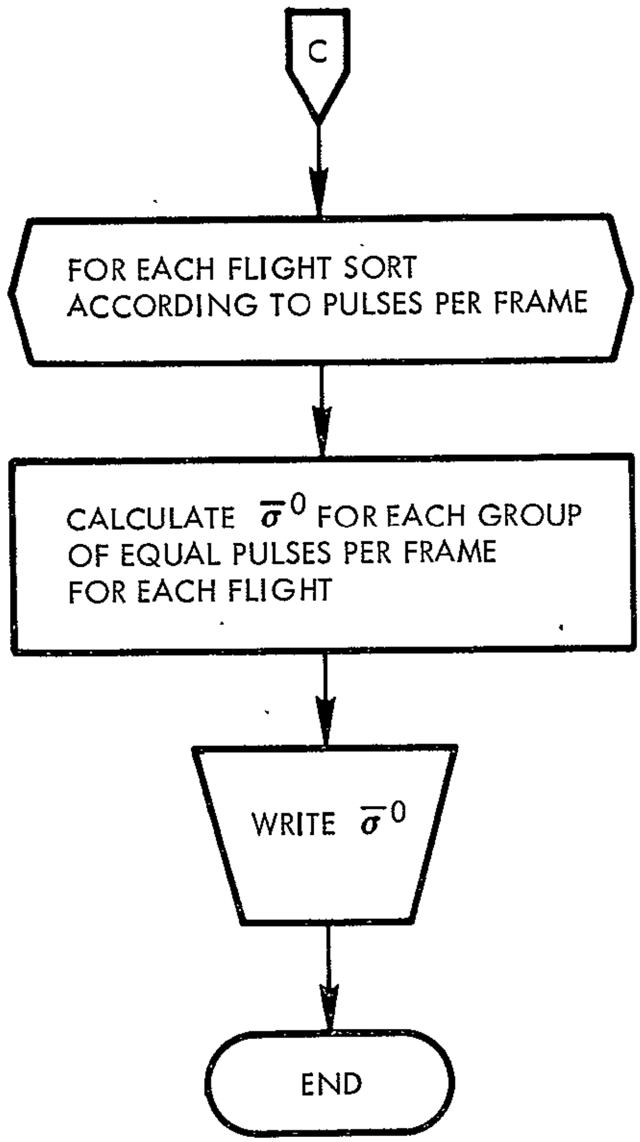

Figure 4-4. Computer Processing Program (Cont.)

4.5 Distribution of Pulse Peaks

The theoretical distribution of pulse peaks for a number of pulses is a Rayleigh distribution. This is actually the circular normal distribution in polar coordinates. The Rayleigh frequency distribution is given as:

$$f(r) = \frac{r}{\sigma^2} e^{-r^2/2\sigma^2}$$

where

$\sigma = [(x-\mu_x)^2 + (y-\mu_y)]^{1/2}$; the distance to the origin in a bivariate normal distribution

$\sigma = \sigma_x = \sigma_y$ (x, y refers to rectangular coordinates)

(See Figure 4-5.) The mean of the distribution equals 1.253 times the standard deviation.

To show that the pulse peaks appear to have a Rayleigh distribution, the distributions of pulse peaks were found for a few frames from each selected test flight. This was done by using a microdensitiometer/isodensitracer which automatically scans and measures the density of points in a film transparency and plots the values as a quantitative two dimensional density map of the scanned area. The following curves (Figures 4-6 through 4-15) are the distributions of pulse peaks for one frame from each flight. The numbers on the vertical axis of the densitometer tracings correspond to the densities of each step of a "21-step wedge" (Kodak Photographic Step Tablet No. 2). The horizontal axis corresponds to the amplitude of the return signal, with the amplitude increasing from left to right. The point where the distribution starts to rise out of the noise level corresponds to the minimum return signal.

As can be seen from the density tracings the distributions appear to be Rayleigh. Further analysis is required to definitely show this relation. The film transfer functions should be considered at that time.

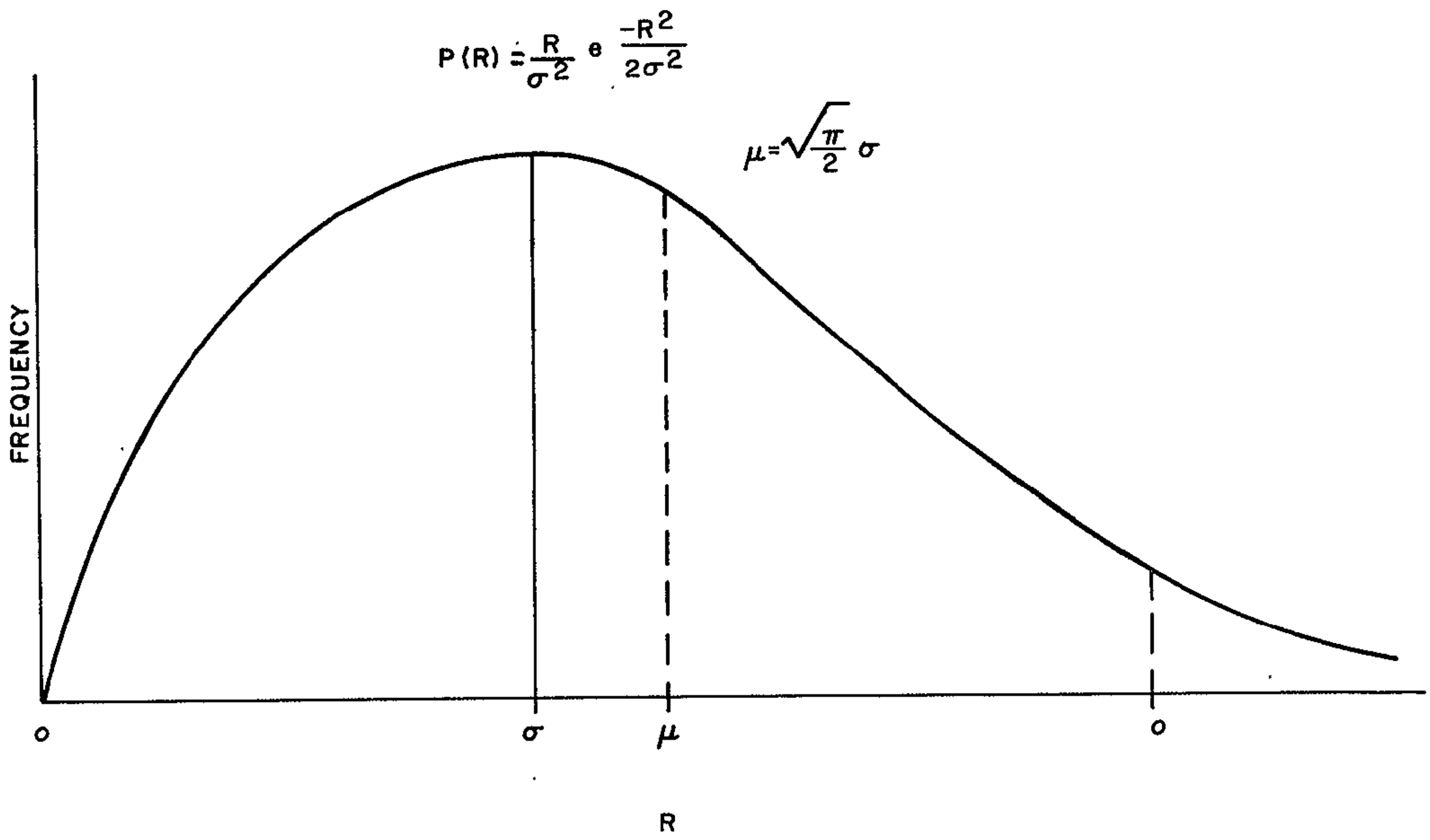

Figure 4-5. Rayleigh Distribution

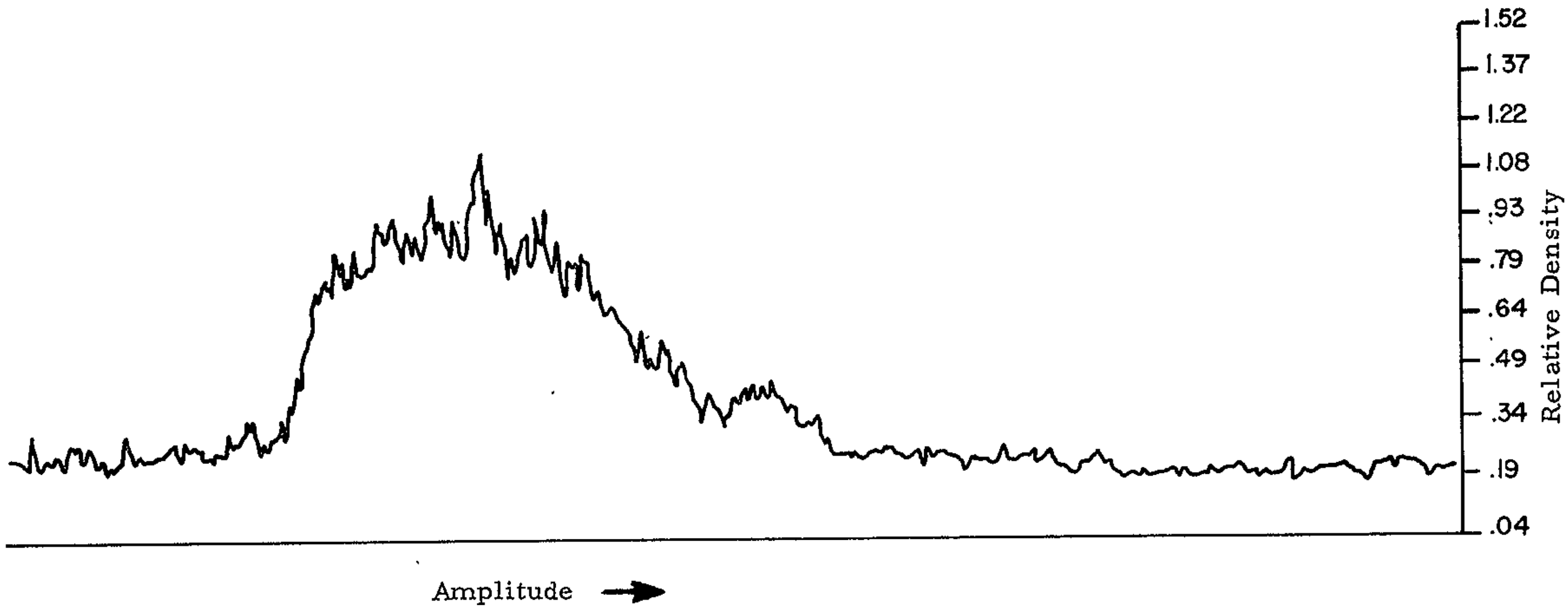

Figure 4-6. Flight 4; Frame 8330

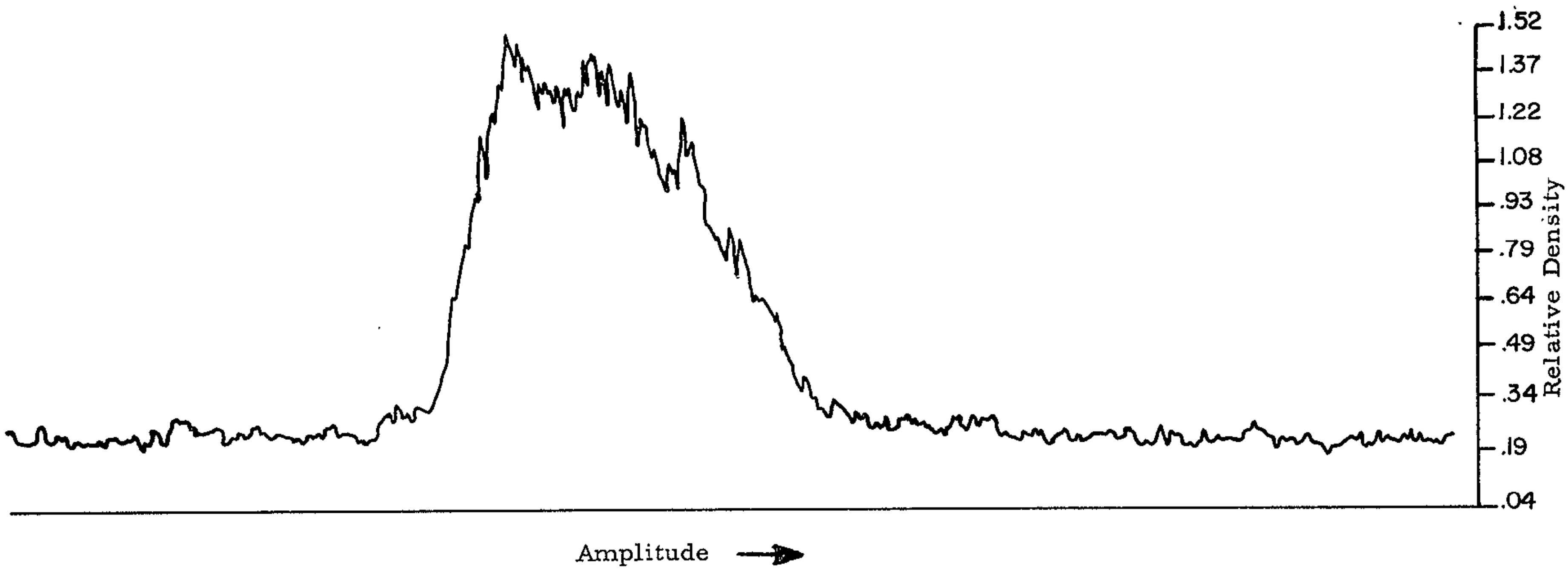

Figure 4-7. Flight 5; Frame 9083

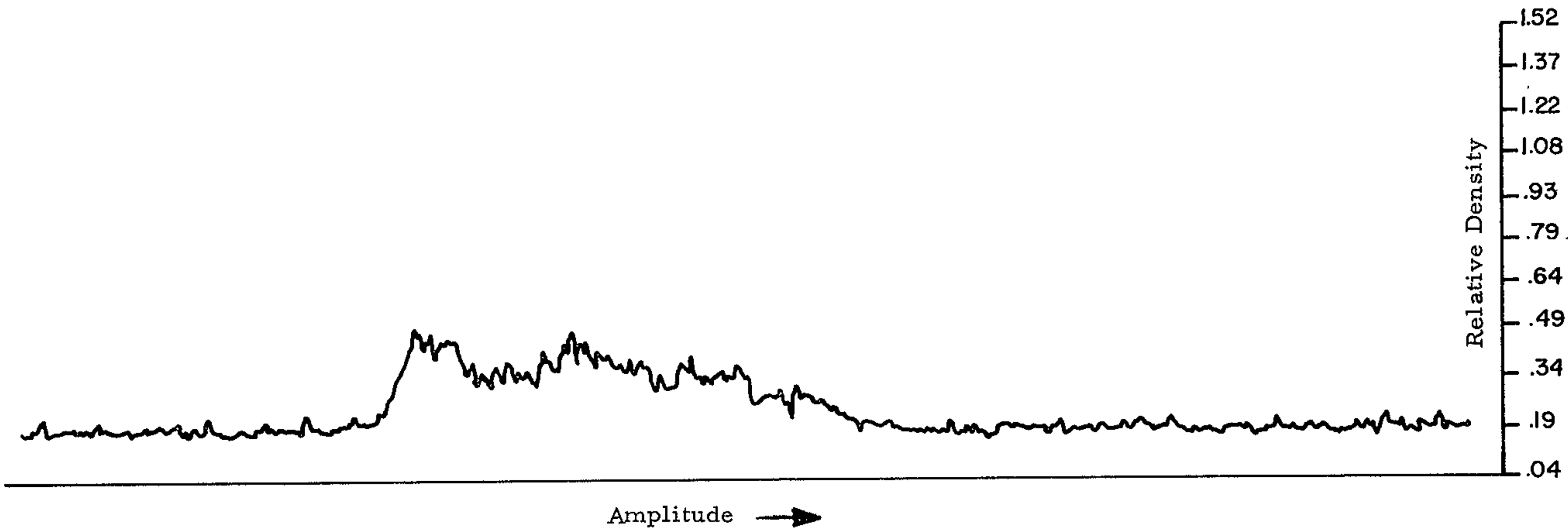

Figure 4-8. Flight 6; Frame 9558

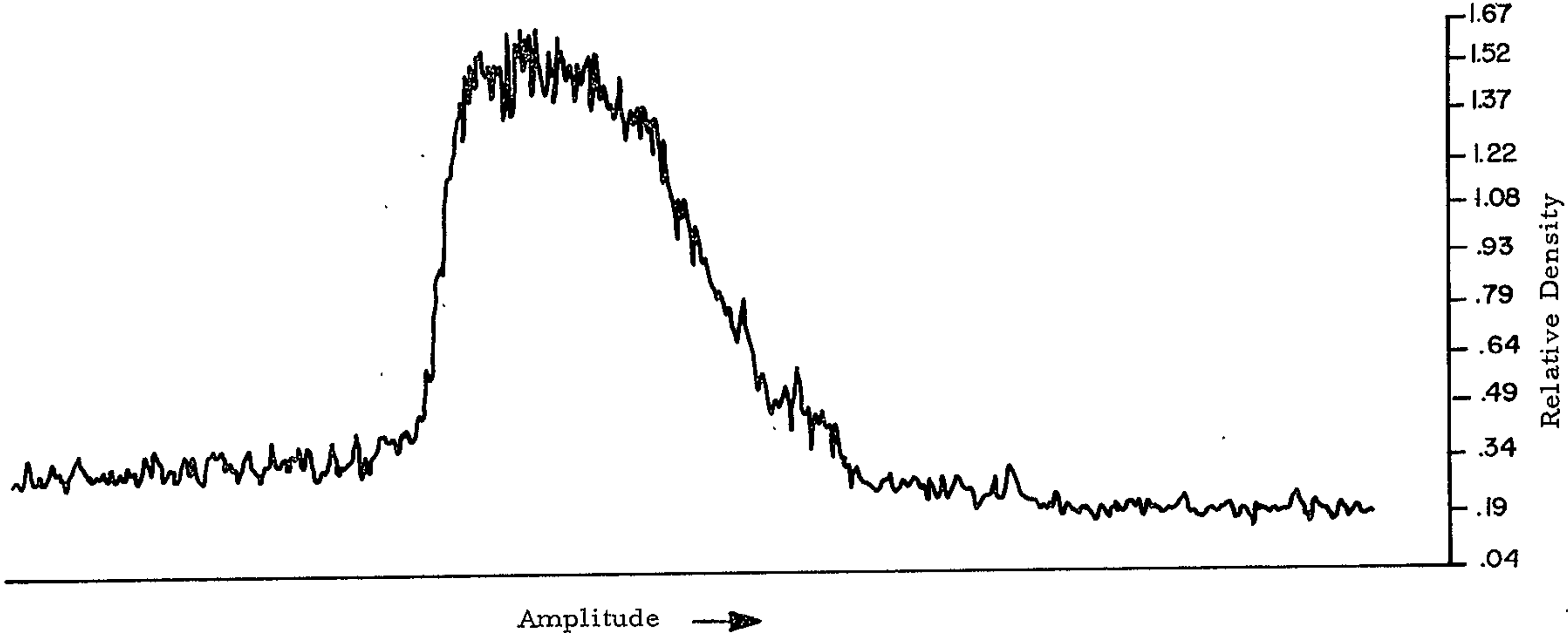

Figure 4-9. Flight 7; Frame 0458

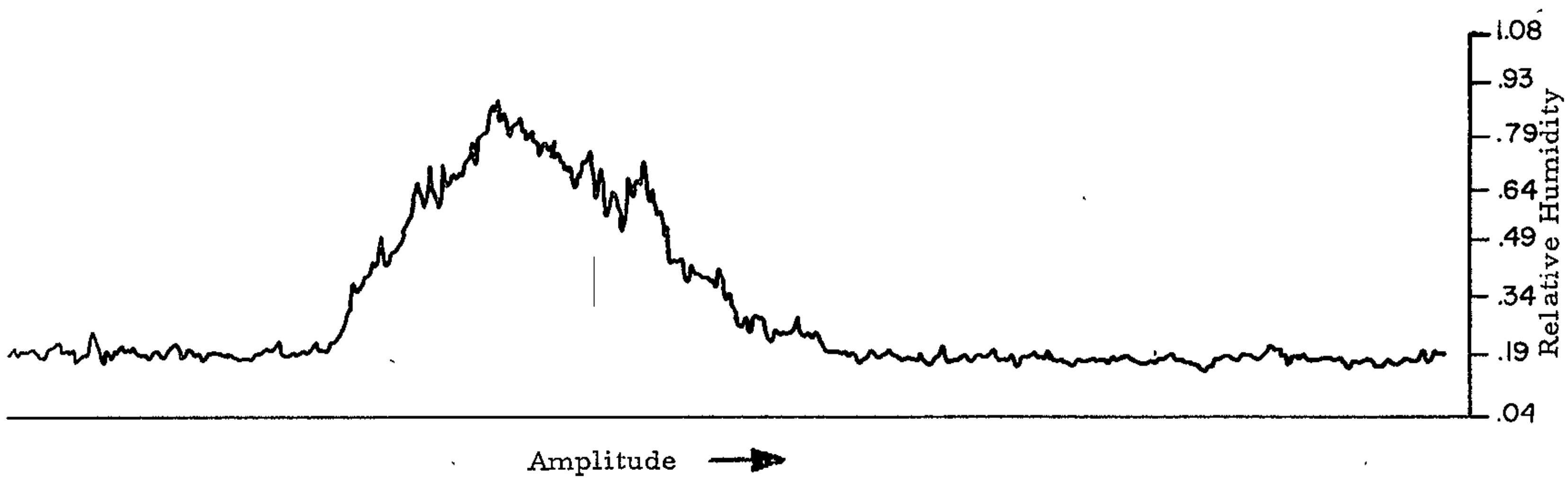

Figure 4-10. Flight 8; Frame 0795

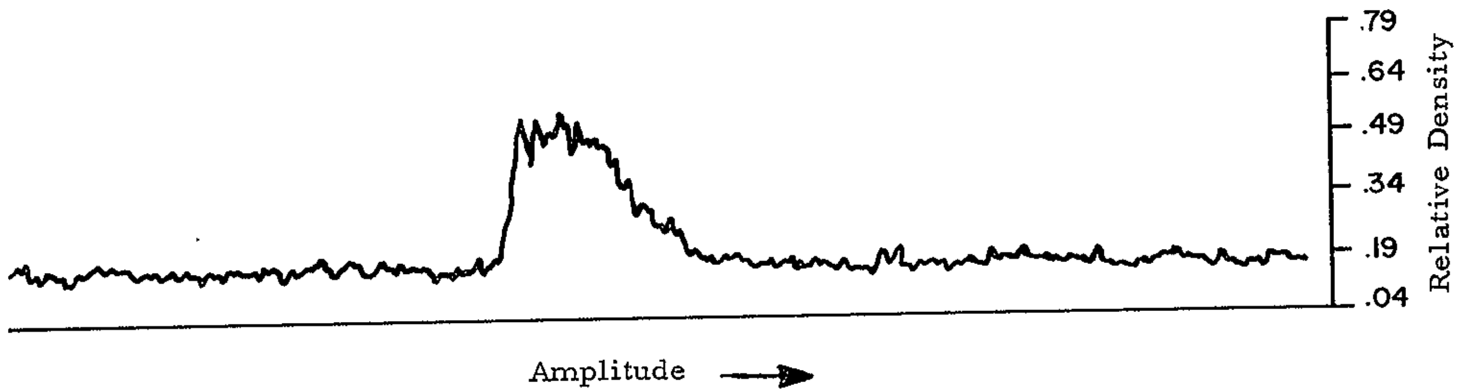

Figure 4-11. Flight 10; Frame 1900

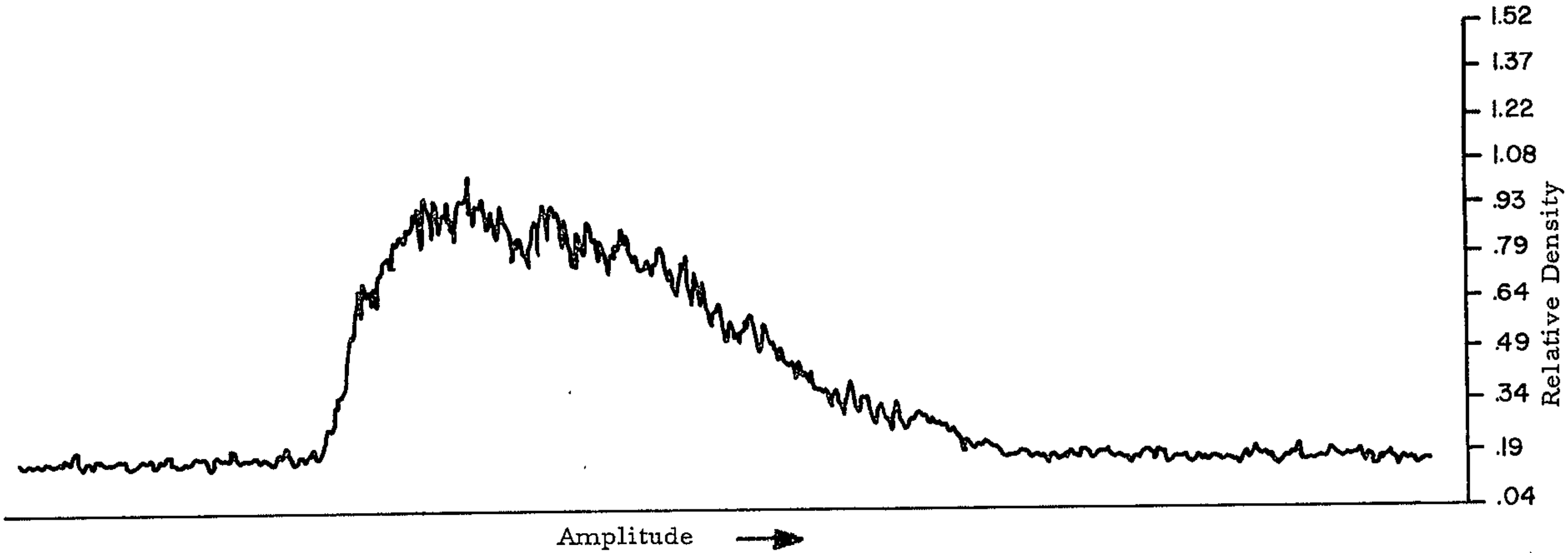

Figure 4-12. Flight 12; Frame 2689

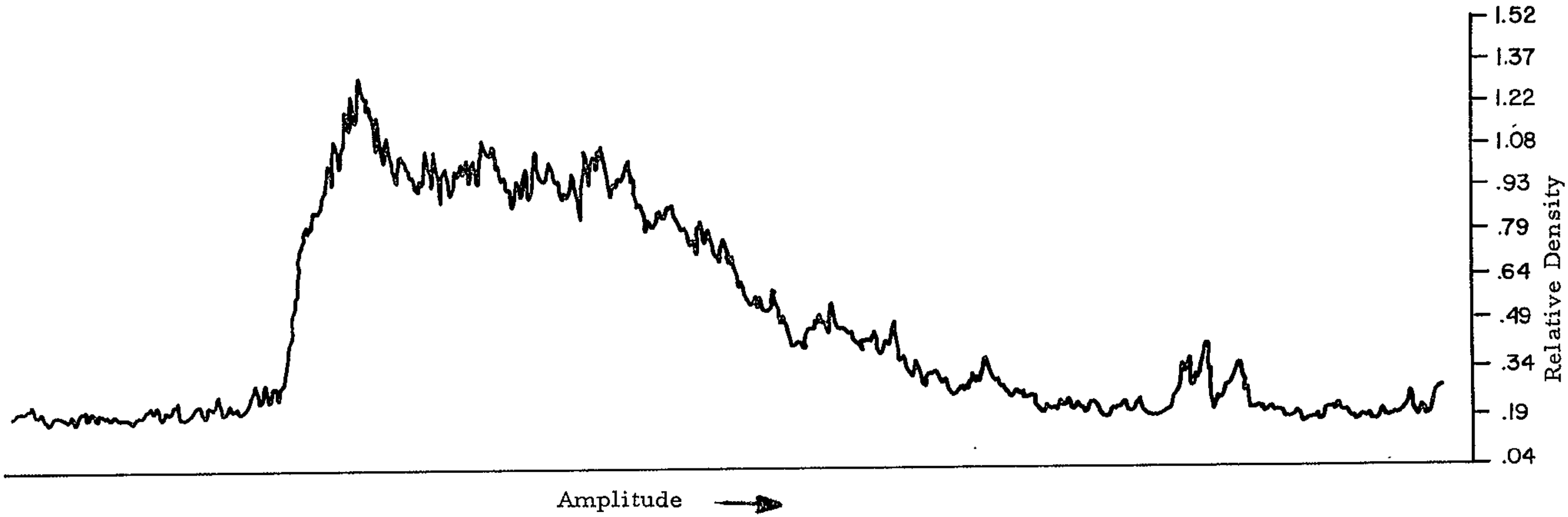

Figure 4-13. Flight 14; Frame 4180

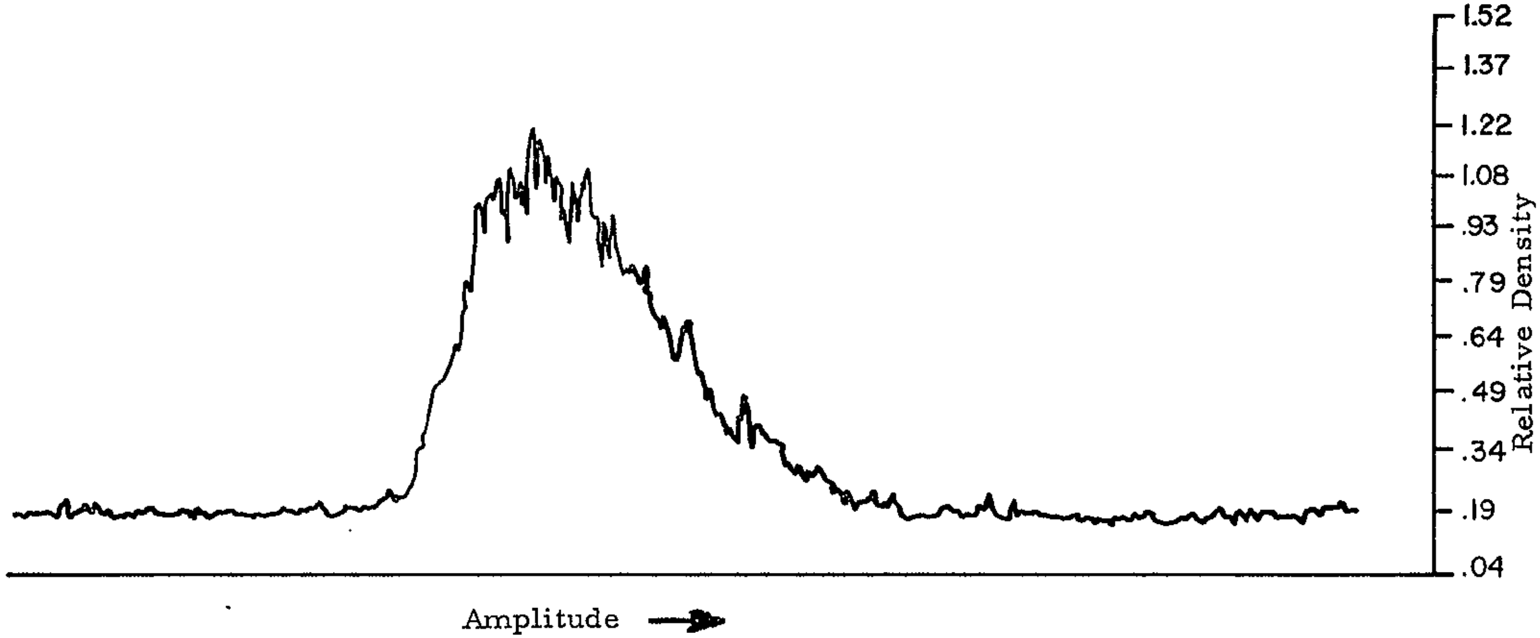

Figure 4-14. Flight 15; Frame 5524

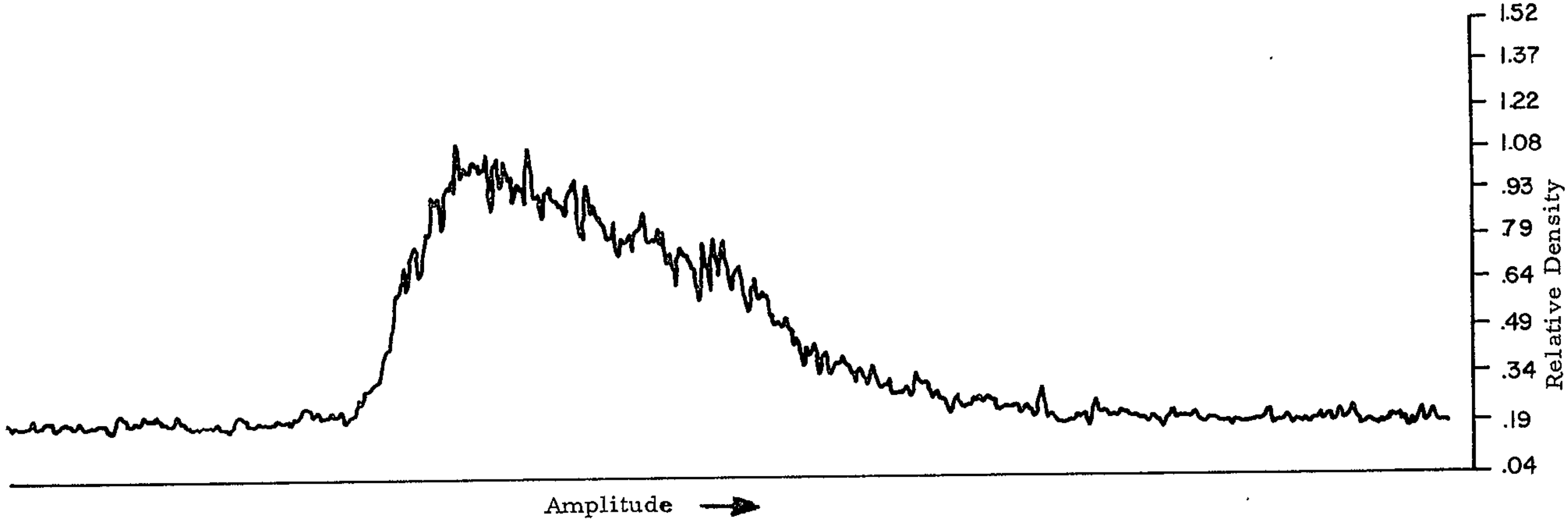

Figure 4-15. Flight 16; Frame 6750

4.6 System Error Analysis

The equation for σ^o has been shown to be

$$\sigma^o = \frac{P_R (4\pi)^3 h^3 L}{P_T G^2 \lambda^2 \pi c \tau}$$

Since the nominal roll (R) and pitch angles (P) are zero, the applicable error equation is

$$\left[\frac{\Delta\sigma^o}{\sigma^o}\right]^2 = \left[\frac{\Delta P_R}{P_R}\right]^2 + \left[\frac{3\Delta h}{h}\right]^2 + \left[\frac{\Delta L}{L}\right]^2 + \left[\frac{\Delta P_T}{P_T}\right]^2 + \left[\frac{2\Delta G}{G}\right]^2 + \left[\frac{2\Delta\lambda}{\lambda}\right]^2 + \left[\frac{\Delta\tau}{\tau}\right]^2$$

To obtain the errors listed in Table 4-1 the calibration errors of the equipments (oscilloscope, power meter, etc.) were used. An additional factor was also included for human error in making the measurements. The major contributors to the error budget are the received power measurement ($\Delta P_R/R_R$), the altitude measurement ($\Delta h/h$), and the transmitted power measurement ($\Delta P_t/P_t$). The power measurements involve the use of: (1) an oscilloscope (accuracy better than 5%); (2) power meter (accuracy better than 2%); and human error (estimated to be 3%) in reading the oscilloscope and/or photograph. The altitude measurement error (5%) is that which was specified by manufacturers of the aircraft altimeter.

The error contribution (standard deviation) expressed in dB is listed in Table 4-1 for each error with a notation describing the sources of each error.

The RSS error for σ^o obtained from these elements is therefore

$$\frac{\Delta\sigma^o}{\sigma^o} \text{ RSS} \approx 0.9 \text{ dB}$$

Table 4-1. FLIGHT TEST ERROR CONTRIBUTIONS

ERROR	PERCENTAGE OF ERROR	1σ VALUE (dB)	SOURCES OF ERROR
(1) $\frac{\Delta P_R}{P_R}$	10%	0.4	VIDEO SCOPE CALIBRATION AND OPERATION. INTERPRETATION OF POINT COORDINATOR MENSURATOR.
(2) $\frac{\Delta L}{L}$	2%	0.1	MEASUREMENT OF SYSTEM LOSSES AND IN CALIBRATION.
(3) $3\frac{\Delta h}{h}$	3 x 5%	0.6	MEASUREMENT OF A/C ALTITUDE BY THE A/C ALTIMETER.
(4) $\frac{\Delta P_T}{P_T}$	10%	0.4	MEASUREMENT OF TRANSMITTED POWER BEFORE FLIGHT AND SCOPE MONITORING OF CHANGES DURING FLIGHT.
(5) $2\frac{\Delta G}{G}$	2 x 4%	0.3	MEASUREMENT OF ANTENNA GAIN AT 9.0 GHz.
(6) $2\frac{\Delta\lambda}{\lambda}$	2%	0.1	MEASUREMENT OF FREQUENCY.
(7) $\frac{\Delta\tau}{\tau}$	4%	0.2	MEASUREMENT OF TRANSMITTED PULSEWIDTH.
RSS	22%	0.9	

SECTION 5. DATA EVALUATION

5.1 Average Radar Cross Section (σ^o)

As described in the previous section, σ^o was obtained by averaging the multiple trace oscilloscope photographs and by computing the average of individual pulses displayed on the oscilloscope. The oscilloscope was used to obtain 1, 50, 147, and 278 pulses per frame. σ^o values obtained by averaging individual pulses were about two dB less than when averages were taken of 50 or more pulse traces.

The plotted values of σ^o on a per flight basis (Figures 5-1, 5-2, 5-3, 5-4) involve the averaging of more than 18 frames per flight with each frame representing 50 pulses.

Plots of σ^o were made for each flight in order to relate σ^o values to ocean conditions. The numbers shown on the Figures 5-1, 5-2, and 5-3 next to the points refer to flight numbers and hence to the day which the data was taken.

The spread of values of σ^o ranges from 8 dB to 21 dB. As can be seen from the plots of σ^o it would be questionable to claim any trend or functional relation to ocean parameters. There seems to be little or no relation between the σ^o value or the change in σ^o value to wave height or wave period. If there is any relation it exists with respect to wind speed (Figure 5-3). A trend line is shown on Figure 5-3 and would apply if a functional relation exists.

Flights 8, 10, and 12 in Figures 5-1 and 5-3 are flights in which the relation between wind and wave height were not related as would be the case in a fully developed sea. Flight 8 had very high seas (greater than 12 ft) but the wind had started to die down. On the other hand flights 10 and 12 were made in inland waters with the wind blowing an insufficient time and fetch to produce a

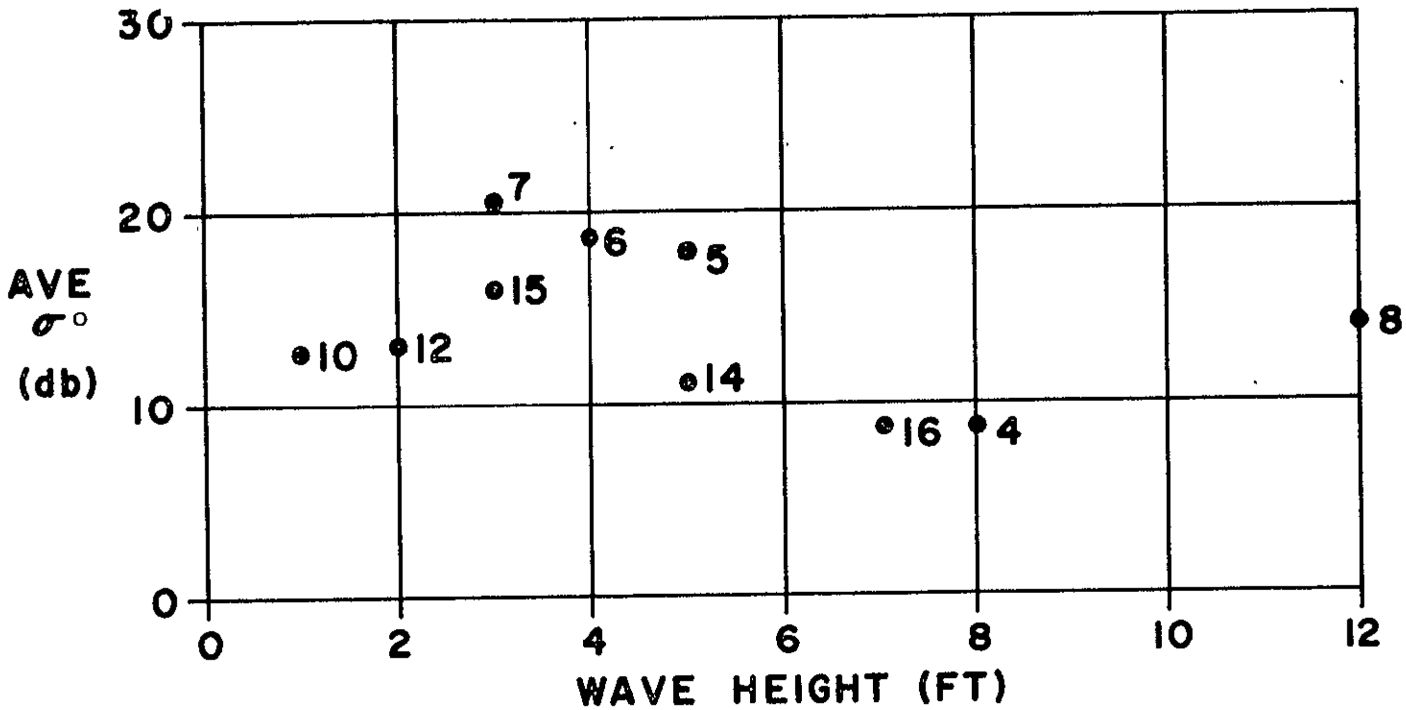

Note: No's Refer to Flight

Figure 5-1. Average σ^o Vs Wave Height (Vertical Incidence)

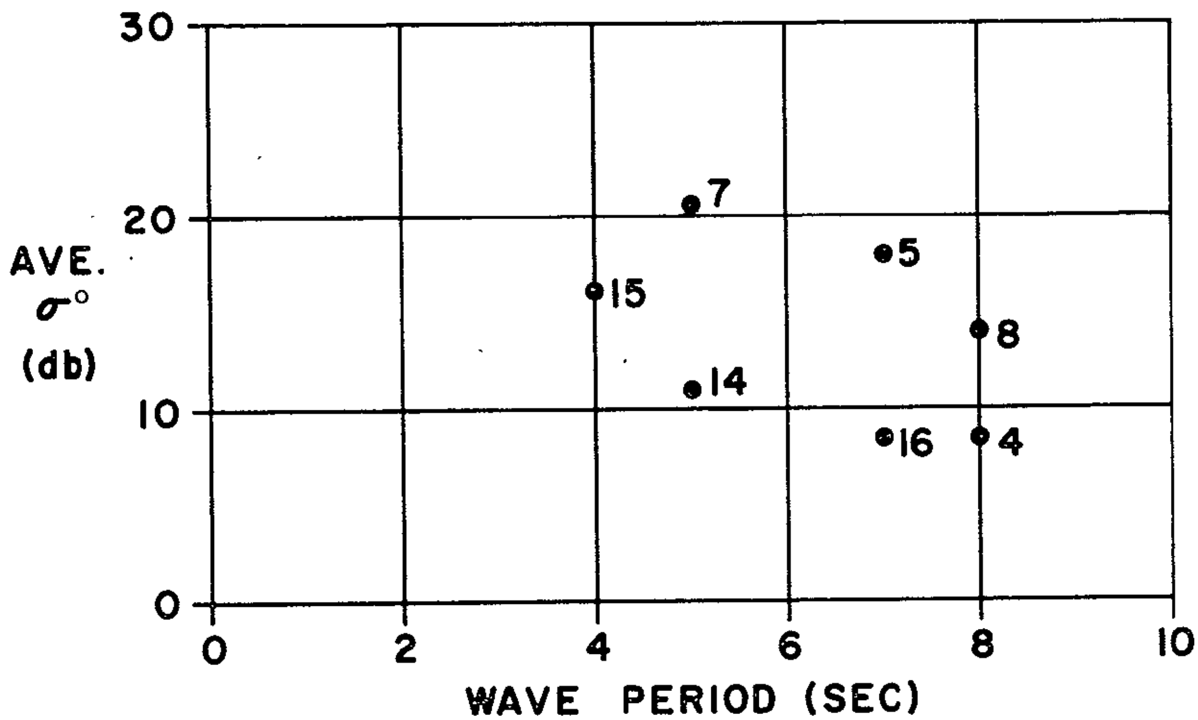

Note: No's Refer to Flights

Figure 5-2. Average σ^o Vs Wave Period (Vertical Incidence)

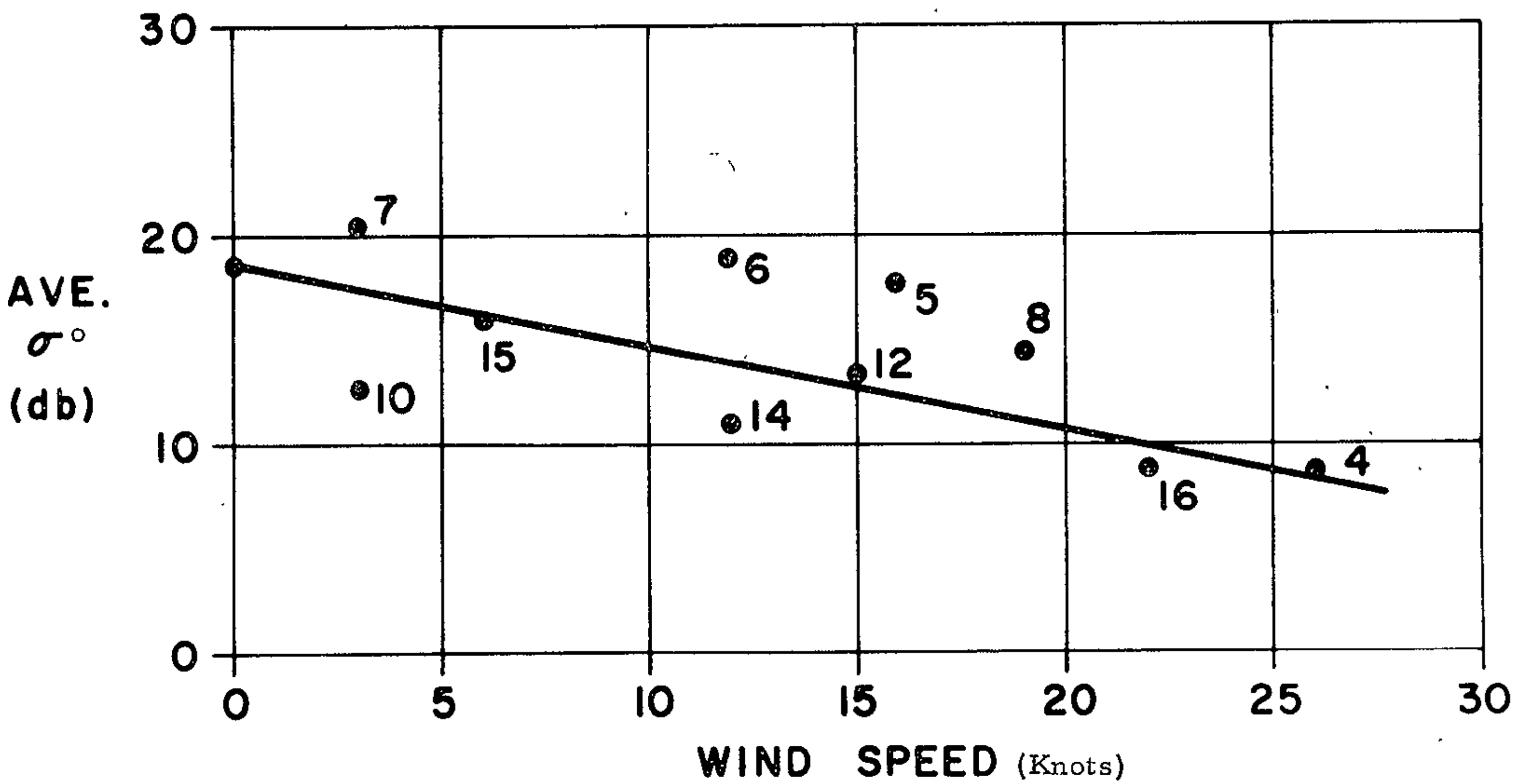

Note: No's Refer to Flights

Figure 5-3. Average σ^o Vs Wind Speed (Vertical Incidence)

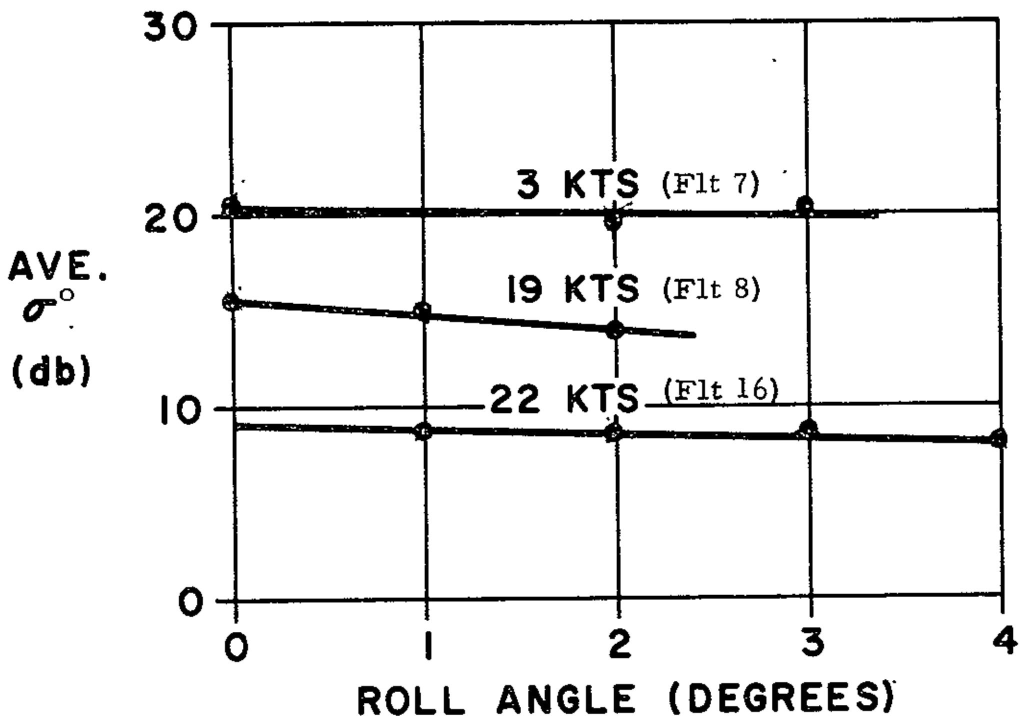

Figure 5-4. Average σ^o Vs Roll Angle (Pitch = 0°)

fully developed sea. It is felt therefore that these three points on Figures 5-1 and 5-3 reinforce the argument that σ^o is functionally related to wind but not to wave height because they improve the fit of the data in Figure 5-3 (σ^o vs wind) but they destroy the fit of the data in Figure 5-1 (σ^o vs wave height).

The ocean data used for making the above plots are the "eyeball" measurements obtained from the NASA ship on location when taking radar data. More definitive ocean parameters are possible from the Stilwell photos taken for each flight but the process of obtaining the necessary two dimensional Fourier transform from these photos in the Stilwell process requires further development (see Section 5-3).

If a relation exists between $\sigma°$ and wind speed, it probably exists because of the relation between wind speed and capillary waves. If $\sigma°$ is in fact related to capillaries (and there is much reason to believe this to be so because the capillary wavelength is comparable to the X-band wavelengths) then some methods for measuring capillaries will have to be devised. To date no such measurement capability exists. Investigations by Kinsman and Molo Christianson and currently underway to measure capillaries. Also, Stilwell photography at low altitudes may make the measurements possible.

Variations of $\sigma°$ as a function of sea direction are negligible and within the measurement accuracy as shown in the representative measurements of Table 5-1. This is further substantiated in the extensive data in Appendix A where additional bearing angles are covered.

Variations of $\sigma°$ as a function of angle from vertical are negligible, as shown in Figure 5-4. This agrees in part with the curves of Moore and Schooley (Figure 5-5).

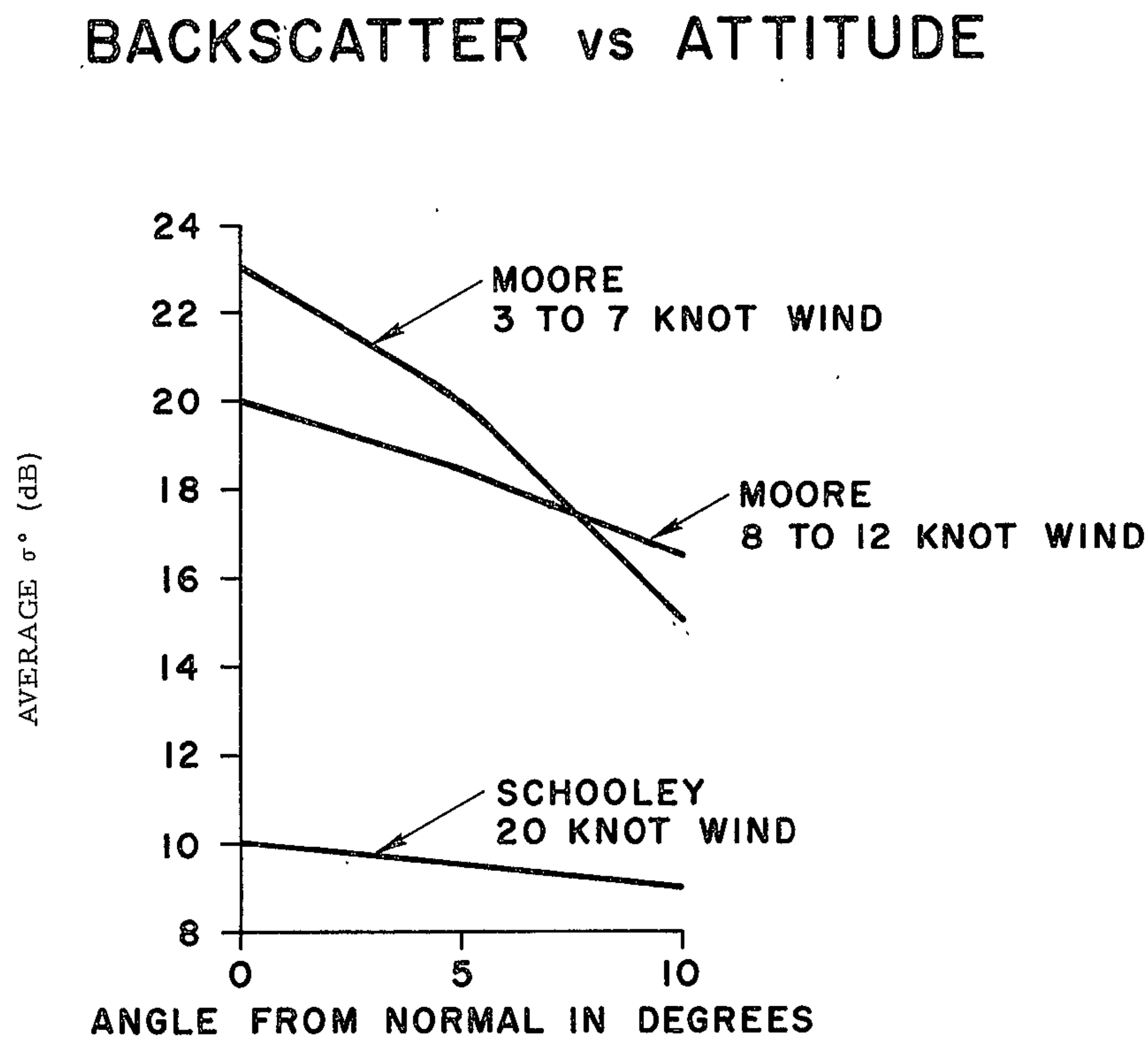

Figure 5-5. Backscatter vs Attitude
(Reference: WHOI Report, No. 65-10, April 1965, Page 23)

Table 5-1

$\sigma°$ vs. Sea Direction

Flight	Run	Bearing*	$\sigma°$
14	9	0	12.9
14	10	90	12.8
14	11	180	13.4
14	12	270	13.0

* Bearing angle with respect to sea direction

5.1.1 Pulse Limited vs Beam Limited

The basic radar range equation defines σ (radar cross section in square meters) as follows:

$$\sigma = \frac{P_R (4\pi)^2 h^4 L}{P_t G^2 \lambda^2} \qquad (5\text{-}1)$$

where

P_R = peak received power

h = altitude

L = system losses

P_t = peak transmitted power

G = antenna gain

λ = wavelength

The average radar cross section (σ^o) is the radar cross section per unit area or

$$\sigma^o = \frac{\sigma}{A} \qquad (5\text{-}2)$$

When the transmitted signal is a pulse, (see Figure 5-6) the return signal will be scattered from the area (A), or footprint, which is a function of time (t) or angle (θ), where:

$$t = \frac{h\theta^2}{c} \tag{5-3}$$

t is here defined from the instant the leading edge of the pulse initiates the first return and θ is the angle from vertical

The maximum value of t is τ (pulsewidth), but the maximum value of θ is not so well defined. The 3 dB point has sometimes been used as the maximum value of θ, but this is purely arbitrary.

The data in this experiment was reduced to σ values by measuring P_r, P_t, and h, and then performing the computation in Equation (5-1). Values of P_R were obtained by measuring the peak and average voltage of the return pulse (see Section 4 for a more detailed description). The σ values were then computed using Equation (5-2) with values of A as follows:

$$A = \pi c \tau h \tag{5-4}$$

This in effect assumes an h^3 relation for the radar range equation - a pulse limited relation. How valid is this assumption?

The area (A) can be related to the angle θ using the simple trigonometric relation $\tan \theta = r/h$:

$$\begin{aligned} A &= \pi r^2 \\ &= \pi h^2 \theta^2 \text{ (for small angle } \theta) \end{aligned} \tag{5-5}$$

Note here that θ is a function of time (t) as follows:

$$\theta^2 = ct/h \tag{5-6}$$

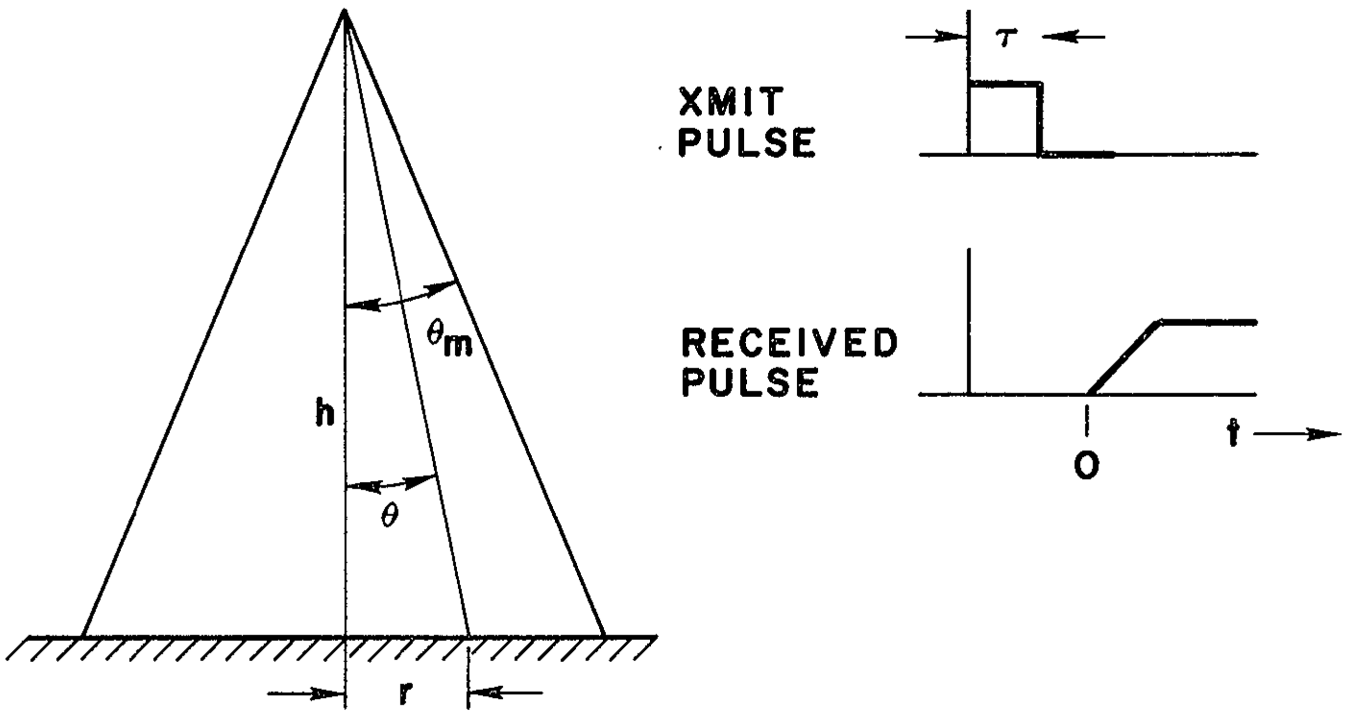

$$\sigma_i = \sigma_o A$$
$$A = \pi r(t)^2$$
$$\approx \pi h^2 \theta_m^2 \quad \text{if } \tau > \frac{h\theta_m^2}{c}$$
$$= \pi h c \tau \quad \text{if } \tau < \frac{h\theta_m^2}{c}$$

Figure 5-6. Geometric Relations

If the maximum value of t ($t = \tau$) is reached before some maximum value of θ ($\theta = \theta_m$), the area then becomes

$$A_\tau = \pi c \tau h \qquad (5\text{-}7)$$

which is the pulse limited situation, or an h cubed relation in the radar range equation.

If however a maximum value of θ ($\theta = \theta_m$) is reached before $t = \tau$ then the area becomes

$$A_\theta = \pi h^2 \theta_m^2 \qquad (5\text{-}8)$$

which is the beam limited situation or an h squared relation in the radar range equation.

The problem is now one of defining θ_m, or beam limiting. To define θ_m as the half beamwidth angle seems indefinite, and some initial calculations of the data with this assumption provided inconsistent values.

The approach used was to work the problem in reverse and determine what θ_m should be. Flight 4 provides the data for making such a determination because on flight 4 nine runs of data were obtained with 100 nsec pulse, and nine runs of data were obtained with a 20 nsec pulse. Even though all runs were at the same altitude and over the same ocean area, it is evident from the data that the received power is functionally related to the pulsewidth.

By comparing the average received power for the two pulse widths we can determine θ_m

If

P_{R_1} = average received power 100 nsec pulse

P_{R_2} = average received power 20 nsec pulse

From the data of flight 4

$$P_{R_1}/P_{R_2} = 4 \tag{5-9}$$

Note here that if the functional relation were proportional to pulse width (τ), then the above ratio should be five rather than four. This indicates that the transistion between pulse limiting and beam limiting at an altitude of 5000 ft occurs somewhere between 20 and 100 μsec. By letting the radar range equations for P_{R_1} and P_{R_2} take the corresponding limiting relations

$$P_{R_1} \sim \theta_m^2/h^2 \tag{5-10}$$

$$P_{R_2} \sim c\tau/h^3, \tag{5-11}$$

we then obtain

$$\theta_m^2 = 4\, c\tau/h. \tag{5-12}$$

This gives a value of

$$\theta_m = 7^o. \tag{5-13}$$

The effective half beamwidth (3 dB) can be computed from the measured beamwidth by assuming a Gaussian distribution and summing the exponents.

$$\frac{1}{\theta_e} = \frac{1}{\theta_{H1}} + \frac{1}{\theta_{H2}} + \frac{1}{\theta_{E1}} + \frac{1}{\theta_{E2}}$$

and

$$\theta_e = \frac{\theta_{H1}\,\theta_{H2}}{\theta_{H\theta} + \theta_{H2}} + \frac{\theta_{E1}\,\theta_{E2}}{\theta_{E1}\,\theta_{E2}} \tag{5-14}$$

where θ_{H1}, θ_{H2}, θ_{E1}, θ_{E2} are half the 3 dB beamwidths measured from the antenna patterns and are equal to 5°, 6.5°, 4.3°, and 6° respectively.

Performing this computation,

$$\theta_e = 2.5^o. \tag{5-15}$$

Comparing this to $\theta_m = 7^o$, we see that the effective angle where beam limiting occurs is much greater than the 3 dB angle.

5.1.2 Maximum Value of σ^o at Vertical Incidence

If we assume that the scattering surface is a flat plate, normal to the transmission and of infinite dimensions (see Figure 5-7), and that the energy impinging upon the flat plate is all reflected to the source, we then can compute the maximum value of σ^o. The radar range equation for the above assumptions becomes:

$$P_R = \frac{P_T G^2 \lambda^2}{(4\pi)^2 4h^2 L}. \tag{5-16}$$

The symbols are the same as previously defined.

This is the equivalent of a transmission and reception one way over a distance 2 h, twice the altitude.

The comparable range equation for a reflected surface is:

$$P_R = \frac{P_T G^2 \lambda^2 \sigma^o A}{(4\pi)^3 h^4 L}. \tag{5-17}$$

Combining equation 5-16 and 5-17 we get

$$\sigma^o = \pi h^2/A. \tag{5-18}$$

The maximum value of A is $\pi h^2 \theta_m^2$ for the beam limited condition, and therefore

$$\sigma^o = 1/\theta^2. \tag{5-19}$$

For the previously obtained value of $\theta_m = 7°$, we obtain a value of

$$\sigma^o = 18.3 \text{ dB}. \tag{5-20}$$

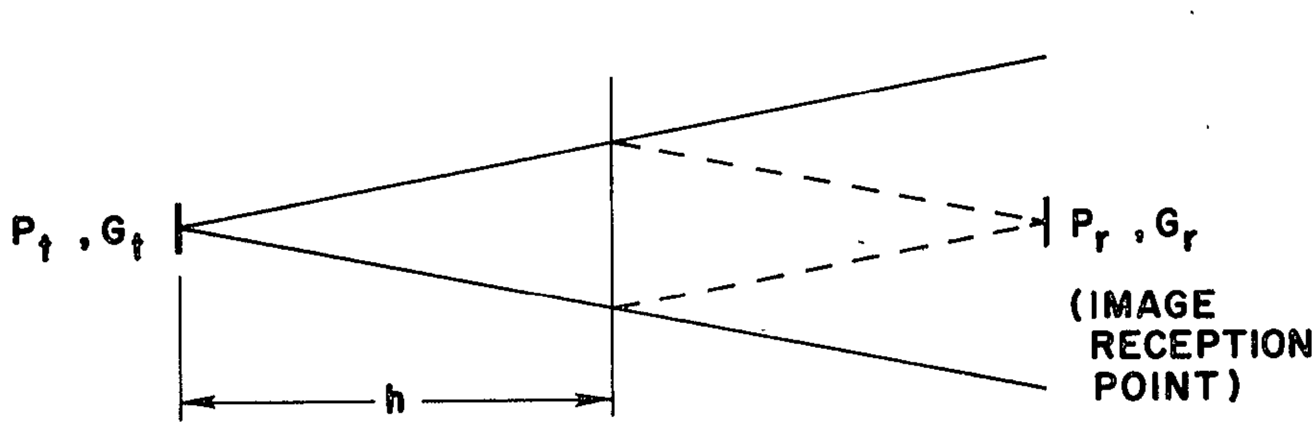

Figure 5-7. Computation of Maximum Value of σ^o

A similar value for the pulse limited condition is obtained, but the computation must be based on a plate of finite dimensions, and the two way path must be taken into account.

5.1.3 Calibration

The values of received and transmitted power used in the computation of σ^o were obtained from oscilloscope photographs. Calibrations of scope deflection voltage as a function of received power (Figure 5-8) were made for the two receivers. Calibrations of detected power level from the transmitted output were also made.

The losses in the system were primarily waveguide and cable losses (Table 5-2). An additional loss factor associated with the antenna pattern was also included (Table 5-3). This pattern loss is due to the peak of the pulse occurring at an angle away from the beam center. In general the values associted with the pattern loss are small enough to be negligible when considering the variability of the data.

The other factor involved in calibration is the antenna gain. Antenna pattern measurements were made with an aircraft mockup. The results of these measurements were used to compute the gain. Table 5-4 is a summary of antenn characteristics.

An overall check on calibration was obtained by flying the aircraft over the Ground Support Equipment (GSE). In this instance the GSE received the signal and the value of the received power was recorded. The GSE then transponded the pulse and transmitted to the aircraft where it was again recorded. Measurements made in this fashion served as a check on the system gains and losses which had been independently calibrated. The operational requirements of this technique were not fully developed. It is felt that coordination and synchronization of the aircraft, radar, and GSE operation must be automated to a considerable degree in order to improve the reliability of this method of calibration.

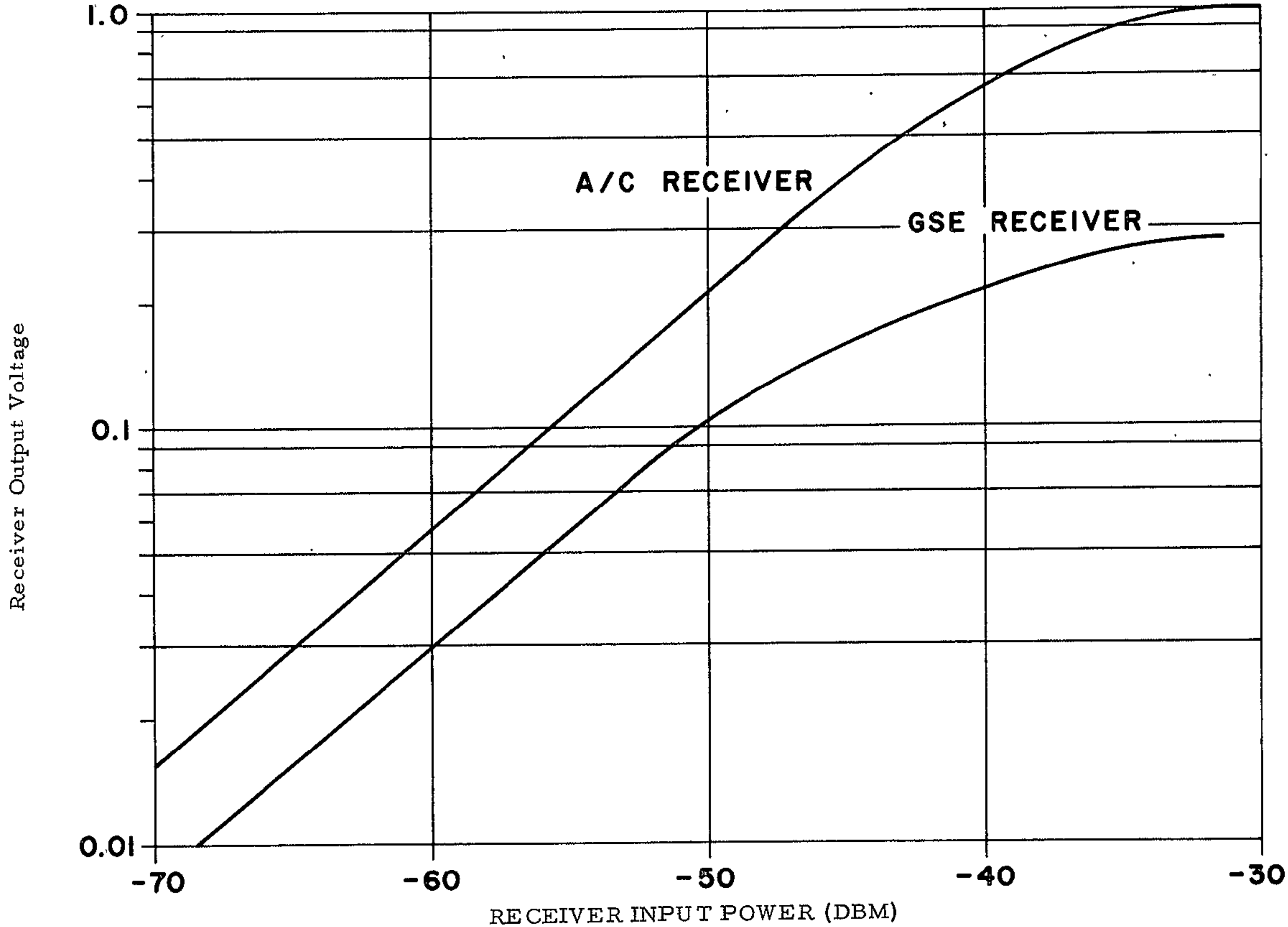

Figure 5-8. Receiver Calibration Curves

Table 5-2. Measured Losses

Transmitter waveguide and coaxial losses		
a.	coaxial from TWT to output coupler	1.2 dB
b.	waveguide loss from attenuation output to transmitter antenna	2.0 dB
c.	insertion loss of variable attenuation	0.5 dB
Receiver waveguide, waveguide switch and all coaxial, flexguide, etc., in both parallel and crossed polarized modes		2.0 dB
Total Losses		5.7 dB

Table 5-3. Pattern Losses

Pulsewidth τ (μsec)	Altitude h (ft)	Loss (dB)
10	5000	0.3
20	5000	0.6
	10000	0.3
	15000	0.2
	20000	0.15
100	5000	3.0
	10000	1.5
	15000	1.0
	20000	0.75

Table 5-4

Antenna Characteristics

f = 9 GHz

Transmitting Antenna - Aircraft	
Beamwidth - H Plane	0.0°
Beamwidth - E Plane	8.5°
Gain	25.2 dB
Receiving Antenna - Aircraft	
Beamwidth - H Plane	13°
Beamwidth - E Plane	12°
Gain	22.1 dB
GSE Antennas	
Beamwidth - H Plane	18°
Beamwidth - E Plane	18°
Gain	18.9 dB

5.2 Pulse Shapes

5.2.1 Theoretical

Before discussing the actual results of return pulse shapes it is necessary to discuss what the expected pulse should look like. Pulse shapes for various pulsewidths, altitudes and σ^o were used to compute the expected waveforms (Figures 5-9, 5-10, 5-11). All waveforms are normalized so that comparisons of the wave shape can be readily made.

Figure 5-9 is based on antenna beamwidth of 6 degrees. The pulse shape corresponding to 100 nsec and 5,000 ft is clearly beam limited, whereas at 20 nsec and 20,000 ft the pulse shape is clearly pulse limited.

Figure 5-10 is for a beamwidth of 12 degrees and the distinction between pulse limiting and beam limiting is less pronounced. As will be seen, the actual pulse shape data more closely resembles the 12 degree beamwidth.

Figure 5-11 is a plot of pulses of 20 nsec width at altitudes 20,000 and 10,000 ft. The pulses are normalized and a σ_o factor is introduced which is based on curves by Moore and Schooley (Figure 5-5). The pulse shape changes very little as a function of changes in σ_o.

5.2.2 Measured Pulse Shapes

Figures 5-12 through 5-37 are actual photographs of multiple pulse returns under various ocean conditions, altitudes, pulse widths, etc. A sampling of the more than 10,000 frames taken is used here to show some significant features.

It first must be pointed out that these are reproductions of reproductions and at each step much information is lost. In fact, the reproductions of the single pulse traces were not visible at all even though they were visible on the original negatives.

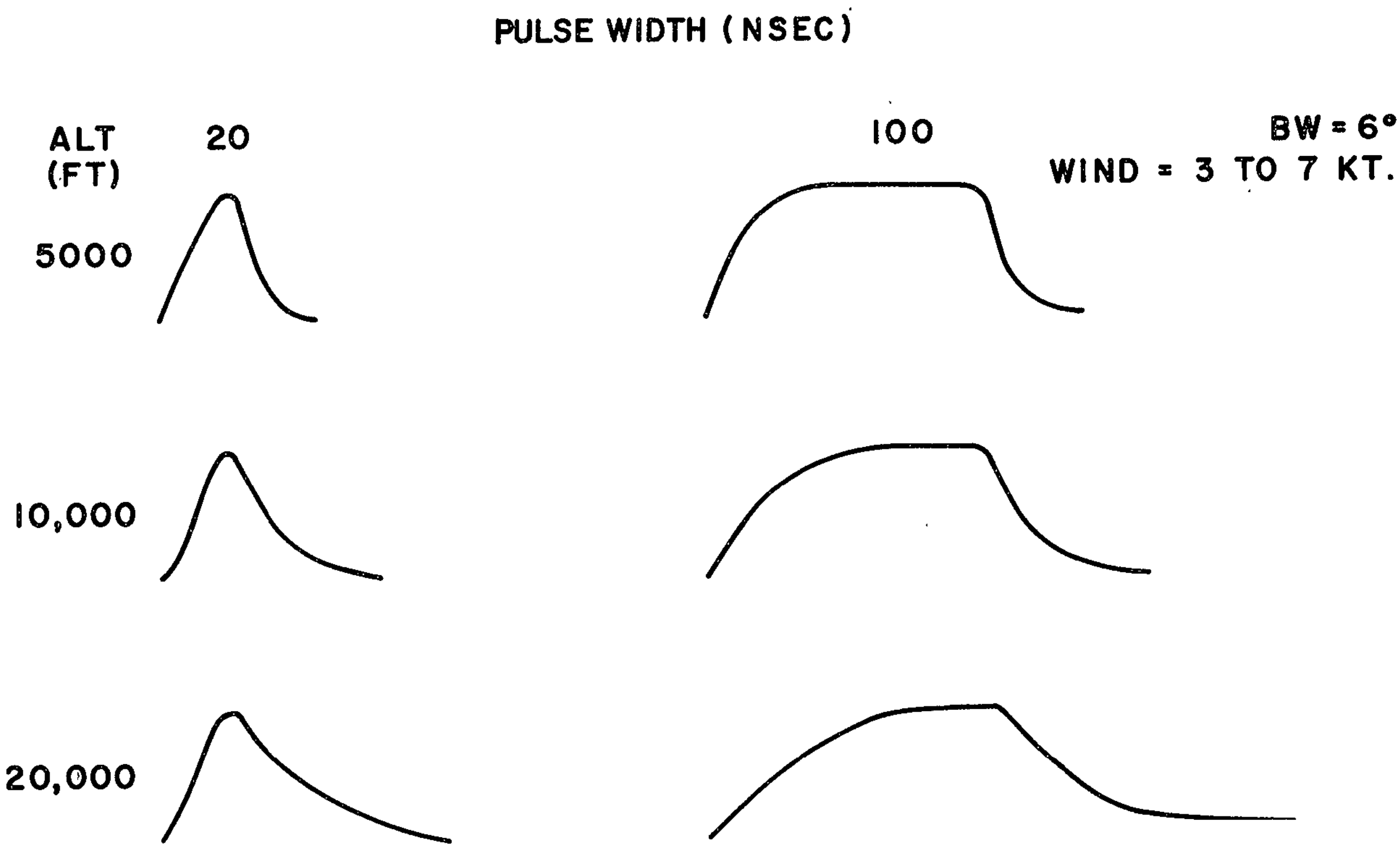

Figure 5-9. Expected Waveforms at BW = 6°, Wind 3-7 Kts

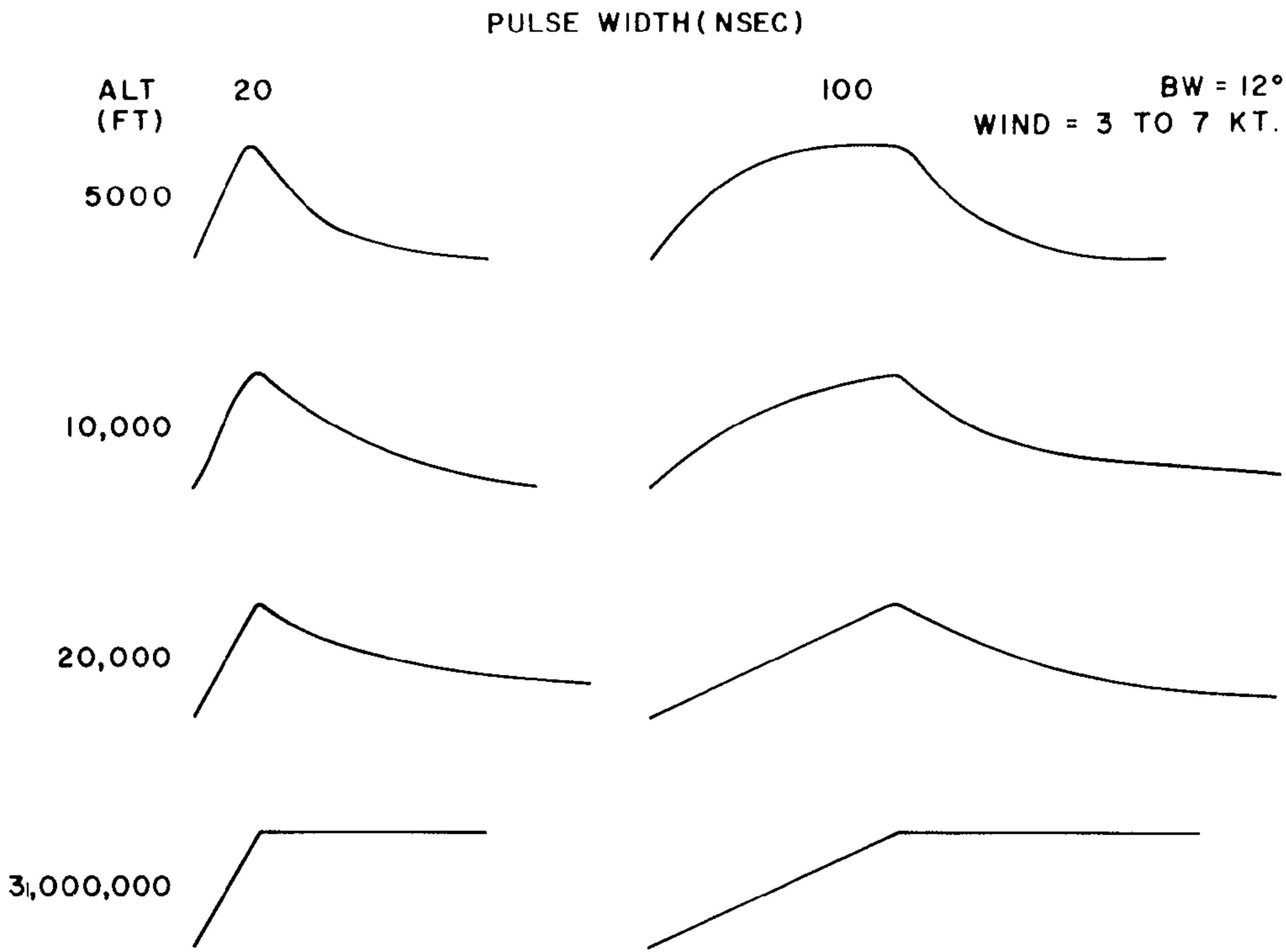

Figure 5-10 Expected Waveforms at BW = 12°, Wind 3-7 Knts

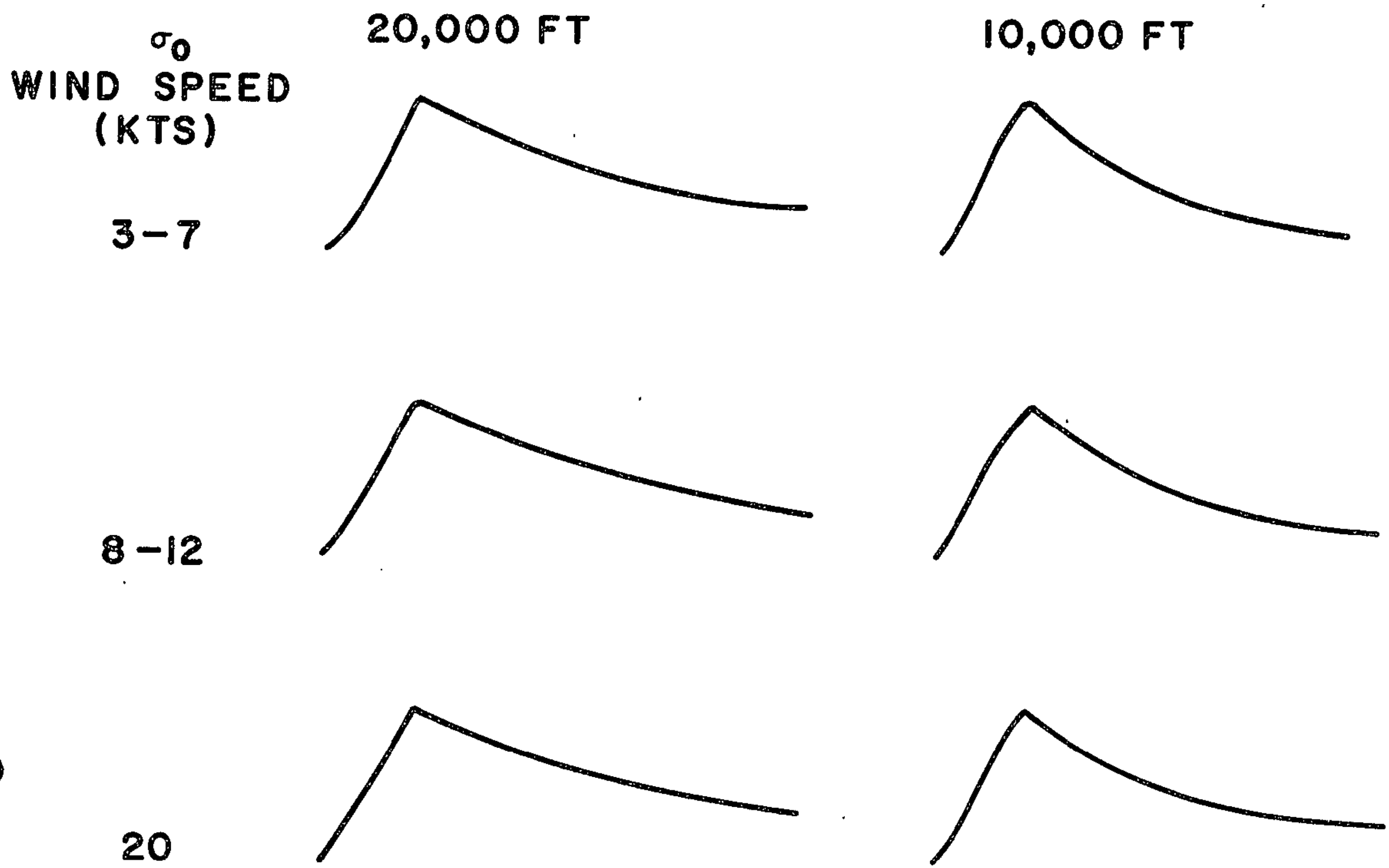

Figure 5-11. Expected Waveforms at Various Wind Velocities and Altitudes

Generally the frames were taken one second apart. It was clear that there was little variation from frame to frame. The sweep speed in all cases was 50 nsec/cm. Selected frames are shown in the following figures:

Flight 4 (Figures 5-12 through 5-17) shows the difference between beam and pulse limiting. Figures 5-15 through 5-21 are based on a 100 nsec pulse where some evidence of a flat peak is visible. Figures 5-12 through 5-14 on the other hand are based on a 20 nsec pulse for the same conditions and here no flat peak exists.

Flight 5 (Figure 5-18 through 5-30) shows true pulse limiting as evidenced by the long trailing edge when the altitude of 10, 000 ft is used with a 20 nsec pulse. This should be compared with the expected values of Figure 5-10. Flight 7 (Figures 5-24, 5-25, and 5-26) shows increased pulse limiting at an altitude of 15, 000 ft for the same 20 nsec pulse. Flight 7 also shows the slight variations in exposure by using three values of pulses per frame (50, 147, and 278).

Flight 10 (Figures 5-27, 5-28) shows 10 nsec pulses over very calm water at 10, 000 ft.

Flight 14 presents a comparison between pulse shapes as a function of sea direction. Figure 5-30 is taken with the polarization of the transmission in the direction of the sea whereas Figure 31, Figure 5-32 and Figure 5-33 are at 90, 180, and 270 bearings with respect to sea direction. It is clear that wave shapes are not related to sea direction.

Flight 14 (Figure 5-34) also shows the results when reception is cross polarized from the transmission. The signal level here was into the noise indicating greater than 30 dB between direct and cross polarized returns.

The returns from ice at low altitude (2, 500 ft) are shown in Figure 5-35.

Figures 5-12 through 5-37. Flight Pulse Data

LEGEND

FLT:	Flight Number
RUN:	Data Run for That Flight
ALT:	Aircraft Altitude in Thousands of Feet
P/F:	Pulses Per Frame
PW:	Transmitted Pulse Width in Nanoseconds
BRNG:	Bearing

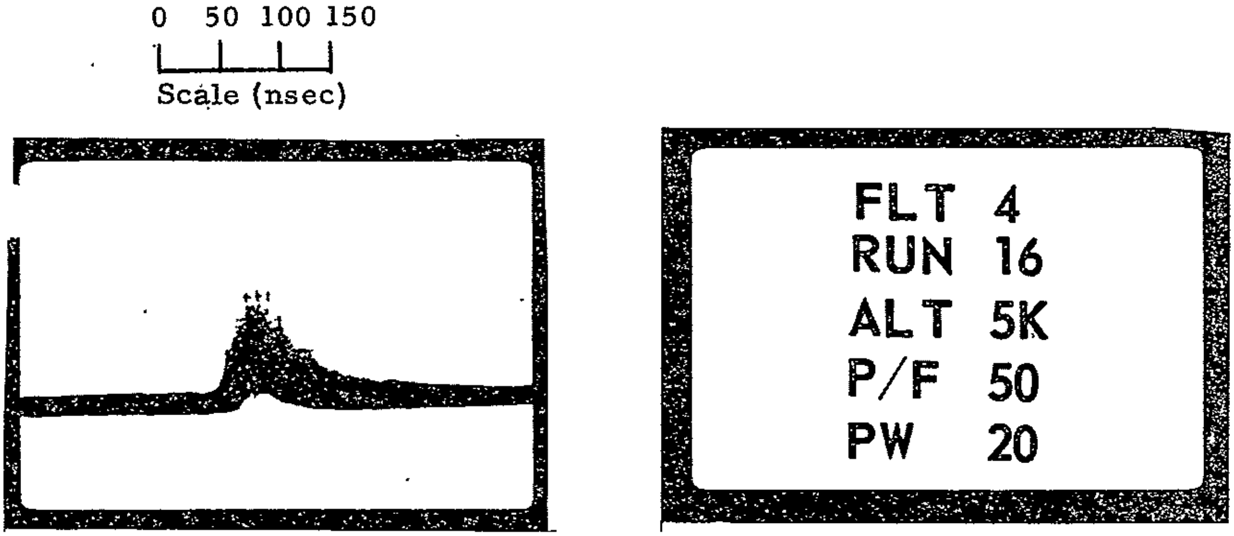

Figure 5-12

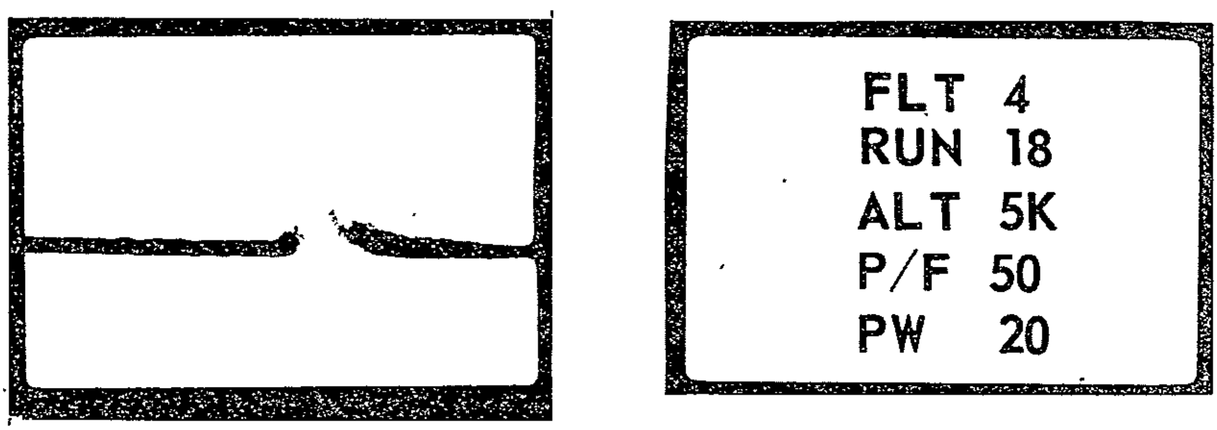

Figure 5-13

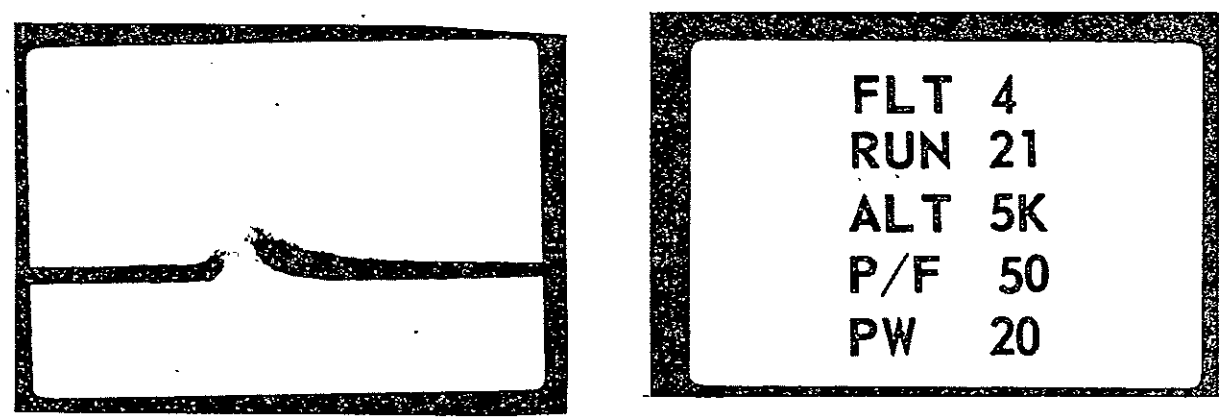

Figure 5-14

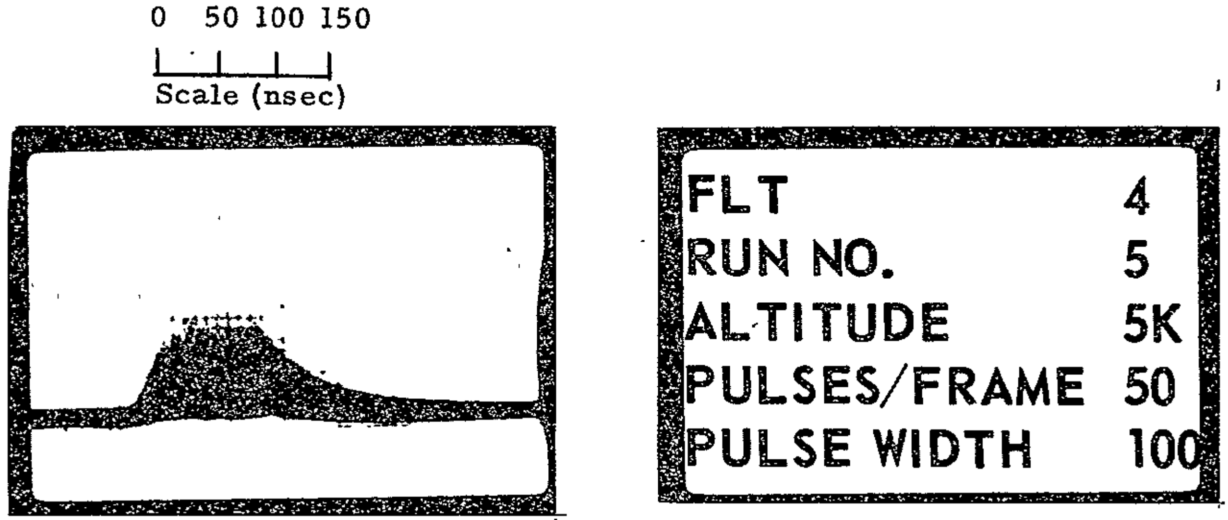

Figure 5-15

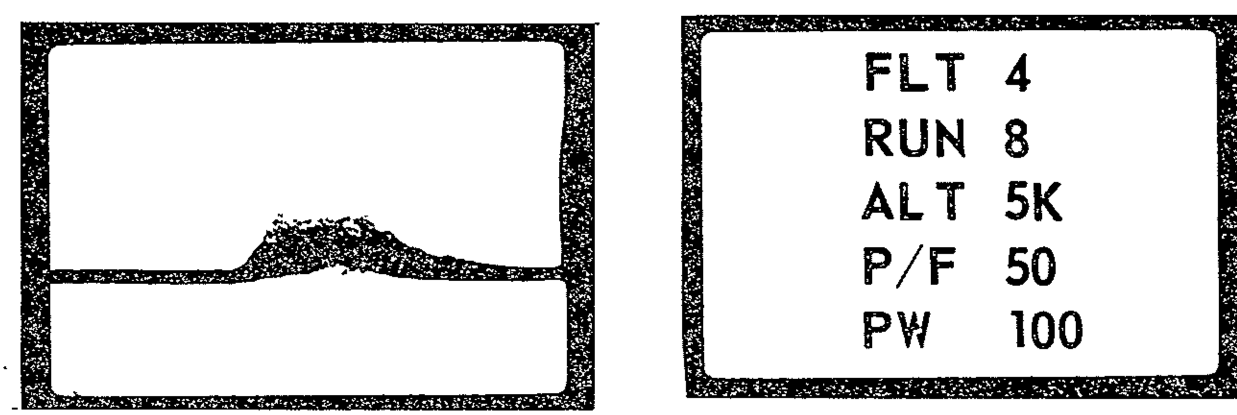

Figure 5-16

Figure 5-17

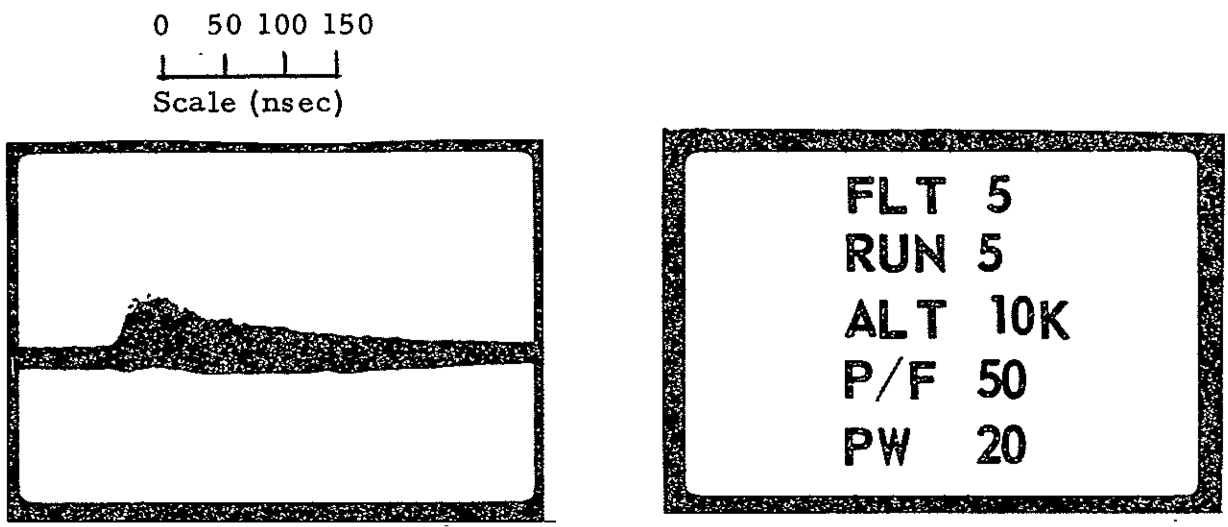

Figure 5-18

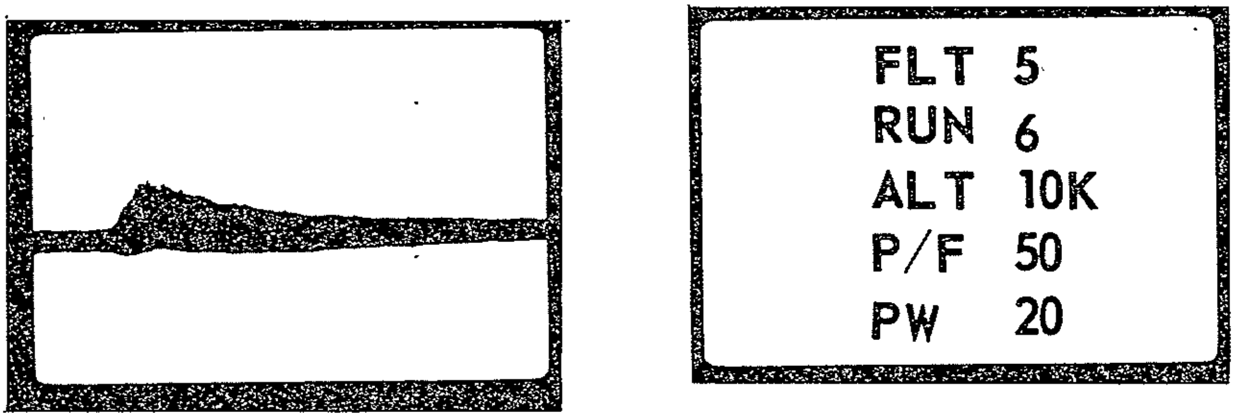

Figure 5-19

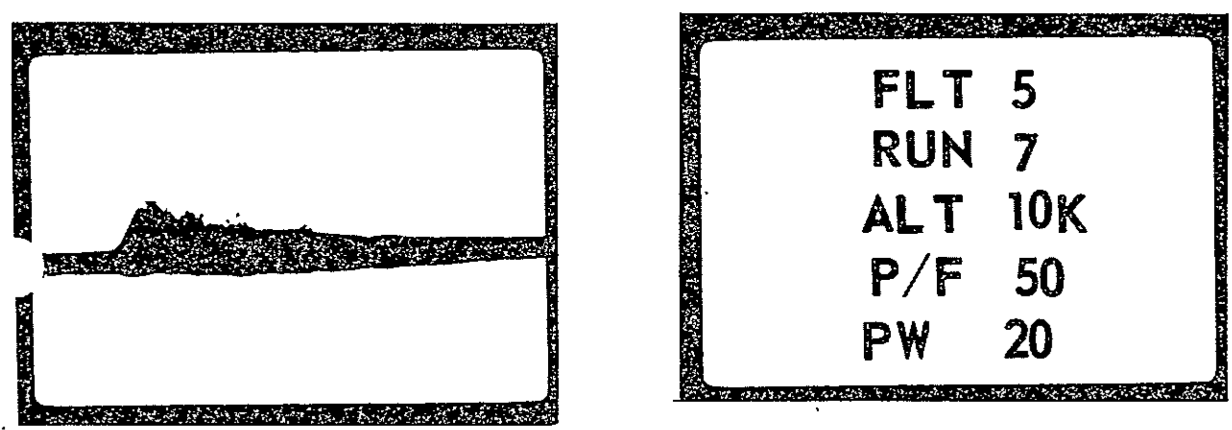

Figure 5-20

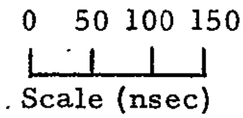

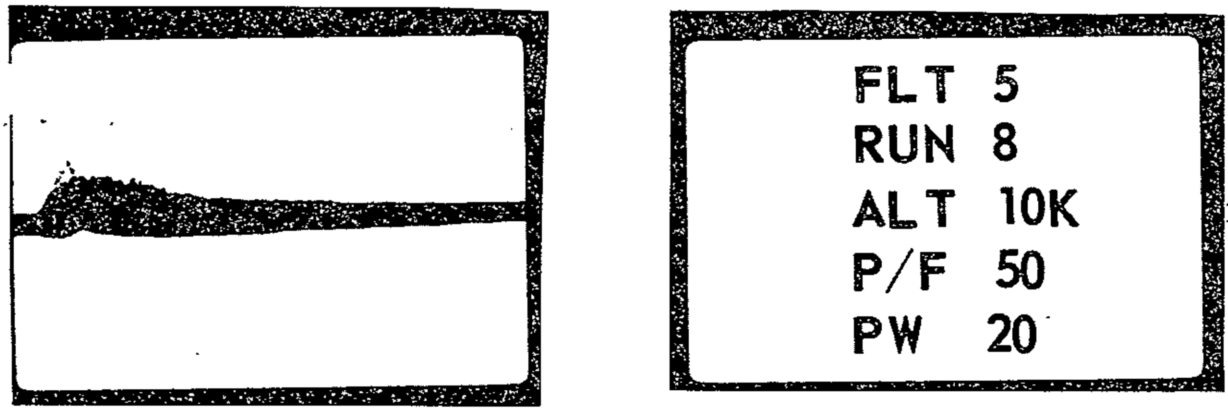

Figure 5-21

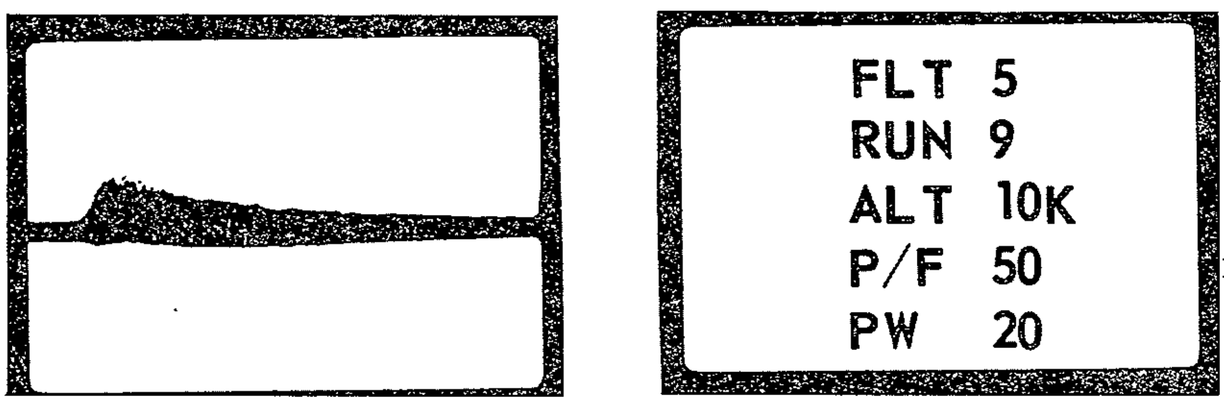

Figure 5-22

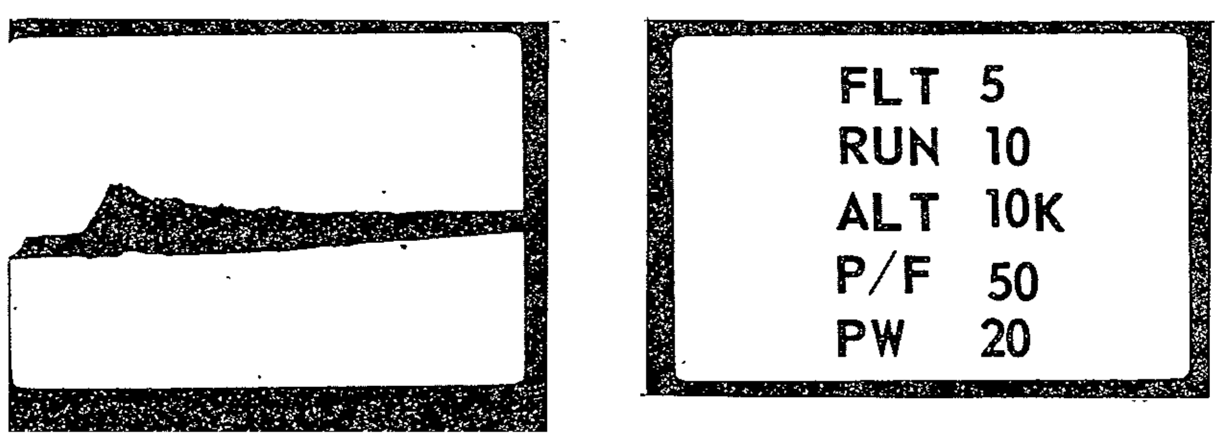

Figure 5-23

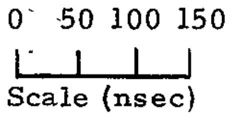

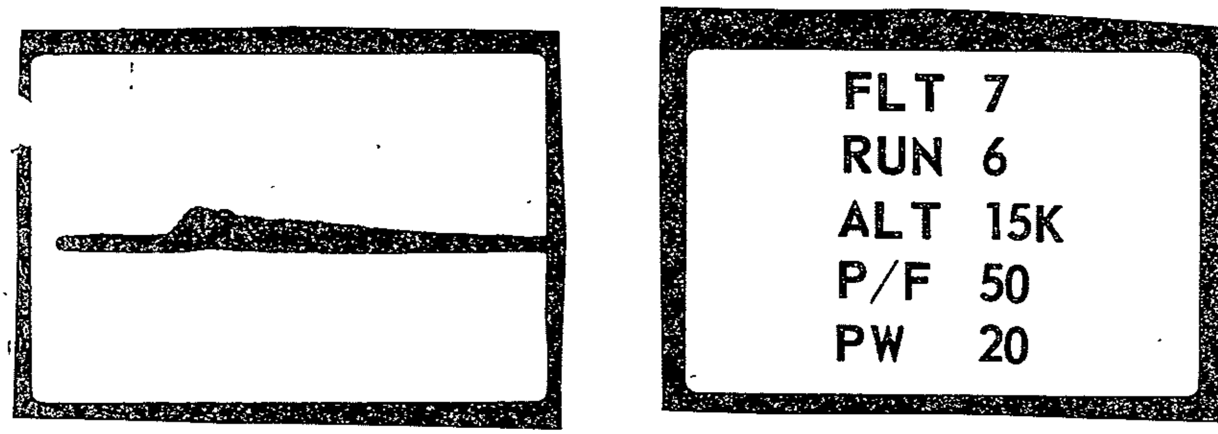

Figure 5-24

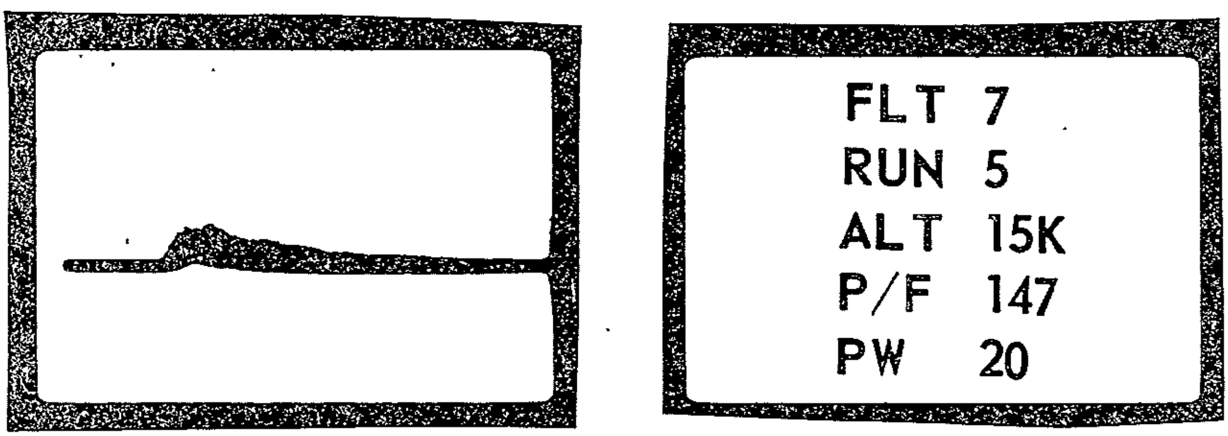

Figure 5-25

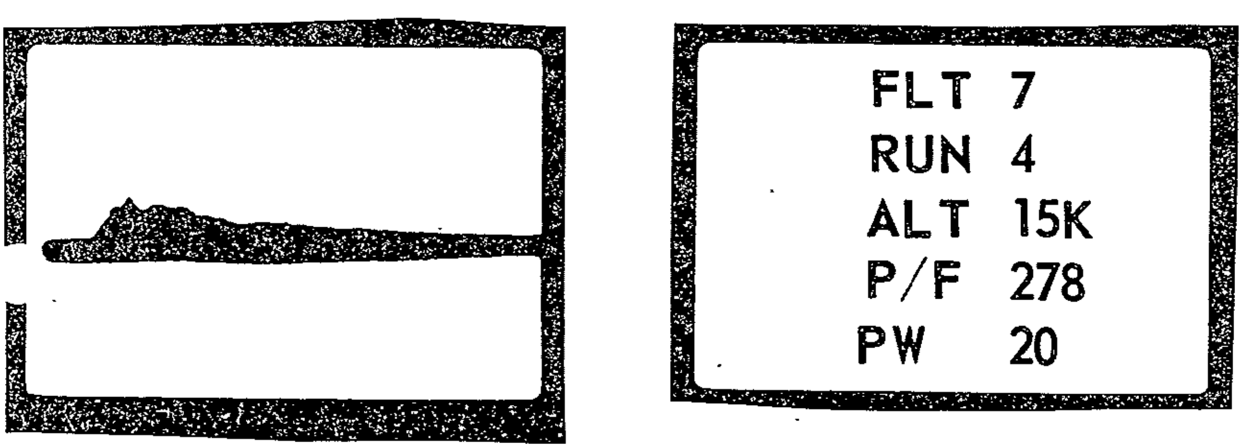

Figure 5-26

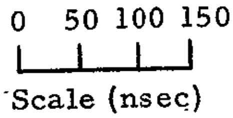

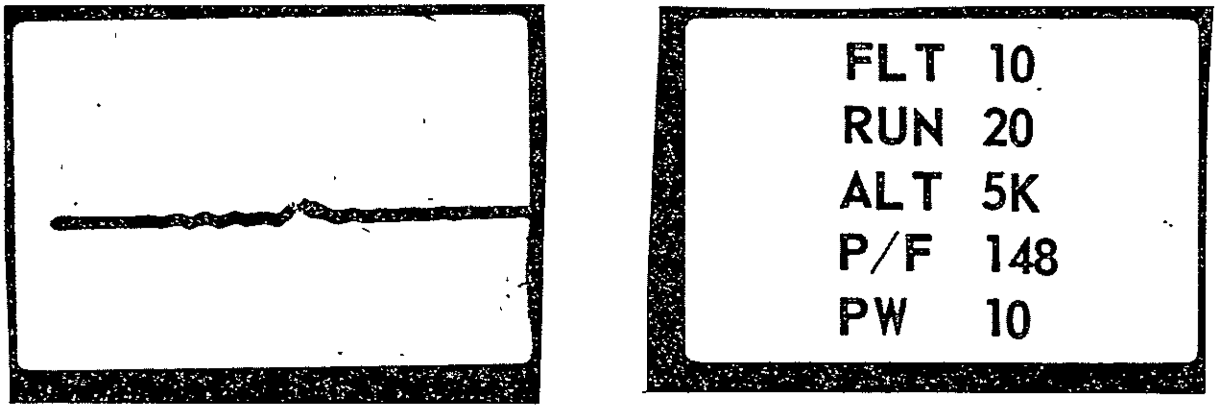

Figure 5-27

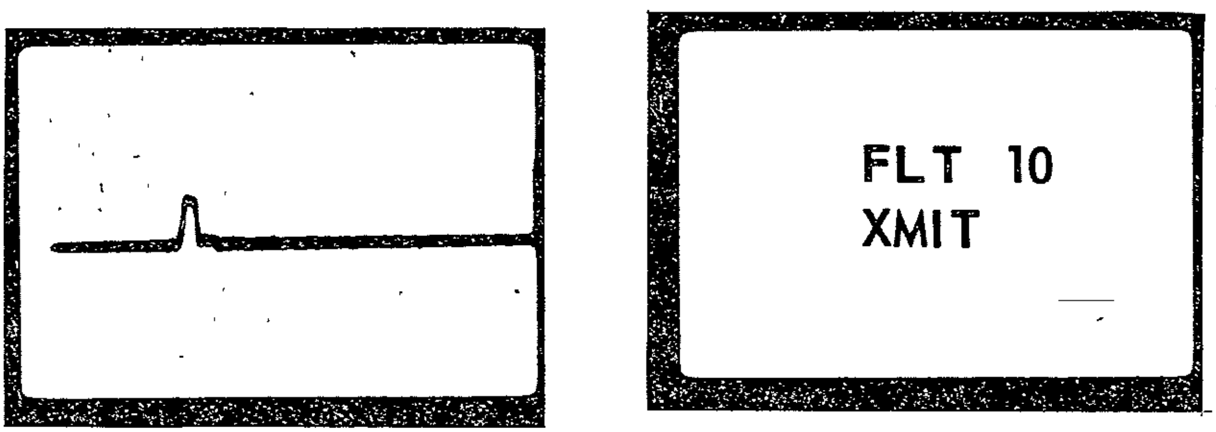

Figure 5-28

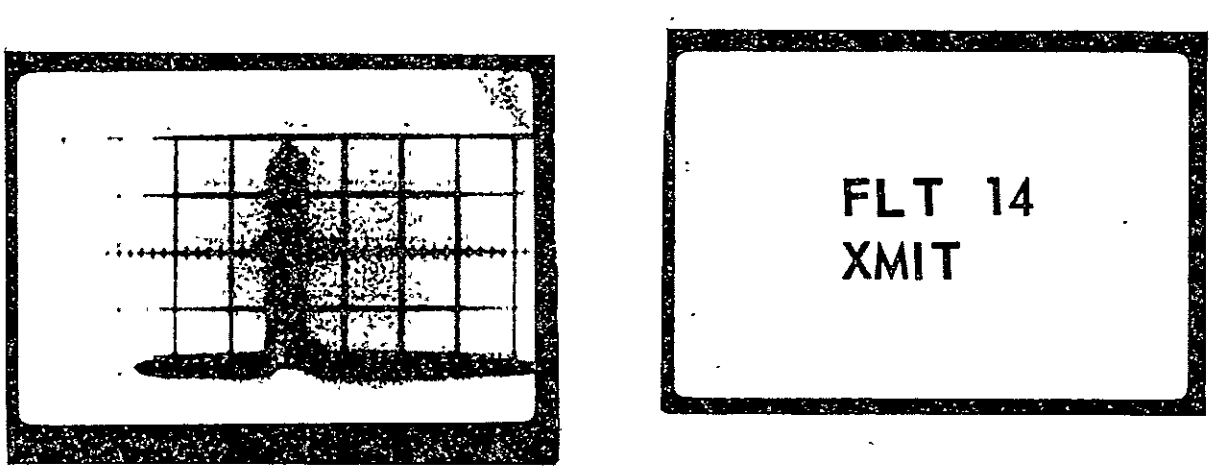

Figure 5-29

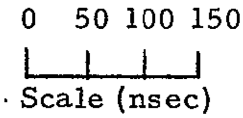

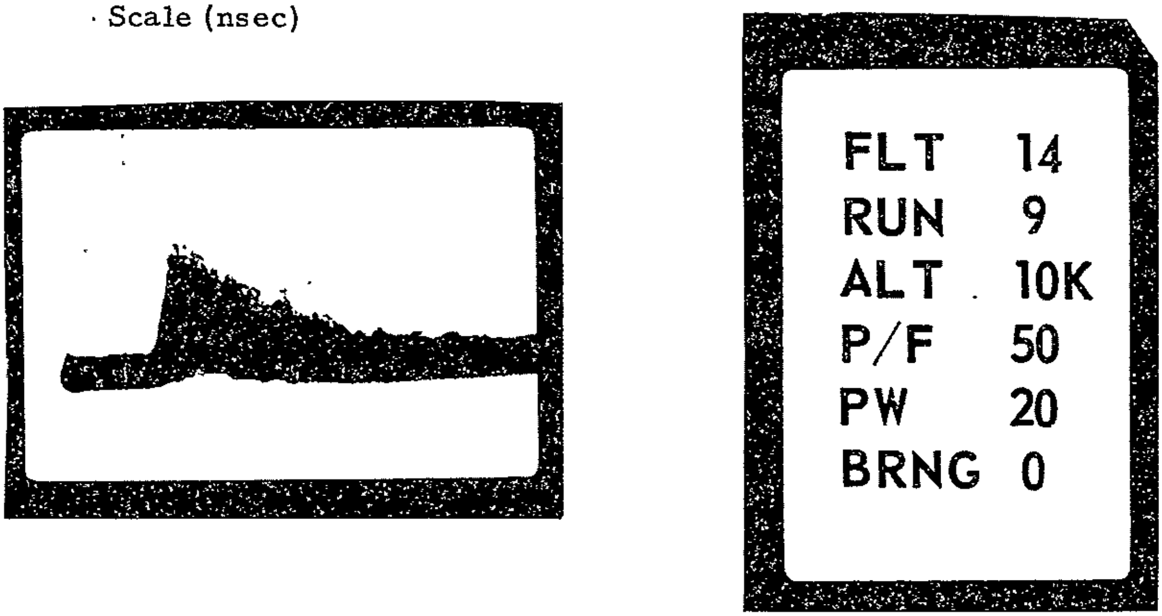

Figure 5-30

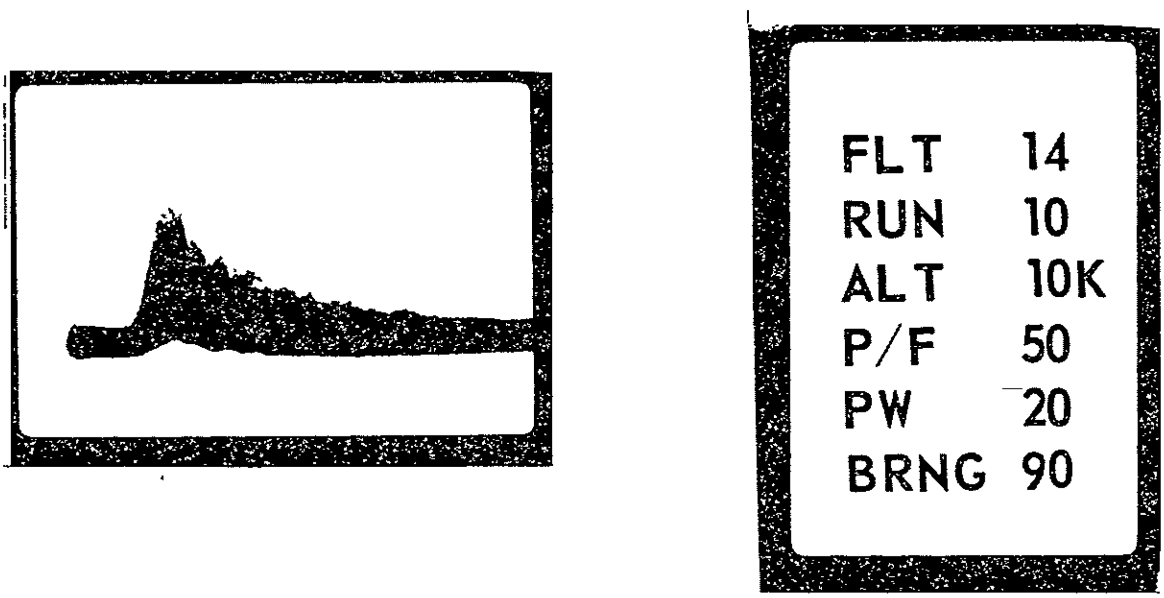

Figure 5-31

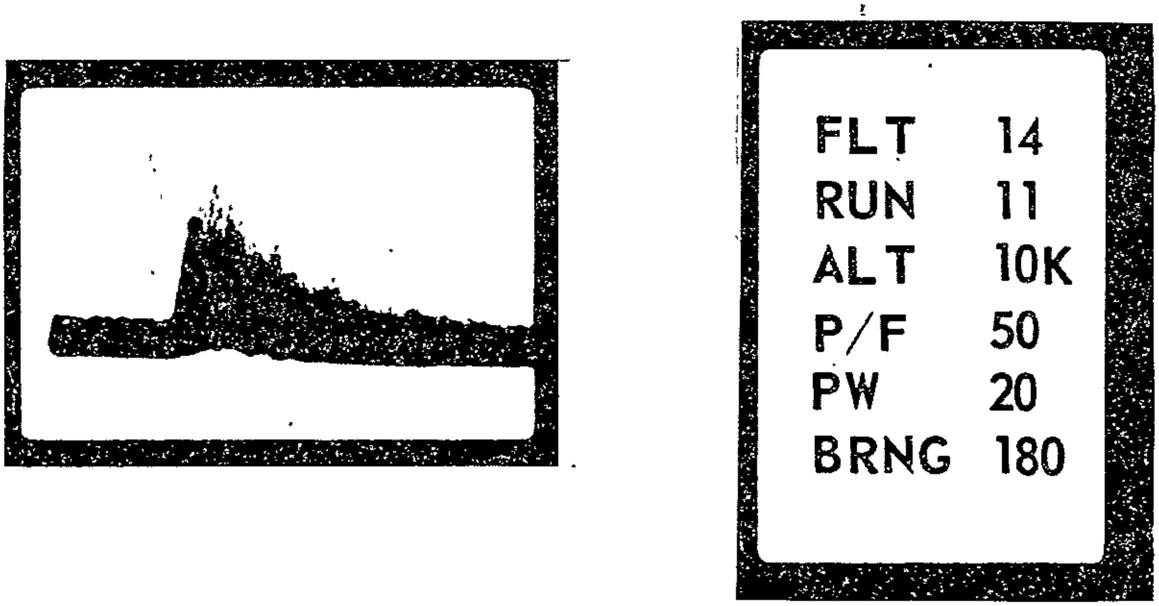

Figure 5-32

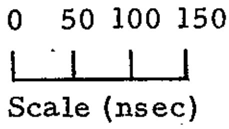

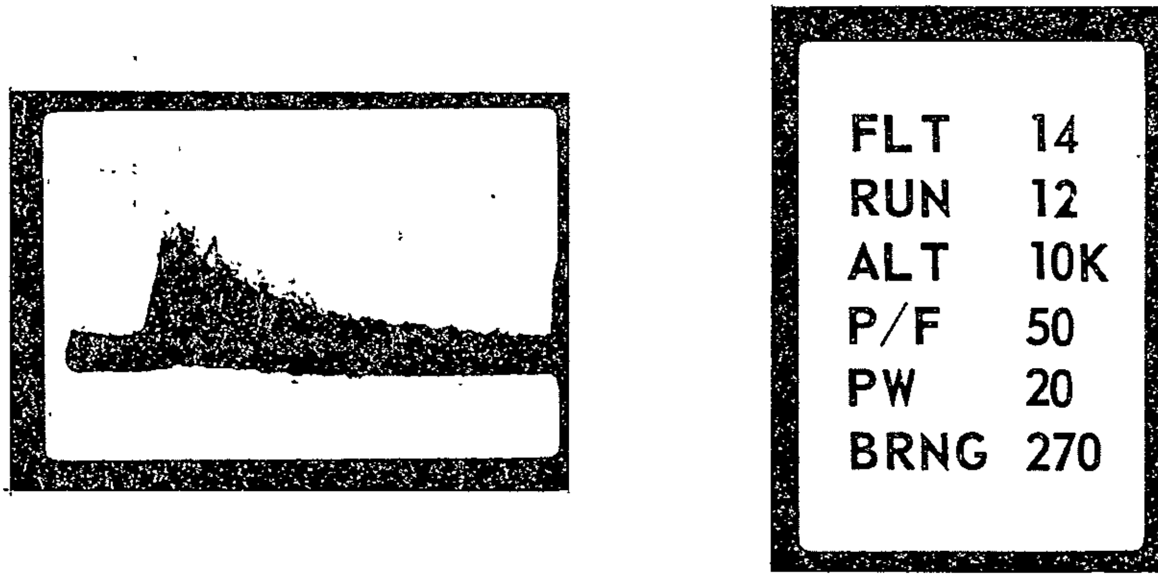

Figure 5-33

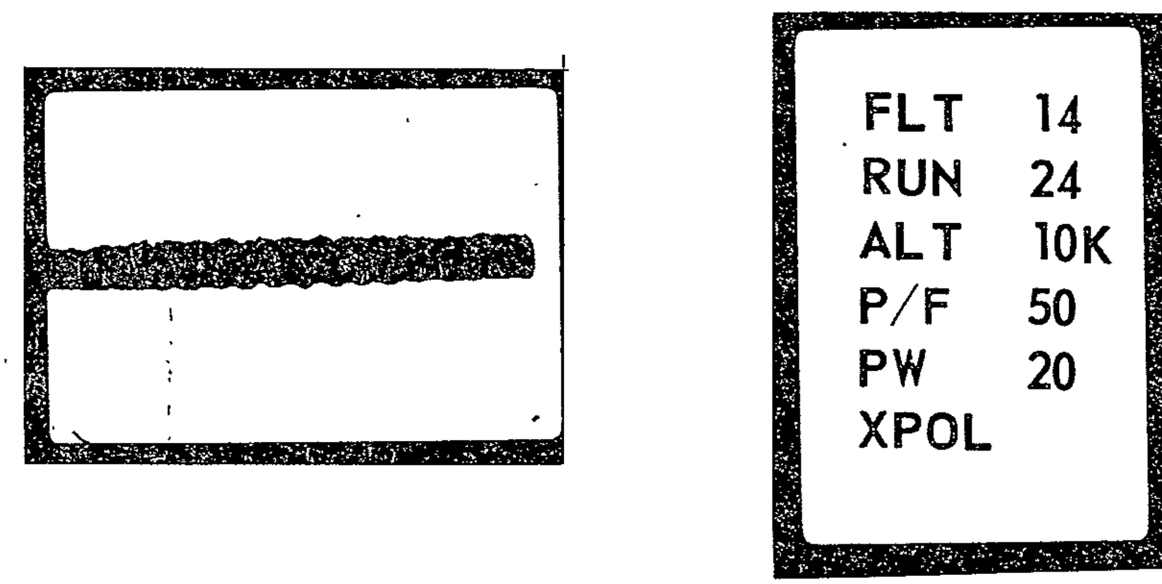

Figure 5-34

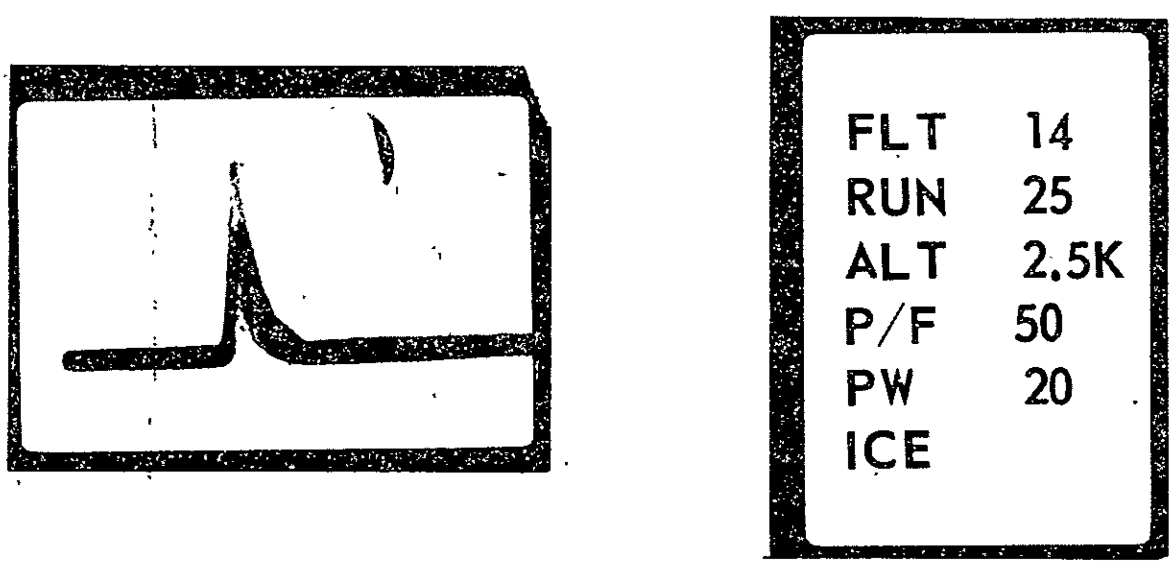

Figure 5-35

0 50 100 150

Scale (nsec)

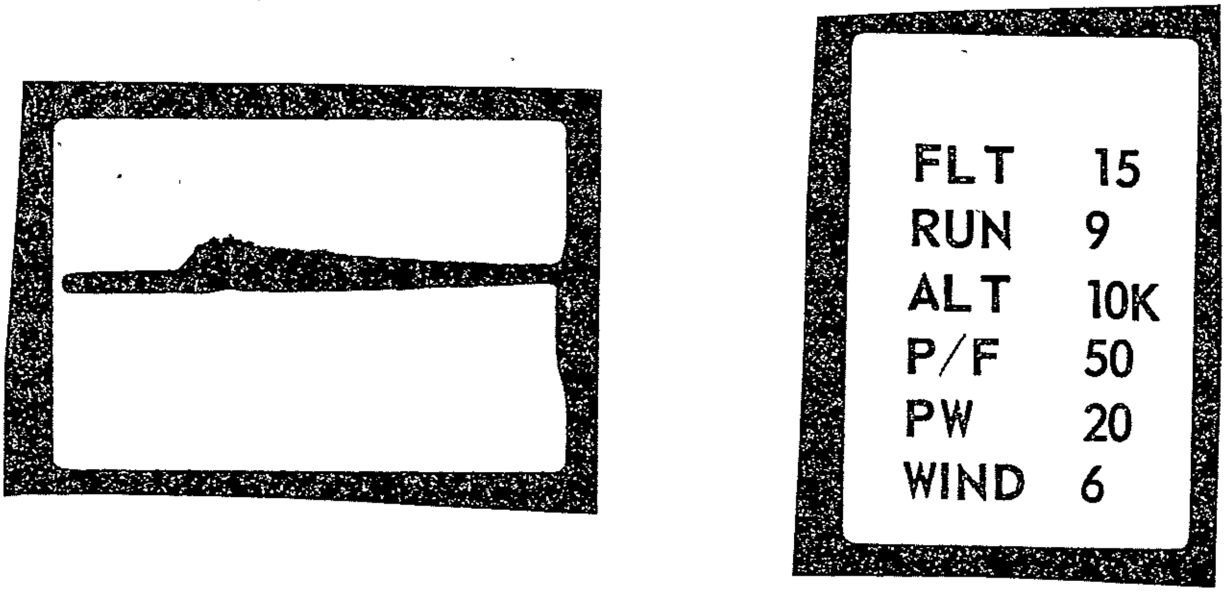

Figure 5-36

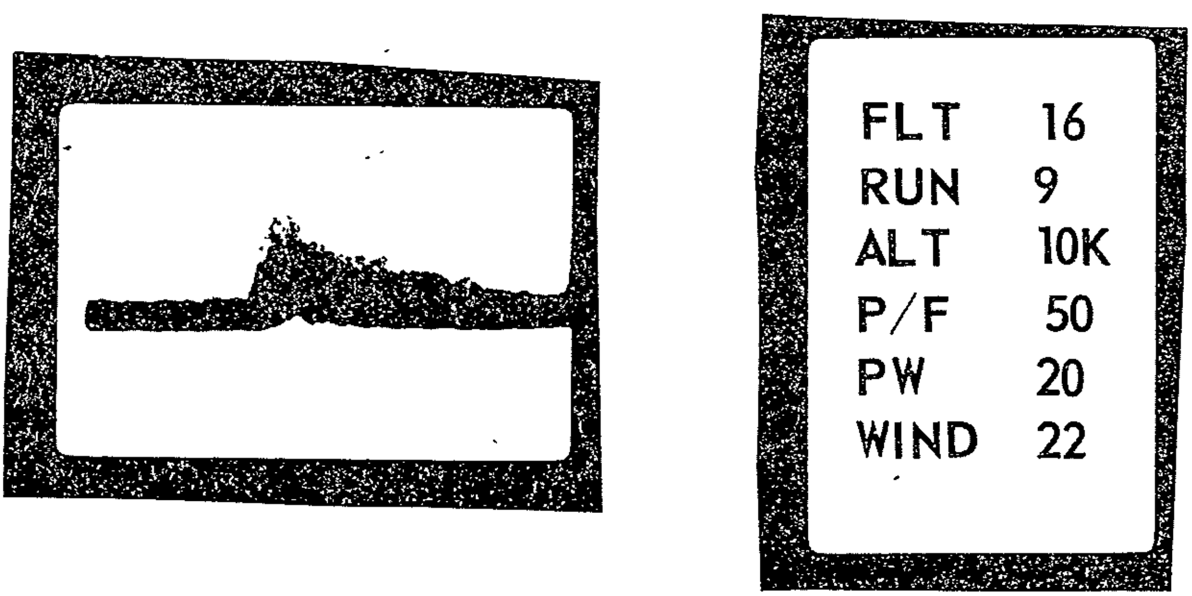

Figure 5-37

The pulse shapes of flights 14, 15, and 16 (Figures 5-33, 5-36, and 5-57) show that winds of 12, 6, and 22 knots, respectively, have little effect on pulse shape.

5.2.3 Individual Pulses

Figure 5-38 represents traces of individual pulses copied directly from the negatives. This procedure was necessary because the faint traces on the negatives were washed out in the reproduction process. Figure 5-39 represents 10 pulses per frame which are barely visible.

It is clear that considerable amplitude variations are visible in the individual pulses and that multiple traces are actually overlaps of individual traces. In general, the leading edges of the individual traces are fairly linear (see Appendix E) and peak at the pulse width. The trailing edges, however, show wide amplitude fluctuations.

5.3 Ocean Truth

Two methods were used to obtain ocean parameters on all flights - observations from a NASA ship stationed in the test area in the area, and Stilwell photographs. In addition, on flights 5 and 6, a Cessna aircraft from Office of Naval Research flew alongside with a laser profilometer aboard.

The ship observations were used in reducing the data because they represent the most complete available information. Comparisons of ship observations with the laser data on flight 5 (see Figure 5-40) show very good correspondence.

The Stilwell photographs (Figure 5-41) offer the greatest potential for ocean truth measurements because,when reduced, they provide a two dimensional spectral representation of the ocean. However, the techniques and computations associated with reducing the data require further development and evaluation before it becomes an acceptable ocean parameter measurement tool. Two photographs from flight 6 were reduced to provide the two dimensional ocean spectrums shown in Figures 5-42 and 5-43. These were in turn converted into line spectra along the dominant wave direction (see Figure 5-44).

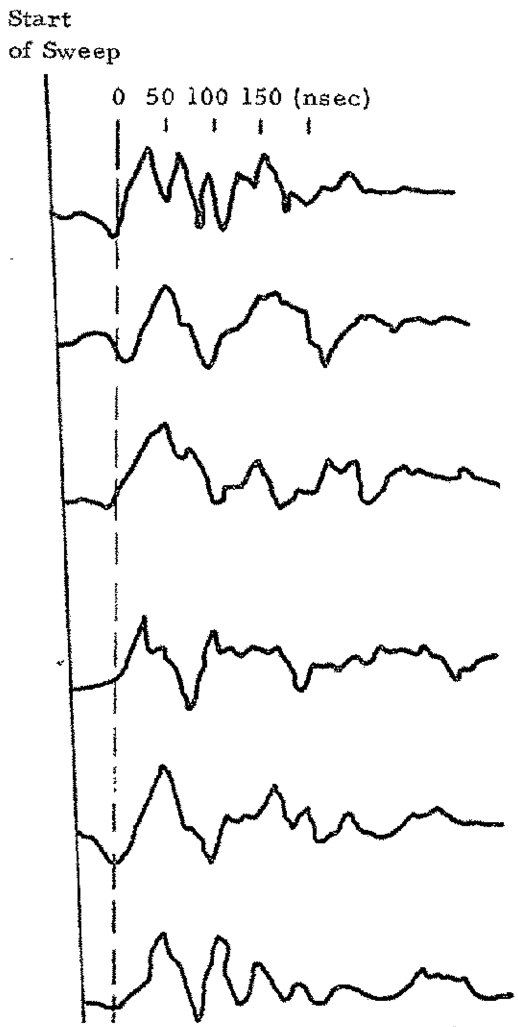

Figure 5-38. Single Pulse Returns, Flight 13

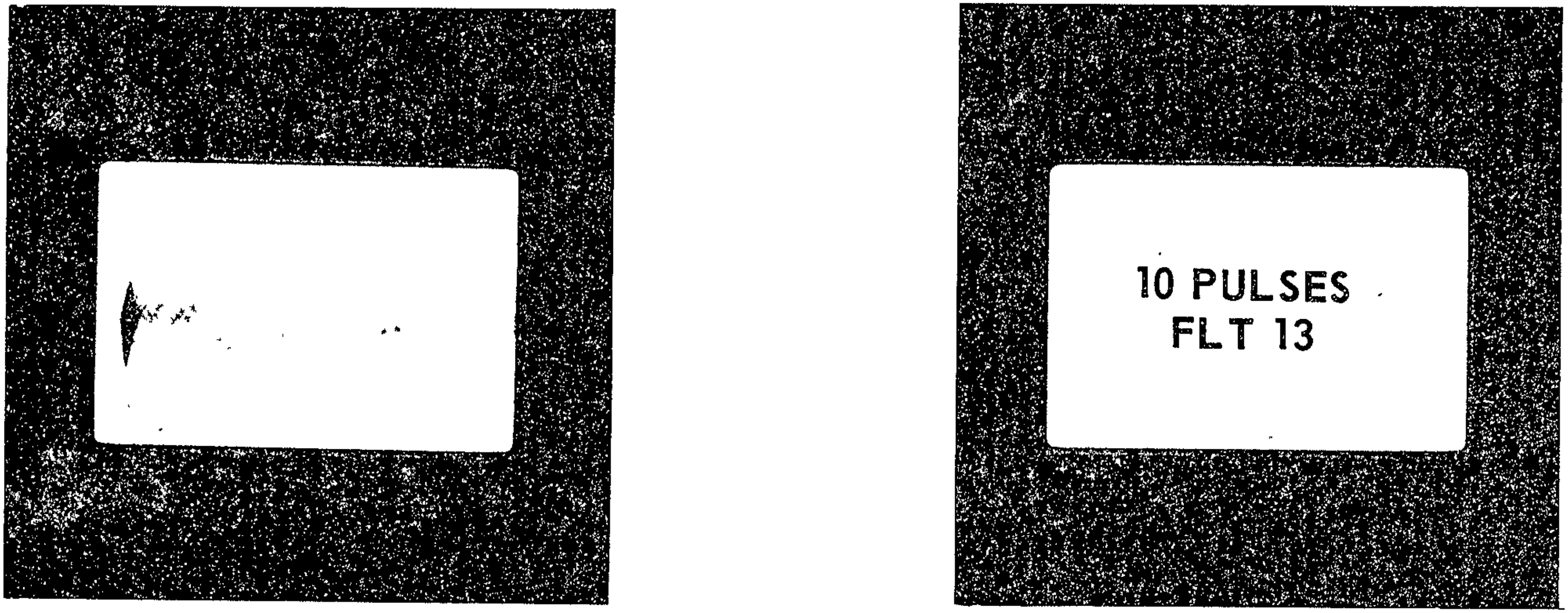

Figure 5-39. 10 Pulses, Flight 13

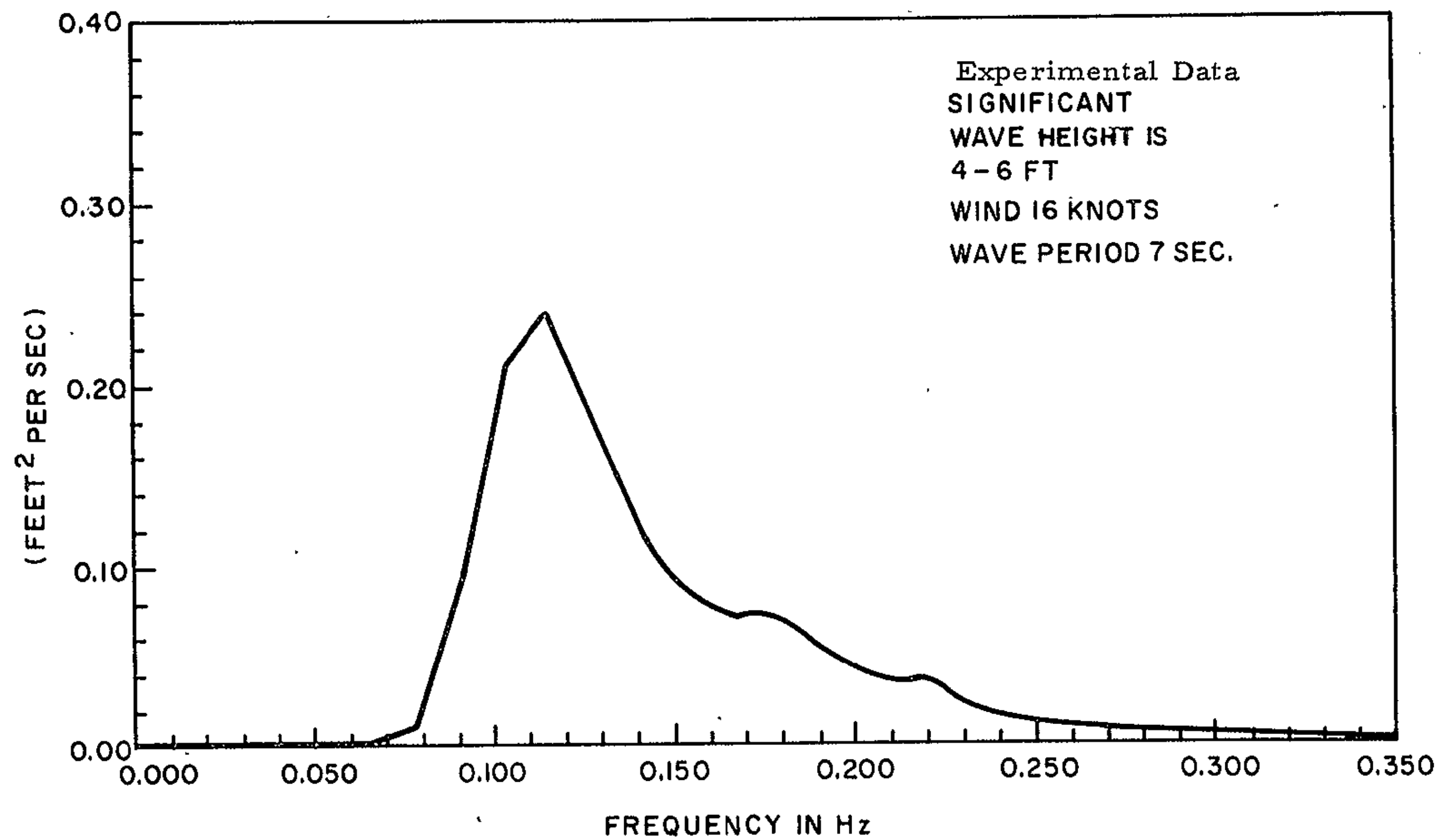

Figure 5-40. Laser Profilometer Data

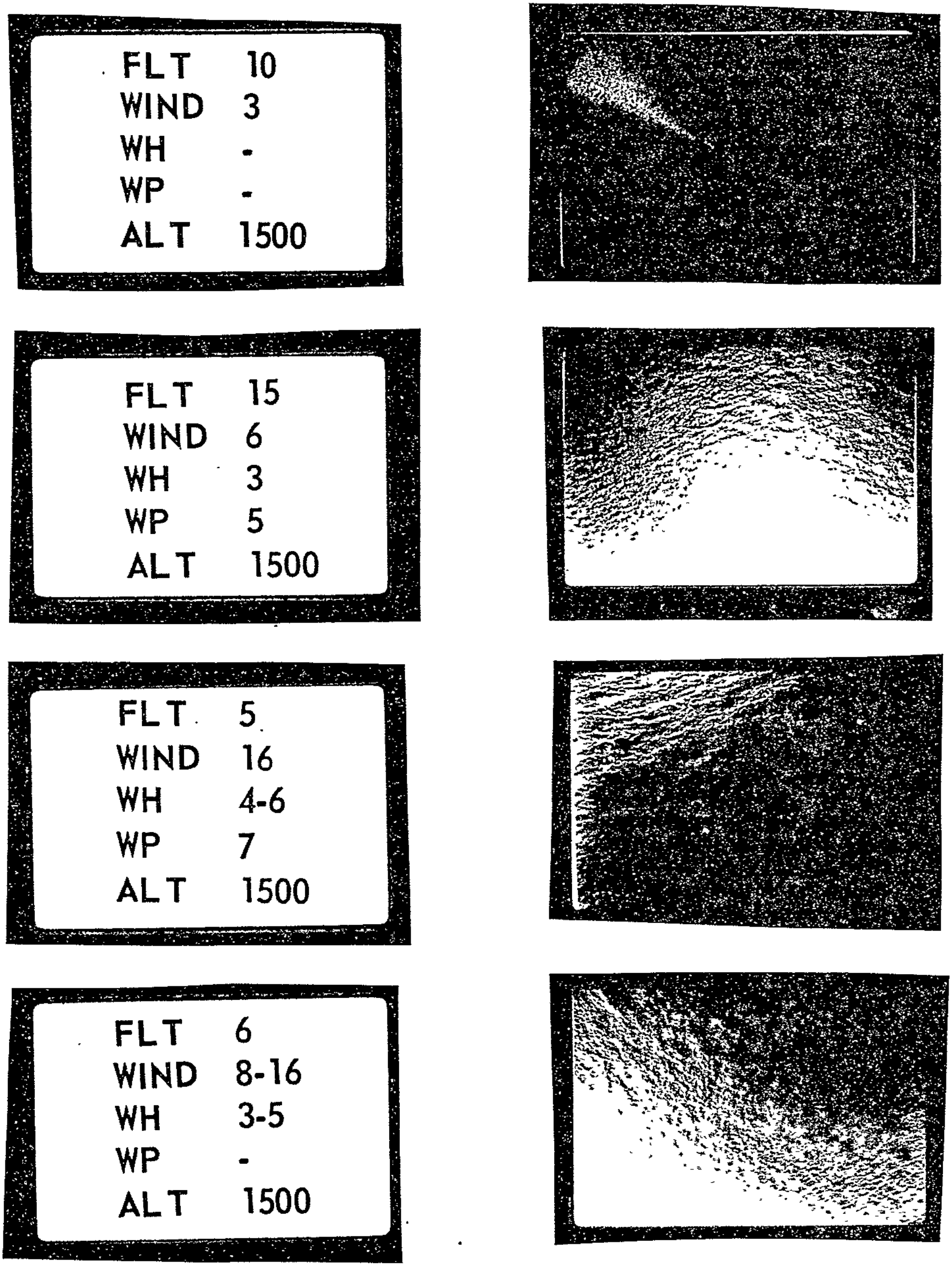

Figure 5-41. Stilwell Photographs

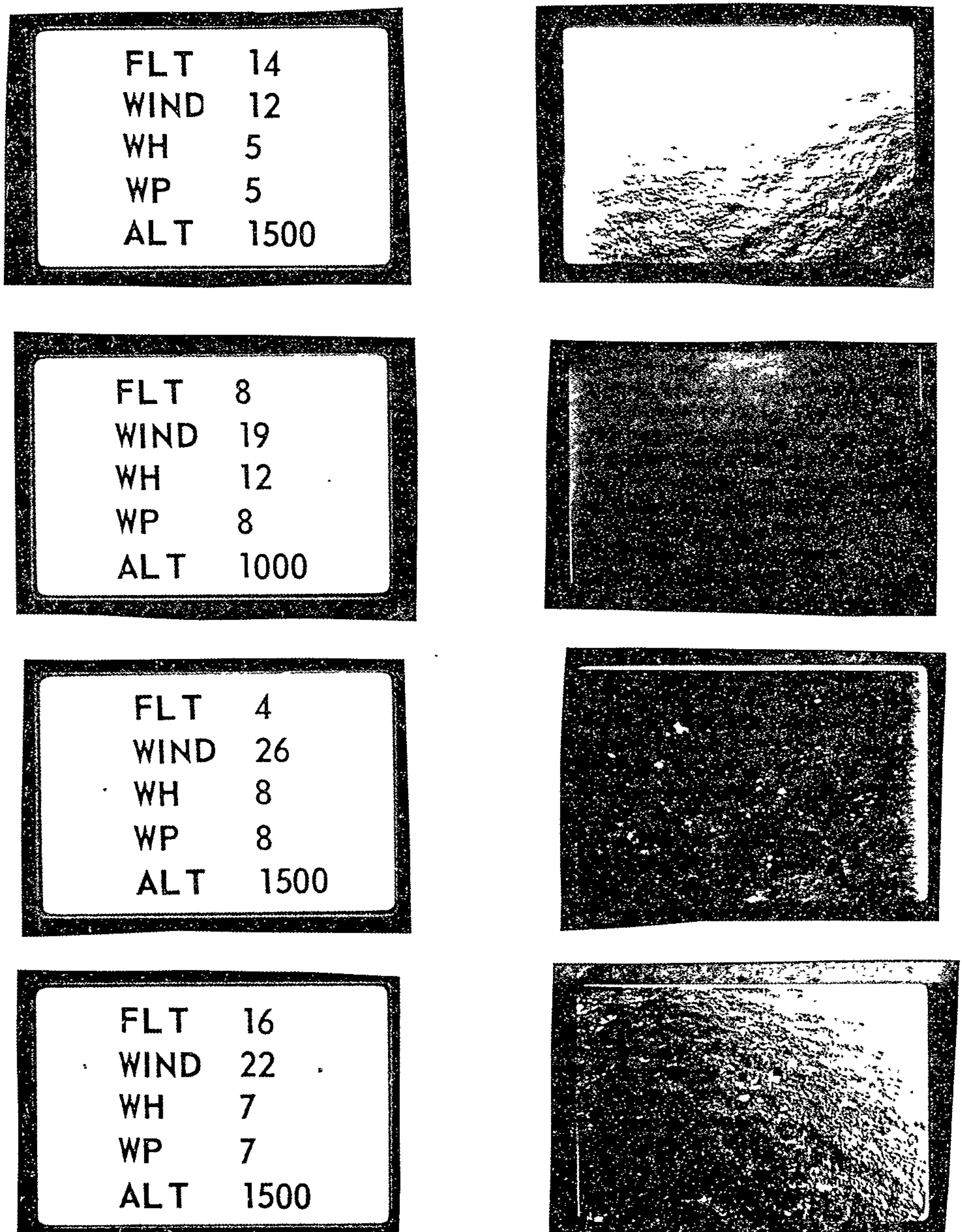

Figure 5-41. Stilwell Photographs (Cont.)

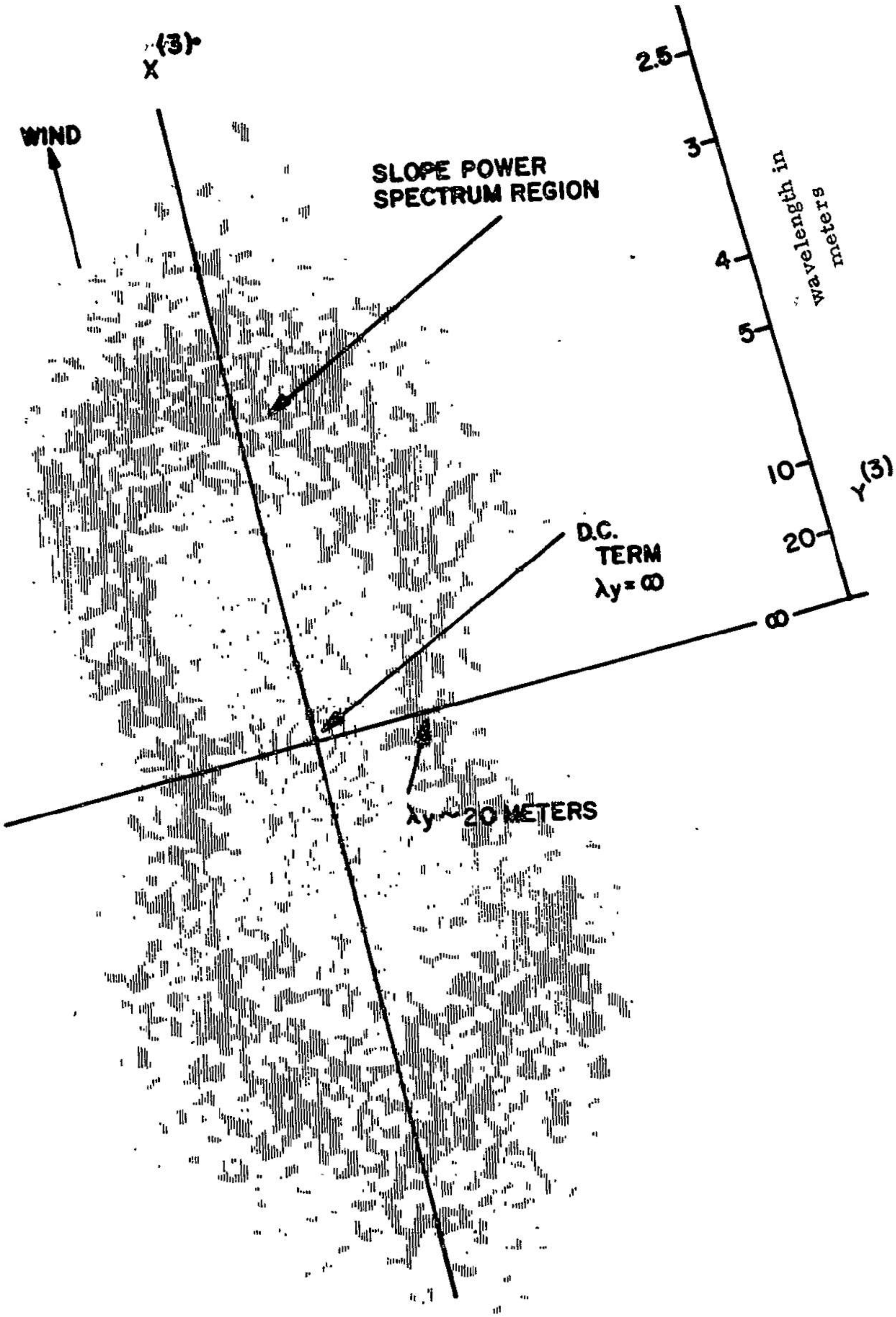

Figure 5-42. Isodensity Tracing of Transform Negative for $\psi = 0$ (Camera Looking in $X^{(3)}$ Directions)

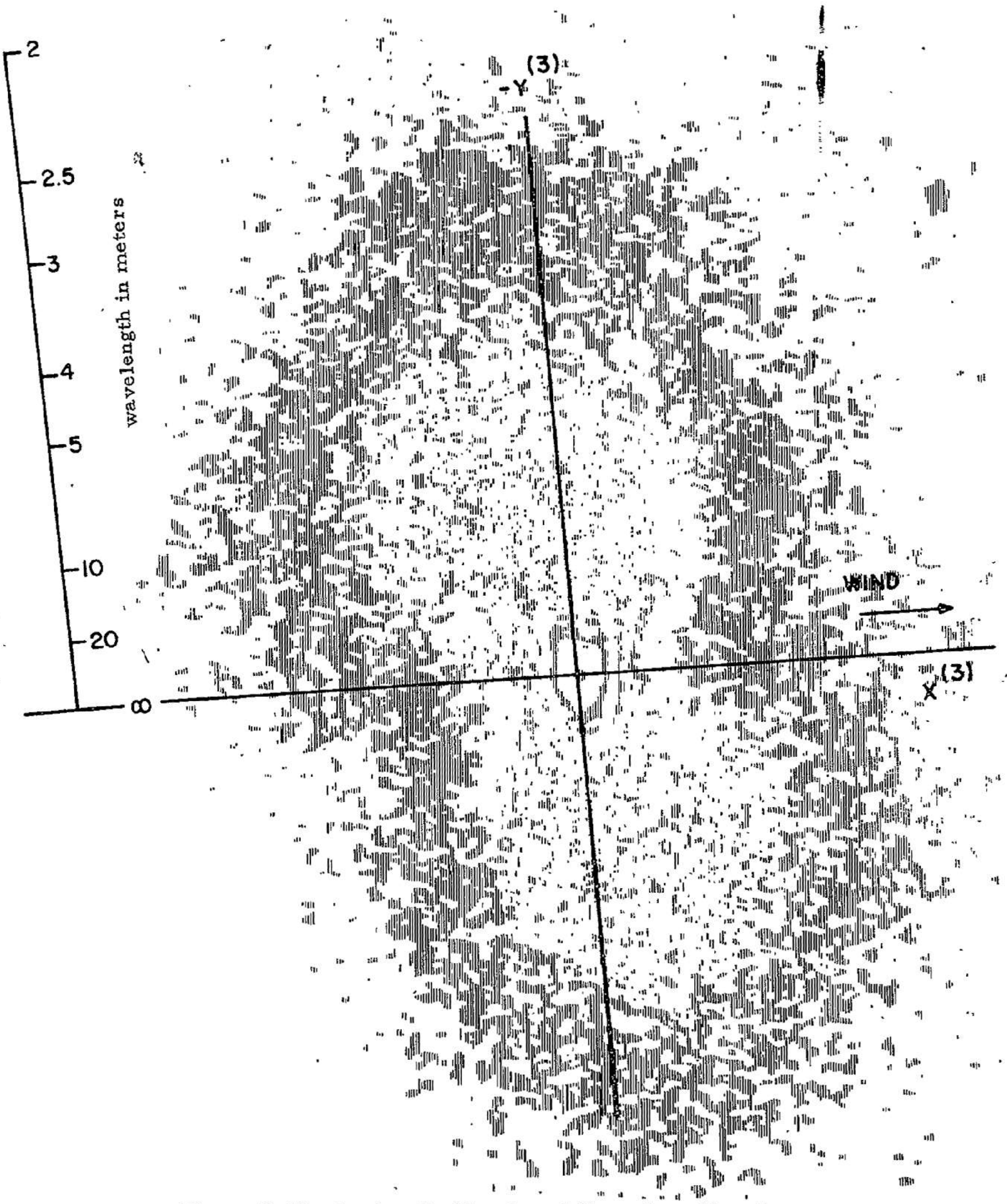

Figure 5-43. Isodensity Tracing of Transform Negative
(Camera Looking in Y (3) Direction of Figure 14)

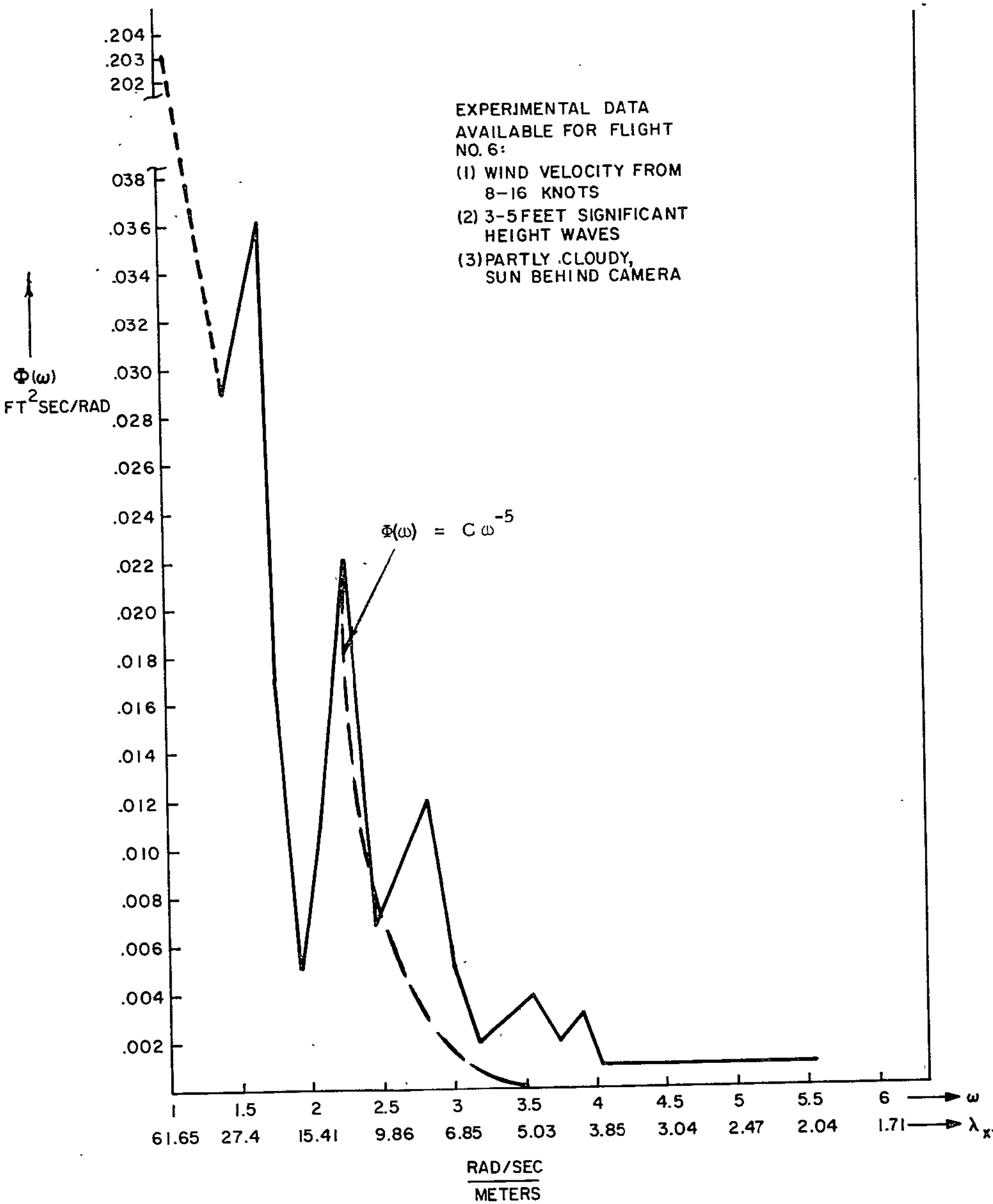

Figure 5-44. Energy Spectrum for Raytheon Flight No. 6

These line spectra agree quite well with line spectra taken by the laser profilometer on the previous day (see Appendix B).

The results of the Stilwell process of ocean spectra measurements are discussed in detail in Appendix B. The technique offers great promise because of the ease of implementation, but further work on processing methods is required before it can be used to provide valuable and reliable outputs.

SECTION 6. CONCLUSIONS AND RECOMMENDATIONS

6.1 Radar Cross Section

The results do not indicate that average cross section ($\sigma°$) is functionally related to the large ocean wave parameters, i.e., wave height (Figure 5-1), wave period (Figure 5-2), or wave direction (Table 5-1). A functional relation appears to exist between $\sigma°$ and wind speed. This seems entirely credible in light of the possible relation between wind speed and the generation of small high frequency capillary waves. This is particularly logical when one considers the dimensions of the capillaries (1.7 cm or less) and the dimensions of the transmitted X-band frequency (3 cm). Mr. John W. Wright[1,2] has shown that X-band backscattering at angles other than normal are highly dependent on capillary waves. Kinsman[3] (see also Appendix C) has also shown that the slopes of capillary waves can be very high, even exceeding 90°, and that the average slope of waves is more affected by capillaries then by the large wind waves or swells.

The results also show that variations in $\sigma°$ over the looking angles of 0 to 4 degrees are small at the various wind speeds (see Figure 5-4). This agrees in part with the curves developed by Moore and Schooley (see Figure 5-5).

Distributions of pulse amplitudes, and hence $\sigma°$, appear to be Rayleigh and independent of ocean parameters.

Cross polarized returns at normal incidence were found to be at least 30 dB down from the directly polarized returns.

6.2 Pulse Shape

Pulse shapes were recorded on film showing the relation between individual pulses and the integrated effect of many pulses. The individual pulses showed wide fluctuations in the trailing edge, especially immediately after the peak. The leading edge of the pulses, however, showed a consistent ramp with little fluctuation. The start of the leading edge did not vary significantly from pulse to pulse.

The multiple pulse tracings showed an integrated average effect which agrees with calculations performed by others[4, 5]. The pulse returns show an integrating effect from the time of the first pulse returns up to the pulse width, and then a decay thereafter. The impulse response can then be determined as follows:

$$h(t) = k \int_0^t f(t)\, dt \qquad 0 < t < \tau \tag{6-1}$$

$$= k e^{-t-\tau/T} \qquad t > \tau$$

where

$f(t)$ = the input pulse

τ = pulse width

T = decay time constant

$= \dfrac{\theta_T^2 h}{2.77c}$ (see Ref. 4)

k = a constant (6-2)

which includes $\sigma°$ and all other radar range parameters.

From this we can derive $H(\omega)$ by performing the Fourier transform

$$H(\omega) = \frac{K}{j(\omega-\omega_o)} \tag{6-3}$$

where $\omega_o = 1/T$

$$K = k e^{\tau/T} \tag{6-4}$$

The above relations assume that the beamwidth of the radar is large compared to $\sqrt{c\tau/h}$, that a pulse limited condition exists. In actual calculations from the reduced data it was found that the transition region between pulse limited and beam limited condition occurred at an angle which was twice as large as the 3 dB beamwidth angle.

In summary, then, average pulse shapes agreed with that predicted by the theoretical computations. The peak pulse amplitude is determined by σ^o. The rise times are linear and equal to the pulse width and the decay times are related to altitude and beamwidth. No changes in σ^o with looking angle were found, and whether these could also affect decay time is unknown, Wave shapes were found to be independent of sea direction.

6.3 Ocean Parameters

As in all experiments involving reflections from a target, the characteristics of the target are never as well defined as they could be. It appears that measurements of capillaries are needed to fully determine a functional relationship between radar and ocean waves.

Of the ocean measuring techniques used in this experiment, the Stilwell process[6] offers the greatest promise. It may provide the most comprehensive quantitative description of the ocean surface and could be operationally easy to implement. However, the total process is still in a research and development stage, and requires further theoretical and experimental evidence before it can be an accepted tool.

The good old-fashioned "eyeball" technique of measuring ocean waves again yielded the most reliable and consistent results, although lacking in definition, accuracy, and resolution. Laser profilometer measurements of wave spectrums did provide some valuable measurements, but the instrumentation and data reduction is more complex than Stilwell photography. Laser profilometry is, however, a more proven technique.

6.4 Recommendations

Further radar backscatter measurements should be made at X-band to verify that a relationship exists between radar cross section and small high frequency waves (capillaries). This is not primarily a radar problem, but it is an ocean parameter measurement problem. Techniques for making the ocean parameter measurements should be further developed, especially the Stilwell process.

An altimeter data processor should be developed which takes into account the leading and trailing edge characteristics discussed in this report. Such a data processor, or range tracker, should take into consideration the wide amplitude variations in the trailing edge near the peak, as well as the relatively minor amplitude variations on the leading edge.

The next phase of precision satellite altimetry experimentation should be started. This involves accurate range or altitude measurements on a ground test range in order to calibrate equipment delays, and in an aircraft in order to measure altitude biases.

Further flight tests should include correlation measurements between pulses, waveform sampling techniques, and evaluation of candidate data processors.

The data gathered in this experiment should be further analyzed in order to determine rise and fall times as well as the distribution of amplitudes as a function of time.

REFERENCES

1. John W. Wright, "Backscattering from Capillary Waves with Application to Sea Clutter," IEEE Transaction AP-14, Nov. 1966.
2. John W. Wright, "A New Model for Sea Cluttèr," IEEE Trans. AP-16, March 1968.
3. B. Kinsman, Wind Waves Prentice Hall Inc. 1965
4. Space Geodesy Altimetry Study, Appendix R-A, Raytheon Company Final Report, R-68-4459, October 1968.
5. R. K. Moore and C.S. Williams, Jr., "Radar Terrain Return at Near Vertical Incidence," Proc. IRE Vol. 45, pg. 228, Feb. 1957.
6. Denzil Stilwell, Jr. Directional Energy Spectra of the Sea from Photographs, JGR Vol. 74, No. 8, Pg. 1974, April 1969.

APPENDIX A

COMPUTER PRINTOUT OF FLIGHT TEST DATA

This appendix contains the results of the data processing program described in Section 4.1.4. It includes a listing of all the ocean and radar parameters for all of the flights, along with σ° calculations for all of the selected frames. Average σ^o's, standard deviations, and frequency distributions were calculated for various groupings of σ^o. The results are divided into five sections as described below.

A-1. σ^o Per Frame

This section includes significant ocean truth and radar parameters for each flight and for each run of each flight, and for each frame the calculated received power, target cross section, and radar cross section per unit area (all values in dB) using both the average return pulse peak and the absolute return pulse peak in the calculation of σ^o.

A-2. Average σ^o Over All Flights

The mean σ° and its standard deviation and sample size calculated over the ten selected flights are presented here.

A-3. Average σ^o for Each Flight

This section includes the mean σ°, its standard deviation, and sample size calculated for σ° based on average power return and for σ°, based in turn on absolute peak power return for each flight. The one standard deviation boundary limits are included for both values of σ^o. A histogram and cumulative probability distribution have also been calculated. The histogram is divided into two parts, the first is a frequency distribution over the spectrum of σ° values with each bar of the histogram being one half of a standard deviation wide, and the second is a frequency distribution for values of $\sigma°$ within the one standard deviation limits, with each bar being one eighth of a standard deviation wide. The cumulative probability was derived from the first histogram.

A-4. <u>Average $\sigma°$ for Selected Runs</u>

The output presented here is similar to the input of the data of Section A-3, except that the results are based on selected runs rather than flights. This shows that $\sigma°$ is independent of sea direction.

A-5. <u>Average $\sigma°$ vs. Pulses Per Frame for Each Flight</u>

Here the average $\sigma°$ is calculated for each variation of pulses per frame during each flight. The values of pulses per frame were 1, 50, 148, or 278.

APPENDIX A

FLIGHT TEST DATA ANALYSIS

A-1 NOTE: A SERIES OF 9'S IN A DATA BLOCK MEANS THAT PIECE OF DATA WAS UNAVAILABLE

FLIGHT	SEA DIRECTION	WAVE HEIGHT(FT)	WAVE PERIOD(SEC)	WIND SPEED(KT)	WIND DIRECTION	WATER TEMP(F)	AIR TEMP(F)	AIR PRES(MB)
1	140	99	99	99	999	99	99	9999.90

RUN	ALTITUDE(FT)	PULSES PER FRAME	PULSE WIDTH(NS)	PEAK POWER	POLARIZATION(1)	C54 HEADING
1	6000	50	100	12	2	999

FRAME	RCVD PWR(DBM)AV	RCVD PWR(DBM)PEAK	SIGMA AV	SIGMA PEAK	SIGMAZ(DB) AV	SIGMAZ(DB) PEAK

FLIGHT	SEA DIRECTION	WAVE HEIGHT(FT)	WAVE PERIOD(SEC)	WIND SPEED(KT)	WIND DIRECTION	WATER TEMP(F)	AIR TEMP	AIR PRES(MB)
2	150	99	99	99	999	99	99	9999.90

RUN	ALTITUDE(FT)	PULSES PER FRAME	PULSE WIDTH(NS)	PEAK POWER	POLARIZATION(1)	C54 HEADING

NO DATA COLLECTED ON THIS FLIGHT

FRAME	RCVD PWR(DBM)AV	RCVD PWR(DBM)PEAK	SIGMA AV	SIGMA PEAK	SIGMAZ(DB) AV	SIGMAZ(DB) PEAK

FLIGHT	SEA DIRECTION	WAVE HEIGHT(FT)	WAVE PERIOD(SEC)	WIND SPEED(KT)	WIND DIRECTION	WATER TEMP(F)	AIR TEMP	AIR PRES(MB)
3	999	99	99	99	999	99	99	9999.90

RUN	ALTITUDE(FT)	PULSES PER FRAME	PULSE WIDTH(NS)	PEAK POWER	POLARIZATION(1)	C54 HEADING
1	1000	50	100	12	1	360
2	1000	50	100	12	1	270
3	20000	50	100	12	1	360
4	20000	50	100	12	1	180
5	20000	50	100	12	1	135
6	20000	50	100	12	1	90
7	20000	50	100	12	1	225
8	20000	50	100	12	1	270
9	20000	50	100	12	1	360

FRAME	RCVD PWR(DBM)AV	RCVD PWR(DBM)PEAK	SIGMA AV	SIGMA PEAK	SIGMAZ(DB) AV	SIGMAZ(DB) PEAK

FLIGHT	SEA DIRECTION	WAVE HEIGHT(FT)	WAVE PERIOD(SEC)	WIND SPEED(KT)	WIND DIRECTION	WATER TEMP(F)	AIR TEMP	AIR PRES(MB)
4	290	4	8	26	293	99	46	9999.90

RUN	ALTITUDE(FT)	PULSES PER FRAME	PULSE WIDTH(NS)	PEAK POWER	POLARIZATION(1)	C54 HEADING

1	1500	1	100	12	1	290
2	1500	1	100	12	1	200
3	1500	1	100	12	1	110
4	1500	1	100	12	1	20
5	5000	50	100	12	1	290
6	5000	50	100	12	1	275
7	5000	50	100	12	1	260
8	5000	50	100	12	1	20
9	5000	50	100	12	1	335
10	5000	50	100	12	1	15
11	5000	50	100	12	1	200
12	5000	50	100	12	1	245
13	5000	50	100	12	1	110
14	5000	50	100	12	1	335
15	5000	50	100	12	1	5
16	5000	50	20	12	1	290
17	5000	50	20	12	1	245
18	5000	50	20	12	1	200
19	5000	50	20	12	1	335
20	5000	50	20	12	1	20
21	5000	50	20	12	1	110
22	1500	1	100	12	1	290
23	1500	1	100	12	1	200
24	1500	1	100	12	1	110
25	1500	1	100	12	1	20

	FRAME	RCVD PWR(DBM)AV	RCVD PWR(DBM)PEAK	SIGMA AV	SIGMA PEAK	SIGMAZ(DB) AV	SIGMAZ(DB) PEAK
5	8330	-56.60	-53.19	60.83	64.24	9.197	12.609
5	8331	-56.92	-55.07	60.51	62.35	8.876	10.724
5	8332	-57.78	-53.64	59.65	63.79	8.015	12.159
8	8407	-58.90	-54.23	58.53	63.19	6.901	11.564
8	8408	-59.22	-55.76	58.21	61.67	6.576	10.035
8	8409	-57.19	-54.94	60.24	62.49	8.605	10.859
13	8528	-58.86	-54.69	58.57	62.74	6.937	11.110
13	8529	-57.19	-54.59	60.24	62.83	8.610	11.204
13	8530	-56.42	-53.82	61.01	63.61	9.381	11.980
16	8618	-63.11	-61.50	54.32	55.93	9.680	11.291
16	8619	-63.48	-59.87	53.95	57.56	9.308	12.920
16	8620	-62.97	-60.11	54.46	57.32	9.820	12.680
18	8662	-64.24	-61.49	53.19	55.94	8.552	11.297
18	8663	-63.22	-60.04	54.20	57.38	9.564	12.744
18	8664	-63.48	-60.07	53.94	57.36	9.303	12.715
21	8731	-65.50	-60.54	51.93	56.89	7.285	12.245
21	8732	-64.01	-60.77	53.42	56.66	8.782	12.016
21	8733	-63.33	-60.44	54.10	56.99	9.459	12.347

FLIGHT	SEA DIRECTION	WAVE HEIGHT(FT)	WAVE PERIOD(SEC)	WIND SPEED(KT)	WIND DIRECTION	WATER TEMP(F)	AIR TEMP	AIR PRES(MB)
5	320	5	7	16	320	99	40	1024.90

RUN	ALTITUDE(FT)	PULSES PER FRAME	PULSE WIDTH(NS)	PEAK POWER	POLARIZATION(1)	C54 HEADING
1	1500	50	20	12	1	320
2	1500	50	20	12	1	230
3	1500	50	20	12	1	140
4	1500	50	20	12	1	50
5	10000	50	20	12	1	320
6	10000	50	20	12	1	275
7	10000	50	20	12	1	230
8	10000	50	20	12	1	5
9	10000	50	20	12	1	50
10	10000	50	20	12	1	140

	FRAME	RCVD PWR(DBM)AV	RCVD PWR(DBM)PEAK	SIGMA AV	SIGMA PEAK	SIGMAZ(DB) AV	SIGMAZ(DB) PEAK
5	9037	-53.45	-51.44	66.02	68.03	18.367	20.375
5	9038	-52.51	-50.46	66.96	69.01	19.308	21.356
5	9039	-55.83	-51.84	63.64	67.62	15.991	19.974
6	9060	-53.96	-51.63	65.50	67.84	17.854	20.190
6	9061	-54.54	-50.62	64.93	68.85	17.277	21.201
6	9062	-52.51	-50.57	66.96	68.90	19.306	21.251
7	9083	-53.68	-51.57	65.79	67.90	18.139	20.248
7	9084	-53.37	-51.11	66.39	68.36	18.744	20.709
7	9085	-55.03	-51.99	64.44	67.48	16.789	19.827
8	9105	-54.33	-51.28	65.14	68.19	17.487	20.540
8	9106	-54.44	-51.17	65.03	68.30	17.380	20.646
8	9107	-55.29	-52.73	64.18	66.74	16.532	19.089
9	9127	-53.14	-51.69	66.33	67.78	18.681	20.132
9	9128	-53.63	-51.14	65.83	68.33	18.184	20.679
9	9129	-55.48	-51.89	63.99	67.58	16.337	19.925
10	9149	-54.81	-50.93	64.66	68.54	17.006	20.891
10	9150	-55.02	-52.22	64.45	67.25	16.795	19.598
10	9151	-52.74	-50.69	66.73	68.78	19.080	21.129

FLIGHT	SEA DIRECTION	WAVE HEIGHT(FT)	WAVE PERIOD(SEC)	WIND SPEED(KT)	WIND DIRECTION	WATER TEMP(F)	AIR TEMP	AIR PRES(MB)
6	330	4	99	12	330	60	43	1028.00

RUN	ALTITUDE(FT)	PULSES PER FRAME	PULSE WIDTH(NS)	PEAK POWER	POLARIZATION(1)	C54 HEADING
1	1500	1	100	12	2	330
2	1500	1	100	12	2	240
3	1500	1	100	12	2	150
4	1500	1	100	12	2	60
5	15000	50	100	12	1	330
6	15000	50	100	12	1	285
7	15000	50	100	12	1	240
8	15000	50	100	12	1	15
9	15000	50	100	12	1	60
10	15000	50	100	12	1	150
11	15000	50	100	12	2	330
12	15000	50	100	12	2	285
13	15000	50	100	12	2	240
14	15000	50	100	12	2	15
15	15000	50	100	12	2	60
16	15000	50	100	12	2	150
17	20000	50	100	12	1	330
18	20000	50	100	12	1	285
19	20000	50	100	12	1	240
20	20000	50	100	12	1	15
21	20000	50	100	12	1	60
22	20000	50	100	12	1	150
23	1500	1	100	12	1	330
24	1500	1	100	12	1	240
25	1500	1	100	12	1	150
26	1500	1	100	12	1	60

	FRAME	RCVD PWR(DBM)AV	RCVD PWR(DBM)PEAK	SIGMA AV	SIGMA PEAK	SIGMAZ(DB) AV	SIGMAZ(DB) PEAK
5	9447	-51.35	-47.64	75.17	78.87	18.765	22.471
5	9448	-51.86	-48.37	74.55	78.14	18.153	21.741
5	9449	[illegible]	-48.23	74.43	78.28	18.031	21.880
7	[illegible]	-51.30	-47.82	75.21	79.69	18.812	22.292
7	[illegible]	-49.74	-46.05	76.77	80.46	20.371	24.062
7	[illegible]	-51.77	-48.76	74.74	77.75	18.339	21.349
10	[illegible]	-51.28	-48.32	75.23	78.19	18.828	21.791
10	[illegible]	-53.10	-48.73	73.36	77.78	16.955	21.380
10	[illegible]	[illegible]	-46.55	76.09	79.96	19.685	23.561

FLIGHT	SEA DIRECTION	WAVE HEIGHT(FT)	WAVE PERIOD(SEC)	WIND SPEED(KT)	WIND DIRECTION	WATER TEMP(F)	AIR TEMP	AIR PRES(MB)
7	320	3	5	3	320	58	49	1020.80

RUN	ALTITUDE(FT)	PULSES PER FRAME	PULSE WIDTH(NS)	PEAK POWER	POLARIZATION(1)	C54 HEADING
1	15000	999	20	12	1	320
2	15000	999	20	12	1	275
3	15000	999	20	12	1	230
4	15000	999	20	12	1	5
5	15000	999	20	12	1	50
6	15000	999	20	12	1	140

RUN	FRAME	RCVD PWR(DBM)AV	RCVD PWR(DBM)PEAK	SIGMA AV	SIGMA PEAK	SIGMAZ(DB) AV	SIGMAZ(DB) PEAK
1	401	-57.53	-54.84	68.99	71.67	19.576	22.257
1	402	-57.46	-53.34	69.06	73.17	19.644	23.760
1	404	-57.87	-54.57	68.65	71.94	19.234	22.532
1	409	-56.74	-54.09	69.78	72.42	20.365	23.008
1	410	-57.27	-54.16	69.25	72.35	19.835	22.943
1	411	-57.82	-55.35	68.69	71.16	19.281	21.749
2	427	-57.35	-54.23	69.16	72.28	19.750	22.874
2	428	-56.83	-52.99	69.68	73.52	20.271	24.110
2	429	-58.44	-55.65	68.08	70.86	18.665	21.451
2	430	-56.36	-53.50	70.15	73.01	20.741	23.604
2	431	-55.12	-53.62	70.40	72.89	20.984	23.482
2	433	-55.71	-52.61	70.80	73.90	21.386	24.493
2	434	-54.53	-50.94	71.69	75.57	22.275	26.164
2	435	-56.76	-52.81	69.76	73.70	20.344	24.289
2	436	-56.32	-52.26	70.19	74.25	20.781	24.842
2	437	-55.70	-51.89	69.82	74.63	20.406	25.216
2	439	-55.10	-52.56	71.41	73.95	21.998	24.536
2	440	-55.16	-52.71	71.35	73.80	21.939	24.391
2	441	-55.64	-52.80	70.87	73.72	21.459	24.304
2	442	-55.70	-51.91	70.82	74.60	21.405	25.188
3	452	-57.65	-53.06	69.46	73.46	20.053	24.044
3	453	-57.15	-54.09	69.46	72.42	20.046	23.009
3	454	-56.11	-53.60	70.40	72.92	20.992	23.505
3	455	-57.45	-53.38	69.06	73.13	19.646	23.720
3	456	-57.11	-54.10	69.40	72.41	19.986	22.999
3	458	-54.79	-50.99	72.12	75.52	22.709	26.111
3	459	-55.96	-51.87	70.55	74.64	21.142	25.233
3	460	-55.63	-51.76	70.88	74.75	21.472	25.340
3	461	-55.25	-51.32	71.26	75.20	21.853	25.784
3	462	-54.92	-51.24	71.60	75.27	22.185	25.861
3	464	-54.58	-51.15	71.93	75.36	22.519	25.952
3	466	-54.96	-52.25	71.56	74.26	22.144	24.853
3	467	-54.47	-51.66	72.04	74.86	22.630	25.446
3	468	-56.41	-52.96	70.10	73.55	20.692	24.137
4	479	-57.74	-54.63	68.77	71.88	19.356	22.467
4	480	-57.50	-54.62	69.01	71.89	19.597	22.479
4	481	-57.03	-54.36	69.48	72.15	20.068	22.738
4	482	-57.10	-52.97	69.41	73.55	20.002	24.135
4	483	-57.66	-53.45	68.86	73.06	19.445	23.652
4	485	-55.73	-52.05	70.78	74.46	21.373	25.046
4	486	-55.89	-52.17	70.62	74.34	21.211	24.931
4	488	-55.92	-52.95	70.60	73.56	21.184	24.149
4	489	-55.86	-53.32	70.65	73.20	21.241	23.785
4	491	-55.74	-52.68	70.77	73.83	21.358	24.416
4	492	-55.54	-52.90	70.97	73.61	21.563	24.202
4	493	-56.60	-53.79	69.91	72.72	20.502	23.306
4	494	-55.57	-53.20	70.94	73.32	21.532	23.905
4	495	-55.92	-52.33	70.60	74.19	21.184	24.774
5	506	-57.73	-54.44	68.78	72.07	19.371	22.663

5	507	-58.47	-54.25	68.04	72.26	18.631	22.854
5	508	-59.76	-53.57	66.76	72.94	17.344	23.528
5	509	-57.88	-54.20	68.63	72.31	19.222	22.901
5	510	-58.39	-54.68	68.13	71.83	18.715	22.422
5	512	-57.18	-53.62	69.34	72.89	19.926	23.476
5	513	-55.19	-52.47	71.32	74.04	21.913	24.627
5	514	-56.06	-53.07	70.46	73.44	21.045	24.033
5	515	-56.48	-52.60	70.03	73.91	20.621	24.502
5	516	-56.62	-52.93	69.89	73.58	20.484	24.170
5	517	-54.74	-52.00	71.77	74.51	22.363	25.101
5	518	-54.95	-52.91	71.56	73.60	22.149	24.192
5	519	-54.39	-52.20	72.13	74.31	22.715	24.903
5	520	-56.00	-53.62	70.51	72.89	21.101	23.479
5	521	-56.30	-53.08	70.21	73.44	20.798	24.024
6	532	-61.14	-56.88	65.37	69.63	15.960	20.222
6	533	-59.69	-55.33	66.82	71.19	17.406	21.775
6	534	-60.92	-57.07	65.59	69.44	16.182	20.029
6	535	-61.63	-56.41	64.88	70.10	15.469	20.690
6	536	-60.45	-56.15	66.06	70.36	16.648	20.949
6	538	-56.41	-53.60	70.10	72.91	20.688	23.499
6	539	-57.68	-53.78	68.83	72.73	19.421	23.317
6	540	-57.63	-53.67	68.88	72.84	19.467	23.431
6	541	-57.85	-54.05	68.66	72.46	19.246	23.047
6	542	-56.43	-53.34	70.08	73.18	20.668	23.765
6	544	-55.94	-52.04	70.57	74.48	21.157	25.065
6	545	-56.03	-52.14	70.48	74.37	21.068	24.962
6	546	-57.49	-53.55	69.03	72.96	19.616	23.552
6	547	-54.72	-51.26	71.79	75.25	22.379	25.839
6	548	-55.73	-51.41	70.78	75.10	21.369	25.692

FLIGHT	SEA DIRECTION	WAVE HEIGHT(FT)	WAVE PERIOD(SEC)	WIND SPEED(KT)	WIND DIRECTION	WATER TEMP(F)	AIR TEMP	AIR PRES(MB)
8	340	13	8	19	340	53	99	1016.00

RUN	ALTITUDE(FT)	PULSES PER FRAME	PULSE WIDTH(NS)	PEAK POWER	POLARIZATION(1)	C54 HEADING
1	10000	1	20	12	1	340
2	10000	1	20	12	1	295
3	10000	1	20	12	1	250
4	10000	1	20	12	1	25
5	10000	1	20	12	1	70
6	10000	1	20	12	1	160
7	10000	2	20	12	1	340
8	10000	2	20	12	1	295
9	10000	2	20	12	1	250
10	10000	2	20	12	1	25
11	10000	2	20	12	1	70
12	10000	2	20	12	1	160
13	10000	50	20	12	1	340
14	10000	50	20	12	1	295
15	10000	50	20	12	1	250
16	10000	50	20	12	1	25
17	10000	50	20	12	1	70
18	10000	50	20	12	1	160
19	10000	278	20	12	1	340
20	10000	278	20	12	1	295
21	10000	278	20	12	1	250
22	10000	278	20	12	1	25
23	10000	278	20	12	1	70
24	10000	278	20	12	1	160

	FRAME	RCVD PWR(DBM)AV	RCVD PWR(DBM)PEAK	SIGMA AV	SIGMA PEAK	SIGMAZ(DB) AV	SIGMAZ(DB) PEAK
1	701	-56.41	-56.41	63.06	63.06	15.410	15.410
1	702	-58.07	-58.07	61.40	61.40	13.747	13.747
1	703	-56.24	-56.24	63.23	63.23	15.579	15.579
1	704	-60.26	-60.26	59.21	59.21	11.562	11.562

2	706	-57.19	-57.19	62.28	62.28	14.629	14.629
2	707	-56.26	-56.26	63.21	63.21	15.563	15.563
2	708	-60.38	-60.38	59.08	59.08	11.434	11.434
2	709	-56.78	-56.78	62.68	62.68	15.034	15.034
2	710	-58.80	-58.80	60.67	60.67	13.022	13.022
3	713	-60.85	-60.85	58.61	58.61	10.964	10.964
3	714	-61.80	-61.80	57.67	57.67	10.020	10.020
3	715	-62.25	-62.25	57.22	57.22	9.567	9.567
3	716	-63.02	-63.02	56.44	56.44	8.794	8.794
4	719	-61.95	-61.95	57.52	57.52	9.872	9.872
4	720	-62.41	-62.41	57.06	57.06	9.409	9.409
4	721	-59.99	-59.99	59.48	59.48	11.832	11.832
4	722	-60.59	-60.59	58.88	58.88	11.227	11.227
5	724	-59.49	-59.49	59.98	59.98	12.326	12.326
5	725	-60.44	-60.44	59.03	59.03	11.379	11.379
5	726	-58.76	-58.76	60.71	60.71	13.055	13.055
5	727	-60.34	-60.34	59.13	59.13	11.475	11.475
5	728	-56.98	-56.98	62.49	62.49	14.838	14.838
6	730	-59.83	-59.83	59.64	59.64	11.992	11.992
6	731	-64.36	-64.36	55.11	55.11	7.463	7.463
6	733	-60.71	-60.71	58.76	58.76	11.108	11.108
6	734	-56.12	-56.12	63.35	63.35	15.698	15.698
13	795	-55.62	-51.12	63.85	68.35	16.200	20.700
13	796	-55.19	-51.83	64.28	67.64	16.625	19.993
13	797	-54.79	-51.11	64.68	68.35	17.026	20.703
13	798	-56.59	-50.27	62.88	69.20	15.228	21.552
13	799	-54.99	-50.54	64.48	68.93	16.829	21.279
13	800	-56.40	-52.02	63.07	67.45	15.418	19.800
13	801	-56.41	-51.41	63.06	68.06	15.405	20.410
13	802	-56.06	-50.15	63.41	69.32	15.756	21.666
13	803	-55.77	-50.57	63.70	68.90	16.047	21.250
13	804	-56.50	-51.31	62.97	68.15	15.319	20.504
13	805	-56.37	-50.62	63.10	68.85	15.448	21.195
13	806	-55.38	-51.74	64.09	67.73	16.438	20.083
13	807	-56.82	-51.64	62.65	67.82	14.997	20.174
13	808	-57.35	-52.63	62.12	66.84	14.465	19.190
13	809	-57.38	-52.09	62.09	67.38	14.440	19.729
13	810	-57.17	-51.57	62.30	67.90	14.650	20.251
13	811	-56.65	-51.20	62.82	68.27	15.171	20.616
13	812	-57.17	-50.98	62.30	68.48	14.652	20.833
13	813	-56.84	-51.03	62.62	68.44	14.973	20.787
13	814	-56.02	-50.85	63.45	68.62	15.803	20.970
14	816	-58.84	-53.78	60.63	65.69	12.978	18.037
14	817	-58.29	-54.02	61.18	65.45	13.533	17.798
14	818	-56.43	-53.22	63.04	66.25	15.390	18.600
14	819	-59.98	-55.99	59.48	63.48	11.834	15.833
14	820	-56.74	-55.26	62.73	64.21	15.080	16.560
14	821	-56.29	-54.57	63.18	64.90	15.527	17.248
14	822	-55.85	-53.97	63.62	65.50	15.968	17.845
14	823	-59.40	-55,57	60.07	63.89	12.423	16.244
14	824	-57.53	-55.11	61.94	64.36	14.293	16.713
14	825	-59.16	-54.82	60.31	64.65	12.659	16.996
14	826	-57.65	-54.69	61.82	64.78	14.173	17.132
14	827	-58.49	-55.18	60.98	64.29	13.329	16.635
14	828	-58.91	-55.37	60.56	64.10	12.910	16.452
14	829	-57.43	-54.57	62.04	64.90	14.391	17.249
14	830	-57.43	-54.45	62.04	65.02	14.392	17.365
14	831	-58.23	-54.94	61.24	64.53	13.589	16.879
14	832	-58.00	-54.88	61.47	64.59	13.821	16.940
14	833	-58.58	-54.98	60.89	64.49	13.238	16.840
14	834	-58.15	-54.10	61.32	65.37	13.670	17.717
14	835	-57.47	-54.77	61.99	64.70	14.344	17.048
15	837	-58.14	-55.16	61.33	64.31	13.678	16.663
15	838	-56.49	-53.92	62.98	65.55	15.330	17.902
15	839	-57.20	-53.88	62.27	65.59	14.623	17.939
15	840	-56.42	-53.46	63.05	66.01	15.399	18.363
15	841	-56.83	-53.17	62.64	66.29	14.985	18.644
15	842	-57.23	-53.44	62.24	66.03	14.593	18.377
15	843	-56.44	-53.31	63.03	66.16	15.381	18.506
15	844	-56.40	-53.29	63.07	66.18	15.423	18.533

15	845	-56.96	-53.64	62.51	65.82	14.855	18.174
15	846	-57.79	-54.47	61.68	65.00	14.026	17.349
15	847	-57.87	-54.09	61.60	65.38	13.946	17.731
15	848	-56.60	-54.01	62.87	65.46	15.217	17.809
15	849	-57.09	-53.86	62.38	65.61	14.732	17.958
15	850	-56.98	-53.40	62.49	66.07	14.835	18.420
15	851	-59.45	-55.34	60.02	64.13	12.366	16.482
15	852	-56.85	-53.78	62.62	65.69	14.968	18.040
15	853	-55.66	-53.55	63.81	65.92	16.155	18.267
15	854	-56.16	-53.32	63.30	66.15	15.653	18.495
15	855	-57.28	-52.89	62.19	66.58	14.542	18.932
15	856	-57.69	-53.98	61.78	65.49	14.131	17.842
16	858	-57.44	-54.68	62.03	64.78	14.375	17.134
16	859	-57.09	-53.91	62.38	65.56	14.728	17.906
16	860	-57.68	-53.35	61.79	66.12	14.142	18.465
16	861	-55.62	-53.00	63.85	66.47	16.195	18.820
16	862	-57.08	-53.14	62.38	66.33	14.734	18.675
16	863	-57.07	-53.76	62.40	65.71	14.746	18.057
16	864	-57.28	-53.25	62.19	66.22	14.543	18.569
16	865	-56.56	-53.30	62.91	66.17	15.255	18.523
16	866	-55.41	-52.72	64.06	66.75	16.411	19.095
16	867	-57.44	-54.60	62.03	64.87	14.376	17.218
16	868	-57.44	-53.89	62.03	65.58	14.377	17.933
16	869	-57.75	-54.26	61.72	65.21	14.067	17.559
16	870	-57.89	-54.92	61.58	64.55	13.927	16.902
16	871	-58.30	-54.64	61.16	64.83	13.514	17.175
16	872	-58.52	-54.17	60.95	65.30	13.301	17.650
16	873	-57.59	-54.54	61.87	64.93	14.224	17.277
16	874	-57.61	-53.78	61.86	65.69	14.210	18.037
16	875	-57.77	-53.54	61.70	65.92	14.045	18.274
16	876	-57.18	-54.20	62.29	65.27	14.643	17.615
16	877	-56.91	-53.34	62.56	66.13	14.909	18.482
17	879	-58.47	-55.45	61.00	64.02	13.353	16.373
17	880	-57.53	-54.21	61.94	65.26	14.291	17.608
17	881	-57.10	-53.99	62.37	65.48	14.719	17.826
17	882	-56.68	-53.97	62.79	65.50	15.142	17.845
17	883	-55.37	-53.63	64.10	65.84	16.446	18.192
17	884	-56.80	-53.66	62.67	65.81	15.016	18.161
17	885	-58.16	-54.21	61.31	65.26	13.658	17.606
17	886	-58.29	-54.46	61.18	65.01	13.533	17.356
17	887	-57.24	-54.02	62.23	65.45	14.579	17.795
17	888	-55.83	-53.59	63.64	65.87	15.985	18.224
17	889	-57.53	-54.11	61.94	65.36	14.291	17.707
17	890	-55.94	-54.23	63.53	65.24	15.878	17.591
17	891	-57.83	-55.79	61.64	63.68	13.986	16.030
17	892	-58.83	-55.09	60.64	64.38	12.987	16.731
17	893	-58.91	-55.41	60.56	64.06	12.912	16.412
17	894	-59.75	-56.23	59.71	63.24	12.064	15.593
17	895	-58.31	-54.66	61.16	64.81	13.512	17.156
17	896	-57.38	-54.38	62.09	65.09	14.441	17.442
17	897	-58.21	-55.41	61.26	64.06	13.608	16.412
17	898	-56.70	-54.57	62.77	64.90	15.116	17.253
18	900	-58.67	-55.04	60.80	64.43	13.147	16.777
18	901	-57.29	-54.30	62.18	65.17	14.532	17.518
18	902	-57.00	-54.18	62.46	65.29	14.814	17.643
18	903	-57.15	-54.11	62.32	65.35	14.665	17.704
18	904	-57.62	-54.02	61.84	65.44	14.194	17.795
18	905	-57.68	-54.13	61.79	65.34	14.137	17.690
18	906	-57.47	-54.67	62.00	64.80	14.346	17.153
18	907	-58.46	-53.87	61.01	65.60	13.363	17.947
18	908	-56.60	-53.97	62.87	65.50	15.220	17.848
18	909	-57.71	-55.26	61.76	64.20	14.113	16.554
18	910	-57.69	-54.89	61.77	64.58	14.124	16.931
18	911	-56.28	-54.62	63.19	64.85	15.542	17.203
18	912	-58.17	-54.69	61.30	64.78	13.647	17.130
18	913	-58.61	-54.61	60.86	64.85	13.208	17.204

18	914	-58.06	-55.14	61.41	64.33	13.758	16.681
18	915	-58.40	-55.39	61.07	64.08	13.423	16.431
18	916	-59.90	-55.85	59.57	63.62	11.915	15.970
18	917	-59.28	-55.86	60.19	63.61	12.542	15.959
18	918	-58.19	-55.45	61.28	64.02	13.632	16.369
18	919	-59.11	-54.35	60.36	65.12	12.707	17.467
19	923	-58.09	-54.68	61.38	64.79	13.733	17.135
19	924	-57.48	-53.99	61.99	65.47	14.337	17.824
19	925	-58.75	-54.95	60.72	64.52	13.065	16.868
19	926	-57.72	-54.82	61.75	64.65	14.102	16.996
19	927	-57.26	-54.53	62.21	64.94	14.555	17.285
21	965	-56.54	-53.79	62.93	65.68	15.281	18.027
21	966	-56.84	-53.63	62.63	65.83	14.979	18.184
21	967	-57.75	-54.06	61.72	65.41	14.067	17.762
21	968	-57.56	-54.40	61.90	65.07	14.254	17.417
21	969	-58.96	-53.90	60.50	65.56	12.854	17.914
24	1032	-56.30	-53.56	63.16	65.91	15.514	18.255
24	1033	-56.90	-54.06	62.56	65.41	14.914	17.759
24	1034	-58.52	-54.29	60.95	65.18	13.300	17.532
24	1035	-56.74	-53.76	62.73	65.71	15.078	18.059
24	1036	-56.72	-53.86	62.75	65.60	15.097	17.953

FLIGHT	SEA DIRECTION	WAVE HEIGHT(FT)	WAVE PERIOD(SEC)	WIND SPEED(KT)	WIND DIRECTION	WATER TEMP(F)	AIR TEMP	AIR PRES(MB)
9	290	7	99	30	290	61	28	1018.50

RUN	ALTITUDE(FT)	PULSES PER FRAME	PULSE WIDTH(NS)	PEAK POWER	POLARIZATION(1)	C54 HEADING

NO DATA COLLECTED ON THIS FLIGHT

FRAME	RCVD PWR(DBM)AV	RCVD PWR(DBM)PEAK	SIGMA AV	SIGMA PEAK	SIGMAZ(DB) AV	SIGMAZ(DB) PEAK

FLIGHT	SEA DIRECTION	WAVE HEIGHT(FT)	WAVE PERIOD(SEC)	WIND SPEED(KT)	WIND DIRECTION	WATER TEMP(F)	AIR TEMP	AIR PRES(MB)
10	888	0	99	3	80	32	27	1019.80

RUN	ALTITUDE(FT)	PULSES PER FRAME	PULSE WIDTH(NS)	PEAK POWER	POLARIZATION(1)	C54 HEADING
1	5000	1	10	3	1	180
2	5000	1	10	3	1	90
3	5000	1	10	3	1	360
4	5000	1	10	3	1	270
5	5000	2	10	3	1	180
6	5000	2	10	3	1	90
7	5000	2	10	3	1	360
8	5000	2	10	3	1	270
9	5000	10	10	3	1	180
10	5000	10	10	3	1	90
11	5000	10	10	3	1	360
12	5000	10	10	3	1	270
13	5000	50	10	3	1	180
14	5000	50	10	3	1	90
15	5000	50	10	3	1	360
16	5000	50	10	3	1	270
17	5000	148	10	3	1	180
18	5000	148	10	3	1	90
19	5000	148	10	3	1	360
20	5000	148	10	3	1	270

	FRAME	RCVD PWR(DBM)AV	RCVD PWR(DBM)PEAK	SIGMA AV	SIGMA PEAK	SIGMAZ(DB) AV	SIGMAZ(DB) PEAK
13	1649	-84.01	-80.87	49.44	52.58	7.812	10.953
13	1650	-82.02	-79.69	51.43	53.76	9.803	12.127
13	1651	-82.33	-79.53	51.12	53.92	9.489	12.289
13	1676	-76.70	-74.83	56.75	58.62	15.116	16.989
14	1690	-80.80	-77.89	52.64	55.56	11.014	13.927
14	1691	-79.67	-76.74	53.78	56.71	12.148	15.077
14	1692	-80.34	-76.92	53.11	56.52	11.480	14.894
15	1732	-82.30	-78.55	51.15	54.89	9.523	13.264
15	1734	-81.14	-78.06	52.31	55.39	10.677	13.763
15	1735	-80.10	-77.96	53.35	55.49	11.716	13.862
16	1774	-80.11	-76.79	53.34	56.66	11.708	15.030
16	1775	-79.17	-77.45	54.28	56.00	12.648	14.367
16	1776	-77.99	-75.72	55.46	57.73	13.826	16.102
17	1816	-77.86	-75.14	55.59	58.31	13.956	16.677
17	1817	-75.93	-73.31	57.52	60.14	15.886	18.509
17	1818	-74.53	-71.54	58.91	61.91	17.284	20.282
17	1819	-75.41	-72.05	58.04	61.40	16.409	19.768
17	1820	-75.85	-73.32	57.60	60.13	15.968	18.500
18	1858	-79.45	-76.16	54.00	57.29	12.368	15.656
18	1859	-79.80	-73.98	53.65	59.47	12.016	17.836
18	1860	-79.68	-76.01	53.77	57.44	12.139	15.812
18	1861	-78.31	-75.16	55.14	58.29	13.507	16.656
18	1862	-78.78	-75.74	54.67	57.71	13.035	16.079
19	1900	-79.86	-77.14	53.58	56.31	11.954	14.679
19	1901	-79.49	-75.99	53.95	57.46	12.325	15.828
19	1902	-80.45	-76.66	52.99	56.79	11.364	15.158
19	1903	-80.29	-77.17	53.16	56.28	11.529	14.647
19	1904	-79.27	-76.04	54.17	57.41	12.544	15.782
20	1942	-80.25	-76.66	53.20	56.79	11.573	15.161
20	1943	-80.40	-75.82	53.05	57.63	11.423	16.003
20	1944	-79.43	-76.08	54.02	57.37	12.388	15.736
20	1945	-80.93	-76.78	52.52	56.67	10.886	15.038
20	1946	-79.47	-76.39	53.98	57.06	12.349	15.427

FLIGHT	SEA DIRECTION	WAVE HEIGHT(FT)	WAVE PERIOD(SEC)	WIND SPEED(KT)	WIND DIRECTION	WATER TEMP(F)	AIR TEMP	AIR PRES(MB)
11	999	99	99	99	999	99	99	9999.90

RUN	ALTITUDE(FT)	PULSES PER FRAME	PULSE WIDTH(NS)	PEAK POWER	POLARIZATION(1)	C54 HEADING

NO DATA COLLECTED ON THIS FLIGHT

FRAME	RCVD PWR(DBM)AV	RCVD PWR(DBM)PEAK	SIGMA AV	SIGMA PEAK	SIGMAZ(DB) AV	SIGMAZ(DB) PEAK

FLIGHT	SEA DIRECTION	WAVE HEIGHT(FT)	WAVE PERIOD(SEC)	WIND SPEED(KT)	WIND DIRECTION	WATER TEMP(F)	AIR TEMP	AIR PRES(MB)
12	265	99	99	15	330	99	99	9999.90

RUN	ALTITUDE(FT)	PULSES PER FRAME	PULSE WIDTH(NS)	PEAK POWER	POLARIZATION(1)	C54 HEADING
1	10000	1	20	3	1	85
2	10000	1	20	3	1	355
3	10000	1	20	3	1	265
4	10000	1	20	3	1	175
5	10000	2	20	3	1	85
6	10000	2	20	3	1	355
7	10000	2	20	3	1	265

8	10000.	2	20	3	1	175
9	10000	10	20	3	1	85
10	10000	10	20	3	1	355
11	10000	10	20	3	1	265
12	10000	10	20	3	1	175
13	10000	50	20	3	1	85
14	10000	50	20	3	1	355
15	10000	50	20	3	1	265
16	10000	50	20	3	1	175
17	10000	148	20	3	1	85
18	10000	148	20	3	1	355
19	10000	148	20	3	1	265
20	10000	148	20	3	1	175
21	10000	278	20	3	1	85
22	10000	278	20	3	1	355
23	10000	278	20	3	1	265
24	10000	278	20	3	1	175

	FRAME	RCVD PWR(DBM)AV	RCVD PWR(DBM)PEAK	SIGMA AV	SIGMA PEAK	SIGMAZ(DB) AV	SIGMAZ(DB) PEAK
17	2642	-63.52	-60.88	61.97	64.61	14.318	16.955
17	2643	-62.65	-61.21	62.84	64.28	15.193	16.626
17	2644	-62.74	-60.73	62.75	64.76	15.097	17.110
17	2645	-63.12	-60.69	62.37	64.80	14.723	17.146
17	2646	-63.12	-60.58	62.37	64.91	14.717	17.260
18	2689	-65.43	-62.91	60.06	62.58	12.408	14.925
18	2690	-64.84	-62.36	60.65	63.13	12.995	15.477
18	2691	-64.43	-62.30	61.06	63.18	13.407	15.534
18	2692	-63.95	-62.12	61.54	63.37	13.888	15.723
18	2693	-64.63	-62.74	60.85	62.74	13.204	15.094
19	2725	-64.36	-62.74	61.13	62.75	13.481	15.100
19	2726	-66.73	-63.91	58.75	61.58	11.104	13.932
19	2727	-66.26	-62.67	59.23	62.82	11.575	15.168
19	2728	-66.00	-62.16	59.49	63.33	11.839	15.679
19	2729	-64.35	-61.36	61.14	64.13	13.485	16.477
20	2767	-67.42	-63.19	58.07	62.30	10.419	14.650
20	2768	-65.50	-62.39	59.99	63.10	12.340	15.448
20	2769	-65.96	-62.86	59.53	62.63	11.878	14.978
20	2770	-65.78	-62.03	59.71	63.46	12.060	15.813
20	2771	-66.02	-62.13	59.47	63.36	11.821	15.706

FLIGHT	SEA DIRECTION	WAVE HEIGHT(FT)	WAVE PERIOD(SEC)	WIND SPEED(KT)	WIND DIRECTION	WATER TEMP(F)	AIR TEMP	AIR PRES(MB)
13	220	9	8	26	220	58	55	1005.90

RUN	ALTITUDE(FT)	PULSES PER FRAME	PULSE WIDTH(NS)	PEAK POWER	POLARIZATION(1)	C54 HEADING
1	10000	1	20	3	1	220
2	10000	1	20	3	1	130
3	10000	1	20	3	1	40
4	10000	1	20	3	1	310
5	10000	10	20	3	1	220
6	10000	10	20	3	1	130
7	10000	10	20	3	1	40
8	10000	10	20	3	1	310
9	10000	50	20	3	1	220
10	10000	50	20	3	1	130
11	10000	50	20	3	1	40
12	10000	50	20	3	1	310
13	10000	148	20	3	1	220
14	10000	148	20	3	1	130
15	10000	148	20	3	1	40
16	10000	148	20	3	1	310
17	10000	278	20	3	1	220
18	10000	278	20	3	1	130
19	10000	278	20	3	1	40

20	10000	278	20	3	1	310
21	10000	50	20	3	2	220
22	10000	50	20	3	2	130
23	10000	50	20	3	2	40
24	10000	50	20	3	2	310

FRAME	RCVD PWR(DBM)AV	RCVD PWR(DBM)PEAK	SIGMA AV	SIGMA PEAK	SIGMAZ(DB) AV	SIGMAZ(DB) PEAK

FLIGHT	SEA DIRECTION	WAVE HEIGHT(FT)	WAVE PERIOD(SEC)	WIND SPEED(KT)	WIND DIRECTION	WATER TEMP(F)	AIR TEMP	AIR PRES(MB)
14	350	5	5	12	360	55	43	1020.30

RUN	ALTITUDE(FT)	PULSES PER FRAME	PULSE WIDTH(NS)	PEAK POWER	POLARIZATION(1)	C54 HEADING
1	10000	1	20	12	1	350
2	10000	1	20	12	1	260
3	10000	1	20	12	1	170
4	10000	1	20	12	1	80
5	10000	10	20	12	1	350
6	10000	10	20	12	1	260
7	10000	10	20	12	1	170
8	10000	10	20	12	1	80
9	10000	50	20	12	1	350
10	10000	50	20	12	1	260
11	10000	50	20	12	1	170
12	10000	50	20	12	1	80
13	10000	148	20	12	1	350
14	10000	148	20	12	1	260
15	10000	148	20	12	1	170
16	10000	148	20	12	1	80
17	10000	50	20	12	2	350
18	10000	50	20	12	2	260
19	10000	50	20	12	2	170
20	10000	50	20	12	2	80
21	10000	50	20	12	1	350
22	10000	50	20	12	1	260
23	10000	50	20	12	1	170
24	10000	50	20	12	1	80

	FRAME	RCVD PWR(DBM)AV	RCVD PWR(DBM)PEAK	SIGMA AV	SIGMA PEAK	SIGMAZ(DB) AV	SIGMAZ(DB) PEAK
1	3919	-62.27	-62.27	57.20	57.20	9.549	9.549
1	3920	-63.49	-63.49	55.98	55.98	8.331	8.331
1	3921	-63.73	-63.73	55.74	55.74	8.089	8.089
1	3922	-65.57	-65.57	53.90	53.90	6.250	6.250
1	3923	-63.57	-63.57	55.90	55.90	8.245	8.245
1	3925	-63.64	-63.64	55.83	55.83	8.178	8.178
1	3926	-66.16	-66.16	53.31	53.31	5.658	5.658
1	3927	-64.54	-64.54	54.92	54.92	7.274	7.274
1	3928	-62.87	-62.87	56.60	56.60	8.950	8.950
1	3929	-65.04	-65.04	54.43	54.43	6.782	6.782
1	3930	-66.98	-66.98	52.49	52.49	4.837	4.837
1	3931	-68.30	-68.30	51.16	51.16	3.513	3.513
1	3932	-68.94	-68.94	50.53	50.53	2.875	2.875
1	3933	-66.36	-66.36	53.11	53.11	5.463	5.463
1	3934	-65.20	-65.20	54.27	54.27	6.619	6.619
1	3935	-63.91	-63.91	55.55	55.55	7.904	7.904
1	3936	-64.53	-64.53	54.94	54.94	7.291	7.291
1	3937	-65.09	-65.09	54.38	54.38	6.732	6.732
1	3938	-63.97	-63.97	55.50	55.50	7.845	7.845
1	3939	-66.48	-66.48	52.99	52.99	5.337	5.337
1	3940	-64.89	-64.89	54.58	54.58	6.929	6.929
1	3941	-63.70	-63.70	55.77	55.77	8.121	8.121

1	3942	-65.12	-65.12	54.35	54.35	6.701	6.701
1	3943	-64.79	-64.79	54.68	54.68	7.026	7.026
9	4180	-61.43	-59.07	57.54	60.40	9.888	12.746
9	4181	-60.85	-58.50	58.62	60.97	10.971	13.316
9	4182	-61.58	-59.07	57.88	60.40	10.234	12.748
10	4221	-61.69	-58.44	57.78	61.03	10.129	13.383
10	4222	-62.83	-58.97	56.64	60.50	8.985	12.846
10	4223	-62.55	-59.36	56.92	60.11	9.268	12.457
11	4263	-60.43	-58.05	59.04	61.42	11.392	13.770
11	4264	-60.60	-58.12	58.87	61.35	11.215	13.700
11	4265	-60.94	-57.96	58.53	61.50	10.883	13.854
12	4305	-62.17	-58.73	57.30	60.74	9.649	13.087
12	4306	-62.05	-58.49	57.42	60.98	9.773	13.327
12	4307	-62.48	-59.18	56.99	60.29	9.337	12.637
13	4347	-57.48	-54.95	61.99	64.52	14.342	16.865
13	4348	-58.01	-55.67	61.46	63.79	13.807	16.144
13	4349	-58.30	-55.43	61.17	64.04	13.519	16.387
13	4350	-58.44	-55.10	61.03	64.37	13.377	16.715
13	4351	-57.31	-54.05	62.16	65.42	14.507	17.772
14	4389	-57.47	-55.07	61.99	64.40	14.344	16.750
14	4390	-57.06	-54.88	62.41	64.59	14.757	16.937
14	4391	-58.87	-55.82	60.60	63.65	12.952	15.997
14	4392	-58.15	-55.49	61.32	63.98	13.666	16.328
14	4393	-57.47	-54.99	62.00	64.48	14.351	16.827
15	4431	-58.50	-54.54	60.97	64.92	13.321	17.273
15	4432	-58.73	-55.82	60.73	63.65	13.084	15.997
15	4433	-58.50	-55.81	60.97	63.66	13.321	16.012
15	4434	-58.07	-55.06	61.40	64.41	13.746	16.757
15	4435	-57.65	-55.35	61.82	64.12	14.166	16.469
16	4473	-59.09	-56.54	60.38	62.92	12.728	15.274
16	4474	-59.31	-56.52	60.16	62.94	12.511	15.293
16	4475	-58.91	-56.72	60.56	62.75	12.909	15.101
16	4476	-59.66	-57.08	59.81	62.39	12.161	14.735
16	4477	-59.59	-56.60	59.88	62.87	12.232	15.215

FLIGHT	SEA DIRECTION	WAVE HEIGHT(FT)	WAVE PERIOD(SEC)	WIND SPEED(KT)	WIND DIRECTION	WATER TEMP(F)	AIR TEMP	AIR PRES(MB)
15	10	3	4	6	10	55	51	1027.80

RUN	ALTITUDE(FT)	PULSES PER FRAME	PULSE WIDTH(NS)	PEAK POWER	POLARIZATION(1)	C54 HEADING
1	10000	1	20	12	1	10
2	10000	1	20	12	1	280
3	10000	1	20	12	1	190
4	10000	1	20	12	1	100
5	10000	10	20	12	1	10
6	10000	10	20	12	1	280
7	10000	10	20	12	1	190
8	10000	10	20	12	1	100
9	10000	50	20	12	1	10
10	10000	50	20	12	1	280
11	10000	50	20	12	1	190
12	10000	50	20	12	1	100
13	10000	148	20	12	1	10
14	10000	148	20	12	1	280
15	10000	148	20	12	1	190
16	10000	148	20	12	1	100
17	10000	278	20	12	1	10
18	10000	278	20	12	1	280
19	10000	278	20	12	1	190
20	10000	278	20	12	1	100
21	10000	50	20	12	1	10
22	10000	50	20	12	1	280
23	10000	50	20	12	1	190
24	10000	50	20	12	1	100

	FRAME	RCVD PWR(DBM)AV	RCVD PWR(DBM)PEAK	SIGMA AV	SIGMA PEAK	SIGMAZ(DB) AV	SIGMAZ(DB) PEAK
1	5222	-55.60	-55.60	63.87	63.87	16.215	16.215
1	5224	-57.50	-57.50	61.97	61.97	14.321	14.321
1	5225	-57.92	-57.92	61.55	61.55	13.902	13.902
2	5254	-57.45	-57.45	62.02	62.02	14.373	14.373
2	5255	-57.54	-57.54	61.93	61.93	14.279	14.279
2	5256	-57.07	-57.07	62.40	62.40	14.750	14.750
2	5257	-57.99	-57.99	61.48	61.48	13.832	13.832
2	5258	-58.98	-58.98	60.49	60.49	12.843	12.843
3	5286	-56.04	-56.04	63.43	63.43	15.776	15.776
2	5287	-55.68	-55.68	63.79	63.79	16.137	16.137
3	5288	-57.04	-57.04	62.43	62.43	14.777	14.777
3	5289	-56.78	-56.78	62.69	62.69	15.042	15.042
3	5290	-56.58	-56.58	62.89	62.89	15.241	15.241
4	5318	-58.09	-58.09	61.38	61.38	13.732	13.732
4	5319	-57.63	-57.63	61.84	61.84	14.189	14.189
4	5320	-60.43	-60.43	59.04	59.04	11.393	11.393
4	5321	-57.04	-57.04	62.43	62.43	14.777	14.777
4	5322	-59.31	-59.31	60.16	60.16	12.512	12.512
9	5484	-55.50	-52.03	63.97	67.44	16.321	19.793
9	5485	-55.86	-53.79	63.61	65.68	15.955	18.025
9	5486	-55.48	-52.89	63.99	66.58	16.337	18.931
9	5487	-54.44	-51.66	65.02	67.81	17.374	20.160
9	5488	-54.89	-51.83	64.58	67.64	16.927	19.990
9	5489	-54.69	-51.64	64.78	67.82	17.131	20.174
9	5490	-54.75	-51.66	64.72	67.81	17.065	20.159
9	5491	-55.01	-51.95	64.46	67.52	16.807	19.865
9	5492	-54.91	-52.05	64.56	67.42	16.912	19.766
9	5493	-54.54	-52.66	64.93	66.81	17.275	19.157
9	5494	-55.92	-52.29	63.55	67.18	15.898	19.532
9	5495	-55.57	-52.37	63.90	67.10	16.253	19.445
9	5496	-55.91	-53.09	63.56	66.38	15.909	18.732
9	5497	-55.12	-52.59	64.35	66.87	16.698	19.224
9	5498	-55.10	-52.10	64.37	67.37	16.717	19.720
9	5499	-55.57	-52.70	63.90	66.77	16.253	19.118
9	5501	-55.63	-52.51	63.84	66.96	16.191	19.313
9	5502	-54.52	-51.97	64.95	67.50	17.302	19.845
9	5503	-55.65	-52.51	63.82	66.96	16.172	19.306
9	5504	-54.56	-52.24	64.91	67.22	17.262	19.574
9	5505	-56.01	-52.14	63.46	67.33	15.811	19.681
9	5506	-56.03	-52.84	63.43	66.63	15.784	18.982
9	5507	-54.06	-51.71	65.41	67.76	17.758	20.105
9	5508	-55.90	-52.68	63.57	66.79	15.919	19.137
9	5509	-55.49	-53.65	63.98	65.82	16.326	18.169
10	5524	-55.11	-52.93	64.36	66.53	16.708	18.884
10	5525	-53.09	-52.28	65.47	67.19	17.824	19.537
10	5526	-55.69	-52.87	63.77	66.59	16.124	18.944
10	5527	-56.50	-53.69	62.97	65.78	15.317	18.129
10	5528	-55.59	-53.36	63.78	66.11	16.131	18.456
10	5529	-54.77	-52.72	64.70	66.75	17.047	19.102
10	5530	-56.20	-53.50	63.27	65.97	15.623	18.321
10	5531	-54.36	-52.79	64.61	66.68	16.961	19.033
10	5532	-55.66	-52.72	63.80	66.75	16.154	19.095
10	5533	-55.50	-52.76	63.97	66.71	16.319	19.057
10	5534	-54.64	-52.83	64.83	66.64	17.175	18.989
10	5535	-54.69	-52.39	64.78	67.08	17.131	19.428
10	5536	-54.80	-52.44	64.66	67.03	17.014	19.378
10	5537	-55.38	-52.54	64.09	66.93	16.441	19.276
10	5538	-54.89	-52.46	64.58	67.01	16.927	19.359
10	5539	-54.81	-52.04	64.66	67.42	17.007	19.774
10	5540	-57.21	-53.07	62.26	66.40	14.609	18.745
10	5541	-59.08	-54.34	60.39	65.13	12.740	17.478
10	5542	-56.45	-52.54	62.52	66.93	14.867	19.281
10	5543	-56.72	-52.79	62.75	66.68	15.095	19.032

10	5544	-56.41	-53.81	62.56	65.66	14.911	18.011
10	5545	-56.07	-53.40	63.40	66.07	15.745	18.421
10	5546	-55.49	-52.56	64.38	66.91	16.729	19.261
10	5547	-55.94	-52.46	64.43	67.01	16.777	19.360
10	5548	-54.69	-52.56	64.78	66.91	17.129	19.260
11	5566	-54.70	-52.30	64.77	67.17	17.121	19.522
11	5567	-55.84	-52.38	63.63	67.09	15.978	19.436
11	5568	-54.61	-51.75	65.45	67.72	17.804	20.067
11	5569	-54.11	-51.97	65.35	67.50	17.704	19.845
11	5570	-54.73	-52.06	64.73	67.41	17.083	19.756
11	5571	-55.77	-52.72	63.70	66.75	16.047	19.102
11	5572	-53.53	-51.46	65.94	68.01	18.291	20.360
11	5573	-54.81	-51.30	64.65	68.17	17.004	20.517
11	5574	-55.20	-51.66	64.27	67.81	16.623	20.162
11	5575	-55.75	-52.85	63.72	66.61	16.070	18.964
11	5576	-54.34	-50.93	65.13	68.54	17.482	20.893
11	5578	-55.77	-52.14	63.70	67.32	16.047	19.674
11	5579	-56.72	-51.72	62.75	67.75	15.095	20.101
11	5580	-54.91	-52.24	64.56	67.23	16.912	19.578
11	5581	-56.22	-52.15	63.25	67.32	15.597	19.670
11	5582	-56.37	-53.20	63.10	66.27	15.446	18.621
11	5583	-56.42	-51.74	63.05	67.73	15.401	20.082
11	5584	-55.64	-51.14	63.83	68.33	16.181	20.680
11	5585	-56.31	-53.05	63.16	66.42	15.505	18.769
11	5586	-57.00	-51.71	62.47	67.76	14.821	20.113
11	5587	-55.66	-52.38	63.81	67.08	16.156	19.434
11	5586	-55.66	-52.72	63.81	66.74	16.159	19.094
11	5589	-55.01	-51.75	64.46	67.72	16.806	20.066
11	5590	-55.31	-51.84	64.16	67.63	16.510	19.976
12	5608	-56.57	-53.34	62.90	66.13	15.247	18.483
12	5609	-57.22	-53.67	62.25	65.80	14.598	18.145
12	5610	-57.55	-54.27	61.92	65.19	14.267	17.545
12	5611	-56.19	-52.67	63.28	66.80	15.633	19.146
12	5612	-56.31	-52.31	63.16	67.16	15.509	19.508
12	5613	-54.98	-51.85	64.49	67.62	16.836	19.967
12	5614	-54.33	-52.49	65.14	66.98	17.485	19.333
12	5615	-56.69	-53.96	62.78	65.51	15.129	17.863
12	5616	-56.35	-53.46	63.12	66.00	15.466	18.354
12	5617	-55.68	-53.10	63.79	66.36	16.137	18.714
12	5618	-56.93	-54.06	62.54	65.41	14.891	17.763
12	5619	-55.24	-53.28	64.23	66.19	16.576	18.543
12	5620	-56.22	-52.61	63.25	66.86	15.603	19.213
12	5621	-54.33	-51.95	65.13	67.52	17.484	19.867
12	5622	-55.19	-52.18	64.28	67.29	16.626	19.643
12	5623	-54.99	-52.43	64.48	67.04	16.831	19.387
12	5624	-55.39	-52.64	64.08	66.82	16.430	19.174
12	5625	-54.93	-52.50	64.54	66.97	16.887	19.319
12	5626	-55.23	-52.80	64.23	66.67	16.584	19.020
12	5627	-55.82	-52.41	63.65	67.06	15.998	19.405
12	5628	-54.18	-52.35	65.29	67.12	17.637	19.472
12	5629	-55.76	-52.21	63.71	67.26	16.057	19.606
12	5630	-55.47	-52.42	64.00	67.05	16.351	19.399
12	5631	-55.54	-52.36	63.93	67.11	16.279	19.455
12	5632	-54.81	-52.37	64.66	67.10	17.009	19.452

FLIGHT	SEA DIRECTION	WAVE HEIGHT(FT)	WAVE PERIOD(SEC)	WIND SPEED(KT)	WIND DIRECTION	WATER TEMP(F)	AIR TEMP	AIR PRES(MB)
16	210	7	7	22	210	55	60	1016.60

RUN	ALTITUDE(FT)	PULSES PER FRAME	PULSE WIDTH(NS)	PEAK POWER	POLARIZATION(1)	C54 HEADING
1	10000	1	20	12	1	210
2	10000	1	20	12	1	120
3	10000	1	20	12	1	30
4	10000	1	20	12	1	300
5	10000	10	20	12	1	210

6	10000	10	20	12	1	120
7	10000	10	20	12	1	30
8	10000	10	20	12	1	300
9	10000	50	20	12	1	210
10	10000	50	20	12	1	120
11	10000	50	20	12	1	30
12	10000	50	20	12	1	300
13	10000	148	20	12	1	210
14	10000	148	20	12	1	120
15	10000	148	20	12	1	30
16	10000	148	20	12	1	300
17	10000	50	20	12	1	210
18	10000	50	20	12	1	120
19	10000	50	20	12	1	30
20	10000	50	20	12	1	300
21	10000	148	20	12	1	210
22	10000	148	20	12	1	120
23	10000	148	20	12	1	30
24	10000	148	20	12	1	300

	FRAME	RCVD PWR(DBM)AV	RCVD PWR(DBM)PEAK	SIGMA AV	SIGMA PEAK	SIGMAZ(DB) AV	SIGMAZ(DB) PEAK
9	6577	-64.74	-60.61	54.73	58.86	7.081	11.210
9	6578	-61.85	-59.09	57.62	60.38	9.970	12.728
9	6579	-63.40	-60.21	56.06	59.26	8.414	11.612
10	6624	-63.13	-60.36	56.33	59.11	8.684	11.457
10	6625	-62.99	-60.72	56.48	58.75	8.826	11.098
10	6626	-63.61	-60.86	55.85	58.61	8.204	10.961
11	6666	-62.66	-59.96	56.80	59.51	9.154	11.856
11	6667	-62.78	-60.60	56.69	58.87	9.036	11.220
11	6668	-62.52	-59.85	56.95	59.62	9.298	11.971
12	6708	-62.40	-60.38	57.07	59.09	9.418	11.440
12	6709	-62.84	-60.32	56.63	59.15	8.982	11.501
12	6710	-63.82	-60.21	56.45	59.26	8.798	11.610
13	6750	-64.61	-62.02	54.86	57.45	7.208	9.798
13	6751	-62.89	-60.62	56.58	58.85	8.933	11.203
13	6752	-64.57	-60.98	54.90	58.49	7.250	10.841
13	6753	-63.59	-61.02	55.78	58.44	8.132	10.793
13	6754	-64.29	-60.66	55.18	58.80	7.529	11.154
14	6792	-63.63	-60.88	55.84	58.59	8.190	10.941
14	6793	-64.05	-61.47	55.42	57.99	7.771	10.344
14	6794	-64.05	-61.73	55.42	57.74	7.767	10.088
14	6795	-63.60	-61.25	55.67	58.21	8.017	10.564
14	6796	-63.24	-60.82	56.23	58.65	8.580	11.003
15	6834	-64.77	-62.28	54.70	57.19	7.045	9.535
15	6835	-62.67	-60.18	56.80	59.29	9.148	11.636
15	6836	-62.55	-59.04	56.92	60.43	9.273	12.778
15	6837	-61.24	-59.52	58.23	59.95	10.581	12.295
15	6838	-62.59	-59.24	56.88	60.23	9.225	12.579
16	6876	-63.91	-60.19	56.46	59.28	8.805	11.632
16	6877	-63.40	-60.46	56.07	59.01	8.417	11.361
16	6878	-63.03	-59.83	56.44	59.63	8.788	11.984
16	6879	-62.50	-59.95	56.97	59.52	9.318	11.865
16	6880	-61.44	-59.83	57.53	59.64	9.882	11.991

1 POLARIZATION CODES 1 DIRECT+2 CROSS

NOTE$FOR FLT7.PULSES PER FRAME VARIED DURING RUN WITH VALUES OF 50,148,278

A-2 OVERALL FLIGHTS

MEAN SIGA(DB)	STD.DEV.	SAMPLE SIZE	MEAN SIGP(DB)	STD.DEV.	SAMPLE SIZE
16.115	15.694	542.0	19.725	19.171	474.0

A-3

FLIGHT	MEAN SIGZ(DB)AV	SAMPLE SIZE	STD.DEV.(DB)	MEAN SIGZ(DB)PK	SAMPLE SIZE	STD.DEV.(DB)
4	8.71	18	2.07	11.88	18	4.51

SIGZAV + 1 STD DEV DB	SIGZAV - 1 STD DEV DB	SIGZPK + 1 STD DEV DB	SIGZPK - 1 STD DEV DB
9.56	7.65	12.61	11.00

FLIGHT HISTOGRAM(NO.OF STD.DEV.FROM MEAN (

FLIGHT	(LT-2)	(-2 TO -1.5)	(-1.5 TO -1)	(-1 TO -.5)	(-.5 TO 0)	(0 TO .5)	(.5 TO 1)	(1 TO 1.5)	(1.5 TO 2)	(GE 2)
4	0	3	1	1	3	2	5	3	0	0

HISTOGRAM.FROM -1 TO -7/8.-7/8 TO -3/4.---7/8 TO 1 STD.DEV.

0 0 1 0 0 0 1 2 1 1 0 0 1 2 2 0

CUMULATIVE PROBABILITY

0.00000 0.00000 .16667 .22222 .27778 .44444 .55556 .83333 1.00000 1.00000 1.00000

$$$$$$$$$$$$$$$$$$$$$$$$$$$$$$$$$$

FLIGHT HISTOGRAM(NO.OF STD.DEV.FROM MEAN

FLIGHT	(LT-2)	(-2 TO -1.5)	(-1.5 TO -1)	(-1 TO -.5)	(-.5 TO 0)	(0 TO .5)	(.5 TO 1)	(1 TO 1.5)	(1.5 TO 2)	(GE 2)
4	0	1	2	4	1	4	1	5	0	0

HISTOGRAM.FROM -1 TO -7/8.-7/8 TO -3/4.---7/8 TO 1 STD.DEV.

1 1 2 0 1 0 0 0 0 2 1 1 1 0 0 0

CUMULATIVE PROBABILITY

0.00000 0.00000 .05556 .16667 .38889 .44444 .66667 .72222 1.00000 1.00000 1.00000

$$$$$$$$$$$$$$$$$$$$$$$$$$$$$$$$$$

FLIGHT	MEAN SIGZ(DB)AV	SAMPLE SIZE	STD.DEV.(DB)	MEAN SIGZ(DB)PK	SAMPLE SIZE	STD.DEV.(DB)
5	17.85	18	11.66	20.47	18	11.93

SIGZAV + 1 STD DEV DB	SIGZAV - 1 STD DEV DB	SIGZPK + 1 STD DEV DB	SIGZPK - 1 STD DEV DB
18.79	16.66	21.04	19.82

FLIGHT HISTOGRAM(NO.OF STD.DEV.FROM MEAN

FLIGHT	(LT-2)	(-2 TO -1.5)	(-1.5 TO -1)	(-1 TO -.5)	(-.5 TO 0)	(0 TO .5)	(.5 TO 1)	(1 TO 1.5)	(1.5 TO 2)	(GE 2)
5	0	0	3	4	3	2	3	1	2	0

HISTOGRAM.FROM -1 TO -7/8.-7/8 TO -3/4.---7/8 TO 1 STD.DEV.

2 0 1 1 1 1 0 1 0 0 2 0 1 0 1 1

CUMULATIVE PROBABILITY

0.00000 0.00000 0.00000 .16667 .38889 .55556 .66667 .83333 .88889 1.00000 1.00000

```
FLIGHT HISTOGRAM(NO.OF STD.DEV.FROM MEAN

FLIGHT (LT-2) (-2 TO -1.5) (-1.5 TO -1) (-1 TO -.5) (-.5 TO 0) (0 TO .5) (.5 TO 1) (1 TO 1.5) (1.5 TO 2) (GE 2)
  5        0          1            1          4         3         4         1          3         1        0
 HISTOGRAM.FROM -1 TO -7/8.-7/8 TO -3/4.---7/8 TO 1 STD.DEV.
   1   2   0   1   1   1   1   0   1   0   2   1   0   1   0   0
CUMULATIVE PROBABILITY
     0.00000   0.00000   .05556   .11111   .33333   .50000   .72222   .77778   .94444   1.00000   1.00000
                              $$$$$$$$$$$$$$$$$$$$$$$$$$$$$$$$

   FLIGHT   MEAN SIGZ(DB)AV   SAMPLE SIZE   STD.DEV.(DB)   MEAN SIGZ(DB)PK   SAMPLE SIZE   STD.DEV.(DB)
     6         15.7[illegible]          9          12.38            22.38              9            16.16
       SIGZAV + 1 STD DEV DB   SIGZAV - 1 STD DEV DB   SIGZPK + 1 STD DEV DB   SIGZPK - 1 STD DEV DB
          1[illegible].[illegible]8                  17.62                   23.31                   21.19
FLIGHT HISTOGRAM(NO.OF STD.DEV.FROM MEAN

FLIGHT (LT-2) (-2 TO -1.5) (-1.5 TO -1) (-1 TO -.5) (-.5 TO 0) (0 TO .5) (.5 TO 1) (1 TO 1.5) (1.5 TO 2) (GE 2)
  6        0          [illegible]            1          2         1         3         0          1         1        0
 HISTOGRAM.FROM -1 TO -7/8.-7/8 TO -3/4.---7/8 TO 1 STD.DEV.
   0   0   1   1   1   0   0   0   3   0   0   0   0   0   0   0
CUMULATIVE PROBABILITY
     0.00000   0.00000   0.00000   .11111   .33333   .44444   .77778   .77778   .88889   1.00000   1.00000
                              $$$$$$$$$$$$$$$$$$$$$$$$$$$$$$$$

FLIGHT HISTOGRAM(NO.OF STD.DEV.FROM MEAN

FLIGHT (LT-2) (-2 TO -1.5) (-1.5 TO -1) (-1 TO -.5) (-.5 TO 0) (0 TO .5) (.5 TO 1) (1 TO 1.5) (1.5 TO 2) (GE 2)
  6        0          0            0          4         2         1         0          1         1        0
 HISTOGRAM.FROM -1 TO -7/8.-7/8 TO -3/4.---7/8 TO 1 STD.DEV.
   1   1   [illegible]   2   1   0   0   1   1   0   0   0   0   0   0   0
CUMULATIVE PROBABILITY
     0.00000   0.00000   0.00000   0.00000   .44444   .66667   .77778   .77778   .88889   1.00000   1.00000
                              $$$$$$$$$$$$$$$$$$$$$$$$$$$$$$$$

   FLIGHT   MEAN SIGZ(DB)AV   SAMPLE SIZE   STD.DEV.(DB)   MEAN SIGZ(DB)PK   SAMPLE SIZE   STD.DEV.(DB)
     7         20.64            78          15.51            24.01             78            18.57
       SIGZAV + 1 STD DEV DB   SIGZAV - 1 STD DEV DB   SIGZPK + 1 STD DEV DB   SIGZPK - 1 STD DEV DB
          21.89                  19.05                   25.10                   22.55
FLIGHT HISTOGRAM(NO.OF STD.DEV.FROM MEAN
```

FLIGHT	(LT-2)	(-2 TO -1.5)	(-1.5 TO -1)	(-1 TO -.5)	(-.5 TO 0)	(0 TO .5)	(.5 TO 1)	(1 TO 1.5)	(1.5 TO 2)	(GE 2)
7	3	3	1	16	13	17	9	8	6	0

HISTOGRAM.FROM -1 TO -7/8,-7/8 TO -3/4,---7/8 TO 1 STD.DEV.

4	5	5	2	6	1	3	3	6	0	5	6	4	4	1	0

CUMULATIVE PROBABILITY

0.00000	.03846	.07692	.11538	.32051	.48718	.70513	.82051	.92308	1.00000	1.00000

$$$$$$$$$$$$$$$$$$$$$$$$$$$$$$$$$$

FLIGHT HISTOGRAM(NO.OF STD.DEV.FROM MEAN

FLIGHT	(LT-2)	(-2 TO -1.5)	(-1.5 TO -1)	(-1 TO -.5)	(-.5 TO 0)	(0 TO .5)	(.5 TO 1)	(1 TO 1.5)	(1.5 TO 2)	(GE 2)
7	2	3	7	12	15	17	9	6	5	2

HISTOGRAM.FROM -1 TO -7/8,-7/8 TO -3/4,---7/8 TO 1 STD.DEV.

2	4	4	2	6	4	4	1	7	5	2	3	1	2	4	2

CUMULATIVE PROBABILITY

0.00000	.02564	.06410	.15385	.30769	.50000	.71795	.83333	.91026	.97436	1.00000

$$$$$$$$$$$$$$$$$$$$$$$$$$$$$$$$$$

FLIGHT	MEAN SIGZ(DB)AV	SAMPLE SIZE	STD.DEV.(DB)	MEAN SIGZ(DB)PK	SAMPLE SIZE	STD.DEV.(DB)
8	14.34	161	9.20	18.19	135	13.70

SIGZAV + 1 STD DEV DB	SIGZAV - 1 STD DEV DB	SIGZPK + 1 STD DEV DB	SIGZPK - 1 STD DEV DB
15.50	12.75	19.51	16.28

FLIGHT HISTOGRAM(NO.OF STD.DEV.FROM MEAN

FLIGHT	(LT-2)	(-2 TO -1.5)	(-1.5 TO -1)	(-1 TO -.5)	(-.5 TO 0)	(0 TO .5)	(.5 TO 1)	(1 TO 1.5)	(1.5 TO 2)	(GE 2)
8	6	7	11	23	30	34	28	11	6	5

HISTOGRAM.FROM -1 TO -7/8,-7/8 TO -3/4,---7/8 TO 1 STD.DEV.

4	5	7	7	8	4	10	8	11	11	6	6	9	7	4	8

CUMULATIVE PROBABILITY

0.00000	.03727	.08075	.14907	.29193	.47826	.68944	.86335	.93168	.96894	1.00000

$$$$$$$$$$$$$$$$$$$$$$$$$$$$$$$$$$

FLIGHT HISTOGRAM(NO.OF STD.DEV.FROM MEAN

FLIGHT	(LT-2)	(-2 TO -1.5)	(-1.5 TO -1)	(-1 TO -.5)	(-.5 TO 0)	(0 TO .5)	(.5 TO 1)	(1 TO 1.5)	(1.5 TO 2)	(GE 2)
8	0	0	6	39	49	19	3	3	5	11

HISTOGRAM.FROM -1 TO -7/8,-7/8 TO -3/4,---7/8 TO 1 STD.DEV.

9	6	9	15	9	13	18	9	6	8	4	1	1	2	0	0

CUMULATIVE PROBABILITY

0.00000	0.00000	0.00000	.04444	.33333	.69630	.83704	.85926	.88148	.91852	1.00000

$$$$$$$$$$$$$$$$$$$$$$$$$$$$$$$$$$

FLIGHT	MEAN SIGZ(DB)AV	SAMPLE SIZE	STD.DEV.(DB)	MEAN SIGZ(DB)PK	SAMPLE SIZE	STD.DEV.(DB)
10	12.87	33	10.30	15.99	33	13.16

SIGZAV + 1 STD DEV DB	SIGZAV - 1 STD DEV DB	SIGZPK + 1 STD DEV DB	SIGZPK - 1 STD DEV DB
14.7[illegible]	9.37	17.81	12.78

FLIGHT HISTOGRAM(NO.OF STD.DEV.FROM MEAN

FLIGHT	(LT-2)	(-2 TO -1.5)	(-1.5 TO -1)	(-1 TO -.5)	(-.5 TO 0)	(0 TO .5)	(.5 TO 1)	(1 TO 1.5)	(1.5 TO 2)	(GE 2)
10	0	0	1	8	15	3	1	1	2	2

HISTOGRAM.FROM -1 TO -7/8.-7/8 TO -3/4.---7/8 TO 1 STD.DEV.

3	0	1	2	5	4	5	1	1	0	1	1	1	0	0	0

CUMULATIVE PROBABILITY

0.00000	0.00000	0.00000	.03030	.27273	.72727	.81818	.84848	.87879	.93939	1.00000

$$$$$$$$$$$$$$$$$$$$$$$$$$$$$$$$$

FLIGHT HISTOGRAM(NO.OF STD.DEV.FROM MEAN

FLIGHT	(LT-2)	(-2 TO -1.5)	(-1.5 TO -1)	(-1 TO -.5)	(-.5 TO 0)	(0 TO .5)	(.5 TO 1)	(1 TO 1.5)	(1.5 TO 2)	(GE 2)
10	0	0	1	6	13	6	0	1	2	2

HISTOGRAM.FROM -1 TO -7/8.-7/8 TO -3/4.---7/8 TO 1 STD.DEV.

1	1	2	2	4	3	2	4	3	0	2	1	0	0	0	0

CUMULATIVE PROBABILITY

0.00000	0.00000	0.00000	.09091	.27273	.66667	.84848	.84848	.87879	.93939	1.00000

$$$$$$$$$$$$$$$$$$$$$$$$$$$$$$$$$

FLIGHT	MEAN SIGZ(DB)AV	SAMPLE SIZE	STD.DEV.(DB)	MEAN SIGZ(DB)PK	SAMPLE SIZE	STD.DEV.(DB)
12	13.21	20	8.22	15.83	20	9.17

SIGZAV + 1 STD DEV DB	SIGZAV - 1 STD DEV DB	SIGZPK + 1 STD DEV DB	SIGZPK - 1 STD DEV DB
14.4[illegible]	11.55	16.68	14.78

FLIGHT HISTOGRAM(NO.OF STD.DEV.FROM MEAN

FLIGHT	(LT-2)	(-2 TO -1.5)	(-1.5 TO -1)	(-1 TO -.5)	(-.5 TO 0)	(0 TO .5)	(.5 TO 1)	(1 TO 1.5)	(1.5 TO 2)	(GE 2)
12	0	0	2	7	2	3	2	2	2	0

HISTOGRAM.FROM -1 TO -7/8.-7/8 TO -3/4.---7/8 TO 1 STD.DEV.

1	3	1	2	0	0	1	1	0	3	0	0	1	0	0	1

CUMULATIVE PROBABILITY

0.00000	0.00000	0.00000	.10000	.45000	.55000	.70000	.80000	.90000	1.00000	1.00000

$$$$$$$$$$$$$$$$$$$$$$$$$$$$$$$$$

FLIGHT HISTOGRAM(NO.OF STD.DEV.FROM MEAN

FLIGHT	(LT-2)	(-2 TO -1.5)	(-1.5 TO -1)	(-1 TO -.5)	(-.5 TO 0)	(0 TO .5)	(.5 TO 1)	(1 TO 1.5)	(1.5 TO 2)	(GE 2)
12	0	1	1	5	7	0	2	1	3	0

HISTOGRAM.FROM -1 TO -7/8.-7/8 TO -3/4.---7/8 TO 1 STD.DEV.

0	2	3	0	1	2	2	2	0	0	0	0	0	1	0	1

CUMULATIVE PROBABILITY

0.00000	0.00000	.05000	.10000	.35000	.70000	.70000	.80000	.85000	1.00000	1.00000

$$$$$$$$$$$$$$$$$$$$$$$$$$$$$$$$$$$

FLIGHT	MEAN SIGZ(DB)AV	SAMPLE SIZE	STD.DEV.(DB)	MEAN SIGZ(DB)PK	SAMPLE SIZE	STD.DEV.(DB)
14	10.99	56	9.21	15.38	32	10.95

SIGZAV + 1 STD DEV DB	SIGZAV - 1 STD DEV DB	SIGZPK + 1 STD DEV DB	SIGZPK - 1 STD DEV DB
13.20	6.25	16.72	13.44

FLIGHT HISTOGRAM(NO.OF STD.DEV.FROM MEAN

FLIGHT	(LT-2)	(-2 TO -1.5)	(-1.5 TO -1)	(-1 TO -.5)	(-.5 TO 0)	(0 TO .5)	(.5 TO 1)	(1 TO 1.5)	(1.5 TO 2)	(GE 2)
14	0	0	6	18	10	4	5	7	5	1

HISTOGRAM.FROM -1 TO -7/8.-7/8 TO -3/4.---7/8 TO 1 STD.DEV.

7	4	5	2	4	3	1	2	1	1	0	2	0	2	2	1

CUMULATIVE PROBABILITY

0.00000	0.00000	0.00000	.10714	.42857	.60714	.67857	.76786	.89286	.98214	1.00000

$$$$$$$$$$$$$$$$$$$$$$$$$$$$$$$$$$$

FLIGHT HISTOGRAM(NO.OF STD.DEV.FROM MEAN

FLIGHT	(LT-2)	(-2 TO -1.5)	(-1.5 TO -1)	(-1 TO -.5)	(-.5 TO 0)	(0 TO .5)	(.5 TO 1)	(1 TO 1.5)	(1.5 TO 2)	(GE 2)
14	0	0	9	3	5	3	5	5	1	1

HISTOGRAM.FROM -1 TO -7/8.-7/8 TO -3/4.---7/8 TO 1 STD.DEV.

1	2	0	0	1	0	1	3	0	0	0	3	1	2	1	1

CUMULATIVE PROBABILITY

0.00000	0.00000	0.00000	.28125	.37500	.53125	.62500	.78125	.93750	.96875	1.00000

$$$$$$$$$$$$$$$$$$$$$$$$$$$$$$$$$$$

FLIGHT	MEAN SIGZ(DB)AV	SAMPLE SIZE	STD.DEV.(DB)	MEAN SIGZ(DB)PK	SAMPLE SIZE	STD.DEV.(DB)
15	16.17	117	10.05	19.34	99	11.12

SIGZAV + 1 STD DEV DB	SIGZAV - 1 STD DEV DB	SIGZPK + 1 STD DEV DB	SIGZPK - 1 STD DEV DB
17.12	14.95	19.95	18.63

FLIGHT HISTOGRAM(NO.OF STD.DEV.FROM MEAN

FLIGHT (LT-2) (-2 TO -1.5) (-1.5 TO -1) (-1 TO -.5) (-.5 TO 0) (0 TO .5) (.5 TO 1) (1 TO 1.5) (1.5 TO 2) (GE 2)

```
15     4     3     14     13     24     19     22     12     5     1

HISTOGRAM.FROM -1 TO -7/8.-7/8 TO -3/4.---7/8 TO 1 STD.DEV.
  3    3    3    4    4    3    6    11    7    5    3    4    5    5    7    5

CUMULATIVE PROBABILITY
     0.00000    .03419    .05983    .17949    .29060    .49573    .65812    .84615    .94872    .99145    1.00000

                                   $$$$$$$$$$$$$$$$$$$$$$$$$$$$$$$$

FLIGHT HISTOGRAM(NO.OF STD.DEV.FROM MEAN

FLIGHT (LT-2) (-2 TO -1.5) (-1.5 TO -1) (-1 TO -.5) (-.5 TO 0) (0 TO .5) (.5 TO 1) (1 TO 1.5) (1.5 TO 2) (GE 2)
15     3     6     7     10     23     21     12     13     1     3

HISTOGRAM.FROM -1 TO -7/8.-7/8 TO -3/4.---7/8 TO 1 STD.DEV.
  1    3    1    5    4    9    2    8    6    7    6    2    4    4    4    0

CUMULATIVE PROBABILITY
     0.00000    .03030    .09091    .16162    .26263    .49495    .70707    .82828    .95960    .96970    1.00000

                                   $$$$$$$$$$$$$$$$$$$$$$$$$$$$$$$$

     FLIGHT    MEAN SIGZ(DB)AV    SAMPLE SIZE    STD.DEV.(DB)    MEAN SIGZ(DB)PK    SAMPLE SIZE    STD.DEV.(DB)
       16         8.70                32            1.66             11.41              32            3.83

          SIGZAV + 1 STD DEV DB    SIGZAV - 1 STD DEV DB    SIGZPK + 1 STD DEV DB    SIGZPK - 1 STD DEV DB
               9.49                     7.74                     12.11                    10.58

FLIGHT HISTOGRAM(NO.OF STD.DEV.FROM MEAN

FLIGHT (LT-2) (-2 TO -1.5) (-1.5 TO -1) (-1 TO -.5) (-.5 TO 0) (0 TO .5) (.5 TO 1) (1 TO 1.5) (1.5 TO 2) (GE 2)
16     0     2     3     5     4     7     7     0     2     1

HISTOGRAM.FROM -1 TO -7/8.-7/8 TO -3/4.---7/8 TO 1 STD.DEV.
  2    0    1    3    0    2    1    1    3    1    2    1    2    3    1    1

CUMULATIVE PROBABILITY
     0.00000    0.00000    .06250    .15625    .34375    .46875    .68750    .90625    .90625    .96875    1.00000

                                   $$$$$$$$$$$$$$$$$$$$$$$$$$$$$$$$

FLIGHT HISTOGRAM(NO.OF STD.DEV.FROM MEAN

FLIGHT (LT-2) (-2 TO -1.5) (-1.5 TO -1) (-1 TO -.5) (-.5 TO 0) (0 TO .5) (.5 TO 1) (1 TO 1.5) (1.5 TO 2) (GE 2)
16     1     2     2     5     6     7     5     1     1     2

HISTOGRAM.FROM -1 TO -7/8.-7/8 TO -3/4.---7/8 TO 1 STD.DEV.
  0    1    1    3    1    3    1    1    3    0    4    0    1    1    3    0

CUMULATIVE PROBABILITY
     0.00000    .03125    .09375    .15625    .31250    .50000    .71875    .87500    .90625    .93750    1.00000

                                   $$$$$$$$$$$$$$$$$$$$$$$$$$$$$$$$
```

A-4 DISTRIBUTIONS FOR SELECTED RUNS

FLIGHT	RUN	MEAN SIGA(DB)	STD.DEV.	SAM.SIZE	MEAN SIGP(DB)	STD.DEV.	SAM.SIZE
8	13	15.61	8.29	20	20.63	12.28	20

RUN HISTOGRAM(NO.OF STD.DEV.FROM MEAN

FLIGHT	RUN	(LT-2)	(-2 TO-1.5)	(-1.5 TO -1)	(-1 TO -.5)	(.5 TO 0)	(0 TO .5)	(.5 TO 1)	(1 TO 1.5)	(1.5 TO 2)	(GE 2)
8	13	0	0	4	3	5	2	2	2	1	1

HISTOGRAM,FROM -1 TO -7/8,-7/8 TO -3/4,---7/8 TO 1 STD.DEV.

0	0	2	1	1	2	2	0	0	2	0	0	1	0	1	0

CUMULATIVE PROBABILITY

0.00000	0.00000	0.00000	.20000	.35000	.60000	.70000	.80000	.90000	.95000	1.00000

$$$$$$$$$$$$$$$$$$$$$$$$$$$$$$$$$$

RUN HISTOGRAM(NO.OF STD.DEV.FROM MEAN

FLIGHT	RUN	(LT-2)	(-2 TO-1.5)	(-1.5 TO -1)	(-1 TO -.5)	(.5 TO 0)	(0 TO .5)	(.5 TO 1)	(1 TO 1.5)	(1.5 TO 2)	(GE 2)
8	13	0	1	2	4	3	4	2	2	2	0

HISTOGRAM,FROM -1 TO -7/8,-7/8 TO -3/4,---7/8 TO 1 STD.DEV.

1	1	1	1	0	1	1	1	2	0	2	0	1	0	0	1

CUMULATIVE PROBABILITY

0.00000	0.00000	.05000	.15000	.35000	.50000	.70000	.80000	.90000	1.00000	1.00000

$$$$$$$$$$$$$$$$$$$$$$$$$$$$$$$$$$

DISTRIBUTIONS FOR SELECTED RUNS

FLIGHT	RUN	MEAN SIGA(DB)	STD.DEV.	SAM.SIZE	MEAN SIGP(DB)	STD.DEV.	SAM.SIZE
8	14	14.01	4.08	20	17.15	9.09	20

RUN HISTOGRAM(NO.OF STD.DEV.FROM MEAN

FLIGHT	RUN	(LT-2)	(-2 TO-1.5)	(-1.5 TO -1)	(-1 TO -.5)	(.5 TO 0)	(0 TO .5)	(.5 TO 1)	(1 TO 1.5)	(1.5 TO 2)	(GE 2)
8	14	0	1	2	4	4	5	0	2	1	1

HISTOGRAM,FROM -1 TO -7/8,-7/8 TO -3/4,---7/8 TO 1 STD.DEV.

0	2	1	1	1	2	1	0	0	1	4	0	0	0	0	0

CUMULATIVE PROBABILITY

0.00000	0.00000	.05000	.15000	.35000	.55000	.80000	.80000	.90000	.95000	1.00000

$$$$$$$$$$$$$$$$$$$$$$$$$$$$$$$$$$

RUN HISTOGRAM(NO.OF STD.DEV.FROM MEAN

FLIGHT	RUN	(LT-2)	(-2 TO-1.5)	(-1.5 TO -1)	(-1 TO -.5)	(.5 TO 0)	(0 TO .5)	(.5 TO 1)	(1 TO 1.5)	(1.5 TO 2)	(GE 2)
8	14	0	1	1	4	6	3	1	3	0	1

HISTOGRAM.FROM -1 TO -7/8,-7/8 TO -3/4,---7/8 TO 1 STD.DEV.

1 1 1 1 2 1 2 1 0 2 1 0 0 0 0 1

CUMULATIVE PROBABILITY

0.00000 [illegible] .05000 .10000 .30000 .60000 .75000 .80000 .95000 .95000 1.00000

$$$$$$$$$$$$$$$$$$$$$$$$$$$$$$$$

DISTRIBUTIONS FOR SELECTED RUNS

FLIGHT	RUN	MEAN SIGP(DB)	STD.DEV.	SAM.SIZE	MEAN SIGP(DB)	STD.DEV.	SAM.SIZE
8	15	14.41	7.30	20	18.06	9.27	20

RUN HISTOGRAM(NO.OF STD.DEV.FROM MEAN

FLIGHT	RUN	(LT-2)	(-2 TO-1.5)	(-1.5 TO -1)	(-1 TO -.5)	(.5 TO 0)	(0 TO .5)	(.5 TO 1)	(1 TO 1.5)	(1.5 TO 2)	(GE 2)
8	15	1	2	2	4	4	5	1	0	1	

HISTOGRAM.FROM -1 TO -7/8,-7/8 TO -3/4,---7/8 TO 1 STD.DEV.

1 1 0 0 0 2 1 1 2 2 0 0 1 1 3 0

CUMULATIVE PROBABILITY

0.00000 [illegible] [illegible] .15000 .25000 .45000 .65000 .90000 .95000 .95000 1.00000

$$$$$$$$$$$$$$$$$$$$$$$$$$$$$$$$

RUN HISTOGRAM(NO.OF STD.DEV.FROM MEAN

FLIGHT	RUN	(LT-2)	(-2 TO-1.5)	(-1.5 TO -1)	(-1 TO -.5)	(.5 TO 0)	(0 TO .5)	(.5 TO 1)	(1 TO 1.5)	(1.5 TO 2)	(GE 2)
8	15	2	1	1	6	2	6	1	1	0	

HISTOGRAM.FROM -1 TO -7/8,-7/8 TO -3/4,---7/8 TO 1 STD.DEV.

0 0 0 1 1 2 2 1 0 1 1 0 2 1 3 0

CUMULATIVE PROBABILITY

0.00000 [illegible] .10000 .15000 .20000 .50000 .60000 .90000 .95000 1.00000 1.00000

$$$$$$$$$$$$$$$$$$$$$$$$$$$$$$$$

DISTRIBUTIONS FOR SELECTED RUNS

FLIGHT	RUN	MEAN SIGP(DB)	STD.DEV.	SAM.SIZE	MEAN SIGP(DB)	STD.DEV.	SAM.SIZE
8	16	14.6	7.42	20	18.01	9.65	20

RUN HISTOGRAM(NO.OF STD.DEV.FROM MEAN

FLIGHT	RUN	(LT-2)	(-2 TO-1.5)	(-1.5 TO -1)	(-1 TO -.5)	(.5 TO 0)	(0 TO .5)	(.5 TO 1)	(1 TO 1.5)	(1.5 TO 2)	(GE 2)
8	16	0	1	2	4	6	5	1	0	0	2

HISTOGRAM.FROM -1 TO -7/8,-7/8 TO -3/4,---7/8 TO 1 STD.DEV.

0 1 1 2 2 3 0 1 1 3 0 1 0 0 1 0

CUMULATIVE PROBABILITY

0.00000 0.00000 0.00000 .10000 .30000 .60000 .85000 .90000 .90000 .90000 1.00000

$$$$$$$$$$$$$$$$$$$$$$$$$$$$$$$$

RUN HISTOGRAM(NO.OF STD.DEV.FROM MEAN

FLIGHT	RUN	(LT-2)	(-2 TO-1.5)	(-1.5 TO -1)	(-1 TO -.5)	(.5 TO 0)	(0 TO .5)	(.5 TO 1)	(1 TO 1.5)	(1.5 TO 2)	(GE 2)
8	16	0	1	4	3	2	3	4	2	1	0

HISTOGRAM.FROM -1 TO -7/8.-7/8 TO -3/4.---7/8 TO 1 STD.DEV.

0 0 1 2 0 0 1 1 2 0 0 1 0 0 3 1

CUMULATIVE PROBABILITY

0.00000 0.00000 .05000 .25000 .40000 .50000 .65000 .85000 .95000 1.00000 1.00000

$$$$$$$$$$$$$$$$$$$$$$$$$$$$$$$$$$$$

DISTRIBUTIONS FOR SELECTED RUNS

FLIGHT	RUN	MEAN SIGA(DB)	STD.DEV.	SAM.SIZE	MEAN SIGP(DB)	STD.DEV.	SAM.SIZE
8	17	14.41	8.62	20	17.33	9.50	20

RUN HISTOGRAM(NO.OF STD.DEV.FROM MEAN

FLIGHT	RUN	(LT-2)	(-2 TO-1.5)	(-1.5 TO -1)	(-1 TO -.5)	(.5 TO 0)	(0 TO .5)	(.5 TO 1)	(1 TO 1.5)	(1.5 TO 2)	(GE 2)
8	17	0	1	2	5	3	3	3	0	2	1

HISTOGRAM.FROM -1 TO -7/8.-7/8 TO -3/4.---7/8 TO 1 STD.DEV.

0 1 3 1 0 1 0 2 1 1 1 0 1 2 0 0

CUMULATIVE PROBABILITY

0.00000 0.00000 .05000 .15000 .40000 .55000 .70000 .85000 .85000 .95000 1.00000

$$$$$$$$$$$$$$$$$$$$$$$$$$$$$$$$$$$$

RUN HISTOGRAM(NO.OF STD.DEV.FROM MEAN

FLIGHT	RUN	(LT-2)	(-2 TO-1.5)	(-1.5 TO -1)	(-1 TO -.5)	(.5 TO 0)	(0 TO .5)	(.5 TO 1)	(1 TO 1.5)	(1.5 TO 2)	(GE 2)
8	17	1	2	3	1	2	5	4	3	0	0

HISTOGRAM.FROM -1 TO -7/8.-7/8 TO -3/4.---7/8 TO 1 STD.DEV.

0 1 0 0 0 0 1 1 1 1 0 3 1 2 1 0

CUMULATIVE PROBABILITY

0.00000 0.00000 .10000 .25000 .30000 .40000 .65000 .85000 1.00000 1.00000 1.00000

$$$$$$$$$$$$$$$$$$$$$$$$$$$$$$$$$$$$

DISTRIBUTIONS FOR SELECTED RUNS

FLIGHT	RUN	MEAN SIGA(DB)	STD.DEV.	SAM.SIZE	MEAN SIGP(DB)	STD.DEV.	SAM.SIZE
8	18	13.90	7.06	20	17.14	8.55	20

RUN HISTOGRAM(NO.OF STD.DEV.FROM MEAN

FLIGHT	RUN	(LT-2)	(-2 TO-1.5)	(-1.5 TO -1)	(-1 TO -.5)	(.5 TO 0)	(0 TO .5)	(.5 TO 1)	(1 TO 1.5)	(1.5 TO 2)	(GE 2)
8	18	0	1	2	4	3	5	2	1	1	1

```
HISTOGRAM,FROM -1 TO -7/8,-7/8 TO -3/4,---7/8 TO 1 STD.DEV.
   0    2    [illegible]    2    [illegible]    2    1    0    0    3    1    1    0    1    0    1

CUMULATIVE PROBABILITY
   0.00000   [illegible]   .15000   .15000   .35000   .50000   .75000   .85000   .90000   .95000   1.00000
                                   $$$$$$$$$$$$$$$$$$$$$$$$$$$$$$$$

RUN HISTOGRAM(NO.OF STD.DEV.FROM MEAN)

FLIGHT RUN (LT-2) (-2 TO-1.5) (-1.5 TO -1) (-1 TO -.5) (.5 TO 0) (0 TO .5) (.5 TO 1) (1 TO 1.5) (1.5 TO 2) (GE 2)
   8   18   0   2   2   3   2   3   4   4   0   0

HISTOGRAM,FROM -1 TO -7/8,-7/8 TO -3/4,---7/8 TO 1 STD.DEV.
   1    0    1    [illegible]    [illegible]    1    0    1    3    0    0    0    1    1    0    2

CUMULATIVE PROBABILITY
   0.00000   0.00000   .10000   .20000   .35000   .45000   .60000   .80000   1.00000   1.00000   1.00000
                                   $$$$$$$$$$$$$$$$$$$$$$$$$$$$$$$$

DISTRIBUTIONS FOR SELECTED RUNS
FLIGHT   RUN   MEAN SIGP(DB)   STD.DEV.   SAM.SIZE   MEAN SIGP(DB)   STD.DEV.   SAM.SIZE
14       1     7.12            2.34       24         0.00            0.00       2

RUN HISTOGRAM(NO.OF STD.DEV.FROM MEAN)

FLIGHT RUN (LT-2) (-2 TO-1.5) (-1.5 TO -1) (-1 TO -.5) (.5 TO 0) (0 TO .5) (.5 TO 1) (1 TO 1.5) (1.5 TO 2) (GE 2)
   14   1   0   2   2   3   6   2   7   0   1   1

HISTOGRAM,FROM -1 TO -7/8,-7/8 TO -3/4,---7/8 TO 1 STD.DEV.
   1    1    [illegible]    1    0    3    2    1    2    0    0    0    2    0    3    2

CUMULATIVE PROBABILITY
   0.00000   [illegible]   .08333   .16667   .29167   .54167   .62500   .91667   .91667   .95833   1.00000
                                   $$$$$$$$$$$$$$$$$$$$$$$$$$$$$$$$

RUN HISTOGRAM(NO.OF STD.DEV.FROM MEAN)

FLIGHT RUN (LT-2) (-2 TO-1.5) (-1.5 TO -1) (-1 TO -.5) (.5 TO 0) (0 TO .5) (.5 TO 1) (1 TO 1.5) (1.5 TO 2) (GE 2)
   14   1   0   [illegible]   0   0   0   0   0   0   0   1

HISTOGRAM,FROM -1 TO -7/8,-7/8 TO -3/4,---7/8 TO 1 STD.DEV.
   0    0    0    [illegible]    0    0    0    0    0    0    0    0    0    0    0    0

CUMULATIVE PROBABILITY
   0.00000   1.00000   0.00000   0.00000   0.00000   0.00000   0.00000   0.00000   0.00000   0.00000   1.00000
                                   $$$$$$$$$$$$$$$$$$$$$$$$$$$$$$$$

DISTRIBUTIONS FOR SELECTED RUNS
FLIGHT   RUN   MEAN SIGP(DB)   STD.DEV.   SAM.SIZE   MEAN SIGP(DB)   STD.DEV.   SAM.SIZE
15       9     15.61           7.93       25         19.47           10.49      25
```

40

RUN HISTOGRAM(NO.OF STD.DEV.FROM MEAN

FLIGHT	RUN	(LT-2)	(-2 TO -1.5)	(-1.5 TO -1)	(-1 TO -.5)	(-.5 TO 0)	(0 TO .5)	(.5 TO 1)	(1 TO 1.5)	(1.5 TO 2)	(GE 2)
15	9	0	[illegible]	6	4	3	3	4	4	0	1

HISTOGRAM.FROM -1 TO -7/8,-7/8 TO -3/4,---7/8 TO 1 STD.DEV.

0	0	2	2	1	0	0	0	0	2	1	0	2	0	1	1

CUMULATIVE PROBABILITY

0.00000	0.00000	0.00000	.24000	.40000	.52000	.64000	.80000	.96000	.96000	1.00000

$$$$$$$$$$$$$$$$$$$$$$$$$$$$$$$$

RUN HISTOGRAM(NO.OF STD.DEV.FROM MEAN

FLIGHT	RUN	(LT-2)	(-2 TO -1.5)	(-1.5 TO -1)	(-1 TO -.5)	(-.5 TO 0)	(0 TO .5)	(.5 TO 1)	(1 TO 1.5)	(1.5 TO 2)	(GE 2)
15	9	2	0	1	5	4	4	4	5	0	0

HISTOGRAM.FROM -1 TO -7/8,-7/8 TO -3/4,---7/8 TO 1 STD.DEV.

1	1	0	3	1	2	0	1	1	1	0	2.	2	1	1	0

CUMULATIVE PROBABILITY

0.00000	[illegible]	[illegible]	.12000	.32000	.48000	.64000	.80000	1.00000	1.00000	1.00000

$$$$$$$$$$$$$$$$$$$$$$$$$$$$$$$$

DISTRIBUTIONS FOR SELECTED RUNS

FLIGHT	RUN	MEAN SIGA(DB)	STD.DEV.	SAM.SIZE	MEAN SIGP(DB)	STD.DEV.	SAM.SIZE
15	10	16.3	9.81	25	18.98	9.64	25

RUN HISTOGRAM(NO.OF STD.DEV.FROM MEAN

FLIGHT	RUN	(LT-2)	(-2 TO -1.5)	(-1.5 TO -1)	(-1 TO -.5)	(-.5 TO 0)	(0 TO .5)	(.5 TO 1)	(1 TO 1.5)	(1.5 TO 2)	(GE 2)
15	10	1	1	4	3	3	4	9	0	1	0

HISTOGRAM.FROM -1 TO -7/8,-7/8 TO -3/4,---7/8 TO 1 STD.DEV.

1	0	1	1	0	0	3	0	1	1	0	2	1	2	3	3

CUMULATIVE PROBABILITY

0.00000	.04000	[illegible]	.20000	.32000	.44000	.60000	.96000	.96000	1.00000	1.00000

$$$$$$$$$$$$$$$$$$$$$$$$$$$$$$$$

RUN HISTOGRAM(NO.OF STD.DEV.FROM MEAN

FLIGHT	RUN	(LT-2)	(-2 TO -1.5)	(-1.5 TO -1)	(-1 TO -.5)	(-.5 TO 0)	(0 TO .5)	(.5 TO 1)	(1 TO 1.5)	(1.5 TO 2)	(GE 2)
15	10	1	2	2	1	3	6	8	1	1	0

HISTOGRAM.FROM -1 TO -7/8,-7/8 TO -3/4,---7/8 TO 1 STD.DEV.

1	0	[illegible]	[illegible]	1	0	1	1	3	2	1	0	3	1	3	1

CUMULATIVE PROBABILITY

0.00000	[illegible]	.12000	.20000	.24000	.36000	.60000	.92000	.96000	1.00000	1.00000

$$$$$$$$$$$$$$$$$$$$$$$$$$$$$$

DISTRIBUTIONS FOR SELECTED RUNS

FLIGHT	RUN	MEAN SIGA(DB)	STD.DEV.	SAM.SIZE	MEAN SIGP(DB)	STD.DEV.	SAM.SIZE
15	11	16.56	9.77	24	19.81	11.07	24

RUN HISTOGRAM(NO.OF STD.DEV.FROM MEAN

FLIGHT	RUN	(LT-2)	(-2 TO-1.5)	(-1.5 TO -1)	(-1 TO -.5)	(.5 TO 0)	(0 TO .5)	(.5 TO 1)	(1 TO 1.5)	(1.5 TO 2)	(GE 2)
15	11	0	1	3	3	6	4	3	1	2	1

HISTOGRAM.FROM -1 TO -7/8.-7/8 TO -3/4.---7/8 TO 1 STD.DEV.

2	0	0	1	1	3	0	0	1	1	1	1	1	2	0	0

CUMULATIVE PROBABILITY

0.00000	0.00000	.04167	.16667	.29167	.54167	.70833	.83333	.87500	.95833	1.00000

$$$$$$$$$$$$$$$$$$$$$$$$$$$$$$

RUN HISTOGRAM(NO.OF STD.DEV.FROM MEAN

FLIGHT	RUN	(LT-2)	(-2 TO-1.5)	(-1.5 TO -1)	(-1 TO -.5)	(.5 TO 0)	(0 TO .5)	(.5 TO 1)	(1 TO 1.5)	(1.5 TO 2)	(GE 2)
15	11	0	2	3	2	5	5	3	2	1	1

HISTOGRAM.FROM -1 TO -7/8.-7/8 TO -3/4.---7/8 TO 1 STD.DEV.

0	0	0	2	2	0	2	1	1	0	1	3	2	1	0	0

CUMULATIVE PROBABILITY

0.00000	0.00000	.08333	.20833	.29167	.50000	.70833	.83333	.91667	.95833	1.00000

$$$$$$$$$$$$$$$$$$$$$$$$$$$$$$

DISTRIBUTIONS FOR SELECTED RUNS

FLIGHT	RUN	MEAN SIGA(DB)	STD.DEV.	SAM.SIZE	MEAN SIGP(DB)	STD.DEV.	SAM.SIZE
15	12	16.21	9.30	25	19.08	10.69	25

RUN HISTOGRAM(NO.OF STD.DEV.FROM MEAN

FLIGHT	RUN	(LT-2)	(-2 TO-1.5)	(-1.5 TO -1)	(-1 TO -.5)	(.5 TO 0)	(0 TO .5)	(.5 TO 1)	(1 TO 1.5)	(1.5 TO 2)	(GE 2)
15	12	0	2	2	5	3	6	4	0	3	0

HISTOGRAM.FROM -1 TO -7/8.-7/8 TO -3/4.---7/8 TO 1 STD.DEV.

1	2	2	1	0	1	1	1	1	2	0	3	0	2	1	1

CUMULATIVE PROBABILITY

0.00000	0.00000	.08000	.16000	.36000	.48000	.72000	.88000	.88000	1.00000	1.00000

$$$$$$$$$$$$$$$$$$$$$$$$$$$$$$

RUN HISTOGRAM(NO.OF STD.DEV.FROM MEAN

FLIGHT RUN (LT-2) (-2 TO-1.5) (-1.5 TO -1) (-1 TO -.5) (.5 TO 0) (0 TO .5) (.5 TO 1) (1 TO 1.5) (1.5 TO 2) (GE 2)

15	12	1	2	2	3	1	5	9	1	1	0

HISTOGRAM,FROM -1 TO -7/8,-7/8 TO -3/4,---7/8 TO 1 STD.DEV.

1	1	0	1	0	0	0	1	1	2	0	2	4	3	0	2

CUMULATIVE PROBABILITY

0.00000	.04000	.12000	.20000	.32000	.36000	.56000	.92000	.96000	1.00000	1.00000

$$$$$$$$$$$$$$$$$$$$$$$$$$$$$$$$$$$

$$$$$$$$$$$$$$$$$$$$$$$$$$$$$$$$$$$

	FRAME	RCVD PWR(DBM)AV	RCVD PWR(DBM)PEAK	SIGMA AV	SIGMA PEAK	SIGMAZ(DB) AV	SIGMAZ(DB) PEAK
5	8330	-56.60	-53.19	60.83	64.24	9.197	12.609
5	8331	-56.92	-55.07	60.51	62.35	8.876	10.724
5	8332	-57.78	-53.64	59.65	63.79	8.015	12.159
8	8407	-58.90	-54.23	58.53	63.19	6.901	11.564
8	8408	-59.22	-55.76	58.21	61.67	6.576	10.035
8	8409	-57.19	-54.94	60.24	62.49	8.605	10.859
13	8528	-58.86	-54.69	58.57	62.74	6.937	11.110
13	8529	-57.19	-54.59	60.24	62.83	8.610	11.204
13	8530	-56.42	-53.82	61.01	63.61	9.381	11.980
16	8618	-63.11	-61.50	54.32	55.93	9.680	11.291
16	8619	-63.48	-59.87	53.95	57.56	9.308	12.920
16	8620	-62.97	-60.11	54.46	57.32	9.820	12.680
18	8662	-64.24	-61.49	53.19	55.94	8.552	11.297
18	8663	-63.22	-60.04	54.20	57.38	9.564	12.744
18	8664	-63.48	-60.07	53.94	57.36	9.303	12.715
21	8731	-65.50	-60.54	51.93	56.89	7.285	12.245
21	8732	-64.01	-60.77	53.42	56.66	8.782	12.016
21	8733	-63.33	-60.44	54.10	56.99	9.459	12.347

A-5 FLIGHT	PULSES PER FRAME	SIGMAZ(DB) AVG	SIGMAZ(DB) PEAK	
4	[illegible]	8.71	11.88	18

$$$$$$$$$$$$$$$$$$$$$$$$$$$$$$$$$$$

	FRAME	RCVD PWR(DBM)AV	RCVD PWR(DBM)PEAK	SIGMA AV	SIGMA PEAK	SIGMAZ(DB) AV	SIGMAZ(DB) PEAK
5	9037	[illegible]	-51.44	66.02	68.03	18.367	20.375
5	9038	-52.51	-50.46	66.96	69.01	19.308	21.356
5	9039	-53.53	-51.84	63.64	67.62	15.991	19.974
6	9060	-53.46	-51.63	65.50	67.84	17.854	20.190
6	9061	-54.54	-50.62	64.93	68.85	17.277	21.201
6	9062	-52.51	-50.57	66.96	68.90	19.306	21.251
7	9083	-53.68	-51.57	65.79	67.90	18.139	20.248
7	9084	-53.07	-51.11	66.39	68.36	18.744	20.709
7	9085	[illegible]	-51.99	64.44	67.48	16.789	19.827
8	9105	-54.33	-51.28	65.14	68.19	17.487	20.540
8	9106	-54.44	-51.17	65.03	68.30	17.380	20.646
8	9107	-55.29	-52.73	64.18	66.74	16.532	19.089
9	9127	-53.14	-51.69	66.33	67.78	18.681	20.132
9	9128	-53.63	-51.14	65.83	68.33	18.184	20.679
9	9129	-55.48	-51.89	63.99	67.58	16.337	19.925
10	9149	[illegible]	-50.93	64.66	68.54	17.006	20.891
10	9150	[illegible]	-52.22	64.45	67.25	16.795	19.598
10	9151	-52.74	-50.69	66.73	68.78	19.080	21.129

FLIGHT	PULSES PER FRAME	SIGMAZ(DB) AVG	SIGMAZ(DB) PEAK	
5	[illegible]	17.85	20.47	18

$$

	FRAME	RCVD PWR(DBM)AV	RCVD PWR(DBM)PEAK	SIGMA AV	SIGMA PEAK	SIGMAZ(DB) AV	SIGMAZ(DB) PEAK
5	9447	-51.45	-47.64	75.17	78.87	18.765	22.471
5	9448	-51.96	-48.37	74.55	78.14	18.153	21.741
5	9449	-52.08	-48.23	74.43	78.28	18.031	21.880
7	9500	-51.30	-47.82	75.21	78.69	18.812	22.292
7	9501	-49.74	-46.05	76.77	80.46	20.371	24.062
7	9502	-51.77	-48.76	74.74	77.75	18.339	21.349
10	9558	-51.28	-48.32	75.23	78.19	18.828	21.791
10	9559	-53.16	-48.73	73.36	77.78	16.955	21.380
10	9560	-50.43	-46.55	76.09	79.96	19.685	23.561

FLIGHT	PULSES PER FRAME	SIGMAZ(DB) AVG	SIGMAZ(DB) PEAK	
6	-	18.76	22.38	9

$$

	FRAME	RCVD PWR(DBM)AV	RCVD PWR(DBM)PEAK	SIGMA AV	SIGMA PEAK	SIGMAZ(DB) AV	SIGMAZ(DB) PEAK
1	401	-57.53	-54.84	68.99	71.67	19.576	22.257
1	402	-57.46	-53.34	69.06	73.17	19.644	23.760
1	404	-57.87	-54.57	68.65	71.94	19.234	22.532
1	409	-56.74	-54.09	69.78	72.42	20.365	23.008
1	410	-57.27	-54.16	69.25	72.35	19.835	22.943
1	411	-57.82	-55.35	68.69	71.16	19.281	21.749
2	427	-57.35	-54.23	69.16	72.28	19.750	22.874
2	428	-56.83	-52.99	69.68	73.52	20.271	24.110
2	429	-58.44	-55.65	68.08	70.86	18.665	21.451
2	430	-56.36	-53.50	70.15	73.01	20.741	23.604
2	431	-56.12	-53.62	70.40	72.89	20.984	23.482
2	433	-55.71	-52.61	70.80	73.90	21.386	24.493
2	434	-54.83	-50.94	71.69	75.57	22.275	26.164
2	435	-56.76	-52.81	69.76	73.70	20.344	24.289
2	436	-56.32	-52.26	70.19	74.25	20.781	24.842
2	437	-56.70	-51.89	69.82	74.63	20.406	25.216
2	439	-55.10	-52.56	71.41	73.95	21.998	24.536
2	440	-55.16	-52.71	71.35	73.80	21.939	24.391
2	441	-55.64	-52.80	70.87	73.72	21.459	24.304
2	442	-55.70	-51.91	70.82	74.60	21.405	25.188
3	452	-57.05	-53.06	69.46	73.46	20.053	24.044
3	453	-57.05	-54.09	69.46	72.42	20.046	23.009
3	454	-56.11	-53.60	70.40	72.92	20.992	23.505
3	455	-57.45	-53.38	69.06	73.13	19.646	23.720
3	456	-57.11	-54.10	69.40	72.41	19.986	22.999
3	458	-54.39	-50.99	72.12	75.52	22.709	26.111
3	459	-55.96	-51.87	70.55	74.64	21.142	25.233
3	460	-55.63	-51.76	70.88	74.75	21.472	25.340
3	461	-55.25	-51.32	71.26	75.20	21.853	25.784
3	462	-54.92	-51.24	71.60	75.27	22.185	25.861
3	464	-54.58	-51.15	71.93	75.36	22.519	25.952
3	466	-54.96	-52.25	71.56	74.26	22.144	24.853
3	467	-54.47	-51.66	72.04	74.86	22.630	25.446
3	468	-56.41	-52.96	70.10	73.55	20.692	24.137
4	479	-57.74	-54.63	68.77	71.88	19.356	22.467
4	480	-57.50	-54.62	69.01	71.89	19.597	22.479
4	481	-57.03	-54.36	69.48	72.15	20.068	22.738
4	482	-57.10	-52.97	69.41	73.55	20.002	24.135
4	483	-57.66	-53.45	68.86	73.06	19.445	23.652
4	485	-55.73	-52.05	70.78	74.46	21.373	25.046
4	486	-55.89	-52.17	70.62	74.34	21.211	24.931
4	488	-55.92	-52.95	70.60	73.56	21.184	24.149

4	489	-55.86	-53.32	70.65	73.20	21.241	23.785
4	491	-55.74	-52.68	70.77	73.83	21.358	24.416
4	492	-55.54	-52.90	70.97	73.61	21.563	24.202
4	493	-56.60	-53.79	69.91	72.72	20.502	23.306
4	494	-55.57	-53.20	70.94	73.32	21.532	23.905
4	495	-55.92	-52.33	70.60	74.19	21.184	24.774
5	506	-57.73	-54.44	68.78	72.07	19.371	22.663
5	507	-58.47	-54.25	68.04	72.26	18.631	22.854
5	508	-59.76	-53.57	66.76	72.94	17.344	23.528
5	509	-57.88	-54.20	68.63	72.31	19.222	22.901
5	510	-58.39	-54.68	68.13	71.83	18.715	22.422
5	512	-57.16	-53.62	69.34	72.89	19.926	23.476
5	513	-55.19	-52.47	71.32	74.04	21.913	24.627
5	514	-56.06	-53.07	70.46	73.44	21.045	24.033
5	515	-56.48	-52.60	70.03	73.91	20.621	24.502
5	516	-56.62	-52.93	69.89	73.58	20.484	24.170
5	517	-54.74	-52.00	71.77	74.51	22.363	25.101
5	518	-54.95	-52.91	71.56	73.60	22.149	24.192
5	519	-54.39	-52.20	72.13	74.31	22.715	24.903
5	520	-56.00	-53.62	70.51	72.89	21.101	23.479
5	521	-56.30	-53.08	70.21	73.44	20.798	24.024
6	532	-61.14	-56.88	65.37	69.63	15.960	20.222
6	533	-59.69	-55.33	66.82	71.19	17.406	21.775
6	534	-60.92	-57.07	65.59	69.44	16.182	20.029
6	535	-61.63	-56.41	64.88	70.10	15.469	20.690
6	536	-60.45	-56.15	66.06	70.36	16.648	20.949
6	538	-56.41	-53.60	70.10	72.91	20.688	23.499
6	539	-57.68	-53.78	68.83	72.73	19.421	23.317
6	540	-57.63	-53.67	68.88	72.84	19.467	23.431
6	541	-57.85	-54.05	68.66	72.46	19.246	23.047
6	542	-56.43	-53.34	70.08	73.18	20.668	23.765
6	544	-55.94	-52.04	70.57	74.48	21.157	25.065
6	545	-56.03	-52.14	70.48	74.37	21.068	24.962
6	546	-57.49	-53.55	69.03	72.96	19.616	23.552
6	547	-54.72	-51.26	71.79	75.25	22.379	25.839
6	548	-55.73	-51.41	70.78	75.10	21.369	25.692

FLIGHT	PULSES PER FRAME	SIGMAZ(DB) AVG	SIGMAZ(DB) PEAK	
7	999	20.64	24.01	78

$$$$$$$$$$$$$$$$$$$$$$$$$$$$$$$$$$$

	FRAME	RCVD PWR(DBM)AV	RCVD PWR(DBM)PEAK	SIGMA AV	SIGMA PEAK	SIGMAZ(DB) AV	SIGMAZ(DB) PEAK
1	701	-56.41	-56.41	63.06	63.06	15.410	15.410
1	702	-58.07	-58.07	61.40	61.40	13.747	13.747
1	703	-56.24	-56.24	63.23	63.23	15.579	15.579
1	704	-60.26	-60.26	59.21	59.21	11.562	11.562
2	705	-57.19	-57.19	62.28	62.28	14.629	14.629
2	707	-56.26	-56.26	63.21	63.21	15.563	15.563
2	708	-60.38	-60.38	59.08	59.08	11.434	11.434
2	709	-56.78	-56.78	62.68	62.68	15.034	15.034
2	710	-58.80	-58.80	60.67	60.67	13.022	13.022
3	713	-60.85	-60.85	58.61	58.61	10.964	10.964
3	714	-61.80	-61.80	57.67	57.67	10.020	10.020
3	715	-62.25	-62.25	57.22	57.22	9.567	9.567
3	716	-63.02	-63.02	56.44	56.44	8.794	8.794
4	719	-61.95	-61.95	57.52	57.52	9.872	9.872
4	720	-62.41	-62.41	57.06	57.06	9.409	9.409
4	721	-59.99	-59.99	59.48	59.48	11.832	11.832
4	722	-60.59	-60.59	58.88	58.88	11.227	11.227
5	724	-59.49	-59.49	59.98	59.98	12.326	12.326
5	725	-60.44	-60.44	59.03	59.03	11.379	11.379
5	726	-58.76	-58.76	60.71	60.71	13.055	13.055
5	727	-60.34	-60.34	59.13	59.13	11.475	11.475
5	728	-56.98	-56.98	62.49	62.49	14.838	14.838

6	730	-59.63	-59.63	59.64	59.64	11.992	11.992
6	731	-64.36	-64.36	55.11	55.11	7.463	7.463
6	733	-60.71	-60.71	58.76	58.76	11.108	11.108
6	734	-56.12	-56.12	63.35	63.35	15.698	15.698

FLIGHT	PULSES PER FRAME	SIGMAZ(DB) AVG	SIGMAZ(DB) PEAK	
8	1	12.78	12.78	26

$$$$$$$$$$$$$$$$$$$$$$$$$$$$$$$$$$$$

	FRAME	RCVD PWR(DBM)AV	RCVD PWR(DBM)PEAK	SIGMA AV	SIGMA PEAK	SIGMAZ(DB) AV	SIGMAZ(DB) PEAK
13	795	-55.62	-51.12	63.85	68.35	16.200	20.700
13	796	-55.19	-51.83	64.28	67.64	16.625	19.993
13	797	-54.79	-51.11	64.68	68.35	17.026	20.703
13	798	-56.59	-50.27	62.88	69.20	15.228	21.552
13	799	-54.99	-50.54	64.48	68.93	16.829	21.279
13	800	-56.40	-52.02	63.07	67.45	15.418	19.800
13	801	-56.41	-51.41	63.06	68.06	15.405	20.410
13	802	-56.06	-50.15	63.41	69.32	15.756	21.666
13	803	-55.77	-50.57	63.70	68.90	16.047	21.250
13	804	-56.50	-51.31	62.97	68.15	15.319	20.504
13	805	-56.37	-50.62	63.10	68.85	15.448	21.195
13	806	-55.38	-51.74	64.09	67.73	16.438	20.083
13	807	-56.42	-51.64	62.65	67.82	14.997	20.174
13	808	-57.35	-52.63	62.12	66.84	14.465	19.190
13	809	-57.38	-52.09	62.09	67.38	14.440	19.729
13	810	-57.17	-51.57	62.30	67.90	14.650	20.251
13	811	-56.65	-51.20	62.82	68.27	15.171	20.616
13	812	-57.17	-50.98	62.30	68.48	14.652	20.833
13	813	-56.84	-51.03	62.62	68.44	14.973	20.787
13	814	-56.02	-50.85	63.45	68.62	15.803	20.970
14	816	-58.84	-53.78	60.63	65.69	12.978	18.037
14	817	-58.29	-54.02	61.18	65.45	13.533	17.798
14	818	-56.43	-53.22	63.04	66.25	15.390	18.600
14	819	-59.98	-55.99	59.48	63.48	11.834	15.833
14	820	-56.74	-55.26	62.73	64.21	15.080	16.560
14	821	-56.29	-54.57	63.18	64.90	15.527	17.248
14	822	-55.85	-53.97	63.62	65.50	15.968	17.845
14	823	-59.40	-55.57	60.07	63.89	12.423	16.244
14	824	-57.53	-55.11	61.94	64.36	14.293	16.713
14	825	-59.16	-54.82	60.31	64.65	12.659	16.996
14	826	-57.65	-54.69	61.82	64.78	14.173	17.132
14	827	-58.49	-55.18	60.98	64.29	13.329	16.635
14	828	-58.91	-55.37	60.56	64.10	12.910	16.452
14	829	-57.43	-54.57	62.04	64.90	14.391	17.249
14	830	-57.43	-54.45	62.04	65.02	14.392	17.365
14	831	-58.23	-54.94	61.24	64.53	13.589	16.879
14	832	-58.00	-54.88	61.47	64.59	13.821	16.940
14	833	-58.58	-54.98	60.89	64.49	13.238	16.840
14	834	-58.15	-54.10	61.32	65.37	13.670	17.717
14	835	-57.47	-54.77	61.99	64.70	14.344	17.048
15	837	-58.14	-55.16	61.33	64.31	13.678	16.663
15	838	-56.49	-53.92	62.98	65.55	15.330	17.902
15	839	-57.20	-53.88	62.27	65.59	14.623	17.939
15	840	-56.42	-53.46	63.05	66.01	15.399	18.363
15	841	-56.83	-53.17	62.64	66.29	14.985	18.644
15	842	-57.23	-53.44	62.24	66.03	14.593	18.377
15	843	-56.44	-53.31	63.03	66.16	15.381	18.506
15	844	-56.40	-53.29	63.07	66.18	15.423	18.533
15	845	-56.96	-53.64	62.51	65.82	14.855	18.174
15	846	-57.79	-54.47	61.68	65.00	14.026	17.349
15	847	-57.87	-54.09	61.60	65.38	13.946	17.731
15	848	-56.60	-54.01	62.87	65.46	15.217	17.809

15	849	-57.09	-53.86	62.38	65.61	14.732	17.958
15	850	-56.98	-53.40	62.49	66.07	14.835	18.420
15	851	-59.45	-55.34	60.02	64.13	12.366	16.482
15	852	-56.85	-53.78	62.62	65.69	14.968	18.040
15	853	-55.66	-53.55	63.81	65.92	16.155	18.267
15	854	-56.16	-53.32	63.30	66.15	15.653	18.495
15	855	-57.28	-52.89	62.19	66.58	14.542	18.932
15	856	-57.69	-53.98	61.78	65.49	14.131	17.842
16	858	-57.44	-54.68	62.03	64.78	14.375	17.134
16	859	-57.09	-53.91	62.38	65.56	14.728	17.906
16	860	-57.68	-53.35	61.79	66.12	14.142	18.465
16	861	-55.62	-53.00	63.85	66.47	16.195	18.820
16	862	-57.08	-53.14	62.38	66.33	14.734	18.675
16	863	-57.07	-53.76	62.40	65.71	14.746	18.057
16	864	-57.28	-53.25	62.19	66.22	14.543	18.569
16	865	-56.56	-53.30	62.91	66.17	15.255	18.523
16	866	-55.41	-52.72	64.06	66.75	16.411	19.095
16	867	-57.44	-54.60	62.03	64.87	14.376	17.218
16	868	-57.44	-53.89	62.03	65.58	14.377	17.933
16	869	-57.75	-54.26	61.72	65.21	14.067	17.559
16	870	-57.89	-54.92	61.58	64.55	13.927	16.902
16	871	-58.30	-54.64	61.16	64.83	13.514	17.175
16	872	-58.52	-54.17	60.95	65.30	13.301	17.650
16	873	-57.59	-54.54	61.87	64.93	14.224	17.277
16	874	-57.61	-53.78	61.86	65.69	14.210	18.037
16	875	-57.77	-53.54	61.70	65.92	14.045	18.274
16	876	-57.18	-54.20	62.29	65.27	14.643	17.615
16	877	-56.91	-53.34	62.56	66.13	14.909	18.482
17	879	-58.47	-55.45	61.00	64.02	13.353	16.373
17	880	-57.53	-54.21	61.94	65.26	14.291	17.608
17	881	-57.10	-53.99	62.37	65.48	14.719	17.826
17	882	-56.68	-53.97	62.79	65.50	15.142	17.845
17	883	-55.37	-53.63	64.10	65.84	16.446	18.192
17	884	-56.80	-53.66	62.67	65.81	15.016	18.161
17	885	-58.16	-54.21	61.31	65.26	13.658	17.606
17	886	[illegible]	-54.46	61.18	65.01	13.533	17.356
17	887	-57.24	-54.02	62.23	65.45	14.579	17.795
17	888	-55.83	-53.59	63.64	65.87	15.985	18.224
17	889	-57.53	-54.11	61.94	65.36	14.291	17.707
17	890	-55.94	-54.23	63.53	65.24	15.878	17.591
17	891	-57.83	-55.79	61.64	63.68	13.986	16.030
17	892	-58.83	-55.09	60.64	64.38	12.987	16.731
17	893	-58.91	-55.41	60.56	64.06	12.912	16.412
17	894	-59.76	-56.23	59.71	63.24	12.064	15.593
17	895	-58.31	-54.66	61.16	64.81	13.512	17.156
17	896	-57.38	-54.38	62.09	65.09	14.441	17.442
17	897	-58.21	-55.41	61.26	64.06	13.608	16.412
17	898	-56.70	-54.57	62.77	64.90	15.116	17.253
18	900	-58.67	-55.04	60.80	64.43	13.147	16.777
18	901	-57.29	-54.30	62.18	65.17	14.532	17.518
18	902	-57.01	-54.18	62.46	65.29	14.814	17.643
18	903	-57.15	-54.11	62.32	65.35	14.665	17.704
18	904	-57.62	-54.02	61.84	65.44	14.194	17.795
18	905	-57.68	-54.13	61.79	65.34	14.137	17.690
18	906	-57.47	-54.67	62.00	64.80	14.346	17.153
18	907	-58.46	-53.87	61.01	65.60	13.363	17.947
18	908	-56.60	-53.97	62.87	65.50	15.220	17.848
18	909	-57.71	-55.26	61.76	64.20	14.113	16.554
18	910	-57.69	-54.89	61.77	64.58	14.124	16.931
18	911	-56.28	-54.62	63.19	64.85	15.542	17.203
18	912	-58.17	-54.69	61.30	64.78	13.647	17.130
18	913	-58.61	-54.61	60.86	64.85	13.208	17.204
18	914	-58.06	-55.14	61.41	64.33	13.758	16.681
18	915	-58.40	-55.39	61.07	64.08	13.423	16.431
18	916	-59.90	-55.85	59.57	63.62	11.915	15.970
18	917	-59.28	-55.86	60.19	63.61	12.542	15.959
18	918	-58.19	-55.45	61.28	64.02	13.632	16.369
18	919	-59.11	-54.35	60.36	65.12	12.707	17.467

FLIGHT	PULSES PER FRAME	SIGMAZ(DB) AVG	SIGMAZ(DB) PEAK	
8	[illegible]	14.60	18.25	120

$$$$$$$$$$$$$$$$$$$$$$$$$$$$$$

	FRAME	RCVD PWR(DBM)AV	RCVD PWR(DBM)PEAK	SIGMA AV	SIGMA PEAK	SIGMAZ(DB) AV	SIGMAZ(DB) PEAK
19	923	[illegible]	-54.68	61.38	64.79	13.733	17.135
19	924	-57.28	-53.99	61.99	65.47	14.337	17.824
19	925	-58.75	-54.95	60.72	64.52	13.065	16.868
19	926	-57.72	-54.82	61.75	64.65	14.102	16.996
19	927	-57.26	-54.53	62.21	64.94	14.555	17.285
21	965	-56.54	-53.79	62.93	65.68	15.281	18.027
21	966	-56.64	-53.63	62.63	65.83	14.979	18.184
21	967	-57.75	-54.06	61.72	65.41	14.067	17.762
21	968	-57.56	-54.40	61.90	65.07	14.254	17.417
21	969	[illegible]	-53.90	60.50	65.56	12.854	17.914
24	1032	[illegible]	-53.56	63.16	65.91	15.514	18.255
24	1033	[illegible]	-54.06	62.56	65.41	14.914	17.759
24	1034	[illegible]	-54.29	60.95	65.18	13.300	17.532
24	1035	[illegible]	-53.76	62.73	65.71	15.078	18.059
24	1036	-56.72	-53.86	62.75	65.60	15.097	17.953

FLIGHT	PULSES PER FRAME	SIGMAZ(DB) AVG	SIGMAZ(DB) PEAK	
8	27	14.41	17.68	15

$$$$$$$$$$$$$$$$$$$$$$$$$$$$$$

	FRAME	RCVD PWR(DBM)AV	RCVD PWR(DBM)PEAK	SIGMA AV	SIGMA PEAK	SIGMAZ(DB) AV	SIGMAZ(DB) PEAK
13	1649	-84.31	-80.87	49.44	52.58	7.812	10.953
13	1650	-82.12	-79.69	51.43	53.76	9.803	12.127
13	1651	-82.33	-79.53	51.12	53.92	9.489	12.289
13	1676	-76.70	-74.63	56.75	58.62	15.116	16.989
14	1690	-81.20	-77.89	52.64	55.56	11.014	13.927
14	1691	-79.57	-76.74	53.78	56.71	12.148	15.077
14	1692	-80.34	-76.92	53.11	56.52	11.480	14.894
15	1732	-82.30	-78.55	51.15	54.89	9.523	13.264
15	1734	-81.14	-78.06	52.31	55.39	10.677	13.763
15	1735	-81.10	-77.96	53.35	55.49	11.716	13.862
16	1774	-80.11	-76.79	53.34	56.66	11.708	15.030
16	1775	-77.17	-77.45	54.28	56.00	12.648	14.367
16	1776	-77.99	-75.72	55.46	57.73	13.826	16.102

FLIGHT	PULSES PER FRAME	SIGMAZ(DB) AVG	SIGMAZ(DB) PEAK	
10	50	11.71	14.33	13

$$$$$$$$$$$$$$$$$$$$$$$$$$$$$$

	FRAME	RCVD PWR(DBM)AV	RCVD PWR(DBM)PEAK	SIGMA AV	SIGMA PEAK	SIGMAZ(DB) AV	SIGMAZ(DB) PEAK
17	1816	-77.80	-75.14	55.59	58.31	13.956	16.677
17	1817	-75.93	-73.31	57.52	60.14	15.886	18.509
17	1818	-74.53	-71.54	58.91	61.91	17.284	20.282
17	1819	-75.41	-72.05	58.04	61.40	16.409	19.768
17	1820	-75.85	-73.32	57.60	60.13	15.968	18.500
18	1858	-79.45	-76.16	54.00	57.29	12.368	15.656
18	1859	-79.80	-73.98	53.65	59.47	12.016	17.836
18	1860	-79.68	-76.01	53.77	57.44	12.139	15.812
18	1861	-78.31	-75.16	55.14	58.29	13.507	16.656

18	1862	-78.75	-75.74	54.67	57.71	13.035	16.079
19	1900	-79.96	-77.14	53.58	56.31	11.954	14.679
19	1901	-79.49	-75.99	53.95	57.46	12.325	15.828
19	1902	-80.45	-76.66	52.99	56.79	11.364	15.158
19	1903	-80.24	-77.17	53.16	56.28	11.529	14.647
19	1904	-79.27	-76.04	54.17	57.41	12.544	15.782
20	1942	-80.25	-76.66	53.20	56.79	11.573	15.161
20	1943	-80.40	-75.82	53.05	57.63	11.423	16.003
20	1944	-79.43	-76.08	54.02	57.37	12.388	15.736
20	1945	-80.93	-76.78	52.52	56.67	10.886	15.038
20	1946	-79.47	-76.39	53.98	57.06	12.349	15.427

FLIGHT	PULSES PER FRAME	SIGMAZ(DB) AVG	SIGMAZ(DB) PEAK	
10	148	13.48	16.80	20

$$$$$$$$$$$$$$$$$$$$$$$$$$$$$$$$$$$$$

	FRAME	RCVD PWR(DBM)AV	RCVD PWR(DBM)PEAK	SIGMA AV	SIGMA PEAK	SIGMAZ(DB) AV	SIGMAZ(DB) PEAK
17	2642	-63.52	-60.88	61.97	64.61	14.318	16.955
17	2643	-62.65	-61.21	62.84	64.28	15.193	16.626
17	2644	-62.74	-60.73	62.75	64.76	15.097	17.110
17	2645	-63.12	-60.69	62.37	64.80	14.723	17.146
17	2646	-63.12	-60.58	62.37	64.91	14.717	17.260
18	2649	-65.43	-62.91	60.06	62.58	12.408	14.925
18	2650	-64.84	-62.36	60.65	63.13	12.995	15.477
18	2651	-64.43	-62.30	61.06	63.18	13.407	15.534
18	2652	-63.95	-62.12	61.54	63.37	13.888	15.723
18	2653	-64.63	-62.74	60.85	62.74	13.204	15.094
19	2725	-64.36	-62.74	61.13	62.75	13.481	15.100
19	2726	-65.73	-63.91	58.75	61.58	11.104	13.932
19	2727	-66.26	-62.67	59.23	62.82	11.575	15.168
19	2728	-66.00	-62.16	59.49	63.33	11.839	15.679
19	2729	-64.35	-61.36	61.14	64.13	13.485	16.477
20	2767	-67.42	-63.19	58.07	62.30	10.419	14.650
20	2768	-65.50	-62.39	59.99	63.10	12.340	15.448
20	2769	-65.96	-62.86	59.53	62.63	11.878	14.978
20	2770	-65.78	-62.03	59.71	63.46	12.060	15.813
20	2771	-65.12	-62.13	59.47	63.36	11.821	15.706

FLIGHT	PULSES PER FRAME	SIGMAZ(DB) AVG	SIGMAZ(DB) PEAK	
12	16	13.21	15.83	20

$$$$$$$$$$$$$$$$$$$$$$$$$$$$$$$$$$$$$

	FRAME	RCVD PWR(DBM)AV	RCVD PWR(DBM)PEAK	SIGMA AV	SIGMA PEAK	SIGMAZ(DB) AV	SIGMAZ(DB) PEAK
1	3919	-62.27	-62.27	57.20	57.20	9.549	9.549
1	3920	-63.49	-63.49	55.98	55.98	8.331	8.331
1	3921	-63.73	-63.73	55.74	55.74	8.089	8.089
1	3922	-65.57	-65.57	53.90	53.90	6.250	6.250
1	3923	-63.57	-63.57	55.90	55.90	8.245	8.245
1	3925	-63.64	-63.64	55.83	55.83	8.178	8.178
1	3926	-66.16	-66.16	53.31	53.31	5.658	5.658
1	3927	-64.54	-64.54	54.92	54.92	7.274	7.274
1	3928	-62.87	-62.87	56.60	56.60	8.950	8.950
1	3929	-65.04	-65.04	54.43	54.43	6.782	6.782
1	3930	-66.98	-66.98	52.49	52.49	4.837	4.837
1	3931	-68.30	-68.30	51.16	51.16	3.513	3.513
1	3932	-68.94	-68.94	50.53	50.53	2.875	2.875
1	3933	-66.36	-66.36	53.11	53.11	5.463	5.463
1	3934	-65.20	-65.20	54.27	54.27	6.619	6.619

1	[illegible]	-63.[illegible]	-63.91	55.55	55.55	7.904	7.904
1	[illegible]	[illegible]	-64.53	54.94	54.94	7.291	7.291
1	3937	-65.[illegible]9	-65.09	54.38	54.38	6.732	6.732
1	3938	-63.[illegible]7	-63.97	55.50	55.50	7.845	7.845
1	3939	-65.[illegible]	-66.48	52.99	52.99	5.337	5.337
1	3940	-64.[illegible]9	-64.69	54.58	54.58	6.929	6.929
1	3941	-63.70	-63.70	55.77	55.77	8.121	8.121
1	3942	-65.12	-65.12	54.35	54.35	6.701	6.701
1	3943	-64.79	-64.79	54.68	54.68	7.026	7.026

FLIGHT	PULSES PER FRAME	SIGMAZ(DB) AVG	SIGMAZ(DB) PEAK	
14	1	7.12	7.12	24

$$$$$$$$$$$$$$$$$$$$$$$$$$$$$$$$$$

	FRAME	RCVD PWR(DBM)AV	RCVD PWR(DBM)PEAK	SIGMA AV	SIGMA PEAK	SIGMAZ(DB) AV	SIGMAZ(DB) PEAK
9	4180	-61.[illegible]	-59.07	57.54	60.40	9.888	12.746
9	4181	-6[illegible].[illegible]5	-58.50	58.62	60.97	10.971	13.316
9	4182	-61.[illegible]6	-59.07	57.88	60.40	10.234	12.748
10	4221	-61.59	-58.44	57.78	61.03	10.129	13.383
10	4222	-62.[illegible]3	-58.97	56.64	60.50	8.985	12.846
10	4223	-62.55	-59.36	56.92	60.11	9.268	12.457
11	4263	-60.43	-58.05	59.04	61.42	11.392	13.770
11	4264	-60.60	-58.12	58.87	61.35	11.215	13.700
11	4265	-60.[illegible]4	-57.96	58.53	61.50	10.883	13.854
12	4305	-62.17	-58.73	57.30	60.74	9.649	13.087
12	4306	-62.[illegible]5	-58.49	57.42	60.98	9.773	13.327
12	4307	-62.68	-59.18	56.99	60.29	9.337	12.637

FLIGHT	PULSES PER FRAME	SIGMAZ(DB) AVG	SIGMAZ(DB) PEAK	
14	5	10.21	13.18	12

$$$$$$$$$$$$$$$$$$$$$$$$$$$$$$$$$$

	FRAME	RCVD PWR(DBM)AV	RCVD PWR(DBM)PEAK	SIGMA AV	SIGMA PEAK	SIGMAZ(DB) AV	SIGMAZ(DB) PEAK
13	4347	-57.48	-54.95	61.99	64.52	14.342	16.865
13	4348	-58.[illegible]1	-55.67	61.46	63.79	13.807	16.144
13	4349	-58.30	-55.43	61.17	64.04	13.519	16.387
13	4350	-58.44	-55.10	61.03	64.37	13.377	16.715
13	4351	-57.31	-54.05	62.16	65.42	14.507	17.772
14	4389	-57.47	-55.07	61.99	64.40	14.344	16.750
14	4390	-57.[illegible]6	-54.88	62.41	64.59	14.757	16.937
14	4391	-58.87	-55.82	60.60	63.65	12.952	15.997
14	4392	-58.15	-55.49	61.32	63.98	13.666	16.328
14	4393	-57.47	-54.99	62.00	64.48	14.351	16.827
15	4431	-58.50	-54.54	60.97	64.92	13.321	17.273
15	4432	-58.73	-55.82	60.73	63.65	13.084	15.997
15	4433	-58.50	-55.81	60.97	63.66	13.321	16.012
15	4434	-58.[illegible]7	-55.06	61.40	64.41	13.746	16.757
15	4435	-57.65	-55.35	61.82	64.12	14.166	16.469
16	4473	-59.[illegible]9	-56.54	60.38	62.92	12.728	15.274
16	4474	-59.31	-56.52	60.16	62.94	12.511	15.293
16	4475	-58.91	-56.72	60.56	62.75	12.909	15.101
16	4476	-59.66	-57.08	59.81	62.39	12.161	14.735
16	4477	-59.59	-56.60	59.88	62.87	12.232	15.215

FLIGHT	PULSES PER FRAME	SIGMAZ(DB) AVG	SIGMAZ(DB) PEAK	
14	148	13.55	16.31	20

$$$$$$$$$$$$$$$$$$$$$$$$$$$$$$$$$$

	FRAME	RCVD PWR(DBM)AV	RCVD PWR(DBM)PEAK	SIGMA AV	SIGMA PEAK	SIGMAZ(DB) AV	SIGMAZ(DB) PEAK
1	5222	-55.60	-55.60	63.87	63.87	16.215	16.215
1	5224	-57.50	-57.50	61.97	61.97	14.321	14.321
1	5225	-57.92	-57.92	61.55	61.55	13.902	13.902
2	5254	-57.45	-57.45	62.02	62.02	14.373	14.373
2	5255	-57.54	-57.54	61.93	61.93	14.279	14.279
2	5256	-57.07	-57.07	62.40	62.40	14.750	14.750
2	5257	-57.99	-57.99	61.48	61.48	13.832	13.832
2	5258	-58.98	-58.98	60.49	60.49	12.843	12.843
2	5287	-55.68	-55.68	63.79	63.79	16.137	16.137
3	5286	-56.04	-56.04	63.43	63.43	15.776	15.776
3	5288	-57.04	-57.04	62.43	62.43	14.777	14.777
3	5289	-56.78	-56.78	62.69	62.69	15.042	15.042
3	5290	-56.58	-56.58	62.89	62.89	15.241	15.241
4	5315	-58.09	-58.09	61.38	61.38	13.732	13.732
4	5319	-57.63	-57.63	61.84	61.84	14.189	14.189
4	5320	-60.43	-60.43	59.04	59.04	11.393	11.393
4	5321	-57.04	-57.04	62.43	62.43	14.777	14.777
4	5322	-59.31	-59.31	60.16	60.16	12.512	12.512

FLIGHT	PULSES PER FRAME	SIGMAZ(DB) AVG	SIGMAZ(DB) PEAK	
15	1	14.49	14.49	18

$$$$$$$$$$$$$$$$$$$$$$$$$$$$$$$$$$

	FRAME	RCVD PWR(DBM)AV	RCVD PWR(DBM)PEAK	SIGMA AV	SIGMA PEAK	SIGMAZ(DB) AV	SIGMAZ(DB) PEAK.
9	5484	-55.50	-52.03	63.97	67.44	16.321	19.793
9	5485	-55.86	-53.79	63.61	65.68	15.955	18.025
9	5486	-55.43	-52.89	63.99	66.58	16.337	18.931
9	5487	-54.44	-51.66	65.02	67.81	17.374	20.160
9	5488	-54.49	-51.83	64.58	67.64	16.927	19.990
9	5489	-54.69	-51.64	64.78	67.82	17.131	20.174
9	5490	-54.75	-51.66	64.72	67.81	17.065	20.159
9	5491	-55.01	-51.95	64.46	67.52	16.807	19.865
9	5492	-54.91	-52.05	64.56	67.42	16.912	19.766
9	5493	-54.54	-52.06	64.93	66.81	17.275	19.157
9	5494	-55.92	-52.29	63.55	67.18	15.898	19.532
9	5495	-55.57	-52.37	63.90	67.10	16.253	19.445
9	5496	-55.91	-53.09	63.56	66.38	15.909	18.732
9	5497	-55.12	-52.59	64.35	66.87	16.698	19.224
9	5498	-55.10	-52.10	64.37	67.37	16.717	19.720
9	5499	-55.57	-52.70	63.90	66.77	16.253	19.118
9	5501	-55.63	-52.51	63.84	66.96	16.191	19.313
9	5502	-54.52	-51.97	64.95	67.50	17.302	19.845
9	5503	-55.65	-52.51	63.82	66.96	16.172	19.306
9	5504	-54.56	-52.24	64.91	67.22	17.262	19.574
9	5505	-56.01	-52.14	63.46	67.33	15.811	19.681
9	5506	-56.03	-52.84	63.43	66.63	15.784	18.982
9	5507	-54.06	-51.71	65.41	67.76	17.758	20.105
9	5508	-55.90	-52.68	63.57	66.79	15.919	19.137
9	5509	-55.49	-53.65	63.98	65.82	16.326	18.169
10	5524	-55.11	-52.93	64.36	66.53	16.708	18.884
10	5525	-53.99	-52.28	65.47	67.19	17.824	19.537
10	5526	-55.69	-52.87	63.77	66.59	16.124	18.944
10	5527	-56.50	-53.69	62.97	65.78	15.317	18.129
10	5528	-55.69	-53.36	63.78	66.11	16.131	18.456
10	5529	-54.77	-52.72	64.70	66.75	17.047	19.102
10	5530	-56.20	-53.50	63.27	65.97	15.623	18.321
10	5531	-54.80	-52.79	64.61	66.68	16.961	19.033
11	5532	-55.66	-52.72	63.80	66.75	16.154	19.095

10	5533	-55.50	-52.76	63.97	66.71	16.319	19.057
10	5534	-54.64	-52.83	64.83	66.64	17.175	18.989
10	5535	-54.69	-52.39	64.78	67.08	17.131	19.428
10	5536	-54.81	-52.44	64.66	67.03	17.014	19.378
10	5537	-55.38	-52.54	64.09	66.93	16.441	19.276
10	5538	-54.89	-52.46	64.58	67.01	16.927	19.359
10	5539	-54.81	-52.04	64.66	67.42	17.007	19.774
10	5540	-57.21	-53.07	62.26	66.40	14.609	18.745
10	5541	-59.08	-54.34	60.39	65.13	12.740	17.478
10	5542	-56.95	-52.54	62.52	66.93	14.867	19.281
10	5543	-56.72	-52.79	62.75	66.68	15.095	19.032
10	5544	-56.91	-53.81	62.56	65.66	14.911	18.011
10	5545	-56.07	-53.40	63.40	66.07	15.745	18.421
10	5546	-55.09	-52.56	64.38	66.91	16.729	19.261
10	5547	-55.04	-52.46	64.43	67.01	16.777	19.360
10	5548	-54.69	-52.56	64.78	66.91	17.129	19.260
11	5566	-54.70	-52.30	64.77	67.17	17.121	19.522
11	5567	-55.84	-52.38	63.63	67.09	15.978	19.436
11	5568	-54.01	-51.75	65.45	67.72	17.804	20.067
11	5569	-54.11	-51.97	65.35	67.50	17.704	19.845
11	5570	-54.73	-52.06	64.73	67.41	17.083	19.756
11	5571	-55.77	-52.72	63.70	66.75	16.047	19.102
11	5572	-53.53	-51.46	65.94	68.01	18.291	20.360
11	5573	-54.81	-51.30	64.65	68.17	17.004	20.517
11	5574	-55.20	-51.66	64.27	67.81	16.623	20.162
11	5575	-55.75	-52.85	63.72	66.61	16.070	18.964
11	5576	-54.34	-50.93	65.13	68.54	17.482	20.893
11	5578	-55.77	-52.14	63.70	67.32	16.047	19.674
11	5579	-56.72	-51.72	62.75	67.75	15.095	20.101
11	5580	-54.91	-52.24	64.56	67.23	16.912	19.578
11	5581	-56.22	-52.15	63.25	67.32	15.597	19.670
11	5582	-56.37	-53.20	63.10	66.27	15.446	18.621
11	5583	-56.42	-51.74	63.05	67.73	15.401	20.082
11	5584	-55.64	-51.14	63.83	68.33	16.181	20.680
11	5585	-56.31	-53.05	63.16	66.42	15.505	18.769
11	5586	-57.00	-51.71	62.47	67.76	14.821	20.113
11	5587	-55.66	-52.38	63.81	67.08	16.156	19.434
11	5588	-55.66	-52.72	63.81	66.74	16.159	19.094
11	5589	-55.01	-51.75	64.46	67.72	16.806	20.066
11	5590	-55.31	-51.84	64.16	67.63	16.510	19.976
12	5608	-56.57	-53.34	62.90	66.13	15.247	18.483
12	5609	-57.22	-53.67	62.25	65.80	14.598	18.145
12	5610	-57.55	-54.27	61.92	65.19	14.267	17.545
12	5611	-56.19	-52.67	63.28	66.80	15.633	19.146
12	5612	-56.31	-52.31	63.16	67.16	15.509	19.508
12	5613	-54.98	-51.85	64.49	67.62	16.836	19.967
12	5614	-54.33	-52.49	65.14	66.98	17.485	19.333
12	5615	-56.69	-53.96	62.78	65.51	15.129	17.863
12	5616	-56.35	-53.46	63.12	66.00	15.466	18.354
12	5617	-55.68	-53.10	63.79	66.36	16.137	18.714
12	5618	-56.93	-54.06	62.54	65.41	14.891	17.763
12	5619	-55.24	-53.28	64.23	66.19	16.576	18.543
12	5620	-56.22	-52.61	63.25	66.86	15.603	19.213
12	5621	-54.33	-51.95	65.13	67.52	17.484	19.867
12	5622	-55.19	-52.18	64.28	67.29	16.626	19.643
12	5623	-54.99	-52.43	64.48	67.04	16.831	19.387
12	5624	-55.39	-52.64	64.08	66.82	16.430	19.174
12	5625	-54.93	-52.50	64.54	66.97	16.887	19.319
12	5626	-55.23	-52.80	64.23	66.67	16.584	19.020
12	5627	-55.82	-52.41	63.65	67.06	15.998	19.405
12	5628	-54.18	-52.35	65.29	67.12	17.637	19.472
12	5629	-55.76	-52.21	63.71	67.26	16.057	19.606
12	5630	-55.47	-52.42	64.00	67.05	16.351	19.399
12	5631	-55.54	-52.36	63.93	67.11	16.279	19.455
12	5632	-54.81	-52.37	64.66	67.10	17.009	19.452

$$$$$$$$$$$$$$$$$$$$$$$$$$$$$$$$

	FRAME	RCVD PWR(DBM)AV	RCVD PWR(DBM)PEAK	SIGMA AV	SIGMA PEAK	SIGMAZ(DB) AV	SIGMAZ(DB) PEAK
9	6577	-64.74	-60.61	54.73	58.86	7.081	11.210
9	6578	-61.85	-59.09	57.62	60.38	9.970	12.728
9	6579	-63.40	-60.21	56.06	59.26	8.414	11.612
10	6624	-63.13	-60.36	56.33	59.11	8.684	11.457
10	6625	-62.99	-60.72	56.48	58.75	8.826	11.098
10	6626	-63.61	-60.86	55.85	58.61	8.204	10.961
11	6666	-62.66	-59.96	56.80	59.51	9.154	11.856
11	6667	-62.78	-60.60	56.69	58.87	9.036	11.220
11	6668	-62.52	-59.85	56.95	59.62	9.298	11.971
12	6708	-62.40	-60.38	57.07	59.09	9.418	11.440
12	6709	-62.84	-60.32	56.63	59.15	8.982	11.501
12	6710	-63.02	-60.21	56.45	59.26	8.798	11.610

FLIGHT	PULSES PER FRAME	SIGMAZ(DB) AVG	SIGMAZ(DB) PEAK	
16	50	8.87	11.58	12

$$$$$$$$$$$$$$$$$$$$$$$$$$$$$$$$

	FRAME	RCVD PWR(DBM)AV	RCVD PWR(DBM)PEAK	SIGMA AV	SIGMA PEAK	SIGMAZ(DB) AV	SIGMAZ(DB) PEAK
13	6750	-64.61	-62.02	54.86	57.45	7.208	9.798
13	6751	-62.99	-60.62	56.58	58.85	8.933	11.203
13	6752	-64.57	-60.98	54.90	58.49	7.250	10.841
13	6753	-63.69	-61.02	55.78	58.44	8.132	10.793
13	6754	-64.29	-60.66	55.18	58.80	7.529	11.154
14	6792	-63.63	-60.88	55.84	58.59	8.190	10.941
14	6793	-64.05	-61.47	55.42	57.99	7.771	10.344
14	6794	-64.05	-61.73	55.42	57.74	7.767	10.088
14	6795	-63. 0	-61.25	55.67	58.21	8.017	10.564
14	6796	-63.24	-60.82	56.23	58.65	8.580	11.003
15	6834	-64.77	-62.28	54.70	57.19	7.045	9.535
15	6835	-62.67	-60.18	56.80	59.29	9.148	11.636
15	6836	-62.55	-59.04	56.92	60.43	9.273	12.778
15	6837	-61.24	-59.52	58.23	59.95	10.581	12.295
15	6838	-62.59	-59.24	56.88	60.23	9.225	12.579
16	6876	-63.01	-60.19	56.46	59.28	8.805	11.632
16	6877	-63.40	-60.46	56.07	59.01	8.417	11.361
16	6878	-63.03	-59.83	56.44	59.63	8.788	11.984
16	6879	-62.50	-59.95	56.97	59.52	9.318	11.865
16	6880	-61.94	-59.83	57.53	59.64	9.882	11.991

FLIGHT	PULSES PER FRAME	SIGMAZ(DB) AVG	SIGMAZ(DB) PEAK	
16	163	8.59	11.31	20

$$$$$$$$$$$$$$$$$$$$$$$$$$$$$$$$

FRAME	RCVD PWR(DBM)AV	RCVD PWR(DBM)PEAK	SIGMA AV	SIGMA PEAK	SIGMAZ(DB) AV	SIGMAZ(DB) PEAK

APPENDIX B

ENERGY SPECTRA OF SEA WAVES FROM PHOTOGRAPHIC INTERPRETATION

R. S. Kasevich*

* Senior Scientist
Advanced Development Laboratory
Raytheon Co., Sudbury, Mass.

TABLE OF CONTENTS

I. INTRODUCTION

The variable amplitude of the sea surface waves constituting a sea wave profile can be recorded on a photographic film if the sky light providing the illumination of the sea surface varies continuously in a linear manner.

The amplitude of the sea surface waves may be defined in terms of a potential energy spectrum of the wave surface.[3] If one thinks in terms of an infinite summation of sinusoids defining the sea surface, each sinusoidal component must be characterized by a frequency and vector wave number. The energy spectrum of the sea surface will then, in general, depend upon surface position and wave number vectors and the time and frequency scalars. The photographic record of sea surface amplitude variations or slope variations is also a representation of the potential energy spectrum of the surface.

The optical density variations on the photographic film, referred to later as the scene negative, are in a one-to-one correspondence with the sea surface displacement or slope, providing the linear sky light illumination condition is satisfied. The optical density characterizes the variable light transmission property of the negative and is defined by the equation $I = I_o 10^{-D}$, where I is the light intensity transmitted through a medium of optical density D, and I_o is the incident light intensity. For a photographic film, the optical density D is related to the light energy which exposes the film by the linear relationship

$$D = \gamma \log E \tag{1}$$

(3) Kinsman, Blair, "Wind Waves, Their Generation and Propagation on the Ocean," Prentice Hall, Englewood Cliffs, N.J., 1965.

for long enough exposure times. The quantity E is the exposing energy density and depends on the product.

$$E = kI\tau \quad \frac{\text{joules}}{m^2} \tag{2}$$

where

I = exposing light intensity, $\frac{\text{watts}}{m^2}$

τ = exposure time, sec.

k = relates to film sensitivity to light

γ = the slope of the film characteristic curve (log E vs D) in the linear region

A camera located above the surface of the sea and looking down in the direction of the water wave propagation will record a two dimensional optical density pattern - D(x, y). As indicated by equation (1), the numerical value of the density at each point on the scene negative will depend upon the light intensity, exposure time, film gamma, and sensitivity.

The light intensity (I) received by the camera lens will depend upon: (1) the geometry of the sea surface and camera position, (2) the manner in which the sky light intensity varies with zenith angle and azimuth angle, and (3) the polarization and frequency sensitive water reflectivity.

A. Linear Sky Assumption

For a basic understanding of how the slope angle ϕ of the sea wave profile is recorded on the scene film, the assumption of a linear sky is a good starting point. If the sky light reflected off the ocean surface varies linearly with zenith angle θ (see Figure 1), then the light intensity that exposes the camera film $I(x')$ will have a functional dependence which is linearly related to the slope angle $\phi(x)$

or wave height $\eta(x)$. This important concept is illustrated below. Assume the sea wave system is such that no azimuth angle dependent light reflection is recorded.

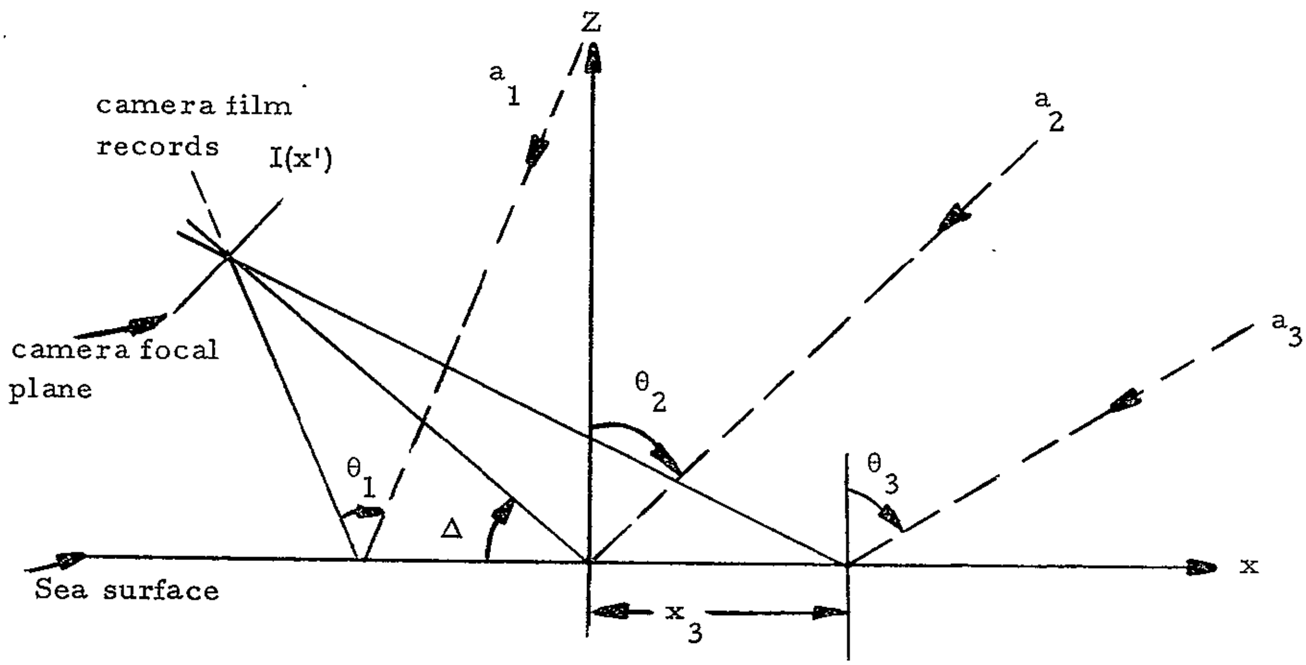

Figure 1. A One-Dimensional View of Ray Geometry for Determining I(x) Under Calm Sea Condition. Distance x' is Measured on the Scene Negative.

In Figure 1, the light intensity $I(x')$ will have the form $I_1 + I_2x'$ provided the sky illumination $a(\theta)$ is linear with zenith angle θ. The light ray a_2 will undergo specular reflection at $x = 0$ and expose the film at a point corresponding to say $x' = 0$. Light ray a_3 will reflect at $x = x_3$ and expose the film at point $x' = x'_3$ with greater light intensity. A measurement of optical density $D(x')$ along the x' axis of the scene negative will be that shown in Figure 2 (microdensitometer tracing)

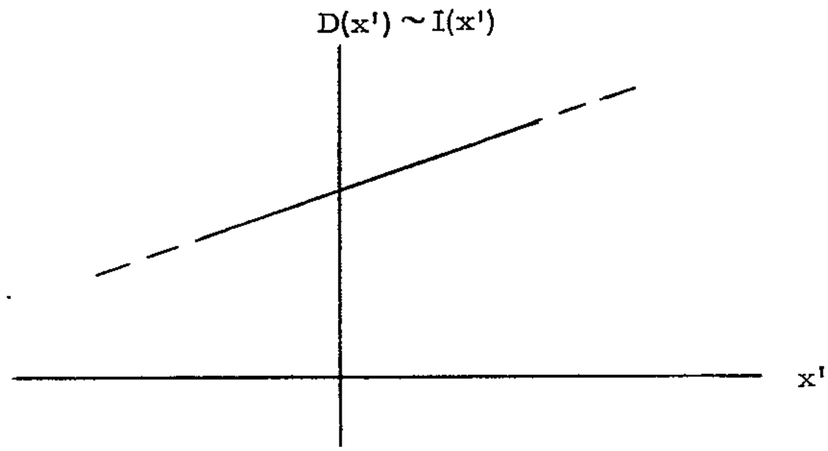

Figure 2. Scene Negative Optical Density Trace for Linear Sky Condition

If the sea surface is now wind driven the camera illumination I(x') is of the form

$$I(x') = I_1 + I_2\ (x' + c_1\phi\ (x')\ ) \qquad (3)$$

where $\phi(x')$ is the slope angle and c_1 is a constant relating angle to distance.

Comparing Figures 1 and 3, it is seen that the tangent plane for specular reflection defined by slope angle $\phi(o)$ in Figure 3 will provide illumination at the camera only by sky ray a_3, and not a_2 (Snell's Law). In terms of the unperturbed sea state of Figure 1, this corresponds to specular reflection from point x_3. Hence, the term $c_1\phi(x')$ must be added to x' to account for the increased light intensity exposing the film at x' = 0 (see Figure 4).

A scene negative will thus contain an optical density pattern D(x')

$$D(x') = \gamma \log \left[I_1 + I_2(x' + c_1\phi(x'))\right] k\,\tau \qquad (4)$$

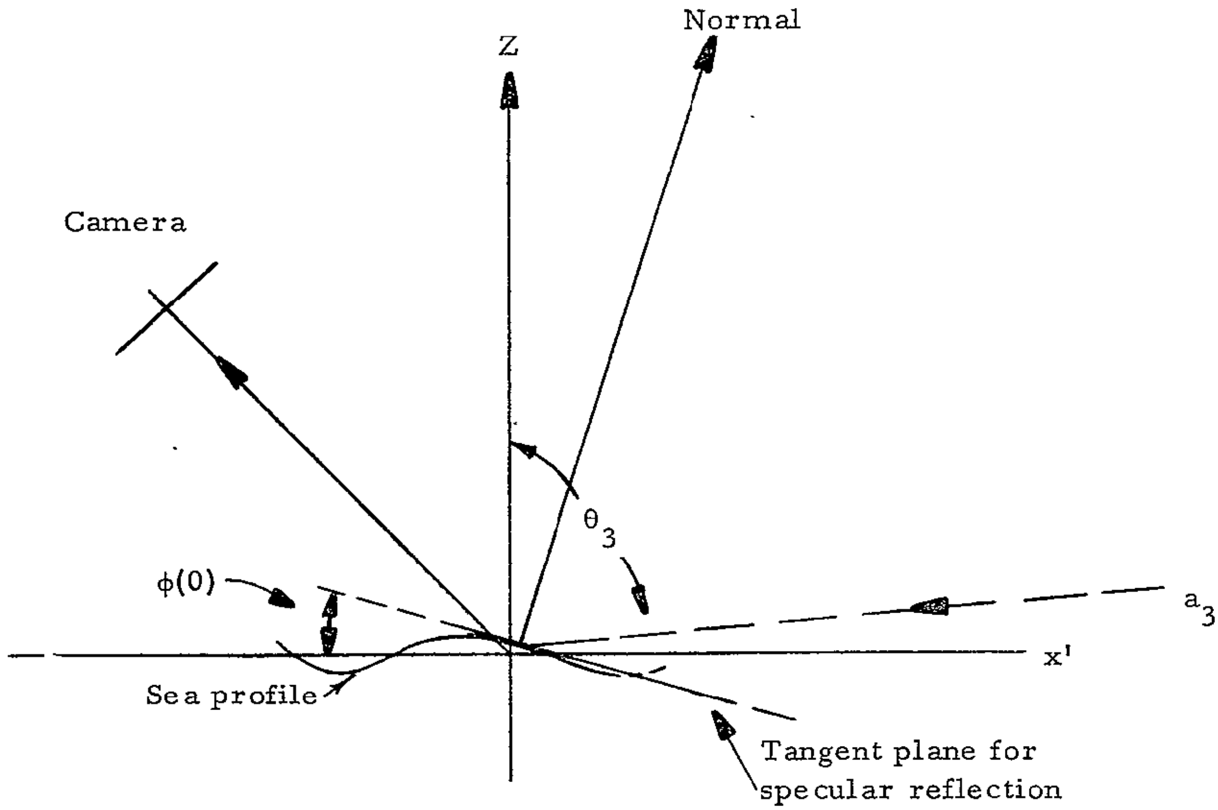

Figure 3. One-Dimensional View of Ray and Slope Geometry for Determining $I(x')$ Under Wind Condition

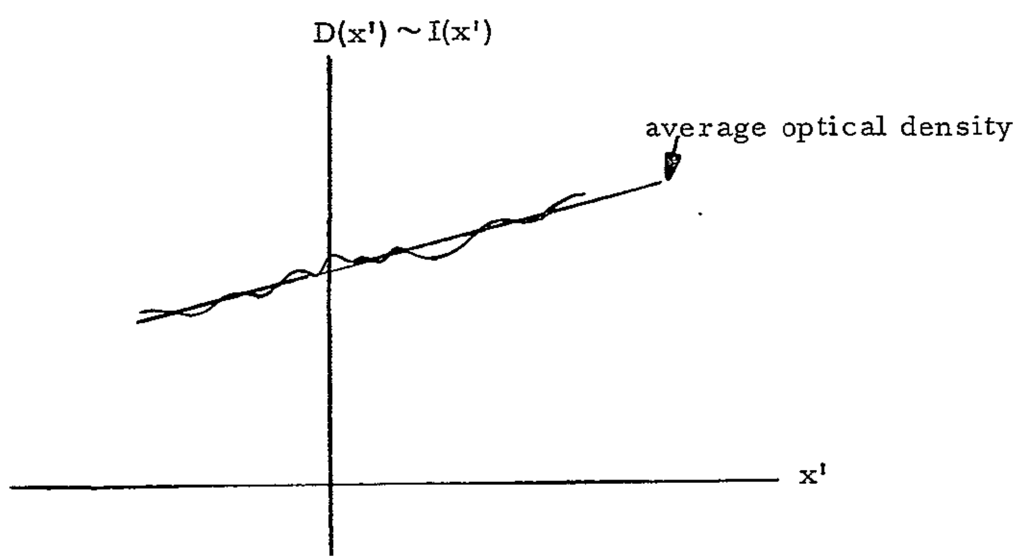

Figure 4. Optical Density Tracing of Scene Film Showing Sea Profile Defined by Slope Angle $\phi(x')$

where if a_o is the amplitude of laser light incident on the scene negative, $a_o 10^{-D(x')/2}$ is the transmitted laser light amplitude.

B. Optical Computer

The Fourier transform of the transmission function $T(x') = 10^{-D(x')}$ is now performed by the optical computer diagramed in Figure 5.

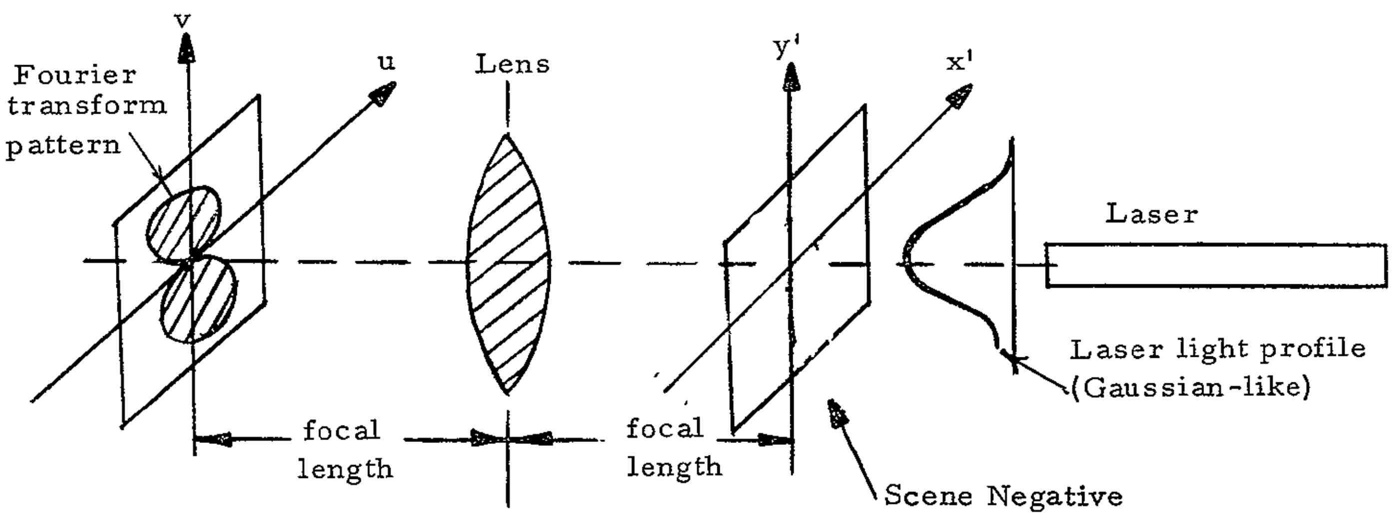

Figure 5. Optical Computer

By placing the scene negative in the x'-y' plane, located in the front focal plane of the lens, and exposing the film to a monochromatic, colliminated light beam (laser), the Fraunhofer diffraction pattern (Fourier transform) of the transmission function $T(x')$ will be recorded by a camera placed in the back focal plane of the lens. This transform negative will contain the spectrum of wave numbers (frequencies that constitute the sea wave profile $\eta(x)$ or slope $\phi(x)$). By simply reading the coordinates of a point in the transform (u_1, v_1), a corresponding vector wave number is calculated by the important relationship

$$\boxed{\left(\frac{\overline{K}}{2\pi}\right) f\lambda = \overline{r}} \qquad (5)$$

where $f\lambda$ is a calibration constant, and $\overline{K}$ is the vector wave number in radians per meter. $\overline{r}$ is the position vector. The vector wave number $\overline{K}_1$ corresponding to the point u_1, v_1 specifies the wavelength, direction, and frequency of one sinusoidal component of the sea wave spectrum.

C. Results of Calculation

The energy spectrum is calculated from the optical density pattern D(u, v) provided by the Fourier transform negative. A two dimensional integration of $10^{-D(u, v)/\gamma}$, the optical density transmission function, and evaluation of appropriate calibration constants determines the energy spectrum. The calibration constants are calculated from microdensitometer tracings of the scene negative, transform negative, laser beam cross-section negative, Ronchi grating transform negative ($f\lambda$ product), and camera focal length and position. The microdensitometer basically measures the optical transmission property of a negative, $10^{-D/\gamma}$.

A one-dimensional energy spectrum calculation for Raytheon Flight No. 6 ocean wave data indicates that the peak spectral component of the wave system is in the range of 0.188-0.226 ft^2-sec at a wave length of approximately 20 meters. Assuming 20 meters to represent the dominant wavelength of the system, the corresponding period is 3.6 seconds. Shore observation recorded a wave period of approximately 5 seconds for this flight. Also, for frequencies greater than two radians per second, the spectral amplitudes decay according to the well known ω^{-5} dependence where ω is the radian frequency.

II. SEA PHOTOGRAPH ANALYSIS

The general two-dimension transmission function $10^{-D(x', y')}$ represented by the scene negative is now derived for the two-dimensional case. The analysis approach follows that given by Stilwell.

Consider the illumination at the camera from light reflected from some arbitrary point on the sea (see Figure 6):

$$I(\Delta) = Ka(\theta)\,\rho(\theta) \qquad (6)$$

where

K = a constant and varies inversely as the square of distance from the point of reflection to the camera position in the sky.

$a(\theta)$ = the luminance of the sky and is a function of zenith angle, θ.

$\rho(\theta)$ = the reflection coefficient of the sea water and depends also on the zenith angle.

Δ = camera angle

In Figure 6, the position vector $\hat{r}$ is drawn perpendicular to a differential area in the focal plane of the camera. $\hat{n}$ is normal to tangent plane.

Equation (6) implies that the illumination of the camera is governed only by light rays that lie in the plane defined by the unit vectors $\hat{r}$ and $\hat{n}$.

The change in camera illumination for a small perturbation of the surface normal unit vector $\hat{n}$ (small slope angle ϕ) is

$$\frac{dI}{d\phi} \doteq K \left(\frac{da(\theta)}{d\theta}\, \rho(\theta) + a(\theta)\, \frac{d\rho(\theta)}{d\theta} \right) \frac{d\theta}{d\phi} \qquad (7)$$

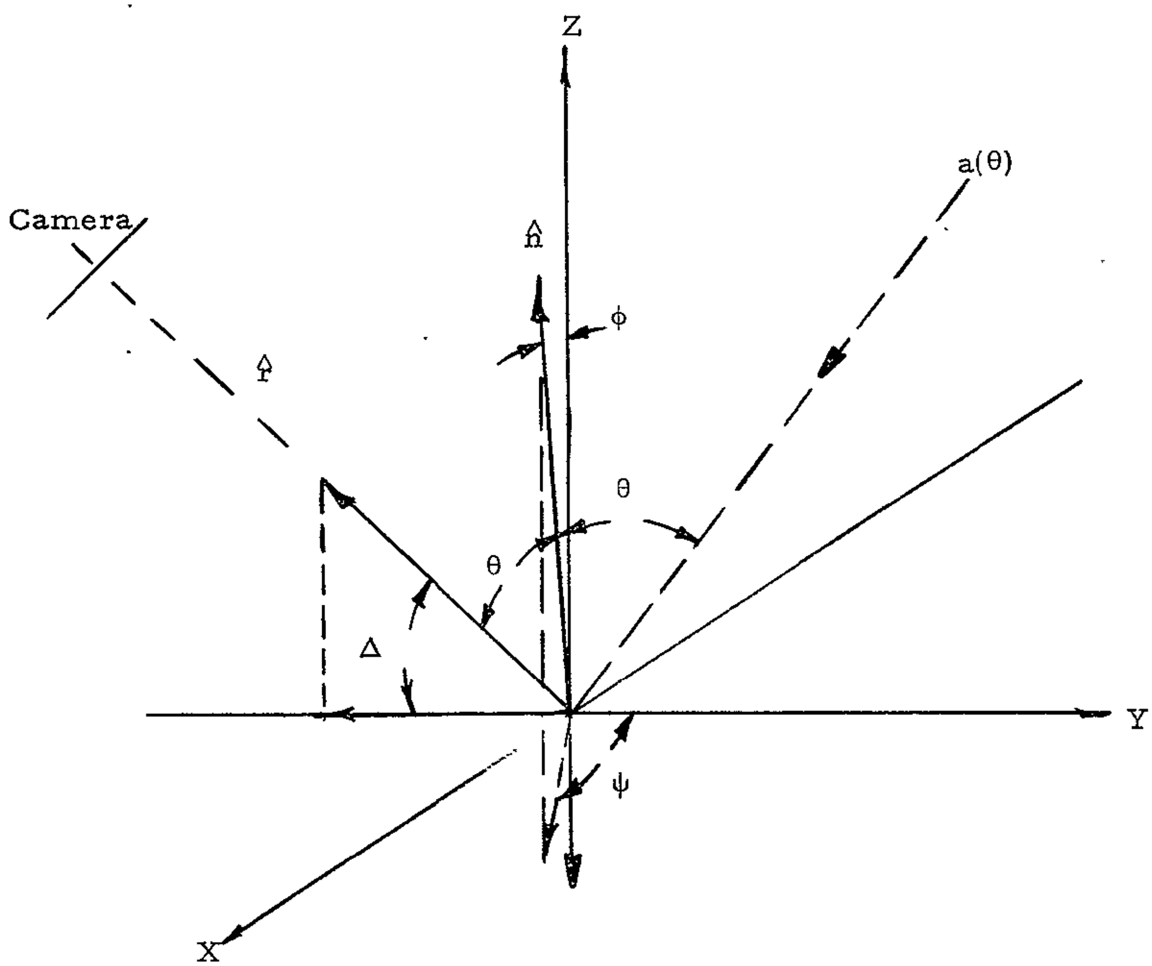

Figure 6. Specular Reflection at a Point on the Surface of the Sea

Assume $\cos\phi \cong 1$, $\sin\phi \cong 0$

The factor $\frac{d\theta}{d\phi}$ is

$$\frac{d\theta}{d\phi} = -\frac{1}{\sin\theta} \cdot \frac{d}{d\phi}(\hat{r} \cdot \hat{n}) \text{ where } \hat{r} \cdot \hat{n} = \cos\theta \qquad (8)$$

$$= -\frac{1}{\sin\theta}\frac{d}{d\phi}\Big[(-\hat{y}\cos\Delta + \hat{z}\sin\Delta) \cdot (\hat{x}\sin\phi\sin\psi +$$

$$\hat{y}\sin\phi\cos\psi + \hat{z}\cos\phi)\Big]$$

$$\cong \cos\psi \text{ for } \theta + \phi + \Delta = 90° \text{ and } \cos\phi = 1, \ \sin\phi = 0 \qquad (9)$$

So

$$\frac{dI}{d\phi} \cong K \left(\frac{da(\theta)}{d\theta} \quad \rho(\theta) + \frac{d\rho(\theta)}{d\theta} \right) \cos\psi \qquad (10)$$

Integrating equation (10) gives

$$I(\theta, \psi, \phi) = K \left(\frac{da(\theta)}{d\theta} \quad \rho(\theta) + a(\theta) \frac{d\rho(\theta)}{d\theta} \right) \cos\psi \cdot \phi + I_o \qquad (11)$$

The constant of integration I_o may be looked upon as the illumination I for $\psi = 90°$ or $\phi = 0$. Equation (11) is simplified by defining

$$K \left(\frac{da(\theta)}{d\theta} \cdot \rho(\theta) + a(\theta) \frac{d\rho(\theta)}{d\theta} \right) = I' = f(\theta) \qquad (12)$$

$$\therefore \ I(\theta, \psi, \phi) = I_o + I' \phi \cos\psi \qquad (13)$$

Equation (13) is the two-dimensional illumination function originally derived by Stilwell.

In terms of general coordinates on the sea surface, Equation (13) is changed to read

$$I(x', y') = I_o(x', y') + I'(x', y') \phi(x', y') \cos\psi \qquad (14)$$

The illumination terms $I_o(x, y)$, and $I'(x, y)$ are assumed to be constants in Stilwell's optical analysis. This would imply that the sky light intensity $a(\theta)$ (see Figure 6) changes linearly with zenith angle θ and all light rays reflected off the sea surface see the same water reflectivity. If this assumption is true, then I' defined by equation (12) would take the form

$$I' = K \frac{da(\theta)}{d\theta} \cdot \rho(\theta) = \text{constant.} \qquad (15)$$

The validity of the assumption $I_o(x, y)$ = constant may be examined by inspection of the optical density plot of the scene negative. (In Figure 2, the average change in optical density is related to $I_o(x')$.)

III. OPTICAL ANALYSIS

A. Average Power Spectrum of Photograph

In general, then, for small slope angles $\phi(x, y)$ ($\cos\phi = 1$, $\sin\phi = 0$)

$$I(x, y) = I_o(x', y') + I'(x', y')\phi(x', y') \cos\psi \qquad (16)$$

A scene negative will record the above illumination function in the form

$$D(x', y') = \gamma \log [k_1 I(x', y')\tau_1] . \qquad (17)$$

The primed coordinates refer to distances measured on the scene film. k_1 is a constant related to the film sensitivity. τ_1 is the film exposure time. A laser beam transmitted through the scene negative, which may be thought of as a diffraction grating, will experience attenuation as shown in Figure 7.

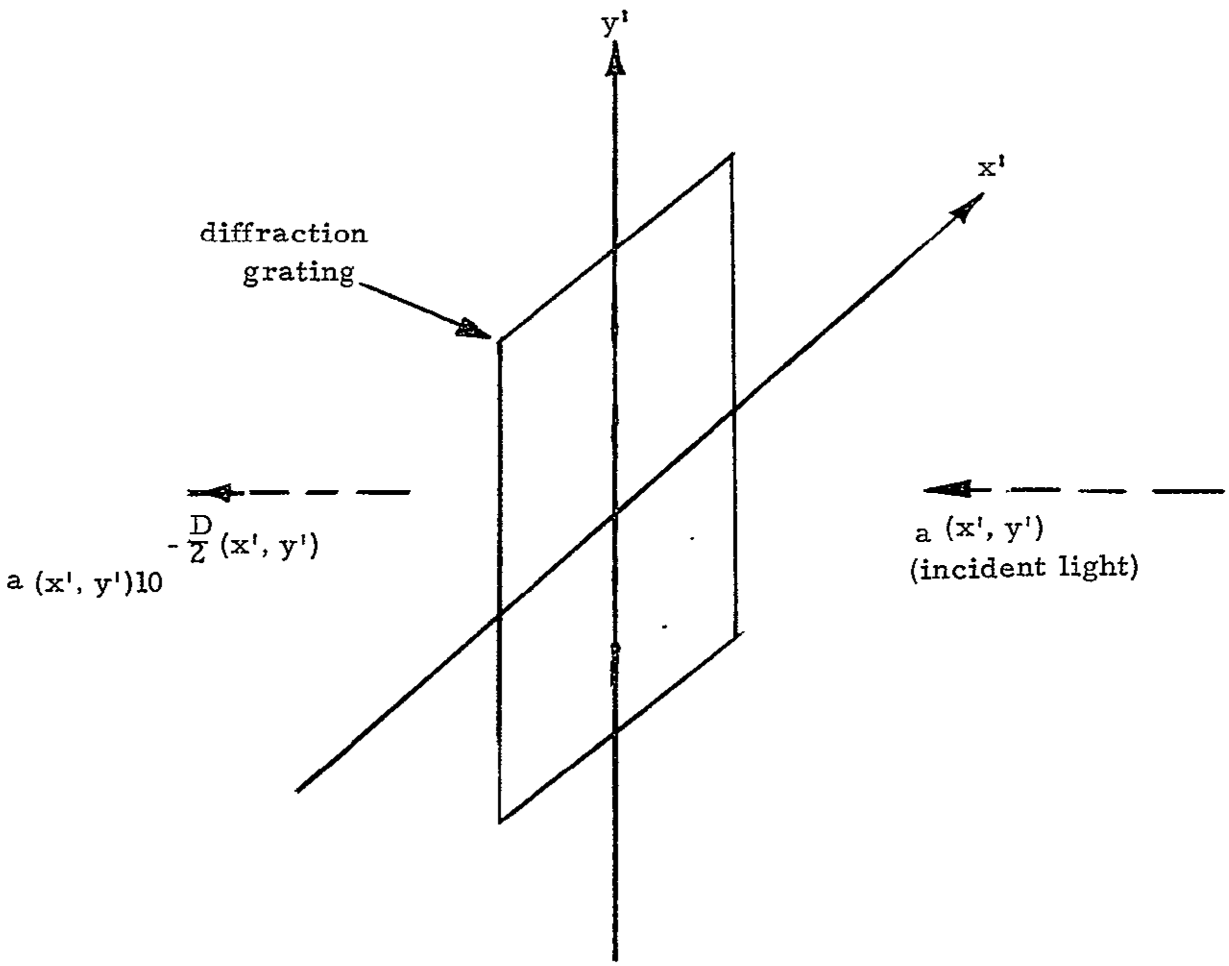

Figure 7. Transmission Through Scene Negative

The transmission function for light amplitude is

$$T'(x', y') = 10^{-D/2(x', y')} = [k_1 I(x', y')\tau_1]^{-\gamma_1/2} \tag{18}$$

where $\gamma_1 k_1, \tau_1$ refers to the scene film. To put equation equation (18) into a form useful for analysis, a binomial expansion is made.

$$T'(x', y') = [\tau_1 k_1 (I_o(x', y') + I'(x', y')\phi(x', y') \cos \psi]^{-\gamma_1/2} \tag{19}$$

$$= [\tau_1 k_1 I_o(x', y')]^{-\gamma_1/2} \left[1 + \frac{I'(x', y')}{I_o(x', y')} \phi(x', y') \cos \psi\right]^{-\gamma_1/2} \tag{20}$$

$$\approx [\tau_1 k_1 I_o(x', y')]^{-\gamma_1/2} \left[1 - \frac{\gamma_1}{2} g(x', y')\phi(x', y') \cos \psi \right] \tag{21}$$

where

$$g(x', y') \triangleq \frac{I'(x', y')}{I_o(x', y')} \tag{22}$$

and the assumption is made that

$$[g(x', y')\phi(x', y') \cos \psi]^2 << 1 . \tag{23}$$

The transmitted light amplitude $a'(x', y')$ is passed through the lens shown in Figure 8, and exposes the film placed in the back focal plane. The light intensity registered by the film is the Fraunhofer diffraction pattern (Fourier transform) of the light amplitude of the front focal plane. Each optical density point on the exposed film is uniquely related to a spatial frequency composing the transmission function of the diffraction grating (scene plane). The value of $D(u, v)$ indicates the relative intensities of the frequency components.

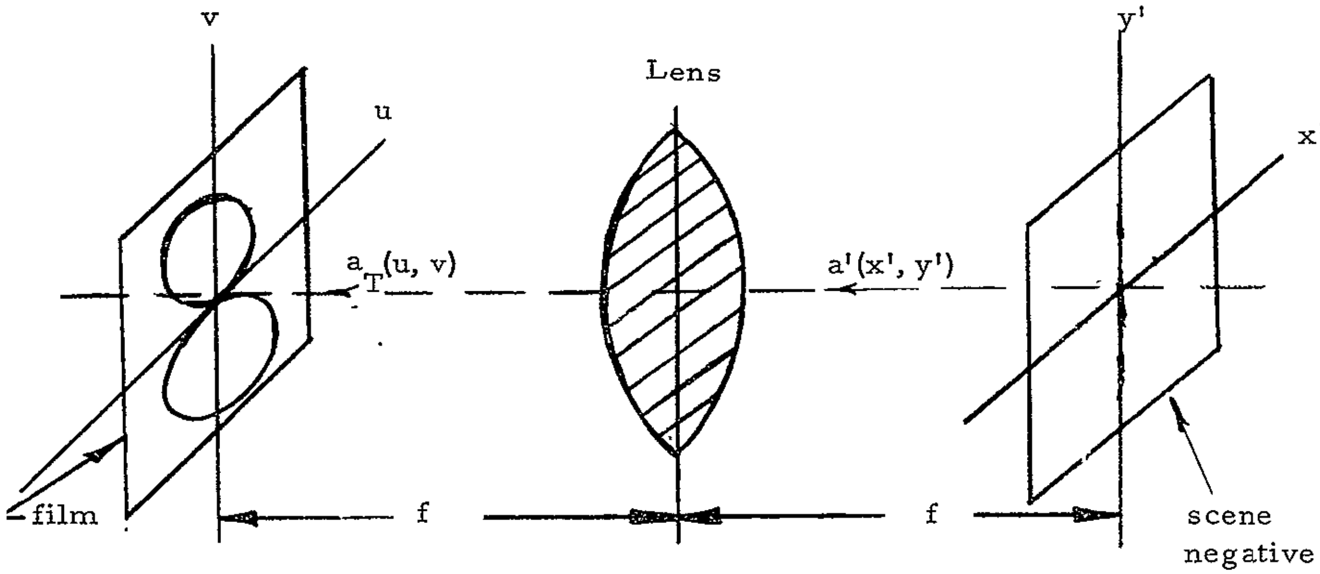

Figure 8

The light amplitude $a_T(u, v)$ exposing the film is therefore

$$a_T(u,v) = \text{const} \int\int_{-\infty}^{+\infty} a'(x',y')\, e^{-\frac{iK_o}{f}(ux'+vy')}\, dx'\, dy' \qquad (24)$$

$$= \text{const} \int\int_{-\infty}^{+\infty} a(x',y')\, T'(x',y')\, e^{-\frac{iK_o}{f}(ux'+vy')}\, dx'\, dy' \qquad (25)$$

$$= \text{const} \int\int_{-\infty}^{+\infty} a(x',y') \left[\tau_1 k_1 I_o(x',y')\right]^{-\gamma_1/2} \left[1 - \frac{\gamma_1}{2} g(x',y') \phi(x',y') \cos \psi\right] \cdot$$

$$e^{-\frac{iK_o}{f}(ux'+vy')}\, dx'\, dy' \qquad (26)$$

The constant of proportionality is $f\lambda$ (see appendix).

$$\therefore \ a_T(u, v) = (f\lambda) \iint_{-\infty}^{+\infty} a(x', y') \ 10^{-\overline{D}_1(x', y')/2} \left[1 - \frac{\gamma_1}{2} g(x', y')\phi(x', y') \cos\psi\right] \cdot e^{-\frac{iko}{f}(ux'+vy')} \, dx' \, dy' \tag{27}$$

where λ is the laser beam wavelength, f is focal length, $k_o = 2\pi/\lambda$, and $10^{-\overline{D}_1(x', y')/2} \triangleq [\tau_1 k_1 I_o(x', y')]^{-\gamma_1/2}$. The film in the u, v plane is sensitive to the light intensity $|a_T(u, v)|^2$. So, the optical density $D_2(u, v)$ is given by

$$k_2 \tau_2 \ |a_T(u, v)|^2 = 10^{D_2(u, v)/\gamma_2} \tag{28}$$

where k_2 is the transform film sensitivity factor, τ_2 is the exposure time, and γ_2 is the gamma of this film.

From equations (27) and (28), we have

$$\left| \iint_{-\infty}^{+\infty} e^{-(1/\sigma^2)(x'^2+y'^2)} \ 10^{-\overline{D}_1(x', y')/2} \left[1 - \frac{\gamma_1}{2} g(x', y')\phi(x', y') \cos\psi\right] e^{-\frac{iko}{f}(ux'+vy')} \, dx' \, dy' \right|^2 \tag{29}$$

$$\equiv \left(\frac{10^{(D_2(u, v)/\gamma_2)}}{k_2 \ \tau_2 \ a_o^2} \right) \cdot (f\lambda)^2 \tag{30}$$

For a Gaussian beam, $a(x', y') = a_o \ e^{-(1/\sigma^2(x'^2+y'^2)}$. Now let (Stilwell assumptions)

$$\underline{10^{-\overline{D}_1(x', y')/2} = \text{constant}} \tag{31}$$

and

$$\underline{\gamma_1 \ g(x', y') \triangleq \frac{\overline{D}_\phi}{\log_{10} e}} \ \text{be constant} \Rightarrow g(x', y') = \text{constant}. \tag{32}$$

Hence

$$\frac{(f\lambda)^2}{(k_2 \tau_2 a_o^2)} \left(10^{(D_2(u,v)/\gamma_2) + \overline{D}_1(x',y')}\right) \cdot \frac{4}{\cos^2\psi} \cdot \frac{\log^2_{10} e}{\overline{D}_\phi^2} \tag{33}$$

$$\cong \left| \int\int_{-\infty}^{+\infty} e^{-(1/\sigma^2)(x'^2+y'^2)} \phi(x',y') \, e^{-\frac{ik_o}{f}(ux'+vy')} dx' \, dy' \right|^2$$

The Fourier integral of the constant term for a finite aperture goes like $\left(\frac{\sin x}{x}\right)$ and will contribute to the frequency spectrum at and near center of the transform ($\omega \cong 0$). In the squaring process, it has been assumed that terms multiplied by the Fourier transform of the constant term do not contribute to the desired power spectrum.

The average power spectrum recorded by the transform photograph is*

$$P(K_x, K_y) = \frac{2\pi}{\sigma^2} \left| \int\int_{-\infty}^{+\infty} e^{-\sigma^{-2}(x'^2+y'^2)} \phi(x',y') \, e^{-\frac{ik_o}{f}(ux'+vy')} dx' \, dy' \right|^2 \tag{34}$$

where

$$\frac{K_o}{f} u = K_x \tag{35}$$

$$\frac{K_o}{f} v = K_y \tag{36}$$

and $u = x'$, $v = y'$ for the geometry of Figure 8.

Equations (35) and (36) relate density points (spectral amplitudes) in the transform to corresponding wave numbers. Equations (33) through (36) are the basic optical analysis formulas.

To gain some insight into the meaning of equation (29), take as an example

$$1 - \frac{\gamma_1}{2} g(x',y') \phi(x',y') = 1 - x' \tag{37}$$

* The factor $2\pi/\sigma^2$ is related to an elemental area in the transform plane and is derived in Stilwell's paper.

Hence

$$\iint_{-\infty}^{+\infty} e^{-\frac{1}{\sigma^2}(x'^2 + y'^2)} e^{-i \frac{k_o}{f}(x'u + vy')} dx' dy' \tag{38}$$

is sketched as curve 1, and

$$-i \iint_{-\infty}^{+\infty} x\, e^{-\frac{1}{\sigma^2}(x'^2 + y'^2)} e^{-i \frac{k_o}{f}(x'u + vy')} dx' dy' \tag{39}$$

is represented by curve 2 in Figure 9.

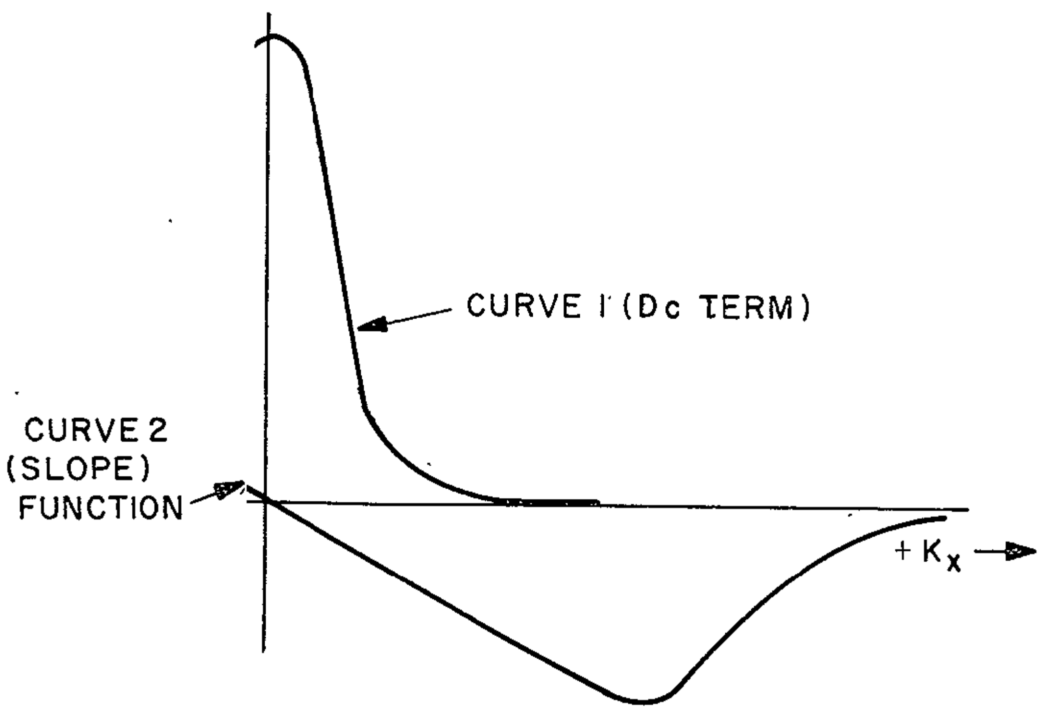

Figure 9. Fourier Transform Components

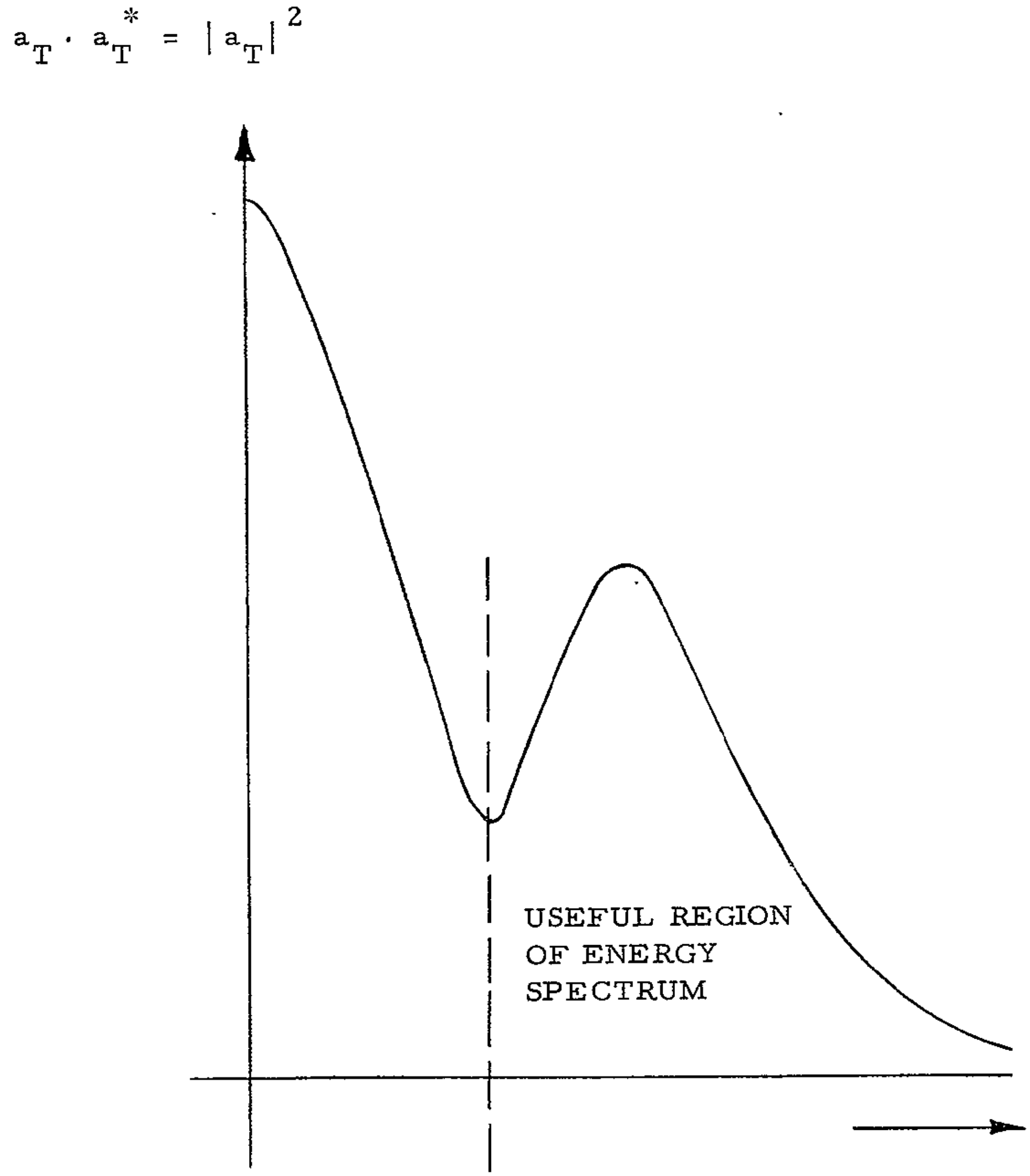

Figure 10. Power Spectrum for
$$1 - \frac{\gamma_1}{2} g(x', y') \phi(x', y') = 1\text{-}x$$

The plot shown in Figure 10 represents the average power spectrum of this hypothetical sea state.

IV. SEA SPECTRA

A. Basic Power Spectra

The sea surface displacement $\eta(x, y, t)$ may be expressed as a linear superposition of sinusoidal components (wave packet) provided that statistically independent, small amplitude components are assumed.[4]

$$\eta(x, y, t) = \iiint_{K_y K_x \omega} B(K_x, K_y, \omega)\, e^{+i(K_x x + K_y y - \omega t)}\, dK_x dK_y d\omega \tag{40}$$

where the amplitude spectrum $B(K_x, K_y, \omega)$ is given by

$$B(K_x, K_y, \omega) = \left(\frac{1}{2\pi}\right)^3 \iiint_{x\,y\,t} \eta(x, y)\, e^{-i(K_x x + K_y y - \omega t)}\, dx\, dy\, dt. \tag{41}$$

The instantaneous power spectrum of the sea surface displacement may be derived from the above relations and is

$$\Phi_\eta(K_x, K_y, \omega, x, y, t) = \left(\frac{1}{2\pi}\right)^2 \iint_{x\,y} \overline{\eta(x, y, t)\eta(x+x_o, y+y_o, t)}\, e^{-i(K_x x_o + K_y y_o)}\, dx_o dy_o \tag{42}$$

where the function

$$H(x, x_o, y, y_o t) \triangleq \overline{\eta(x, y, t)\, \eta(x+x_o, y+y_o, t)} \tag{43}$$

is the autocorrelation function of the sea surface displacement. (The bar indicates mean value.) Its inverse is

$$H(x, x_o, y, y_o, t) = \iiint_{K_x K_y \omega} \Phi_\eta(K_x, K_y, \omega, x, y, t)\, e^{+i(K_x x_o + K_y y_o)}\, dK_x dK_y d\omega. \tag{44}$$

For a homogeneous sea (one independent of the reference position for measurement) and stationary wave process, we have, dropping the x, y and t dependence,

$$H(x_o, y_o) = \iiint_{K_x K_y \omega} \Phi(K_x, K_y, \omega)\, e^{+i(K_x x_o + K_y y_o)}\, dK_x dK_y d\omega \tag{45}$$

(4) Ibid (3)

$$= \iint_{K_x K_y} \Phi(K_x, K_y)\, e^{i(K_x x_o + K_y y_o)}\, dK_x dK_y \tag{46}$$

where

$$\Phi(K_x, K_y) = \int_{\omega} \Phi(K_x, K_y, \omega)\, d\omega \tag{47}$$

$\Phi(K_x, K_y)$ is the two-dimensional wave number spectrum. The function $\Phi_\eta(K_x, K_y, \omega)$ is the three-dimensional spectrum for a spatially homogeneous and temporarily stationary wave field. Kinsman states that "$\Phi(K_x, K_y, \omega)$ represents the waves generated on an ocean of infinite extent over which a statistically uniform wind has been and will be blowing forever". "More reasonably, it isn't a bad model for the interior of a three- or four-day North Atlantic storm covering an area of 500 by 500 nautical miles."

The spectrum that is easily measured in practice (Spar Buoy) is the one-dimensional frequency spectrum given by

$$\Phi(\omega) = \iint_{K_x K_y} \Phi(K_x, K_y, \omega)\, dK_x\, dK_y \tag{48}$$

It gives the contribution to the potential energy of the wave coming from each frequency ω, irrespective of the vector wave numbers associated with that frequency. The frequency spectrum gives no information about which directions the various waves come from. (They add up at a point to define the potential energy of the composite wave.)

A typical frequency spectrum is shown in Figure 11.

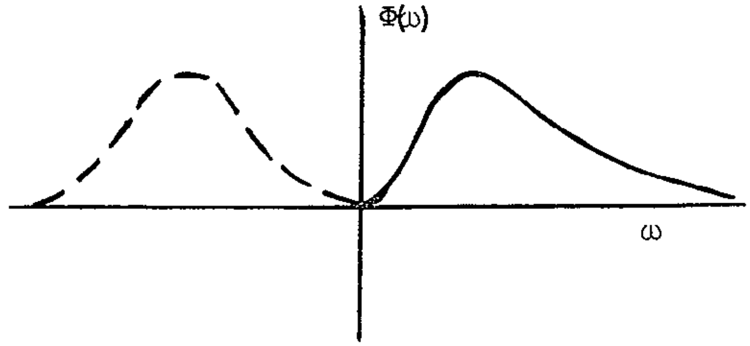

Figure 11

Thus, for the ocean wave process, there are three basic power spectra:

(1) The three-dimensional spectrum - $\Phi_\eta(K_x, K_y, \omega)$

(2) The two-dimensional wave-number spectrum - $\Phi_\eta(k_x, k_y)$.

(3) The one-dimensional frequency spectrum - $\Phi_\eta(\omega)$

B. <u>One-Dimensional Frequency Spectrum</u>

A relationship between the wave number spectrum and frequency spectrum for infinitesimal waves which have a unique connection between wave d frequency. For small amplitude, deep water waves, the relationship

$$\Phi_\eta(\omega) = \frac{2\omega^3}{g^2} \int_0^{2\pi} \Phi_\eta(K, \psi)\, d\psi \tag{49}$$

where g is the gravitational constant, ψ is the azimuth angle (see Figure 2) and

$$\omega^2 = gK \text{ where } g = 9.8 \frac{\text{meters}}{\text{sec}^2},\ K = \frac{\text{radians}}{\text{meter}}. \tag{50}$$

Kinsman points out "that finite amplitude waves do not have a unique relationship between wave number and frequency but yet the application of equation (49) seems to give very good results."

For each wave vector $\overline{K} = K_x \hat{x} + K_y \hat{y}$ there is a energy given by $\Phi_\eta(K_x, K_y)$. All wave vectors of the same length $\sqrt{K_x^2 + K_y^2}$ and corresponding frequency $\omega = \sqrt{gK}$ lie on a circle of radius $|K| = \frac{\omega^2}{g}$ in the K_x, K_y plane (see Figure 12).

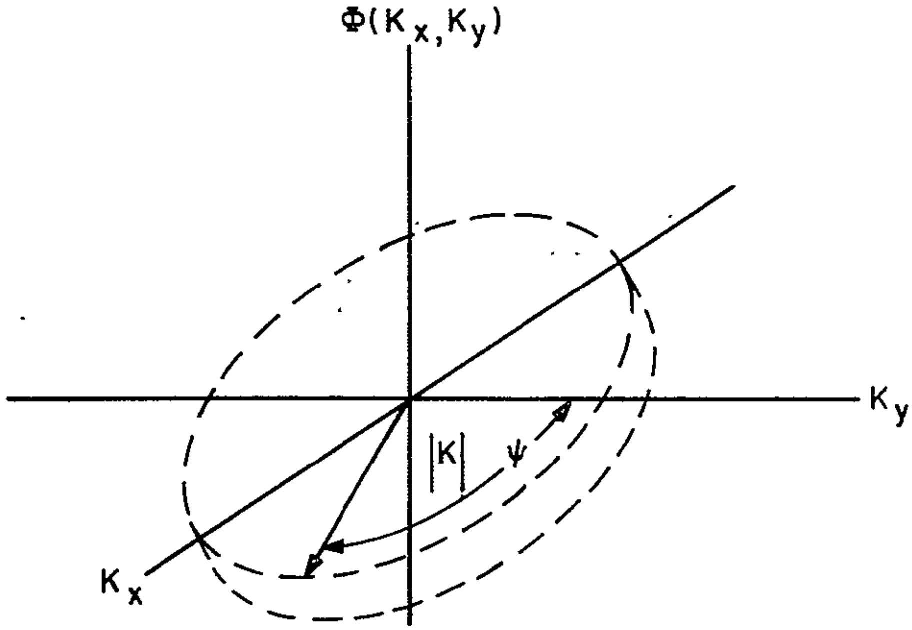

Figure 12. Energy Spectrum Evaluation

Quoting Kinsman, Equation (49) says, "Add up all the energy on this circular ring and you will have located all the energy which is batting around at frequency ω."

V. RELATIONSHIP BETWEEN SEA SPECTRUM AND PHOTOGRAPHIC SPECTRUM

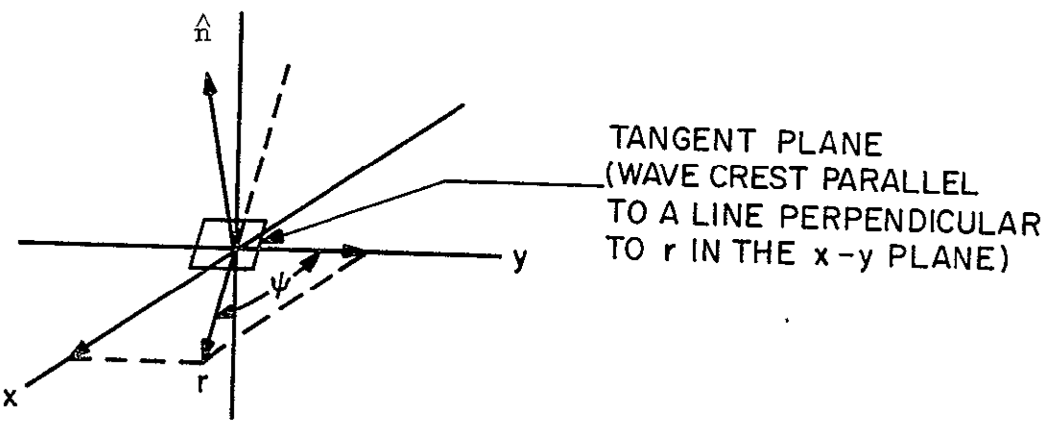

Figure 13. Geometry for Calculating Relationship Between $\Phi_\eta(K_x, K_y)$ and $\Phi_\phi(K_x, K_y)$

The wave height spectrum $\Phi_\eta(\omega)$ is related to the slope spectrum $\Phi_\phi(\omega)$ as follows:

For a wave propagating in the r direction in x-y plane (see Figure 13),

$$\frac{\partial\eta}{\partial r}(x, y) = \tan\phi\,(x, y) \doteq \phi(x, y) \tag{51}$$

and $x = r \sin \psi$

so

$$\frac{\partial \eta}{\partial x}(x, y) = \phi \sin \psi . \quad (52)$$

For a stationary wave process, equation (40) gives

$$\eta(x, y) = \int_{K_x} \int_{K_y} \int_{\omega} B(K_x, K_y, \omega)\, e^{i(K_x x + K_y y)}\, dK_x\, dK_y\, d\omega \quad (53)$$

$$\therefore \frac{\partial \eta}{\partial x}(x, y) = iK_x \int\int\int B(K_x, K_y, \omega)\, e^{i(K_x x + K_y y)}\, dK_x\, dK_y\, d\omega \quad (54)$$

$$= iK_x \eta(x, y)$$

$$= \phi(x, y) \sin \psi$$

or

$$\phi(x, y) = \frac{iK_x}{\sin \psi}\, \eta(x, y) . \quad (55)$$

$$\therefore \phi(x, y) = iK\eta(x, y) . \quad (56)$$

Therefore, equation (41)

$$B(K_x, K_y, \omega) = \left(\frac{1}{2\pi}\right)^2 \int_{K_x} \int_{K_y} \eta(x, y)\, e^{-i(K_x x + K_y y)}\, dx\, dy \quad (57)$$

becomes

$$B(K_x, K_y, \omega) = \left(\frac{1}{2\pi}\right)^2 \left(\frac{1}{iK}\right) \int\int \phi(x, y)\, e^{i(K_x x + K_y y)}\, dx\, dy \quad (58)$$

and the power spectrum given by

$$\Phi_\eta(K_x, K_y, \omega) = \left(\frac{1}{2\pi}\right)^2 \iint_{x\,y} \overline{\eta(x, y)\eta(x+x_o, y+y_o)}\, e^{-i(K_x x_o + K_y y_o)}\, dx_o dy_o \tag{59}$$

becomes

$$\Phi_\eta(K_x, K_y, \omega) = \left(\frac{1}{2\pi}\right)^2 \frac{1}{K^2} \iint_{x\,y} \overline{\phi(x, y)\phi(x + x_o, y + y_o)}\, e^{-i(K_x x_o + K_y y_o)}\, dx_o dy_o \tag{60}$$

or

$$K^2 \Phi_\eta(K_x, K_y, \omega) = \Phi_\phi(K_x, K_y, \omega) \tag{61}$$

and

$$K^2 \Phi_\eta(K_x, K_y) = \Phi_\phi(K_x, K_y)\ ) \tag{62}$$

(both for small $\phi(x, y)$.

The power spectrum defined by the equations (33) and (34) is proportional to $\Phi_\phi(K_x, K_y)$:

$$\phi(K_x, K_y) \propto \left[\left(\frac{2\pi}{\sigma^2}\right) \frac{(f\lambda)^2}{(K_2\, \tau_2\, a_o^2)}\, 10^{(D_2(u, v)/\gamma_2)+\overline{D}_1} \cdot 4 \sec^2\phi \cdot \frac{\log_{10}^2 e}{\overline{D}_\phi^2} \right]. \tag{63}$$

The constant of proportionality is $\left(\frac{\beta_x \beta_y}{2\pi^3}\right)$ where β_x, β_y are scale transformation factors relating the sea coordinates x, y to the transform coordinates x', y'.[5]

(5) Ibid (1).

VI. CALCULATION PROCEDURE

The calculation of wavelength is based upon Equation (5) which relates various points in the Fourier transform to corresponding vector wave numbers. The $f\lambda$ product is determined from either the optical bench or the Ronchi grating transform. f is the focal length of the lens and λ is the wavelength of the laser beam. Knowing the focal length and position of the camera used in taking the scene picture, a scale factor relating a distance on the ocean surface to a distance on the transform can be determined. A calibration equation relating a distance in the transform $x^{(3)}$ to a corresponding wavelength λ_x is therefore determined. (Propagation along the orthogonal axis has been ignored.)

The computation of the energy spectrum function $\Phi(\omega)$ is based upon Equations (49, (62) and (63). Required for this evaluation are the calibration equation and microdensitometer tracings of:

(1) laser beam cross-section

(2) scene negative

(3) transform negative or isodensitometer of transform negative.

The transform density tracing shows rapid oscillations with frequency. An averaging process has been applied to the transform for a reasonable estimate of the spectrum function.

(A) Wavelength Calibration

The vector wave numbers and frequencies comprising the sea state energy spectrum $\Phi_\phi(K_x, K_y)$ are calculated from the relationship between vector positions in the transform or isodensity tracing of the transform and wave number K. A typical Fourier transform and its corresponding isodensity tracing is shown in Figures 14 - 17 for $\psi = 0$ and $\psi = 90°$. The major axis of the pattern indicate the general direction of wave propagation.

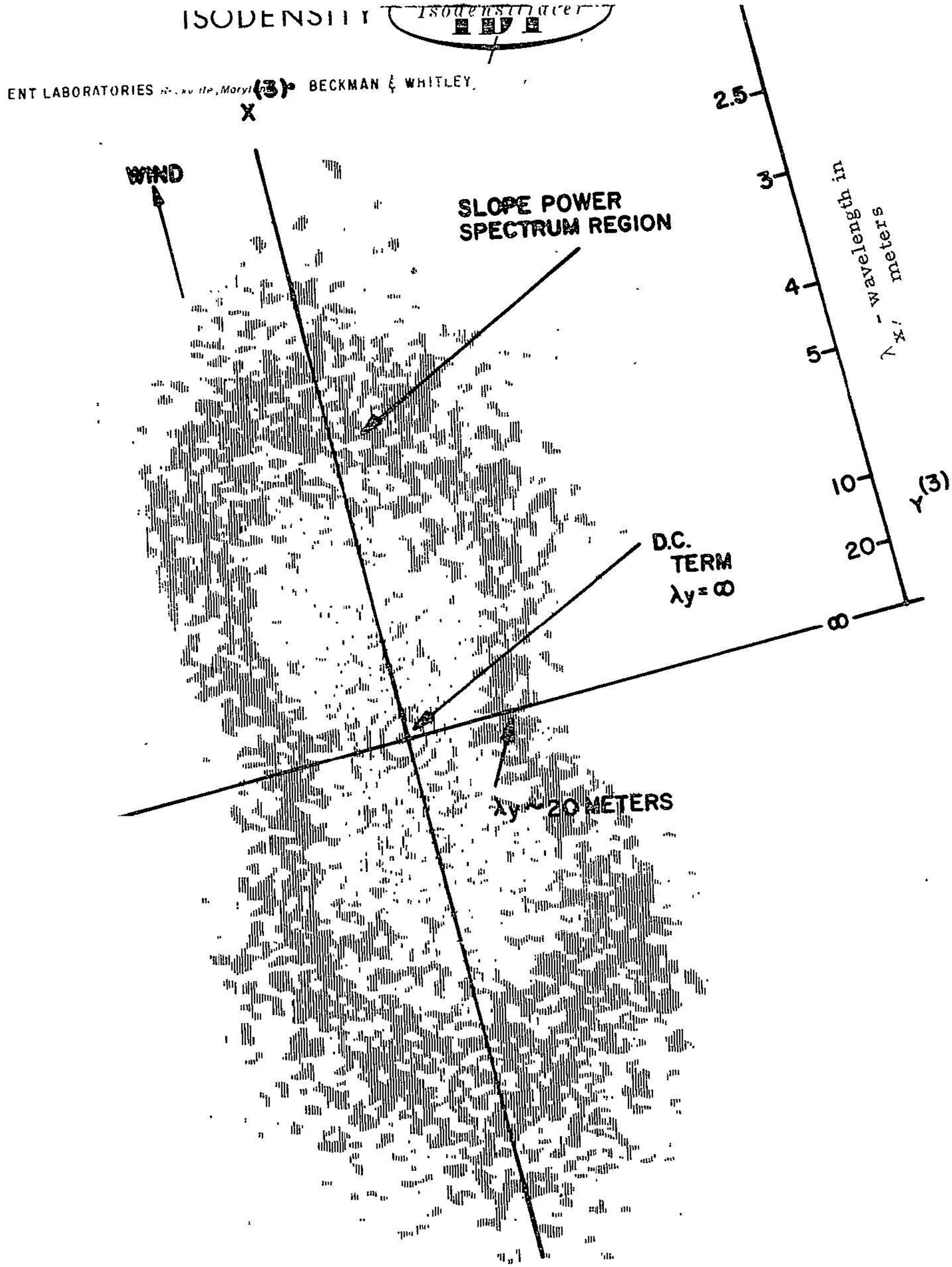

Figure 14. Isodensity Tracing of Transform Negative for $\psi = 0$ (Camera Looking in $X^{(3)}$ Directions)

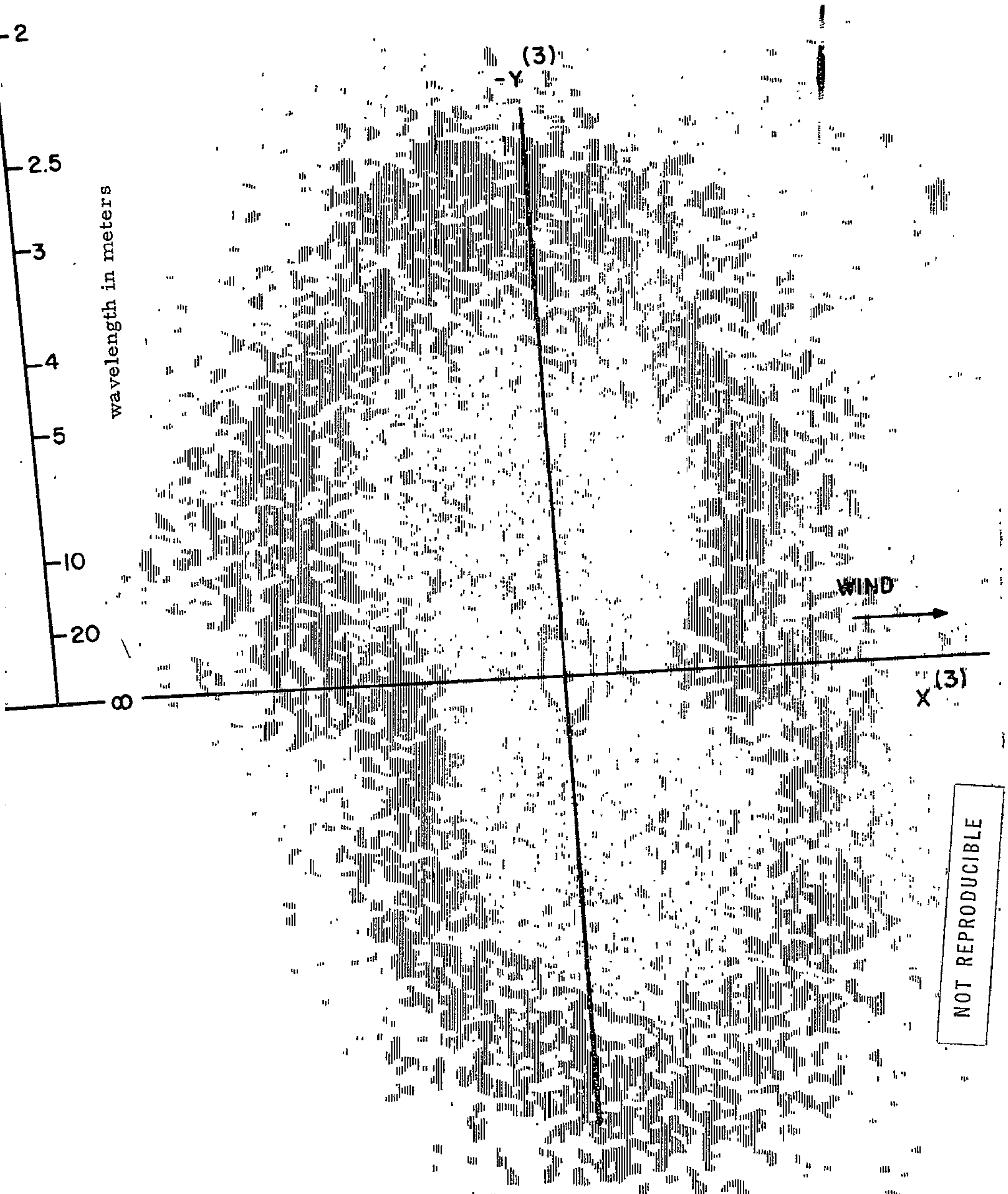

Figure 15. Isodensity Tracing of Transform Negative (Camera Looking in $Y^{(3)}$ Direction of Figure 14)

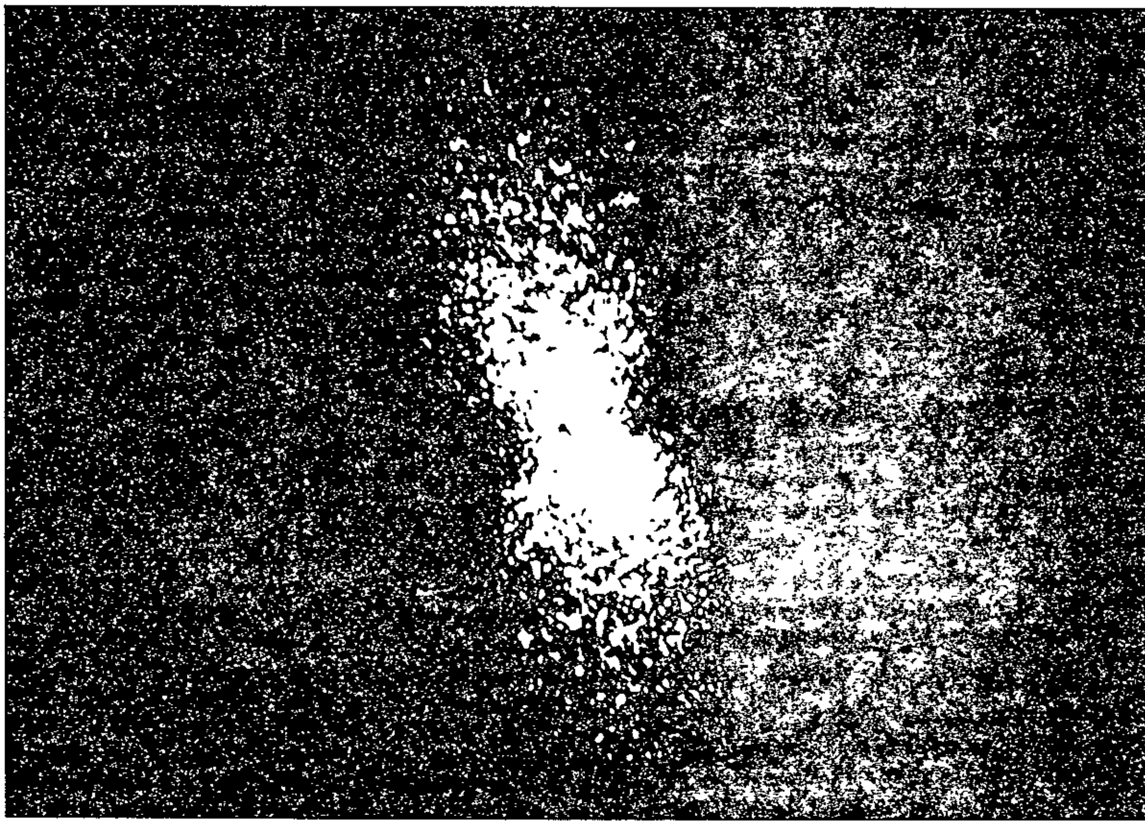

Figure 16. Fourier Transform for Flight No. 6, $\psi = 0$
Camera located in y - z plane

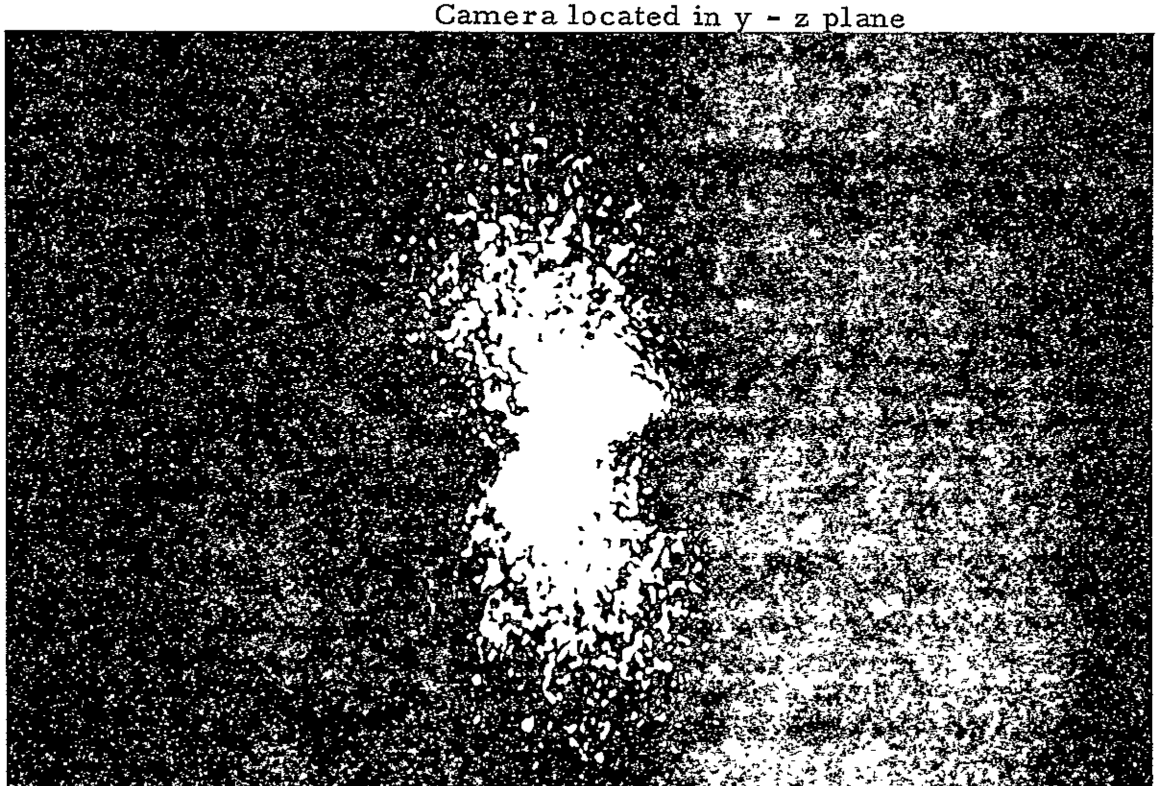

Figure 17. Fourier Transform for Flight No. 6, $\psi = 0°$
Camera located in x - z plane

The following relations apply for all points in the transforms:

$$(f\lambda)\left(\frac{K_x}{2\pi}\right) = x^{(3)} \tag{64}$$

and

$$(f\lambda)\left(\frac{K_y}{2\pi}\right) = y^{(3)}. \tag{65}$$

f is the focal length of the lens and λ is the wavelength of the monochromatic, collimated laser beam.

Alternatively, the $f\lambda$ product can be determined by analyzing the far field pattern (transform) of the Ronchi grating. The basic equation is

$$\Delta x_b = \frac{\lambda f}{2b} \tag{66}$$

where 2b is the distance between grating lines and Δx_b is the distance between two maxima in the transform recording. (See Figure 19).

The first step in the wavelength calibration procedure is to determine the scale factors relating a distance on the sea surface Δx, Δy to a distance in the transform or isodensity tracing of the transform, and a wave number K_x, K_y of the sea state to a wave number in the transform.

In Figure 18 is shown the camera position relative to the ocean surface (ψ=0).

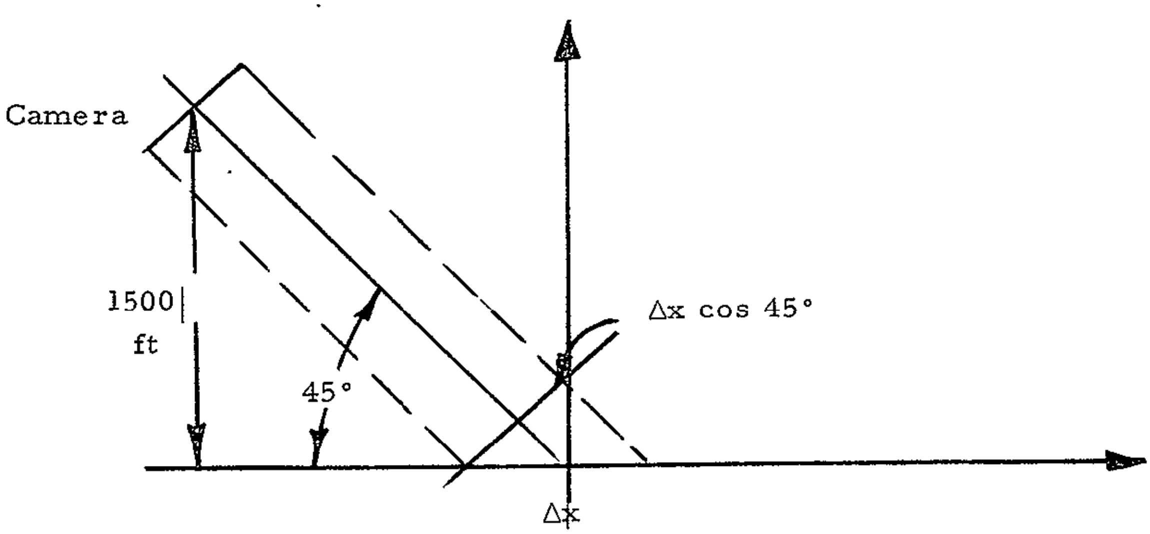

Figure 18. Calibration Geometry for One-Dimensional Spectrum

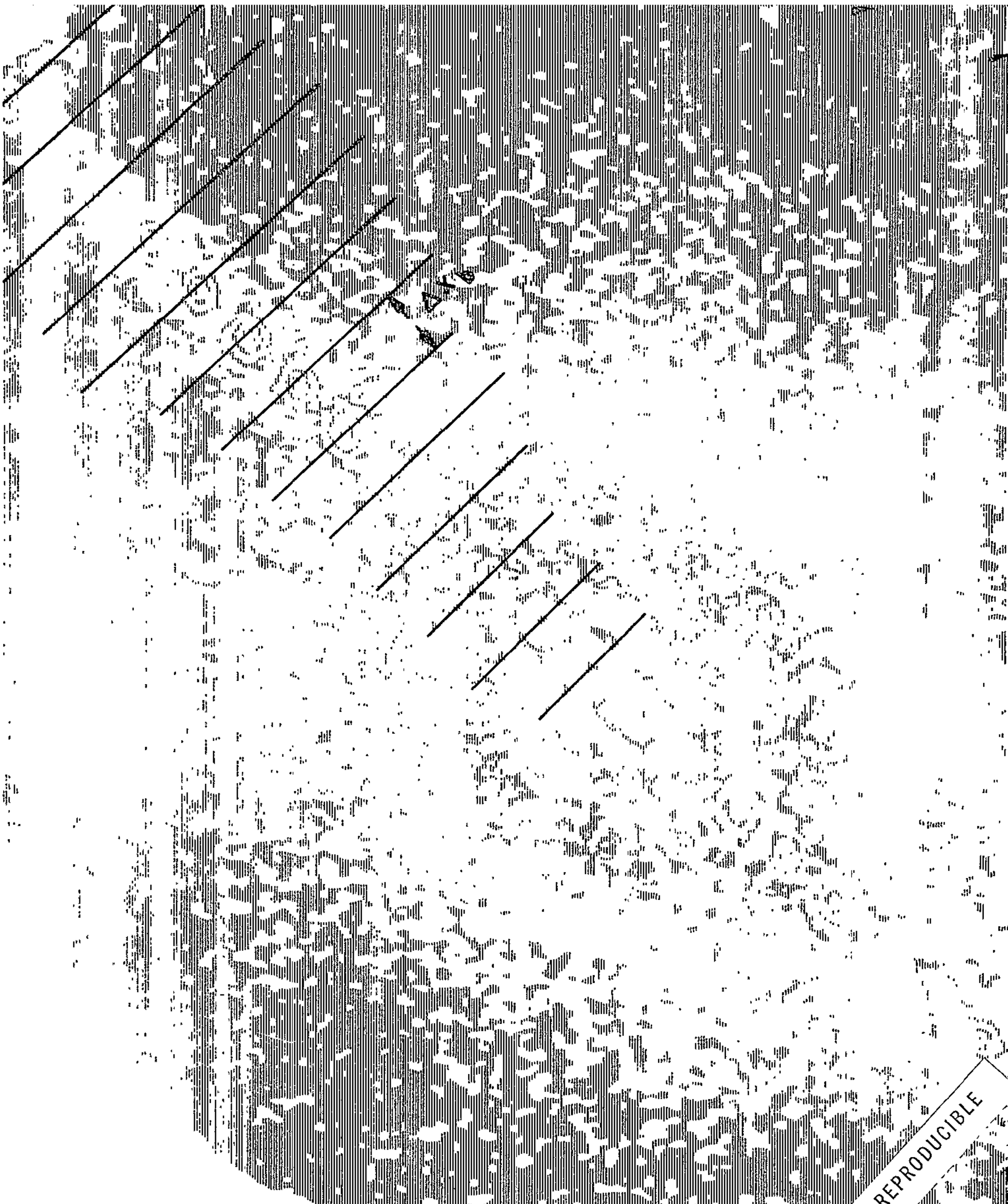

Figure 19. Ronchi Grating Isodensity Tracing for Measuring $f\lambda$. $f\lambda = 2b\,\Delta x_b$ and Line Spacing is 2 lines/mm

Let

Δx = incremental distance on sea surface

$\Delta x^{(1)}$ = incremental distance on a 9 inch film in camera (scene negative)

$\Delta x^{(2)}$ = incremental distance on a 35 mm film (scene negative)

$\Delta x^{(3)}$ = incremental distance on isodensity tracing of transform

and K_x, $K_x^{(1)}$, $K_x^{(2)}$, $K_x^{(3)}$ are the corresponding wave numbers.

It will be assumed that the power spectrum is highly directional along the x axis and therefore all $K_y \doteq 0$.

Now, for flight No. 6 and follow-on film processing work,

$$\frac{\Delta x^{(1)}}{\Delta x \cos 45°} = \frac{\text{focal length of camera}}{\text{range}}$$

$$= \frac{1}{1500\sqrt{2}}$$

so

$$\Delta x^{(1)} = \frac{\Delta x}{3000} \tag{67}$$

The 9 inch film is now reduced to 35 mm film:

$$\frac{\Delta x^{(2)}}{\Delta x^{(1)}} = \frac{1}{14.4} \tag{68}$$

The isodensity tracing of the transform is enlarged 10 times over the 35 mm transform.

$$\frac{\Delta x^{(3)}}{\Delta x^{(2)}} = 10$$

The scale factor β_x is

$$\frac{1}{\beta_x} \triangleq \cdot \frac{\Delta x^{(1)}}{\Delta x} \cdot \frac{\Delta x^{(2)}}{\Delta x^{(1)}} \cdot \frac{\Delta x^{(3)}}{\Delta x^{(2)}} \cdot \qquad (69)$$

or

$$\frac{\Delta x}{\Delta x^{(3)}} = \beta_x = 4320 \qquad (70)$$

and since wave number K_x is dimensionally $\frac{\text{radians}}{\text{unit length}}$

$$\frac{K_x^{(3)}}{K_x} = 4320. \qquad (71)$$

The position-wave number calibration equation is

$$\Delta x^{(3)} = (f\lambda)\ \frac{K_x^{(3)}}{2\pi}$$

$$= (2b\ \Delta xb)\ \frac{4320}{2\pi}\ K_x . \qquad (72)$$

The line spacing Δx_b is measured on the Ronchi grating isodensity transform (see Figure 19) as approximately 0.50 inches. The grating is specified as having 2 lines per mm, so, 2b = 0.5 mm. The result is

$$\boxed{\Delta x^{(3)} = \frac{27.4}{\lambda_x} \times 10^{-2} \text{ meters}^2 \qquad \text{Calibration Equation}} \qquad (73)$$

(B) Frequency Spectrum Calculation - $\Phi_\phi(\omega)$

The two dimensional wave number spectrum in terms of the photographic parameters is

$$\Phi_\phi(K_x, K_y) = \frac{\beta_x \beta_y}{\sigma^2 \pi^2} \left(\frac{(f\lambda)}{k_2 \tau_2 a_0^2} \, 10^{(D_2/\gamma_2) + \overline{D}_1} \qquad \frac{4 \sec^2 \psi}{D_\psi^2} \log_{10}^2 e \right) \quad (74)$$

and using

$$\Phi_\phi (K_x, K_y) = K^2 \, \Phi_\eta (K_x, K_y) \quad (75)$$

and

$$\Phi_\eta(\omega) = \frac{2\omega^3}{g^2} \int_0^{2\pi} \Phi_\eta (K_x, K_y) \, d\psi \quad (76)$$

we have

$$\boxed{\Phi_\phi(\omega) = \left(\frac{\beta_x \beta_y}{\sigma^2 \pi^2 K^2} \right) \left(\frac{2\omega^3}{g^2} \right) \frac{(f\lambda)^2}{k_2 \tau_2 a_0^2} \; \frac{10^{\overline{D}_1} \, 4 \log^2 e}{\overline{D}_\phi^2} \int_0^{2\pi} 10^{(D_2(u,v))/\gamma_2} \sec^2 \psi \, d\psi} \quad (77)$$

Equation (77) is the basic equation for the energy spectrum evaluation. The following numerical values apply:

(1) $\beta_x = 4320, \; \beta_y = 1$

($\beta_y = 1$ because a one-dimensional spectrum is calculated)

(2) $K^2 = \frac{\omega^4}{g^2}$

so

$$\frac{1}{K^2} \frac{\omega^3}{g^2} = \frac{1}{\omega} \quad \text{where}$$

$\omega^2 = Kg$ for small amplitude, deep water waves.

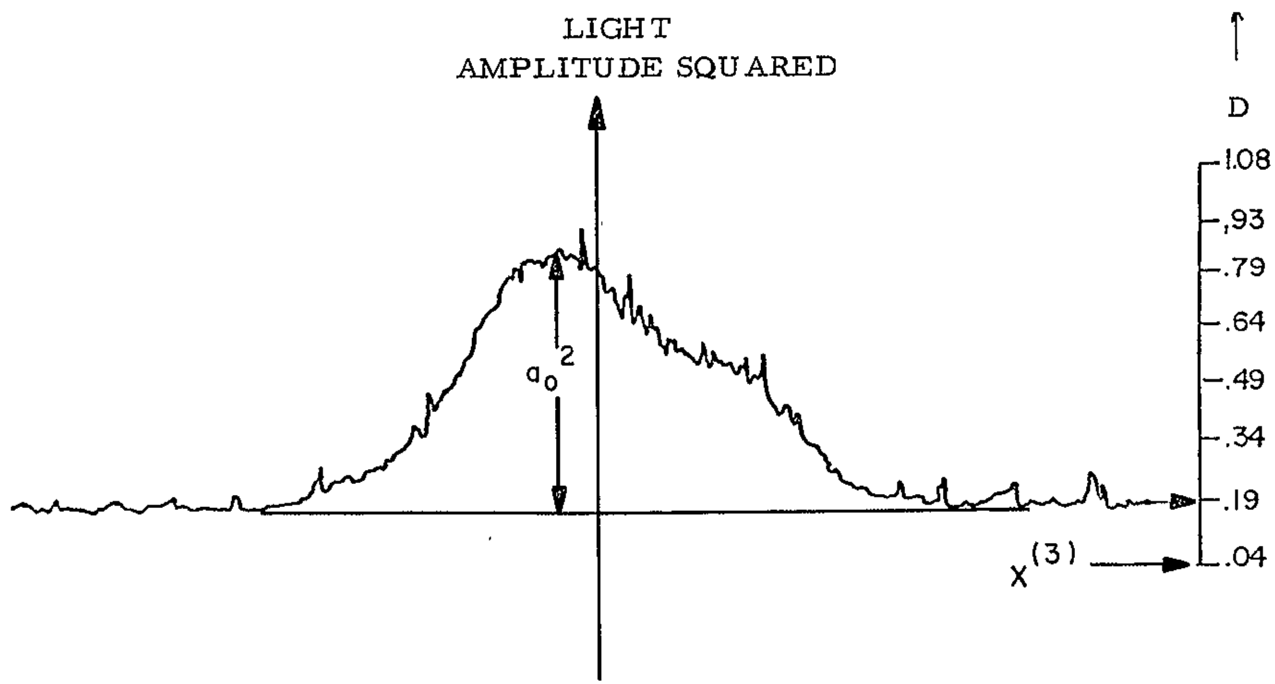

Figure 20. One-Dimensional Laser Beam Profile

(3) σ^2 = gaussian beamwidth of laser beam.

From the one-dimensional density tracing of the film negative of the laser beam exposure (see Figure 20) (which is not gaussian! σ is approximately 0.875 inches.

On the 35 mm negative, this corresponds to

$$\sigma = 22.2 \times 10^{-4} \text{ meters.}$$

(4) $f\lambda = 0.65 \text{ mm}^2$ (Ronchi grating data) (see Figure 19).

(5) The factor $k_2 \tau_2 a_o^2$ is equivalent to the term $10^{D/\gamma}$, in which D/γ is the optical density arising by exposing film in the scene plane to laser intensity a_o^2. From the gaussian beam density trace of Figure 20, the peak value of D is approximately 0.62.

$$k_2 \tau_2 a_o^2 = 10^{0.62} = 4.16 \text{ (Assume } \gamma = 1 \text{ in calculations)}$$

(6) The term $10^{\overline{D}_1}$ is related to the $I_o(x, y)$ of the illumination function $I(x, y)$ and corresponds to the average optical density of the scene negative. Figure 21 is a one-dimensional density trace of the scene negative used for this example.

$$10^{\overline{D}_1} \doteq 10^{0.74} = 5.5$$

(7) The term

$$\overline{D}_\phi = \frac{\gamma I'(x', y')}{I_o(x', y')} \log_{10} e$$

is related to the slope of the average optical density trace of the scene negative (see Figure 21).

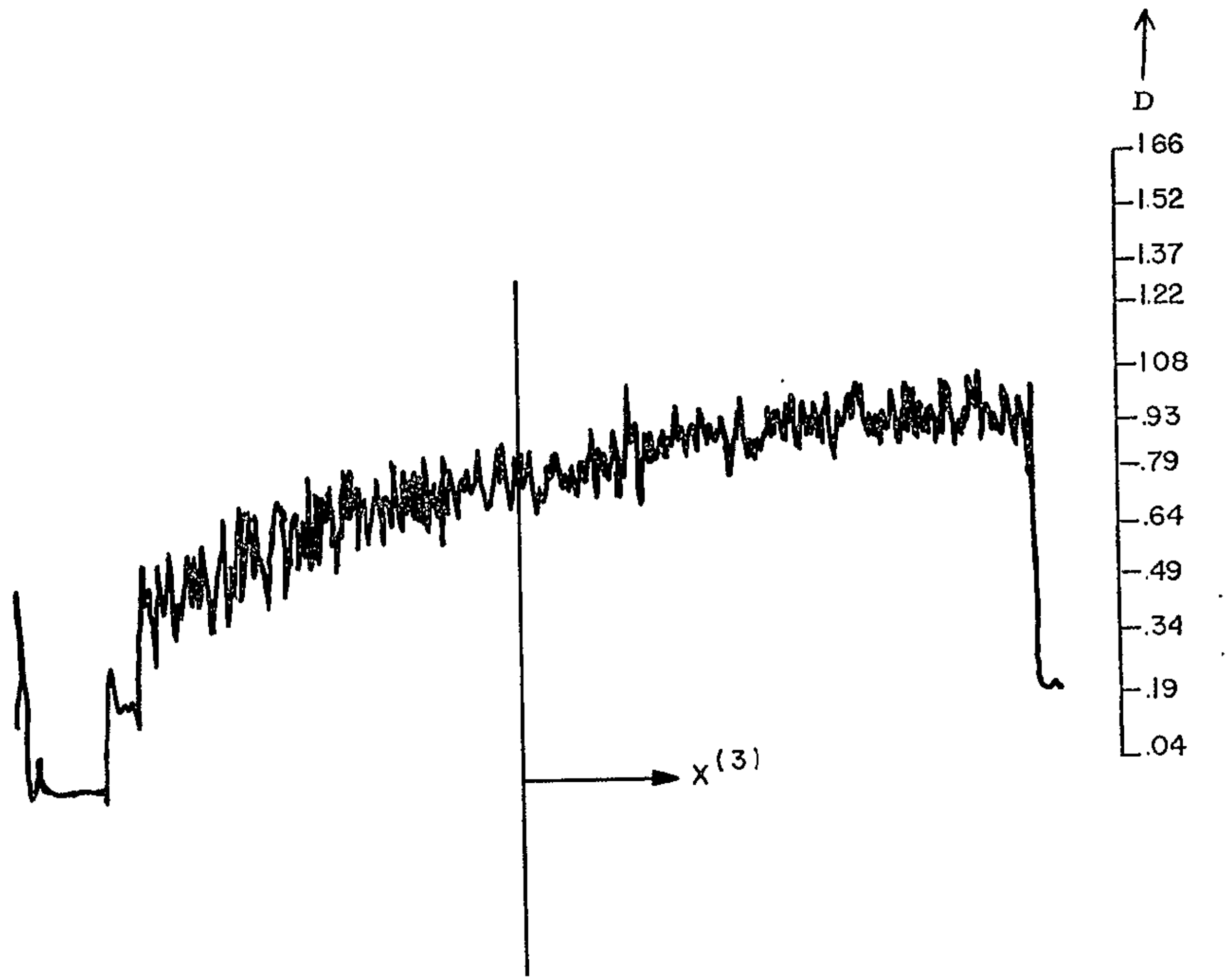

Figure 21. Density Tracing of Scene Negative for Determining I_o and $\overline{D}_\phi$

If we assume (Stilwell linear approximation) that

$$\overline{D}_\phi = 2 \frac{dD}{dx} \frac{dx}{d\phi}.$$

then

$$\overline{D}_\phi = 0.47.$$

The frequency spectrum, $\Phi(\omega)$, is therefore given as

$$\Phi_\eta(\omega) = \frac{(2)(4320)(0.65\ mm^2)^2 (5.5)(4)\log_{10}^2 e}{(22.2 \times 10^{-4})^2 \pi^2 \omega (4.16)(0.47)^2} \int_0^{2\pi} 10^{D_2(u,v)/\gamma_2} \sec^2\psi d\psi$$

$$\frac{meter^2 - sec}{radian} \tag{78}$$

$$= \frac{3.69}{\omega} \times 10^{-3} \int_0^{2\pi} 10^{D_2(u,v)/\gamma_2} \sec^2 \psi\, d\psi\ FT^2\text{-sec}. \tag{79}$$

From the calibration equation (78),

$$\omega = \sqrt{K_x g} = \sqrt{\frac{(9.8)(6.28)\Delta x^{(3)}}{27.4 \times 10^{-2}}} = 15\sqrt{\Delta x^{(3)}} \tag{80}$$

$$\boxed{\therefore\ \omega = 15\sqrt{\Delta x^{(3)}}} \tag{81}$$

for $\Delta x^{(3)}$ in meters.

Equations (79) and (81) and the density tracing of the Fourier transform shown in Figures 22 and 23 were used to calculate both the one dimensional energy spectrum ($K_y \doteq 0$) and wavelength calibration scale for the isodensitometers shown in Figures 14 and 15. A 21 point calculation of the energy spectrum was based upon the smooth curve construction shown in Figure 23. The smooth curve values and equation (78) resulted in the energy spectrum plot of Figure 24 (positive wave numbers only). An experimentally determined energy spectrum for a different Raytheon flight is shown in Figure 26.

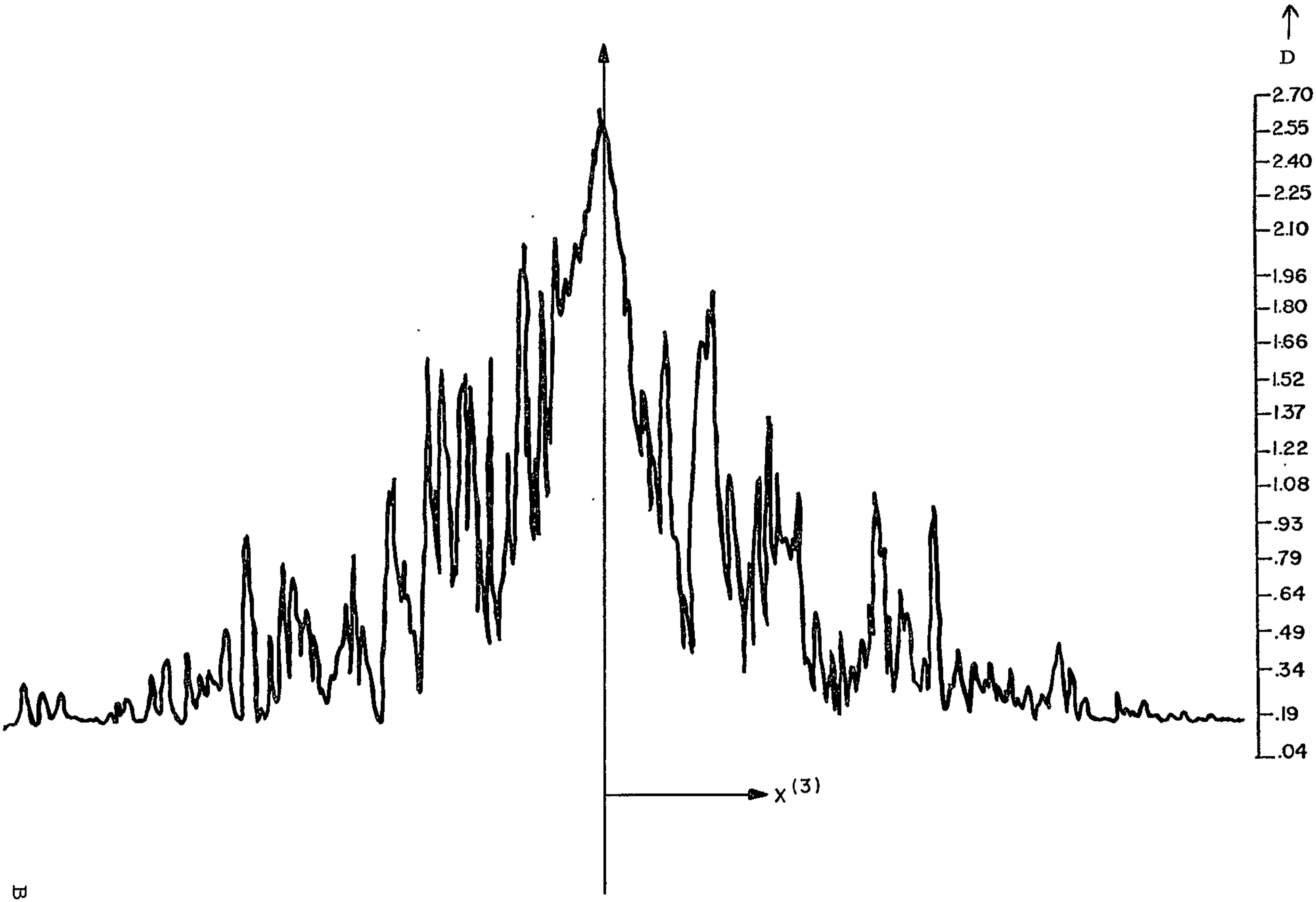

Figure 22. One-Dimensional Density Tracing of Fourier Transform
(ψ = 0)

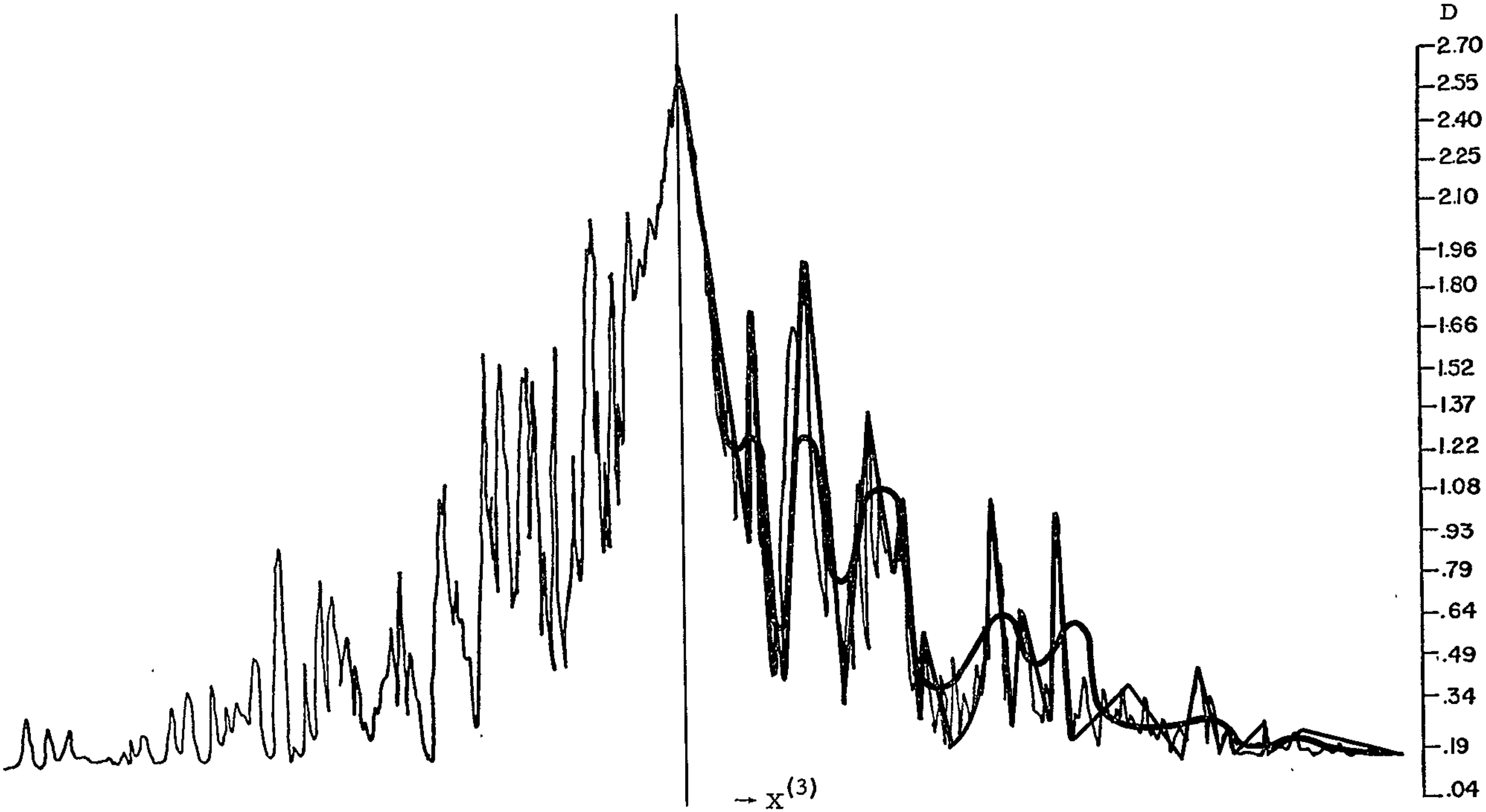

Figure 23. Smooth Curve Construction of Fourier Transform

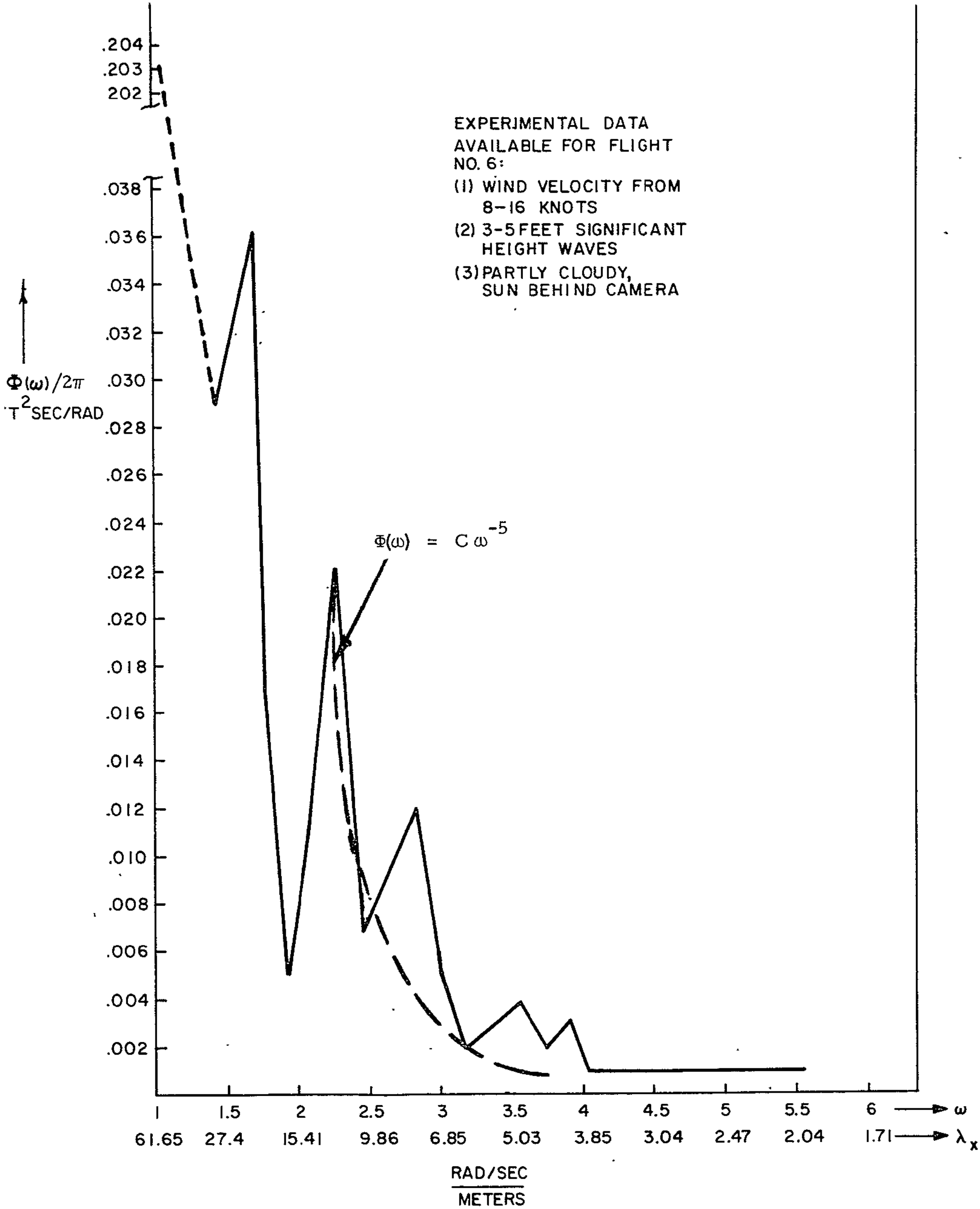

Figure 24. Energy Spectrum for Raytheon Flight No. 6

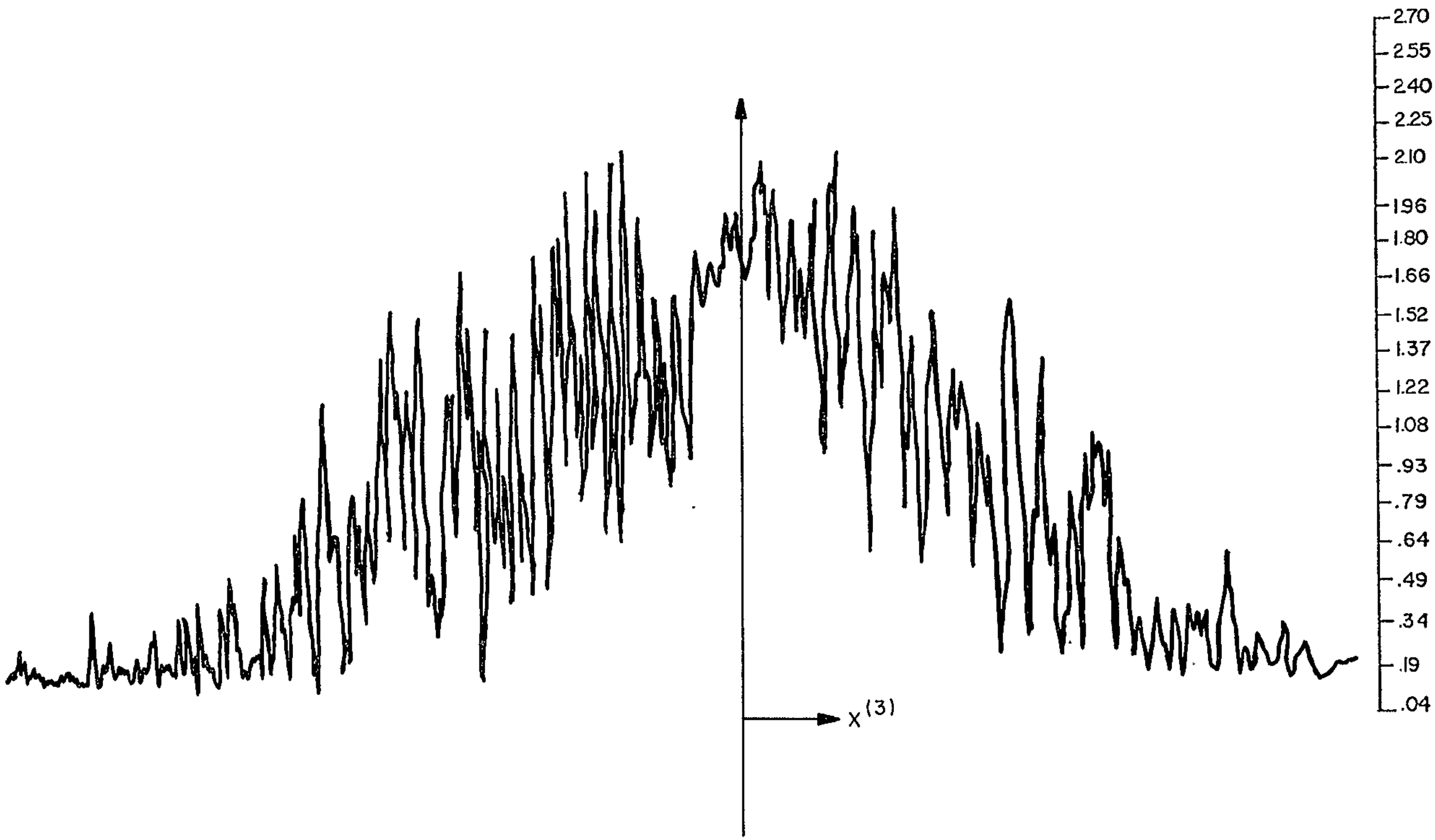

Figure 25. Transform Density Tracing for Figure 15 Isodensity Transform

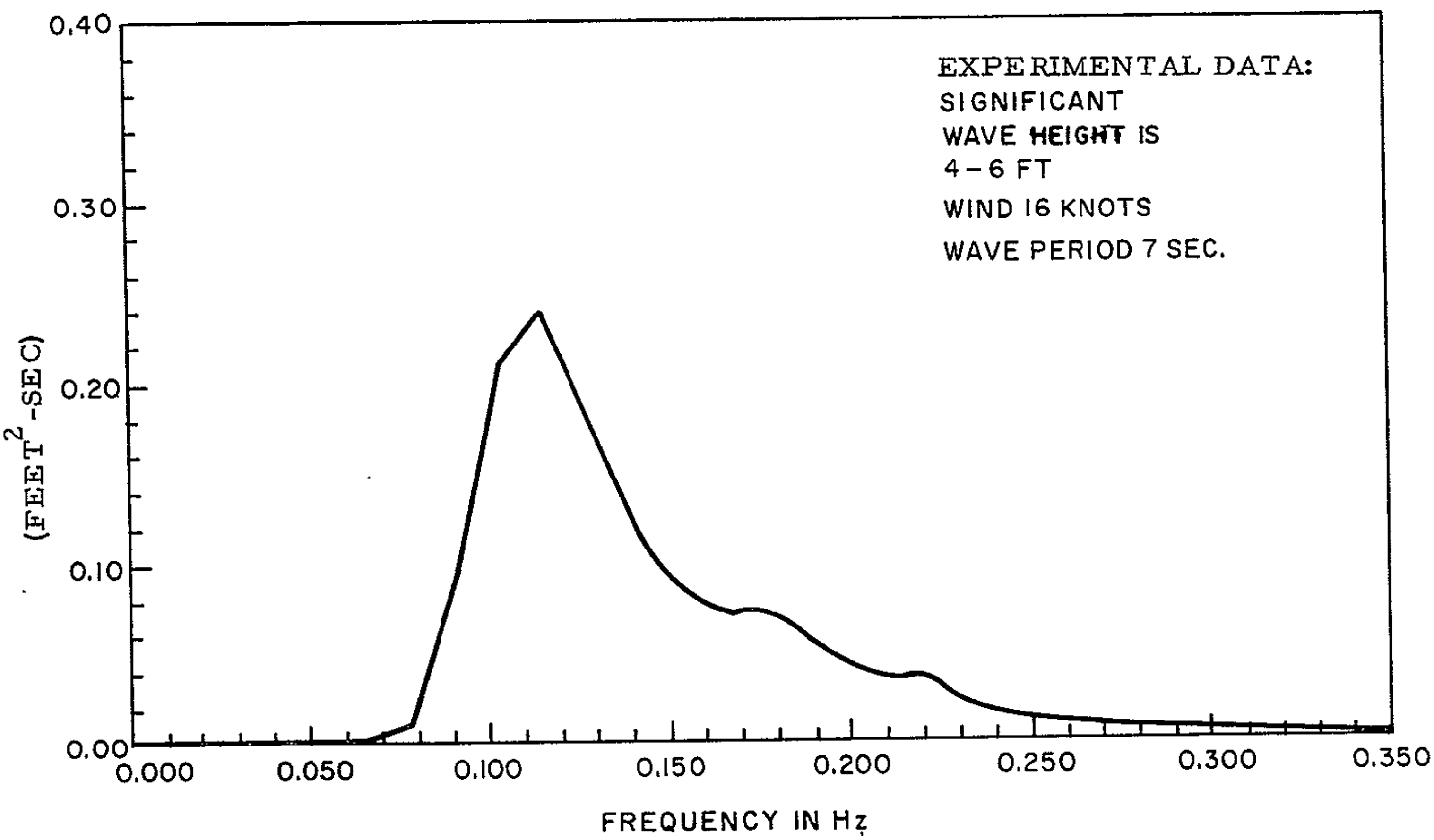

Figure 26. Laser Profilometer Data. The average optical density that appears in the scene negative density tracing and manifests itself as a dc term (ω=0) in the Fourier transform does not appear in Figure 26

VII. CONCLUSIONS

The calculations presented in the preceding section outline the basic computational technique developed by Stilwell for analyzing a sea energy spectrum from photographs. The particular sea photograph analyzed was taken on Raytheon Flight No. 6, and the resultant calibration photographs and transforms were done by D. Stilwell at Naval Research Laboratories. The microdensitometer tracing work was done at Raytheon, Autometrics Division, under the supervision of S. Hendrickson.

The method of energy spectrum analysis of sea waves as outlined by D. Stilwell has been applied to Raytheon Flight No. 6 ocean wave data.

The calculated wavelength calibration equation and one-dimensional energy spectrum $\Phi(\omega)$ indicates that the peak spectral component of the wave system is in the range 0.188 - 0.226 $\frac{ft^2\text{-seconds}}{\text{radian}}$ at a wavelength of approximately 20 meters. (See Figure 24). Assuming 20 meters to represent the dominant wavelength of the ocean wave system (gravity waves) of the photograph, the corresponding period is 3.6 seconds.

As pointed out by O.M. Phillips[6], the consideration of wind generated waves when the duration and fetch of the wind are large, justifies the consideration of an equilibrium range in the energy spectrum for large values of frequency ω. The spectrum obeys the relationship $\Phi(\omega) = c\omega^{-5}$, where c is a constant. Application of this asymtotic rule to the calculated spectrum is shown in Figure 24.

(6) O.M. Phillips, The Equilibrium Range in the Spectrum of Wind-- Generated Waves, J. Fluid Mech., 4, 426-434, 1958.

Shore observation data recorded a wave period of approximately 5 seconds and a significant wave height within the range of 3-5 feet. The time average wind velocity was 8 knots with 16 knot gusts. Aircraft observation reported that the seas for this flight, unlike that of previous flights, appeared somewhat confused. Even though there appeared to be a well defined wave propagation direction, other wave directions were observed.

Experimental measurements of the energy spectrum were made with a laser profilometer. Results for a different flight are shown in Figure 26. Raytheon Flight No. 6 data was not available.

The basic theory of sea wave energy spectrum evaluation from photographic data as developed by D. Stilwell rests on assumptions that require a good deal of physical insight into ocean wave properties. It appears that the really fundamental aspect of the entire process is the requirement for understanding what sky-sea-state is necessary to obtain scene photographs that indicate an accurate measure of the instantaneous power spectrum of the local sea state. The sky-sea-state referred to above should be related to such parameters as:

(1) Type of wave system (capillary, gravity, infragravity, etc.)

(2) Position of sun relative to camera position.

(3) Optimum sky condition (uniform overcast, partial overcast, etc.)

(4) Wind velocity and direction (related to type of wave system).

(5) Wave profile function $\eta(x, y)$ (white caps, sinusoidal, etc.)

(6) Reflectivity characteristics of ocean surface.

Condition (3) related to the average sky illumination with zenith angle can be determined from examination of the optical density tracing of the scene negative. A linear change in density along the x or y axis of the scene negative constitutes what Stilwell refers to as a "good picture." If the linear sky condition is not met, the spectrum evaluation does not represent the power spectrum of the two dimensional slope angle $\phi(x, y)$ characterizing the sea wave profile. The illumination function $I(x, y, \Delta)$* that characterizes a scene photograph is really the most important function in the entire optical analysis. Its mathematical form must be understood before detailed analysis of the sea wave system energy spectrum can be made. With $I(x, y, \Delta)$ known, one could then give an accurate interpretation of the scene negative density tracing as far as identifying the local sky-sea-state. Consequently, the Fourier Integral of the height function $\eta(x, y)$ or slope angle function $\phi(x, y)$ could be clearly identified in the transform isodensity plot, or in other words, the region in K-space that corresponds to the energy spectrum of the slope angle function would be known.

Several observations based upon the analysis and calculation are given below:

(1) The scale factors that relate distances and wavelengths of the sea surface to distances and wavelengths in the transform are two dimensional functions, $\beta_x(x, y)$, $\beta_y(x, y)$.

(2) The transform isodensity tracing shows an asymmetric spectrum plot and one that varies rapidly with wave number. It is suggested by Cox, Monk, and Stilwell that an averaging process be applied to this density function so that the general trend in the spectrum behavior be ascertained. It is this trend which is subjected to optical analysis in order to evaluate real sea energy spectra.

---

* The illumination function represents the light intensity reflected into camera from sea surface.

(3) The collimated monochromatic laser beam is not truly Gaussian. As indicated in the optical analysis a Gaussian beam is assumed and is used to calculate the Fourier transform of the scene plane transmission function T(x', u') modified by the beam function

$$\exp \sigma^{-2} (x'^2 + y'^2).$$

The Fourier transform is

$$(FT \; T'(x', y') \; e^{-1/\sigma^2 (x'^2 + y'^2)}.$$

One is actually performing the Fourier transform of the slope angle function multiplied by the beam shape function, resulting in a distortion of the slope angle power spectrum recorded in the transform plane.

(4) The theory as developed by Stilwell does not allow the energy spectrum evaluation for all azimuth angles

$$\Phi(\omega) \sim \int_0^{2\pi} 10^{\Delta 2} \sec^2 \psi \, d\psi$$

since $\sec^2 \psi \rightarrow \infty$ as $\psi \rightarrow \frac{\pi}{2}$. The transforms generally indicate a non-zero wave number (K) near the center of the transform.

(5) The density tracing of the scene negative could be enlarged and a detailed analysis of slope function made. A mathematical description of this function could then be employed in a digital computer, Fourier transform calculation.

(6) The question of accuracy of results in the optical analyses of energy spectrum remains to be answered. For example:

(a) finite granularity of film

(b) grain characteristics of film

(c) camera movement and wave movement during exposure time

(d) the number of photographs necessary of a particular sea state to completely characterize its energy spectrum.

(e) aperture size of microdensitometer slit used for plotting the transform

(f) lens field of view as related to calculating the scale factors.

(g) Statistical limitations of calculated energy spectrum $\Phi(\omega)$.

VIII. RECOMMENDATIONS FOR FUTURE WORK

(1) Extend mathematical analysis of entire Stilwell process, i. e., linear sky assumption, non-Gaussian laser beam effect on calculated spectrum, camera field of view as related to scale factors, etc.

(2) Develop theoretical understanding of the statistical limitations of calculated energy spectrum.

(3) Examine optical bench assemblies that would provide efficient calibration of scene negatives and transforms. Use photoelectric cell or microdensitometer for calibration equipment.

(4) Optically process existing Raytheon ocean wave data based on part (3), and present knowledge of optical evaluation technique. Select those scene negatives that have a linear variation of optical density and experimental data (laser profilometer and shore data). Compare in detail, experimental data with optical analysis data for a large number of scene negatives.

(5) Study the Stilwell process for application to radar scattering measurements. What, if any, correlation exists between energy spectrum $\Phi(\omega)$ and the corresponding radar cross-section σ ?

IX. APPENDIX

A. Relationship of Optical Power in Scene Plane to Optical Power in Transform Plane

In the back focal plane of the lens (transform plane), the light amplitude $a_T(u, v)$ is the Fourier Transform of $a'(x', y')$, the light amplitude distribution of the scene plane

$$a_T(u, v) = (\text{const.}) \int\int_{-\infty}^{+\infty} a'(x', y')\, e^{-(iK_o/f)(ux'+vy')}\, dx'\, dy'.$$

The corresponding light intensity is

$$u_T(u, v) = |a_T(u, v)|^2$$

$$= c^2 \left| \int\int_{-\infty}^{+\infty} a'(x', y')\, e^{-(iK_o/f)(ux'+vy')}\, dx'\, dy' \right|^2$$

where c^2 is the constant to be determined.

The light amplitude distribution $a'(x', y')$ is

$$a'(x', y') = \underbrace{a_o\, e^{-1/\sigma^2(x'^2+y'^2)}}_{\substack{\text{laser beam} \\ \text{(Gaussian)}}} \quad \underbrace{T'(x', y')}_{\substack{\text{Transmission} \\ \text{function of} \\ \text{scene negative}}}$$

In the absence of the scene negative ($T'(x', y') \rightarrow 1$) and evoking the requirement of equal optical power flow in the input and output focal planes, we have

$$\int_0^{2\pi}\int_0^{\infty} a_o^2 e^{-2/\sigma^2\, r'^2}\, r' dr' d\theta' =$$

$$c^2 \int_0^{2\pi}\int_0^{\infty} \underbrace{\left| \int\int_{-\infty}^{+\infty} a_o\, e^{-1/\sigma^2(x'^2+y'^2)}\, e^{-(iK_o/f)(x''^2+y''^2)}\, dx'\, dy' \right|}_{\text{output plane power density}} r''\, dr''\, d\theta''$$

where the independent variables are cylindrical coordinates about the optic axis. The single prime refers to the scene plane and the double prime refers to the transform plane.

The power density

$$\left| \iint_{-\infty}^{+\infty} a_o e^{-1/\sigma^2(x'^2+y'^2)} e^{-(iK_o/f)(x''^2+y''^2)} dx' dy' \right|^2 = a_o^2 \pi^2 \sigma^4 e^{-\frac{\pi^2 \sigma^2 r''^2 8}{f^2 \lambda^2}}$$

$r''^2 = x''^2 + y''^2$, f = focal length, and λ = beam wavelength in angstroms = $2\pi/K_o$.

and

$$2\pi a_o^2 \int_0^\infty e^{-(2/\sigma^2)r'^2} r'dr' = \frac{1}{2}\pi a_o^2 \sigma^2$$

so that

$$\frac{1}{2}\pi a_o^2 \sigma^2 = 4c^2 a_o^2 \pi^2 \sigma^2 \int_0^{2\pi} \int_0^{\infty} e^{-\frac{4\pi^2 \sigma^2 r''^2 8}{f^2 \lambda^2}} r'' dr'' d\theta''$$

$$= c^2 a_o^2 \pi^2 \sigma^4 \cdot 8\pi \frac{1}{\pi^2 \sigma^2} \frac{f^2 \lambda^2}{16}$$

or

$$c^2 = \frac{1}{f \lambda}^2$$

APPENDIX C

THE FINE STRUCTURE OF THE SEA SURFACE

Dr. B. Kinsman*

Radar altimetry over the ocean confronts difficult problems -- not the least being how to describe the target. In a search for an answer it has turned to the oceanographers and has found little comfort. Waves are a primary response of the ocean to the wind -- and extended regions of calm seldom exist for very long. The waves of the sea are highly irregular, they run rapidly across the surface, and they constantly change their forms. It is only since the second World War that oceanographers have made a start at understanding waves as they exist on the ocean and have begun to create usable forecasting methods. Understandably, their attention has been focused on "practical" problems, which in this case means the larger waves -- those big enough to interfere with amphibious landings, refueling, and air-sea rescues. Now radar altimetry tells us that the small waves, those with lengths of the order of 1 to 10 centimeters, are of intense "practical" interest. They are the ones which have the greatest effect on radar.

For waves on the water surface with lengths in the range 0(1cm) to 0(10 cm) both gravity and surface tension may be important restoring forces. Waves with lengths greater than 5.47 cm are primarily gravity waves; the effect of the surface tension on their phase speeds is less than 5% of the effect of gravity. Waves with lengths less than 0.54 cm are capillary waves; gravity contributes less than 5% to their phase speeds. For waves with lengths between 0.54 cm and 5.47 cm both gravity and surface tension are important.

A great deal is known about the physics of these small waves. The 19th century hydrodynamicists did not neglect them. Lamb's "hydrodynamics," for example, records this extensive body of results. Our theory even provides us in

* Oceanographer
Chesapeake Bay Institute
John Hopkins University

Crapper's wave that very rare commodity: an exact solution to a nonlinear problem. Further, theory has been abundantly confirmed by experiment. Small waves are relatively easy to house in a laboratory.

What clues, then, do theory and experiment offer us? The linear first-order, small-amplitude theory is satisfied by a sinusoidal wave and, because of linearity, by sums of sinusoids. The theory tells us that each component wave will run at a phase speed or celerity, c,

$$c^2 = (pg/k + kT)/(\rho \coth kh)$$

where

ρ = the density of the water,

T = its surface tension, and

h = its depth;

while

g = the acceleration of gravity and

k = the radian wave number which is 2π divided by the wave length, L.

When the water depth h is greater than half the wave length, the waves are in "deep water," $\coth kh \approx 1$, and the phase speed is very closely approximated by

$$c^2 \approx (g/k) + (T/\rho)k \ . \qquad \text{(C-1)}$$

For waves on the range 0 (1 cm) to 0 (10 cm), even if we interpret 0 (10 cm) as 50 cm, any depth h > 25 cm will be deep water so that (1) applies to most of the ocean.

Equation C-1 has a number of interesting features. The effects of gravity and of surface tension on the phase speed are additive. It is on the basis of (1) that a simple calculation yields the wave lengths for 5% residuals previously given. Thus with an error of no more than 5% in the phase speed c we may use for gravity waves

$$c^2 \approx g/k \quad \text{whenever} \quad L > 5.47 \text{ cm} \tag{C-2}$$

and for capillary waves

$$c^2 \approx (T/\rho)k \quad \text{whenever} \quad L < 0.54 \text{ cm.} \tag{C-3}$$

If $0.54 \text{ cm} < L < 5.47$ cm the waves may be called ripples and the full approximation, equation (C-1), is required.

The phase speed for gravity waves is a monotonic increasing function of the wave length, $c \sim L$. For capillary waves it is a monotonic decreasing function of wave length, $c \sim 1/L$. Clearly, within the ripple band there must be a minimum phase speed which can be found by searching equation (C-1) for extrema. One finds that no wave can travel slower then $c_m = (4g\ T/\rho)^{1/4}$ which corresponds to a wave number $k_m = (g\rho/T)^{1/2}$. Using $g = 980$ cm sec^{-2}, $T = 74$ dynes cm^{-1}, and $\rho = 1$ g cm^{-3} one finds a slowest speed of $c_m = 23.2$ cm sec^{-1} associated with the wave of length $L_m = (2\pi)/k_m = 1.73$ cm. Waves either shorter or longer than 1.73 cm travel faster. From Figure C-1 it is clear that there is always a pair of these waves, one shorter than 1.73 cm and one longer, which travel at a common speed. For such a pair the short wave will appear as a fixed roughness on the longer wave. There will be other short waves whose speeds are near those of the long wave which will appear as a slowly changing roughness on the long wave. Such phenomena do occur in a wind driven sea and are clearly apparent to the eye. That they are precisely described by the linear theory may be doubted since the linear theory was developed for small-amplitude (mathematically infinitesimal) waves. If you can see it, its not small-amplitude.

When the small-amplitude restriction is removed theory tells us that the sinusoids become deformed. For gravity waves one solution is an inverted prolated trochoid. Such curves can be generated by tracing the locus of a point on the radius of a circle which is being rolled along the under side of a straight fine. Figure C-2 shows a trochoid which is improbable as an ocean wave because β and k were selected to be 1. Ocean waves theoretically never become that "pointy", the maximum angle just before they break being 120°. If you look at the ocean or at plunger generated gravity waves you will see that the trochoid, while too regular to be a good description of the sea surface, is still much more realistic than the sinusoid. The sinusoid always has smoothly rounded crests while the crests of the trochoid have an edge. A sinusoid is symmetric about a level halfway between crest and trough. You can't tell whether it is upside down or right side up. The trochoid has troughs which are long and flattened and crests which are short and angular so that mean water level is not half way between crest and trough. Further, its wave steepness, i.e., the ratio of its height H to its length L, $\delta \equiv H/L$ has some sizable value. It is not infinitesimal as δ must be for the small-amplitude sinusoid. Thus the trochoidal wave can be visible to the eye. The effect of this finite steepness is to make the trochoidal wave run slightly faster than the speed given by equation (C-2) as shown in Figure C-3.

For capillary waves the exact solution of the nonlinear problem which makes no obeisance to the small amplitude assumption yields a water surface shown in Figure C-4. As drawn, the uppermost line is the water surface for a capillary of maximum steepness, $\delta = 0.73$ in the sense that locally, near the troughs, the slopes have become vertical and the surface recurved so that the surface is about to coalesce. The lower lines are streamlines of the flow for this extreme capillary. However, if a capillary has a steepness of $\delta = 0.53$ the second line is the shape of the wave and the lower lines remain streamlines. So

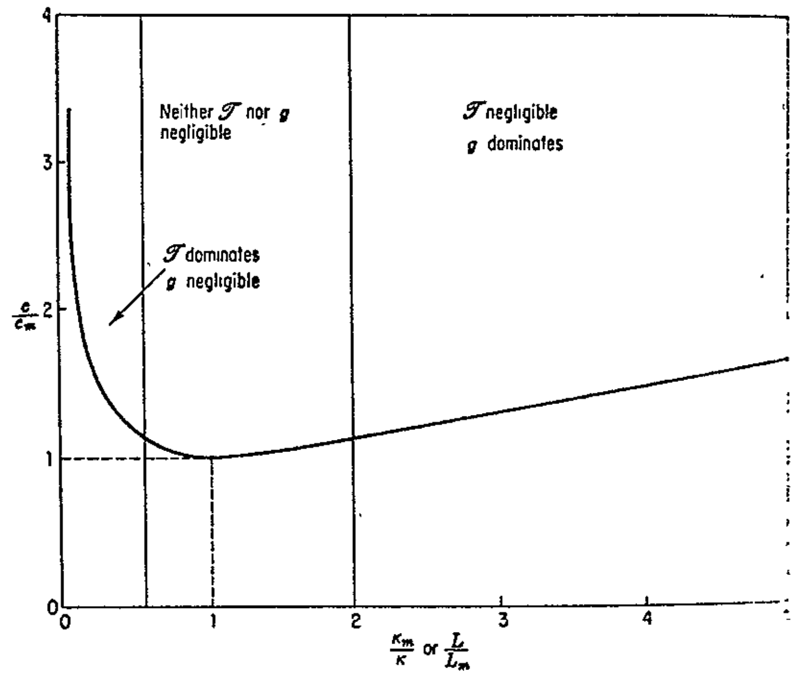

Figure C-1. Wave Speed as a Function of Wavelength (or wave number) When Both Gravity and Surface Tension are Considered

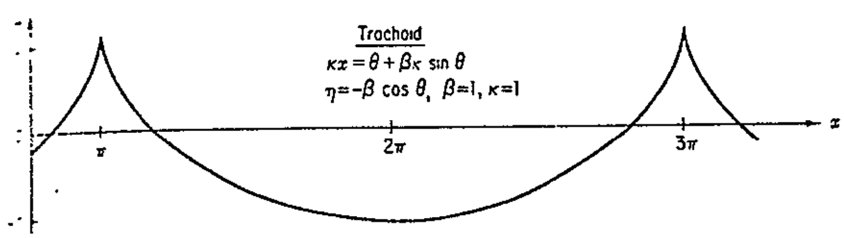

Figure C-2

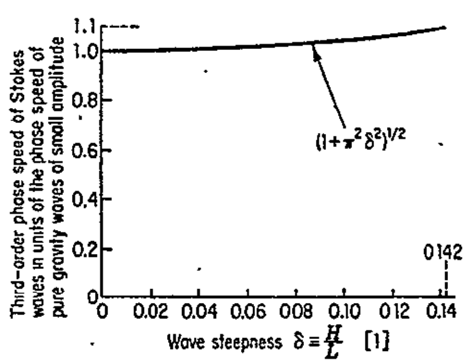

Figure C-3. Phase Speed Correction Factor for Gravity Waves as a Function of Wave Steepness also for the others. What you see in Figure C-4 may seem startling since most of the waves you have looked at have probably been gravity waves that resembled Figure C-2. Here it is the crests which are broader and rounded while it is the troughs which are narrower and more pointed. However, in any process governed by surface tension, as, for instance, the formation of droplets on a non-wetting surface, the shape taken is always as near spherical as the other forces acting permit. Strange as they may seem these wave forms have been shown to exist in laboratory experiments. I think the bearing of such wave forms on radar should be obvious. The larger waves of the sea are like trochoids whose maximum steepness is $\delta = 1/7 = 0.143$. Observed values even in young seas which tend to be steepest seldom show values greater than $\delta = 0.12$. Even locally they don't become very steep. However, these longer waves may be and frequently are covered with short waves. If the short waves are capillaries then the overall slope may reach $\delta = 0.73$ and the surface can locally approach the perpendicular.

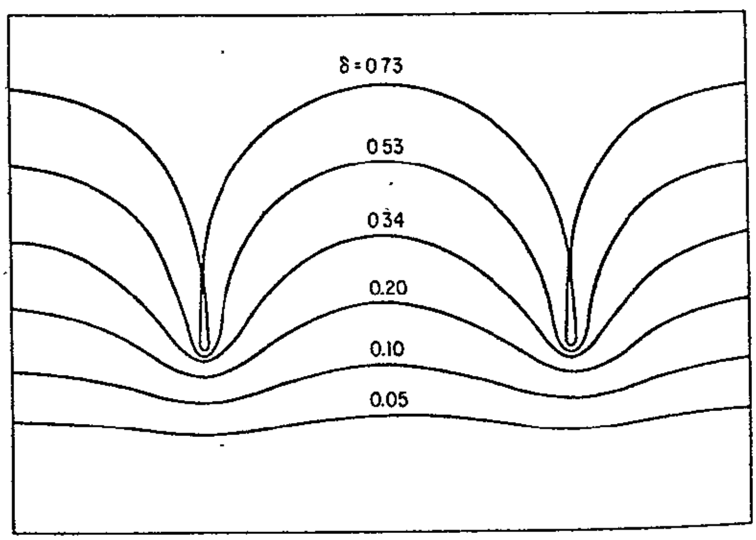

Figure C-4. Streamlines for Crapper's Wave

As with the trochoidal wave there is a correction to the phase speed given by equation (C-3) which involves the finite steepness as shown in Figure C-5. In this case the effect of the finite amplitude correction is to slow the wave a bit. The combined effect on Figure C-1 of the corrections shown in Figures C-3 and C-5 is to raise the curve a bit when $L/L_m < 1$. It may also change the value of k_m used for scaling but only very very slightly.

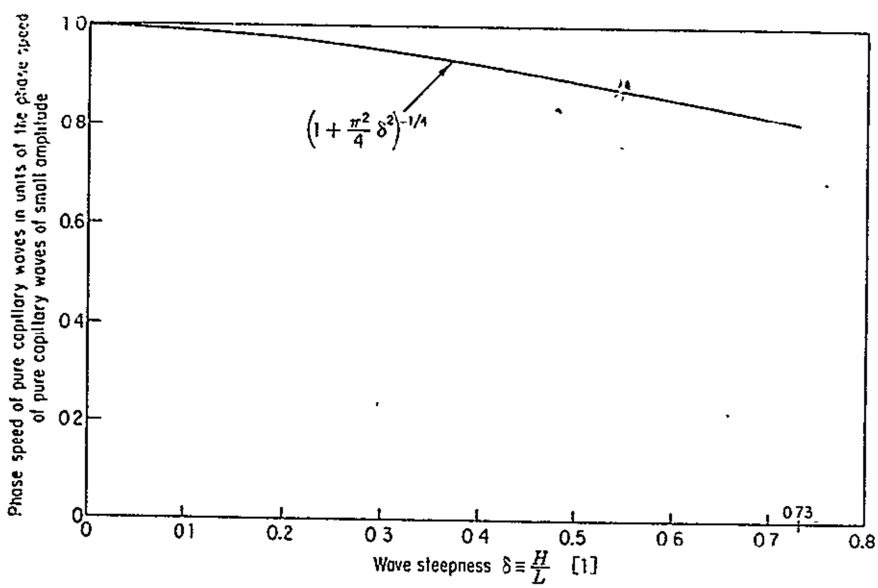

Figure C-5. Phase Speed Correction Factor for Pure Capillary Waves as a Function of Wave Steepness

Even casual observation of wind driven seas shows that a fine structure of small waves riding the longer, larger waves is the rule rather than the exception in reasonably strong winds. As recently as 14 years ago we had no remotely satisfying deduction from physical principles to tell us how the wind might make these small waves; those with lengths less than 5.47 cm for which surface tension must be reckoned with. Certainly if surface tension is important then viscous dissipation will probably be important and these waves will have to be continually regenerated by the wind. Further, when a wind strong enough to make waves flows over a calm water surface the first thing that always happens is the formation of waves with lengths of a centimeter or so running, not with the wind, but symmetrically at an angle to both sides of the wind. They form a typical diamond shaped or rhomboidal pattern on the water surface. In 1957 Phillips offered the first mechanism deduced from hydrodynamic principle that could account for some of what we see. This is hardly the place to attempt an account of the Phillips generation theory. Suffice it to say that the generation of small waves by his process depends critically on a resonance between the waves and the pressure field on the water surface created and swept over the water surface by the turbulent wind. The resonance is selective for the short wave lengths and the off-wind angles of wave propagation. However, if the turbulent wind does not contain appreciable energy in the small pressure structure it can be strong and still create no small waves. The locus of resonantly excited wave numbers in wave-number space is shown in Figure C-6 which may puzzle you a bit. Actually it has been borrowed and contains more information than we need here. The k_1 wave-number component axis is lined up with the mean wind so that the k_2-axis is cross-wind. This is only half the plot. There is a mirror image in the $k_1 > 0$ $k_2 < 0$ quadrant. Further, it is assumed that the pressure field on the water surface expressed in wave-number space has no appreciable energy (for whatever reason -- viscous dissipation in the turbulent wind, perhaps) at wave-numbers outside the circular sector AOB . Under these conditions Phillips has shown that there is a critical angle to the mean wind which defines a locus in $\vec{k}$-space and a narrow band associated with it (the shaded part) in which resonance will strongly excite and continue to feed energy into surface waves with wave-numbers within the band. Note that beyond the arc AB the band has been left unshaded. This represents waves with wave numbers which could be excited but are not since the surface pressures necessary to excite them are lacking. You can see from Figure C-6 how it may be possible that a strong wind may not generate waves by this mechanism. If the wind is uniform and lacking small structure itself, the radius OA of the sector AOB shrinks and, if OA becomes less than OD it falls below the resonance locus. Should that happen no small waves will be created by this mechanism. The mechanism is probably not unique but so far it is the only one which has been worked out that accounts for small waves and it is an excellent start. Theory could tell us many other things about waves with lengths 0 (1 cm) to 0 (10 cm) but I doubt that they would be any more useful in the real world than what we have already.

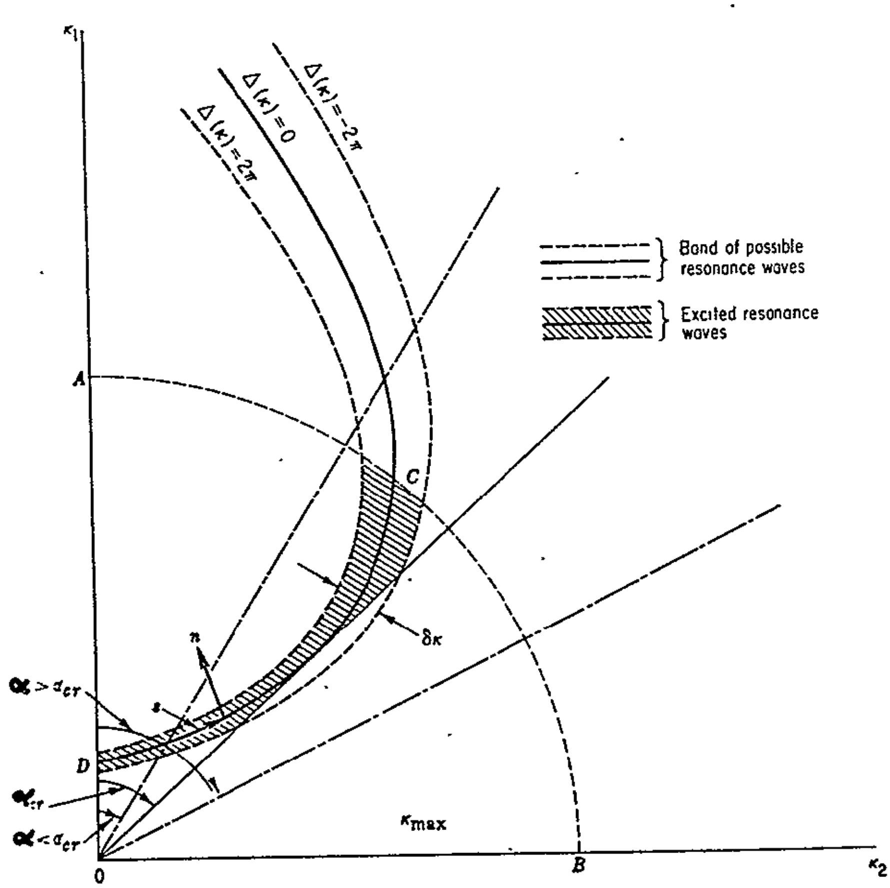

Figure C-6. The Locus of Resonantly Excited Waves in Wave-Number Space

The real ocean can be a very confusing place and, lacking good data, perhaps the best I can do is to describe a few of the things I, myself, have seen. One thing I can hardly overstress in the patchiness and evanescence of the fine structure. When a wind begins to generate waves on a calm surface you often find the rippled surface in cat's paws separated by regions of still calm water. The cat's paws may be small, 10, to 12 wave lengths, or relatively large, 500 to 1000 wave lengths. They may persist, spread, and coalesce until the entire surface is rippled. However, if the wind is puffy and dies momentarily, the cat's paws may disappear again in a few seconds. If the wind sets in steadily and freshens, the longer gravity waves soon appear and the fine structure, while still there and wide spread, is usually very different in character on the different parts of the longer waves. Often the down-wind faces of the large waves are covered with much more prominent fine relief than are the up-wind faces.

Sometimes the small waves on the down wind faces are moving at almost the same speeds as the larger waves and seem to hang fixed on them. I remember watching something like this in the Miles River for an hour or so. The wind was blowing about 30 kts over a fetch of perhaps 5 NM. The large waves were around 3 ft high with characteristic lengths near 30 ft. Over and over again a packet of 5 to 10 very steep small waves with lengths around 5 to 10 cm would suddenly pop up on the forward faces of the large waves. They ran just a little slower than the large wave so that ultimately they were overtaken by the crest and they disappeared as the crest went by. Before this happened, however, the small waves seemed to catch each other up; steepening on their forward faces until they looked like the overlapping tiles of a tile roof. At that time their forward faces were a centimeter or two high. The entire process from formation to vertical forward faces to obliteration when overrun by the crest occupied no more than 10 seconds. The phenomenon was just as local spatially occupying an area of perhaps 10 m^2.

One more situation may perhaps be of interest as illustrating the need for fine wind structure if fine wave structure is to be excited. My pier is located on an arm of South River. The water runs north-south and is perhaps a quarter of a mile wide. A twenty-five knot wind had been blowing from the south for some hours with an unobstructed fetch of 3/4 mi. The usual slope of gravity waves with periods around a second was running. What struck me when I looked at it was that it was abnormally smooth. For a wind that strong there were very few small waves. As I looked up to windward I saw a pier that had been toppled by the winter ice and was lying half submerged across the wind. In its lee the water was entirely covered with a plume of rhomboidal fine structure which extended some 30 ft to leeward where it suddenly disappeared. Looking further, every obstruction to the wind that I could see had its own pendant plume. I feel sure that this was an instance of the OA radius in Figure C-6 being less than OD. As the wind tripped over the obstructions small scale turbulence was generated in it and OA momentarily became greater than OD which permitted the small off-wind waves to be created. However, energy dissipation in the air flow rapidly sapped the energy from the small scales and, once it was gone, the small waves no longer had an energy source. With nothing to sustain them, they were rapidly destroyed by viscosity. I cannot prove that the story I have told is true but it certainly provides a rational explanation of what I saw: no fine structure on the open water even with a strong wind and plumes of rhomboidal fine structure behind each obstacle to the airflow.

Considering the spottiness, rapidity of change, and variety of form of the fine structure it is interesting to turn to the results presented in the body of this report in Figures 5-1 to 5-3. Figure 5-1 plot average σ^o against wave height while Figure 5-2 plots it against wave period. Both the wave height and the wave period are visual observations which notoriously fail to take proper account of the small waves. It is well known that if you have a record of water elevation made at the same time and place a visual observation is made, you can usually duplicate the visual height observation very closely by reading all the heights on the record, putting them in order of size, and then taking the mean of only the highest one-third. The period estimate also ignores the small waves. But the practically important waves for radar, and consequently for σ^o, are the small ones. Thus one can say a priori that no connection is to be expected. This is precisely what the plotted points in Figures 5-1 and 5-2 confirm.

Figure 5-3 plots average σ^o against wind speed and this is something else. The wind speed, whether estimated or computed as a mean from cup anemometer data, is just as "gross" a parameter as the wave height or wave period. It tells us nothing about the turbulent structure of the airflow. However, the higher the wind speed the higher the Reynolds number and the higher the Reynolds number the more turbulent the airflow is likely to be. There is at least some reason to anticipate a connection between small waves and wind speed since the higher wind speeds are more likely to contain appreciable energy in the small eddies necessary to excite small waves. It isn't a tight connection but something ought to be there. Figure 5-3 suggests that there is and further, that you aren't going to be able to say anything about fine wave structure very precisely if all you know is the mean wind.

The problems of the hydrodynamics of the fine structure of the sea and how to characterize it usefully urgently posed by radar altimetry over the ocean needs and deserves close study.

APPENDIX D

FLIGHT PLANS

This section includes the flight plans for all 16 flights. These plans were formulated before the scheduled flights. Comparing the flight plans with the flight summaries (Section 3.2) will indicate where and for what reason(s) the flight plans could not be followed.

Flight 1 - Nov-24-1969

Low Altitude Shakedown

1. Pre-Flight Briefing
2. Take-Off 3:00 P.M.
3. Fly to Test Area (Coastal Waters Near Wallops)
4. Fly Stilwell Pattern at 6000ft.
5. Fly Rectangular pattern at 6000ft. with the following parameters:

   Pulse Width = 100 nsec
   Pulses/frame = 50
   Polarization = cross
   Peak Power = 12 watts
   Sweep speed = 50 nsec/cm
   Attentuation = 0 dB
   No. of Runs = 4

6. Fly Stilwell pattern at 6000 ft.
7. Return to Wallops

Flight 2 - Dec-11-1969

A) High Altitude Shakedown

1. Briefing (Pre-Flight)
   a. Desire course rather than track
   b. Define Sea Direction
   c. Reference names
   d. Required data
2. Take-Off and fly to test area
3. Fly Stilwell pattern at 100 ft.
4. Fly flight Pattern 2 (6 runs)

B) Radar Parameters

Pulse width = 100 nsec; runs 1, 2, 3
20 nsec; runs 4, 5, 6
Pulses/Frame = 50
Polarization = cross
Peak Power = 12 watts
A/C Attitude = 0°
Sweep speed = 50 nsec/cm
Frame rate = 1/sec
Attentuation = 0 dB
No. of Runs = 6

1. Fly Stilwell at max. altitude
2. Fly Stilwell at 1000 ft.

Flight 3 - Dec-12-1969

A) 2nd High Altitude Shakedown

1. Pre-Flight Briefing
2. Take-Off and fly to test area
3. Fly Stilwell pattern at 1000 ft.
4. Fly to max. altitude 18K ft.
5. Fly flight pattern 2 (6 runs)

B) Radar Parameters

Pulse width = 100 nsec
Pulses/Frame = 50
Polarization = cross (3 runs); Direct (3 runs)
Peak power = 12 watts
A/C Attitude = 0^{o}
Sweep speed = 100 nsec/cm
Frame rate = 1/sec
No. of runs = 6

6. Fly Stilwell pattern at max. altitude
7. Fly Stilwell pattern at 1000 ft.
8. Return to Wallops

Flight 4 - Dec-15-1969

1. Briefing (9:00 AM)

Discuss:

a. Course vs. track (we desire course)
b. Definition of Sea Direction
c. Reference name of those on flight
d. Inform crew of data required during flight

2. Take-Off (10:00)
3. Calibrate GYRO Compass of both A/C (Cessna and the DC-4) by flying together to the ship (Ship will be at Lat. 37^{o} 07', Long. 73^{o} 38' ie. Section 9, Quad. D.)
4. Pilot contact ship and request to start recording data

5. Start Stilwell pattern at ship with first heading in same direction as sea. DC-4 at 1000 ft., Cessna flying same pattern at 700 ft.
6. Both A/C repeat Stilwell pattern; DC-4 at 5000 ft., Cessna at 700 ft.
7. Both A/C fly flight pattern 1 (12 runs) DC-4 5000 ft., Cessna at 700 ft.

A) Radar Parameters

Pulse width = 100 nsec
Pulses/Frame = 1; for 1st 5 frames
50; rest of run
Polarization = cross
Peak Power = 12 watts
A/C attitude = 0^{o}
Sweep Speed = 50 nsec/cm
Frame rate = 1 /sec
Attenuation = 0 dB
No. of runs = 12

8. Repeat step 6 (Stilwell pattern).
9. Return to Wallops

3.2.5 <u>Flight 5 - Dec-17-1969</u>

1. Briefing (8:30)
2. Take-Off 9:30 A. M.
3. Fly to Wallops sec 9-D; Lat. 37° 07'; Long. 73° 38'
4. Pilot contact ship at earliest time and ask for weather data (sea direction etc.).
5. At test area; DC-4 fly Stilwell at 1500 ft; Cessna fly profilometer pattern at 300 ft. (single pulse radar runs)
6. DC-4 fly to 10,000 ft. and fly pattern 2 (6 runs) with following parameters:

Pulse width = 20 nsec
Pulse/Frame = 50
Polarization = direct
Sweep speed = 50nsec/cm
Frame rate = 1/sec
Attenuation = 0 dB

7. Fly pattern 2 again (6 runs): Same parameters as #6 except: Polarization = cross
8. Fly to 15000 ft. and fly pattern 2 (6 runs) with same parameters as #6
9. Fly Stilwell at 15000 ft. (or below ceiling): Also fly radar pattern #2 with parameters of #7
10. DC-4 fly to 1500 ft. and fly Stilwell pattern. Cessna fly profilometer pattern at 300 ft.
11. Return to Wallops.

Flight 6 - Jan-5-1970

1. Pre-flight briefing 8:30 A. M.
2. Take-off 9:30 A. M.
3. Fly to Wallops Sec. 9-D; Lat. 37° 07' ; Long. 73° 38'
4. Pilot contact ship at earliest time and request weather data.
5. At target area: DC-4 fly Stilwell pattern at 1500 ft. Cessna fly profilometer at 300 ft.
6. DC-4 fly to 15000 ft. and fly pattern 2 (6 runs) with following parameters:

   Pulse width = 100 nsec
   Pulse/frame = 50
   Polarization = direct
   Sweep speed = 50 ns/cm
   Frame rate = 1/sec
   Attenuation = 0 dB

7. Fly pattern 2 again (6 runs); same parameters as #6 except: Polarization = cross
8. Fly to 20, 000 ft. and fly pattern 2 (6 runs) with same parameters as #6.
9. Fly Stilwell at 20, 000 ft. (or below ceiling): also fly radar pattern #2 with parameters of #7.
10. DC-4 fly to 1500 ft. and fly Stilwell pattern. Cessna fly profilometer pattern at 300 ft.
11. Return to Wallops

Flight 7 - Jan-6-1970

1. Pre-flight briefing 8:30 A. M.
2. Take-Off 9:30 A. M.
3. Fly to Wallops Sec. 9-D; Lat. 37° 07' , Long. 73° 38'

4. Pilot contact ship at earliest time and request weather data.
5. At test area fly Stilwell pattern at 1500 ft.
6. Fly to 15, 000 ft. and fly pattern 2 (6 runs) with following parameters:

   Pulse width = 20 nsec
   Pulse/Frame = 50, 100, 500, 1000*
   Polarization = Direct
   Sweep speed = 50 nsec/cm
   Frame rate = 1/sec
   Attenuation = 0 dB

   * 4 frames for each pulse/frame

7. Fly Stilwell at 15, 000 ft. (if weather permits)
8. Fly Stilwell pattern at 1500 ft.
9. Return to Wallops
10. Fly over hanger at 5000 ft. GSE will be ready for calibration.
11. Land

3.2.8 <u>Flight 8 - Jan-8-1970</u>

1. Pre-flight briefing 8:30 A.M.
2. Take-Off 9:30 A.M.
3. Make 3 passes overy runway (parallel with runway) at 5000 ft.; make another 3 passes over runway at 10, 000 ft. All 6 passes at minimum speed. Calibration using GSE will be made during passes.
4. Fly to test area, Wallops Sec. 9-D; Lat. 37° 07', Long. 73° 38'
5. Pilot contact ship at earliest time and request weather data.
6. Fly Stilwell pattern at 1500 ft.
7. Fly Stilwell pattern at 10, 000 ft.
8. Fly pattern 2 (6 runs) with following parameters (10, 000 f

   Pulse width = 20 nsec
   Pulse/Frame = 1
   Polarization = direct
   Sweep speed = 50 nsec/cm
   Attenuation = 0 dB
9. Repeat Step 8 with Pulse/Frame = 2
10. Repeat Step 8 with Pulse/Frame = 50
11. Repeat Step 8 with Pulse/Frame = 500

12. Fly Stilwell pattern at 1500 ft.
13. Return to Wallops*
14. Repeat step 3
15. Land

* Pilot notify Wallops plot when starting back to Wallops

Flight 9 - Jan-9-1970

1. Pre-flight briefing
2. Take-Off 9:30 A. M.
3. Fly to Wallops Sec. 9-D; Lat. 37° 07'; Long. 73° 38'
4. Pilot contact ship at earliest time and request weather data
5. At test area, fly Stilwell pattern at 1500 ft.
6. Fly pattern 2 (6 runs) at 10, 000 ft. with following parameters:

   Pulse width = 20 nsec
   Pulse/Frame = 10
   Polarization = Direct
   Sweep speed = 50. nsec/cm
   Attenuation = 0 dB

7. Fly pattern 2 again

   Pulse/Frame = 20

8. Fly pattern 2 again

   Pulse/Frame = 148

9. Fly Stilwell pattern at 10, 000 ft.
10. Fly Stilwell pattern at 1500 ft.
11. Notify ship that we are leaving the area.
12. Return to Wallops

Flight 10 - Jan-20-1970

1. Pre-flight briefing 8:30 A. M.
2. Take-Off 9:30 A. M.
3. Fly to Tangier Sound; Lat. 38° 04', Long. 75° 00'
4. Pilot request weather data from range recover ship
5. Fly Stilwell pattern at 1500 ft.
6. Fly pattern 3 (4 runs) at 5000 ft. with following parameters:

   Pulse width = 10 nsec
   Pulse/Frame = 1
   Polarization = Direct

Sweep speed = 50 nsec/cm
Attenuation = 20 dB
(40 frames/run)

7. Fly pattern 3 with:

   Pulse/Frame = 2

8. Fly pattern 3 with:

   Pulse/Frame = 10

9. Fly pattern 3 with:

   Pulse/Frame = 20

10. Fly pattern 3 with:

    Pulse/Frame = 50

11. Fly pattern 3 with:

    Pulse/Frame = 148

12. Fly pattern 3 with:

    Pulse/Frame = 278

13. Fly Stilwell pattern at 5000 ft.
14. Fly Stilwell pattern at 1500 ft.
15. Return to Wallops

<u>Flight 11 - Jan-21-1970</u>

1. Pre-flight briefing 8:30 A. M.
2. Take-Off 9:30 A. M.
3. Fly to Tangier Sound, Lat. 38° 04'; Long. 75° 00'
4. Pilot request weather data from ship
5. Fly Stilwell pattern at 1500 ft.
6. Fly pattern 3 (4 runs) at 10, 000 ft. with following parameters:

   Pulse/width = 20 nsec
   Pulse/Frame = 1
   Polarization = direct
   Sweep speed = 50 ns/cm
   Attenuation = 0 dB
   (40 frames/run)

7. Fly pattern 3 with:

   Pulse/Frame = 2

8. Fly pattern 3 with:

   Pulse/Frame = 10

9. Fly pattern 3 with:

   Pulse/Frame = 50

10. Fly pattern 3 with:

    Pulse/Frame = 147

11. Fly pattern 3 with:

    Pulse/Frame = 278

12. Fly Stilwell pattern at 10,000 ft.
13. Fly Stilwell pattern at 1500 ft.
14. Return to Wallops

<u>Flight 12 - Jan-22-1970</u>

1. Pre-Flight 8:00 A. M.
2. Take-Off 8:30 A. M.
3. Fly to Long Island Sound (Middle Ground)
4. Determine Sea and Wind direction
5. Take 10 frames of transmitted pulse
6. Fly six rectangular patterns with:

   Altitude = 10,000 ft.
   Pulse/width = 20 nsec
   Polarization = direct
   Sweep speed = 50 nsec/cm
   Attenuation = 0 dB

Pulse/Frame	= 1	30 frames
	= 2	30 frames
	= 10	30 frames
	= 50	40 frames
	= 148	40 frames
	= 278	40 frames

7. Take 10 frames of xmitted pulse
8. Land at JFK

<u>Flight 13 - Jan-26-1970</u>

1. Pre-Flight briefing 8:30 A. M.
2. Take-Off 9:30 A. M.
3. Fly to Wallops Sec 9-D; Lat. 37° 07', Long. 73° 38'

4. Contact Range Recoverer ship and request weather information
5. Fly Stilwell pattern at 1500 ft.
6. Take 10 frames of transmitted pulse
7. Fly six rectangular patterns with:

Altitude = 10, 000 ft.
Pulse Width = 20 nsec
Sweep speed = 50 nsec/cm
Attenuation = 0 dB

Peak Power = 3 watt

run #	pulse/frame	polar
1	1	direct
2	10	direct
3	50	direct
4	147	direct
5	278	direct
6	50	cross

8. Fly Stilwell pattern at 10, 000 ft.
9. Take 10 frames of transmitted pulse
10. Fly Stilwell pattern at 1500 ft.
11. Return to Wallops

Flight 14 - Jan-27-1970

1. Pre-Flight briefing 8:30 A. M.
2. Take-Off 9:30 A. M.
3. Fly to Wallops Sec 9-D
4. Take 10 frames of transmitted pulse
5. At test area fly Stilwell pattern at 1500 ft.
6. Fly six rectangular patterns with following radar parameters:

Pulse Width = 20 nsec
Peak power = 12 watts
Altitude = 10, 000 ft.
Attenuation = 0 dB
Sweep speed = 50 nsec/cm

Pattern #	Pulse/Frame	Polarization	Roll Angle
1	1	direct	0^o
2	10	direct	0^o
3	50	direct	0^o
4	148	direct	0^o
5	50	cross	0^o
6	50	direct	3^o

7. Fly Stilwell pattern at 10, 000 ft.
8. Fly Stilwell pattern at 1, 500 ft.
9. Take 10 frames of transmitted pulse
10. Return to Wallops (fly over Tangier Sound to check on ice cover).

Flight 15 - Jan-28-1970

1. Pre-Flight Briefing 8:30 A. M.
2. Take-Off 9:30 A. M.
3. Fly to Wallops Sec 9-D
4. Take 10 frames of transmitted pulse
5. Fly Stilwell pattern at 1500 ft.
6. Fly six rectangular patterns at 10, 000 ft with:

   Pulse width = 20 nsec
   Peak power = 12 watts
   Attenuation = 0 dB
   Sweep speed = 50 nsec/cm
   Polarization = direct

Pattern #	Pulse/Frame	Roll Angle
1	1	0°
2	10	0°
3	50	0°
4	148	0°
5	278	0°
6	50	5°

7. Take 10 frames of transmitted pulse
8. Fly Stilwell pattern at 10, 000 ft.
9. Fly Stilwell pattern at 1500 ft.
10. Return to Wallops

Flight 16 - Jan-29-1970

1. Pre-Flight briefing 8:30 A. M.
2. Take-Off 9:30 A. M.
3. Fly to Wallops Sec 9-D; 37° 07' , 73° 38'
4. Take 10 frames of transmitted pulse
5. Contact range recover for weather data
6. At test area, fly Stilwell at 1500. ft.

7. Fly six rectangular patterns at 10, 000 ft. with:

Pulse width = 20 nsec
Peak power = 12 watts
Attenuation = 0 dB
Sweep speed = 50 nsec/cm
Polarization = direct

Pattern #	Pulse/Frame	Film
1	1	B & W
2	10	B & W
3	50	B & W
4	148	B & W
5	50	Color
6	148	Color

8. Take 10 frames of transmitted pulse
9. Fly Stilwell pattern at 10, 000 ft
10. Fly Stilwell pattern at 1500 ft.
11. Contact Range Recoverer when leaving area
12. Return to Wallops

APPENDIX E

SHARP LEADING EDGE OF MULTIPLE PULSE RETURN FROM OCEAN SCATTERING

E-1. Introduction

It is interesting to note that the leading edge of the multiple return pulse signal is more sharply defined then the top of these pulses (see Figure E-1). There are several reasons why the observer should expect this to be true. The variance of the signal strength at any time during the pulse is proportional to the amplitude at that point so that lower signal values on the leading edge results in less signal variance. In addition the density variance of leading edge traces is measured in a direction perpendicular to that leading edge; while the variance of the pulse at the top of the pulse is measured perpendicular to the time base. From Figure E-2 we see that when the pulse has a slope to the leading edge this results in the variance of trace density being reduced by a factor of the cosine of the slope angle; therefore, the full variance appears on the top of the pulse while the variance on the leading edge in trace density is reduced by two factors, the slope of the leading edge and by the lesser expected amplitude of the signal on the leading edge.

A formula is derived for the variance of a square law detected Rayleigh fading signal corrupted by additive Gaussian noise. In the special case of the ramp-like waveforms that arise in satellite altimetry, the formula for the time dependence of the variance of the detector output is developed and sketched for comparison with flight test data.

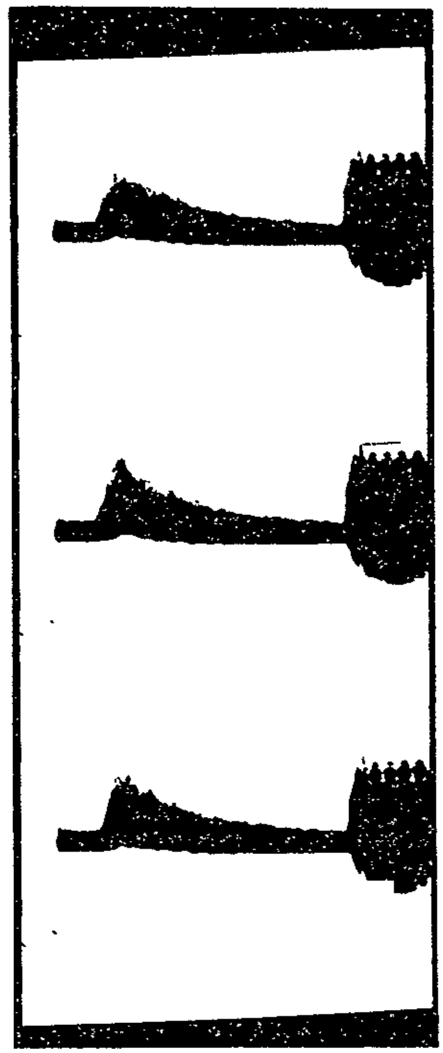

Figure E-1. Multiple Pulse Returns

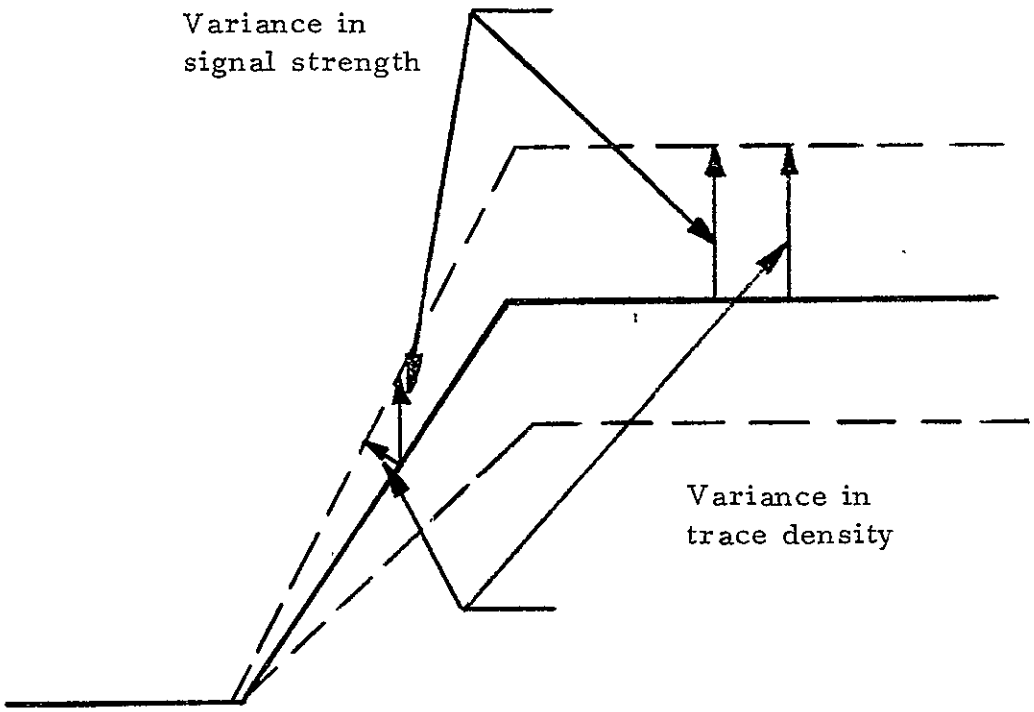

Figure E-2. Expected Waveform and Variance

E-2. Analysis

A narrowband Gaussian (i.e., Rayleigh fading) signal s(t) with power profile

$$E[s^2(t)] = P(t) \tag{1}$$

is corrupted by additive zero mean stationary Gaussian noise n(t) of variance N. The combination y(t) = s(t) + n(t) is subjected to square law detection. We seek the variance of the square law detector output $v(t) = y^2(t)$, namely

$$\sigma^2(v(t)) \triangleq E[v^2(t)] - E^2[v(t)] \tag{2}$$

where E denotes the statistical expectation operator.

From Eqs. (9) and (A-2) of Reference 1 we have, respectively,

$$E[v(t)] = P(t) + N \tag{3}$$

$$E[v^2(t)] = 3[P(t) + N]^2 . \tag{4}$$

(In deriving (4) we have made use of the fact that $\rho_s(t, t) = \rho_n(0) = 1$.) It follows that

$$\boxed{\sigma^2(v(t)) = 2[P(t) + N]^2} \tag{5}$$

Observe that the ratio of the standard deviation of v(t) to the mean of v(t) is

$$\frac{\sigma(v(t))}{E[v(t)]} = \sqrt{2} \tag{6}$$

independent of t. Accordingly, the RMS value of the fluctuation of the signal is proportional† to the expected value of the signal at each instant.

E-3. Results Applied to Satellite Altimetry

In satellite altimetry one receives a signal whose power profile is a ramp,

$$P(t) = Pt/T , \quad 0 \leq t \leq T .$$

when a square pulse is transmitted and a wideband receiver is used. The standard deviation of the square law detector output therefore grows linearly with time during the interval [0, T]. Accordingly, under low noise conditions ($P/N \gg 1$) we expect the square law detector output pulses to have the general appearance sketched in Figure E-3.

---

† The constant in (6) is $\sqrt{2}$ rather than 1 because in Reference 1 we assumed for simplicity that the signal was comprised solely of an in-phase component. Actucally, it has both in-phase and quadrature components, each with peak power $P/2$, and similarly for the noise. When this is taken into account, the $\sqrt{2}$ in (6) reduces to 1.

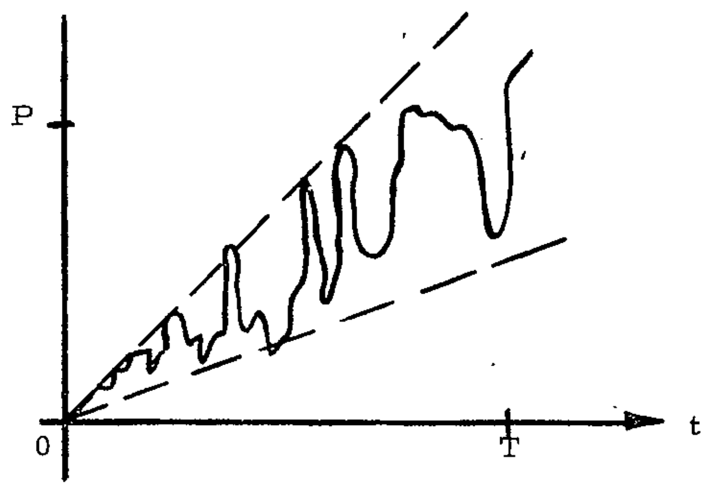

Figure E-3

RAYTHEON

RAYTHEON COMPANY
EQUIPMENT DIVISION